Ferrocene-based Chiral Monomers and Oligomers for Sensing Applications

by

Andrea Mulas

UNIVERSITY OF BIRMINGHAM

A thesis submitted to
The University of Birmingham
For the degree of
DOCTOR OF PHILOSOPHY

School of Chemistry
College of Engineering and Physical Sciences
University of Birmingham
April 2013

Abstract

Chiral sensing is a challenging field for the chemist. Not many sensors for chiral recognition have been studied, and only a few examples of electrochemical chiral sensors are known in the literature. The aim of this project was to synthesise novel ferrocenyl-based chiral receptors, and to study their applications for chiral sensing in solution or upon incorporation onto gold surfaces as self-assembled monolayers (SAMs). From the solution studies it was possible to gain further information on the electrochemical behaviour of ferrocenyl-based receptors during the sensing of chiral carboxylates. The incorporation of receptors onto electrode surfaces led to an economy on the amount of compound required and higher sensitivity in analyte detection. However, the chiral recognition properties and the stability of the SAMs still need to be improved. Multifunctional receptors containing BINOL and ferrocenyl reporting groups were investigated to compare the use of electrochemistry and fluorescence spectroscopy in the chiral recognition of carboxylic acids, amino acid derivatives, or amino acid anions. Finally, a DNA analogue in which ferrocenyl units were incorporated in the backbone was studied. The electrochemical properties of this system as a single strand and in its interaction with complementary strands of DNA and PNA were investigated.

Table of Contents

Acknowledgements

First of all I would like to thank my supervisor Prof. Jim Tucker, for giving me the opportunity to carry out my PhD project in his group. He has always been present and available for advice and suggestions, but also for friendly chats and nice summer barbecues with great entertainment (too bad he is incredibly good at table tennis, he kicked me out of the competition too soon!). And thanks also for the support in various applications, proof-reading, participation in conferences and for giving me the opportunity to have a great USA adventure (thanks also to Prof. Lin Pu and his group members, especially Shanshan, for welcoming me for one month in their lab at the University of Virginia). Thanks to all the members of Tucker Group, especially the other two musketeers, Jack and Antoine, for the awesome three years spent together. Thanks also to Giorgio for introducing me to electrochemistry and for giving me good advice, but also for the good time in the few weeks we spent living under the same roof. Thanks to Yasmine for being available by e-mail communication: although we never met, her help has been really appreciated. Thanks to Luciana for the help with the NMR and for the *mate* sessions in the afternoon, I miss that quite a lot. And last but not least, thanks to Rosie, Gemma, Pete, James, Jean-Louis, John and Huy for proof-reading the chapters of this thesis and speeding up its production.

Thanks also to another member of the staff of the University of Birmingham, Dr. Sarah Horswell, for helping me in improving my understanding of electrochemistry, for having being available to proof-read posters and abstracts, and for giving me the opportunity to participate in the Midlands Electrochemistry Group Meetings.

Thanks to the staff of the analytical facilities for running a smooth service and always being available to provide useful information. In particular I would like to thank Mr Graham Burns

for the HPLC characterisation, Mr Peter Ashton and Mr Nick May for the Mass Spectroscopy, Dr. Louise Male for the resolution of the crystal structures and Dr. Neil Spencer for keeping the automated NMR always working, and for the interesting chats during the NMR titrations. I am grateful to the EPSRC and the School of Chemistry for funding my research and for contributing to the funding that allowed me to carry out my exchange project in the USA.

A very special thanks to my family in Italy: without their support I would probably not be here now. Thanks to my dad for believing in me and giving me always his support: I know he would be proud of me, as he has always been. Thanks to my mum for always being there, and for being strong and affectionate. Thanks to my sister and her beautiful daughters, to bring me delight when I visit home and being close despite far the rest of the time. In the same way thanks to my friends scattered everywhere, but especially Antioco, Katia, Raffo and Pam for making every moment we spend together like the time never passed.

Thanks to the friends I have had the pleasure to meet here in Birmingham: Antonio, John, Marta, Giulia, Sylwia, Alice and finally Elisa, for the fun during the various years; Carlotta for always being a good and attentive friend (maybe sometimes a bit overprotective); with her Antoine, Myrto, Alex, Chris, Dr. Dave and all the people that participated in great evenings in the staff house and out for dinner or in town; Damian and Natalia for being great housemates in the mythical Reservoir Road, and then Luca, despite for a short time but rich of *merende*; Michel and Manu for welcoming me in their house during the last month, and for the great barbecues over the years. And finally thanks to one special person that made me laugh and made me cry, for the good as well as the bad: in the end, *c'est la vie*.

List of Abbreviations

α	Transfer Coefficient
$[\alpha]_D$	Specific Rotation
A	Electrode Surface Area (cm^2)
A	Hydrogen Bond Acceptor
Abs	Absorption
AC	Alternate Current
AcO	Acetate
AFM	Atomic Force Microscopy
Ar	Aromatic
β	Overall Equilibrium Constant
BINOL	1,1'-bi-2-naphthol
Bn	Benzyl
br s	Broad Singlet
Bu	Butyl
Γ	Surface Coverage (mol cm^{-2})
C	Concentration (mol/cm^3)
Cp	Cyclopentadienyl
CV	Cyclic Voltammetry
δ	Chemical Shift (ppm)
δ_0	Shift of the proton resonance observed for the host in absence of substrate
δ_{comp}	Shift of the proton resonance observed for the host upon full complexation
δ_{obs}	Observed shift of the proton resonance monitored
ΔE_{obs}	$E^{o\prime}_{HG} - E^{o\prime}_{H}$
d	Doublet
D	Diffusion Coefficient (cm^2/s)
D	Hydrogen Bond Donor
de	Diastereomeric Excess
DIAD	Diisopropyl Azodicarboxylate
DME	Dimethoxyethane

DMF	Dimethylformamide
dmfc	Decamethylferrocene
DMSO	Dimethylsulfoxide
DNA	Deoxyribonucleic Acid
dopa	3,4-dihydroxyphenylalanine
DPPA	Diphenylphosphoryl Azide
DPV	Differential Pulse Voltammetry
ε	Molar Absorptivity
e^-	Electron
E	Potential (V)
$E^{o'}$	Formal Potential (V)
ee	Enantiomeric Excess
E_p^a	Anodic Peak (V)
E_p^c	Cathodic Peak (V)
eq.	Molar Equivalents
ES	Electrospray
Et	Ethyl
F	Faraday Constant
F(000)	Effective number of electrons in the crystal unit cell
Fc	Ferrocene
FcNA	Ferrocene Nucleic Acid
G	Guest
H	Host
HG	Complex
HPLC	High Performance Liquid Chromatography
HRMS	High Resolution Mass Spectrometry
i	Intensity of Current (A)
i^{lim}	Limiting Current (A)
IPA	Isopropyl Alcohol
i_p^a	Anodic Peak Current (A)

i_p^c	Cathodic Peak Current (A)
IR	Infrared
J	Coupling Constant
K	Binding Constant
k^o	Rate constant of the standard heterogeneous electron transfer
m	Multiplet
MA	Mandelic Acid
Me	Methyl
MeCN	Acetonitrile
Mp	Melting Point
Ms	Mesylate
MS	Mass Spectrometry
v	Scan Rate ($V\ s^{-1}$)
n	Number of Electrons
n	Volume of Host (µl)
NIBC	*N*-isobutyl-cysteine
NMR	Nuclear Magnetic Resonance
ODN	Oligodeoxyribonucleotide
Ox	Oxidised
PNA	Peptide Nucleic Acid
ppm	Parts per Million
PTSA	*para*-Toluene Sulphonic Acid
q	Quartet
Q	Charge Transfer (C)
QCM	Quartz Crystal Microbalance
R	Universal Gas Constant
r	Radius of the Electrode (cm)
R^2	Deviation from Linearity
Red	Reduced
ret.	Retention

Rf	Retardation Factor
rt	Room Temperature
s	Singlet
SAM	Self-Assembled Monolayer
sept	Septet
SP	Stylus Profilometry
STM	Scanning Tunnelling Microscopy
SWV	Square Wave Voltammetry
θ	Step (s)
t	Triplet
T	Absolute Temperature (K)
TBA	Tetrabutylammonium
THF	Tetrahydrofuran
toc	Total Organic Carbon
UFF	Universal Force Field
UV-Vis	Ultra Violet – Visible
vs.	Versus
WE	Working Electrode
Z	Number of molecules in the crystal unit cell

CHAPTER 1: INTRODUCTION

1.1 Supramolecular chemistry

In the past few decades a new branch of coordination chemistry has achieved more importance and consideration, resulting in a novel field with numerous potential applications known as "supramolecular chemistry". Jean-Marie Lehn, Nobel prize winner for chemistry in 1987 together with Donald Cram and Charles Pedersen, defined this science as "the chemistry of molecular assemblies and of the intermolecular bond"[1] or as "chemistry beyond the molecule, bearing on the organised entities of higher complexity that result from the association of two or more chemical species held together by intermolecular forces".[2] Such interactions are typically ion-dipole, hydrogen bonding, π-π interactions and hydrophobic interactions.[3] The basic hypothesis is that molecular recognition occurs between the receptor molecule (host) and a substrate (guest), with an interaction between the two species that should be as selective and specific as possible. To achieve specificity, it is possible to organise the molecule to maximise the interaction with a particular substrate rather than other possible guests; for example, shaping the receptor and positioning the binding sites. With this approach it is possible to achieve a reversible and selective complexation that allows the receptor to behave as a sensor for specific guest molecules, as presented schematically in Figure 1.1.

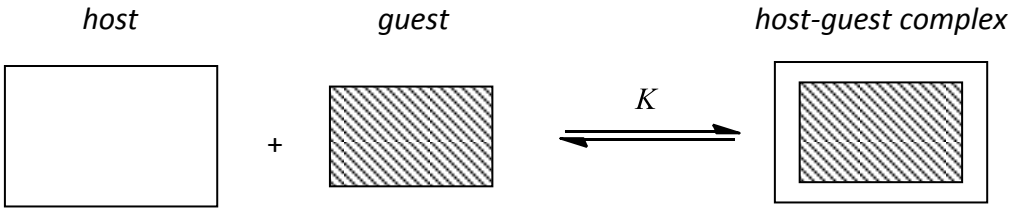

Figure 1.1: *Reversible complexation of a guest molecule due to the interaction with a host molecule. The binding constant, K, represents the equilibrium of the complexation*.

The first example of selective complexation of metal cations was described by Pedersen in 1967, with the synthesis of cyclic polyethers. The most famous of this new class of compounds is 18-crown-6,[4] which is able to selectively bind K^+ cations in solution as in **1.1**.

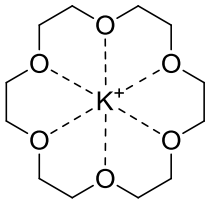

1.1

Two years later Lehn and coworkers expanded the field with the synthesis of cryptands, such as [2.2.2]-cryptand **1.2**.[5] This can be considered a three-dimensional analogue of the crown ethers, with greatly improved preorganisation and selectivity.

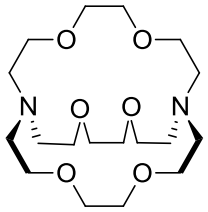

1.2

1.2 Anion binding

Many sensors have been designed with the presence of specific binding sites to enhance the complementarity and recognition of anions. The design is usually more complex than that of cation receptors, because anions often differ in shape and geometry, and they are bigger than cations with the same but opposite charge. However in general, the same design strategies as in the development of cation sensors[6] can be employed. The efficiency and selectivity of the binding event depends on the ligand arrangement, features of the analyte, and the properties of the solvent, plus ionic strength and pH for aqueous solutions.[7] An

effective way to bind an anion strongly is the use of a charged receptor, which exploits electrostatic interactions.[8] Alternatively, the receptor can include atoms that act as Lewis acids and give strong interactions via a good orbital overlap.[9] However, an interaction often exploited is the hydrogen bond donor-acceptor interaction, which is useful because of its directionality and its particular strength.[10] Receptors for anions that use the hydrogen bond can be separated into different categories depending on which hydrogen bond donor group they contain: amide, urea and thiourea, pyrrole and indole, hydroxyl groups, and charged receptors (guanidium, imidazolium, ammonium).[11-14]

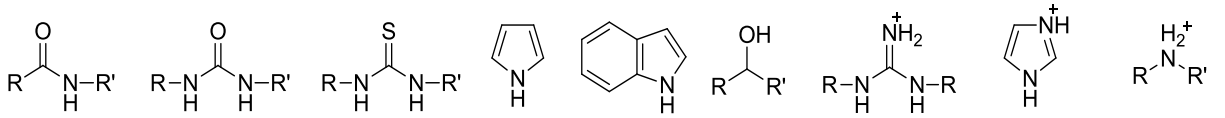

The first example of a receptor for anions was reported by Simmons and Park in 1968,[15] with the synthesis of macrobicyclic amines and the studies on the encapsulation of halide ions within their cavities. In 1976 Lehn and coworkers developed macrotricyclic receptors which were able to selectively bind anions when their amine groups were protonated. A recent example of ammonium based receptor was reported by Hossain and coworkers with receptor **1.3**.[16] This aza-cryptand was able to bind three nitrate anions when octa-protonated.

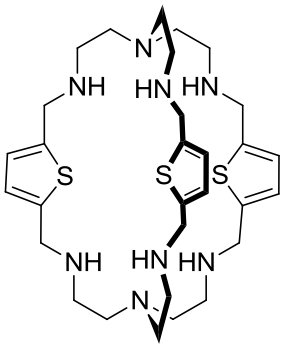

1.3

Neutral hydrogen-bonding receptors have been widely exploited. In 1990 Hamilton published a paper in which receptor **1.4** was synthesised.[17] This was found to bind dicarboxylic acids through the amidopyridine units in nonpolar organic solvents.

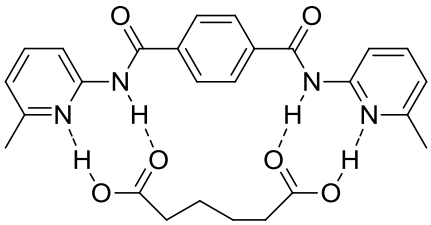

1.4

He then improved the ability of this class of receptors to hydrogen-bond in highly competitive solvents such as DMSO-d_6, by replacing the amidopyridine moieties with urea or thiourea binding sites, such as receptors **1.5** and **1.6**.[18]

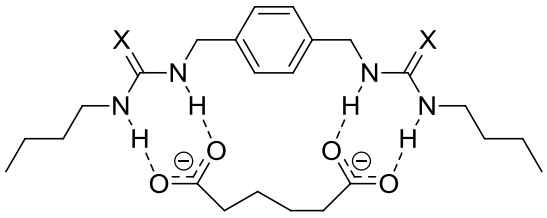

1.5 X=O
1.6 X=S

This type of receptor was able to bind effectively bis-tetrabutylammonium salts of glutaric acid in DMSO-d_6. The binding was supported by the detection of a downfield shift of the resonances relative to the urea protons using ^{1}H NMR spectroscopy.

Gale and coworkers synthesised a series of anion receptors **1.7-1.9** based on *o*-phenylendiamine.[19] Receptor **1.9** was previously synthesised by Cheng and coworkers,[20] who investigated its anion binding properties with a series of anions, excluding carboxylates. Gale and coworkers then discovered that the most efficient receptor in the series was the urea-

based **1.8**, which was selective towards carboxylates due to the formation of four hydrogen-bonds with the guests, as displayed in the crystal structures collected.

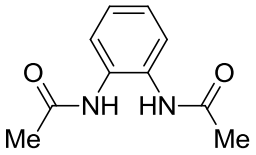

1.7

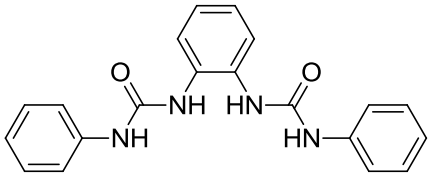

1.8

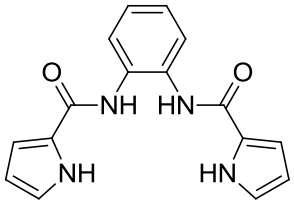

1.9

A recent example of anion binding using a urea-containing receptor was described by Lin and coworkers.[21] The synthesis of the tris(urea) receptor **1.10** was reported. The binding studies with dihydrogenphosphate anions showed good selectivity and affinity, as proven by UV-Vis spectroscopy and by the chemical shifts observed in the ^{1}H NMR.

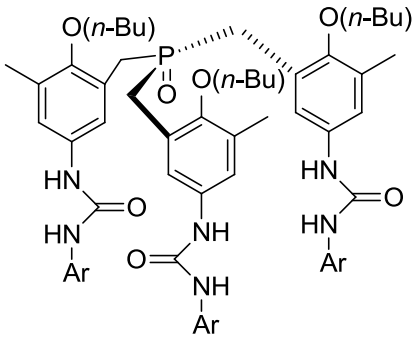

1.10

Numerous studies have been carried out subsequently on anion binding through hydrogen-bonding formation, as summarized in the comprehensive reviews published by Gale and coworkers in the last decades.[11, 13, 14, 22-26]

1.3 Supramolecular Sensing

According to IUPAC, a chemical sensor is a system that transforms chemical information into a signal (such as pH modifications, light emission, colour change or electronic distribution).[27] Supramolecular sensing can be achieved by attaching a functional reporting group in close proximity to a binding site. A generic system such as this is called a supramolecular device (Figure 1.2).[28]

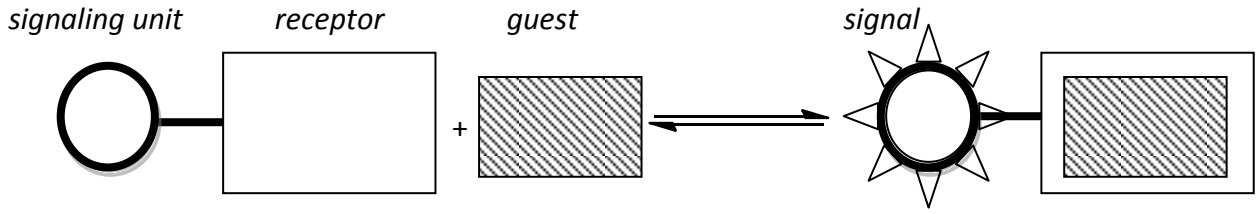

Figure 1.2: *Signaling and sensing in a supramolecular device.*

After complexation of the guest it is possible to observe a change in the properties of the signaling unit; this could correspond to a change in the optical properties that would cause emission in the case of a fluorescent sensor, a change in the absorption properties that could cause a change in colour in the case of a colourimetric sensor, or a modification of the redox properties of the receptor in the case of an electrochemical sensor.

In an optical sensor the signaling unit must be able to modify its photophysical properties, such as fluorescence or absorbance, when the recognition of the substrate occurs. A typical signaling unit exploited in fluorescent sensing is anthracene.

One of the first examples of fluorescent sensors was reported by de Silva and coworkers in 1992 with the synthesis of the anthracenyl functionalised aza-crown ethers **1.11** and **1.12**.[29] These fluorescent sensors were able to sense protons, showing different fluorescent intensity depending on the pH of the solution.

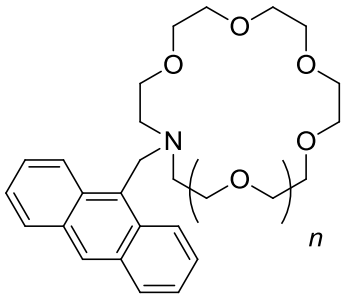

1.11 *n*=0
1.12 *n*=1

Subsequently, Gunnlaugsson and coworkers studied a series of receptors **1.13-1.16** that used hydrogen-bonding to anions through thiourea groups to achieve a photochemical response of the fluorophore,[30-32] that was reflected in selective emission quenching in the presence of fluoride in DMSO.

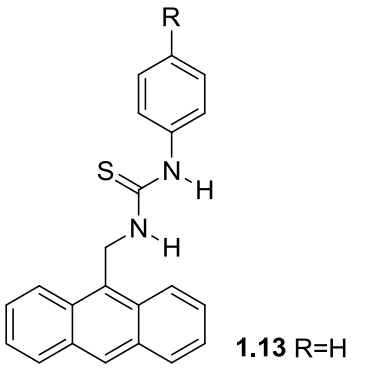

1.13 R=H
1.14 R=CF_3

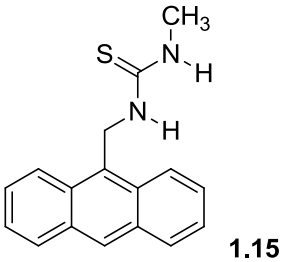

1.15

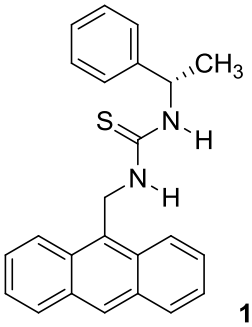

1.16

In colourimetric sensors the absorbance properties are influenced by the presence of the analyte. They are particularly versatile because the response can be followed by observation

with the naked eye. In these kind of sensors, active unit and signaling unit are the same and the colour variation is due to a modification in the energy of the HOMO and LUMO orbitals of the chromophore.

In 2003 Gale and coworkers reported studies on receptor **1.17**,[33] which is based on 2,5-diamidepyrrole and contains 4-nitrophenyl groups.

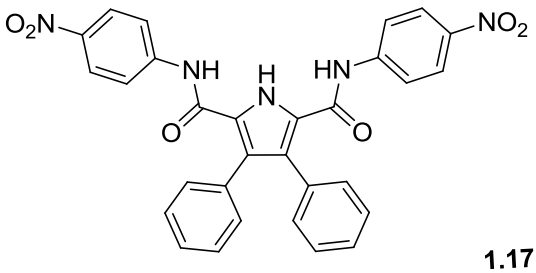

1.17

These increased the acidity of the NH groups *via* an electron withdrawing effect, and in the presence of basic anions such as fluoride, a colour variation towards blue was observed, due to deprotonation (Figure 1.3).

Figure 1.3: *Solutions of receptors* ***1.17*** *(2 mM) in MeCN with various anions, added as TBA salts (20 mM). From left* ***1.17****,* F^- *+* ***1.17****,* Cl^- *+* ***1.17****,* Br^- *+* ***1.17****,* BzO^- *+* ***1.17****,* $H_2PO_4^-$ *+* ***1.17****.* [33]

1.4 Electrochemical Sensing

Electrochemistry is a powerful tool for monitoring supramolecular interactions.[34, 35] Electrochemical sensing can be achieved by attaching an electrochemical active reporting group in close proximity to the binding site.[36] After complexation of the guest it is possible to observe a change in the redox potential of the reporting group. The square scheme (Scheme 1.1) shows the correlation between host H, guest G and complex HG species in their reduced "red" and oxidised "ox" forms.[36]

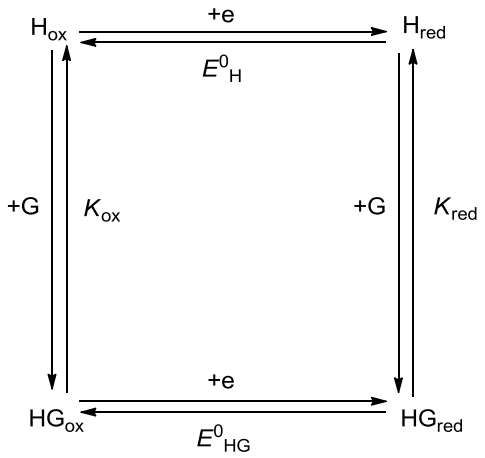

Scheme 1.1*: The square scheme for guest binding and electron transfer.*[36]

According to Beer and coworkers,[37] the ΔE_{obs} values depend on K_{ox}/K_{red}, following equation 1.1:

$$\frac{(E^{o\prime}{}_{H}-E^{o\prime}{}_{HG})nF}{RT} = \ln\left(\frac{K_{ox}}{K_{red}}\right) \qquad \textbf{\textit{Equation 1.1}}$$

Ferrocene is a popular choice as the functional component, for its well-characterised and reversible electrochemistry. In addition, ferrocene can be easily functionalised with a variety

of receptor groups that act as binding sites, and chirality can be readily introduced.[38] Ferrocene undergoes a monoelectronic reversible oxidation to the ferrocenium ion at easily attainable potentials. It also presents the advantage of being rather stable in protic solvents and in the presence of molecular oxygen. Unfortunately, the ferrocene groups are also known for a loss of stability in aqueous solutions when in the presence of some anions.[39] A ferrocenium cation ($FeCp_2^+$) can decompose if the cyclopentadienyl anion (Cp^-) exchanges with other nucleophiles present in solution, such as OH^-, Cl^-, and NO^{3-}. The rate depends on the donor strength of the nucleophile.[40] However, the stability of the ferrocene groups can be increased by functionalisation of both Cp rings. The ferrocene reporting group can act as a redox antenna. Its redox potential is affected by the binding with specific guests,[35] for instance, if the binding site is in proximity to the ferrocene unit.

One of the first examples of ferrocene-based electrochemical sensors was the synthesis of pentaoxo(13)ferrocenphane **1.18** by Saji and coworkers in 1986.[41]

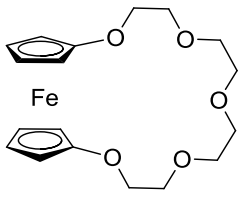

1.18

They studied the effect of its oxidation on the affinity towards metal cations, discovering that oxidation of the ferrocene unit causes an abrupt decrease in the binding constants for the association with the cations.

The first example of a metallocene derivative as a redox-active sensor for anions was reported by Beer and coworkers in 1989.[42] In the literature there are now many examples of the synthesis and study of redox-active receptors for anions that contain urea as a binding group and ferrocene as a reporting group,[43, 44] as described below.

Kaifer and coworkers synthesised a series of redox-active dendrimers of different size.[45] These receptors were based on a diaminobutane core and each branch of the dendrimer was functionalised with a ferrocenylurea group. The resulting series of receptors **1.19**-**1.22** featured 4 to 32 ferrocenylurea groups.

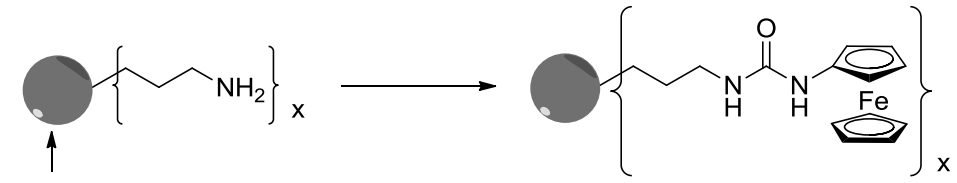

DAB-dendrimer

1.19 x=4
1.20 x=8
1.21 x=16
1.22 x=32

The binding of anions to **1.19**-**1.22** was studied using SWV, as this technique is more sensitive compared to cyclic voltammetry, which has a higher detection limit (see Section 1.9.2). Tetrabutylammonium salts of $H_2PO_4^-$, HSO_4^- and Cl^- were added to the dendrimers in DMSO containing 0.1 M tetrabutylammonium hexafluorophosphate as supporting electrolyte. $H_2PO_4^-$ induced significantly larger shifts compared to the other anions. For example, using dendrimer **1.19** as a receptor, when one equivalent of $H_2PO_4^-$ was added for each ferrocene group, a cathodic shift of -112 mV was observed in the ferrocene redox potential, compared to -40 mV with HSO_4^- and -16 mV with Cl^-. Larger shifts of the redox

potential were observed with receptors **1.20** and **1.21**. However, the largest dendrimer **1.22** bound $H_2PO_4^-$ more weakly than **1.20** or **1.21**.

In 2003 Beer published the synthesis of mono- and bis-urea derivatised ferrocene receptors **1.23**-**1.26.**[46] ^{1}H NMR anion titration studies with Cl^- and $H_2PO_4^-$ were carried out. Electrochemical studies showed that these receptors were able to electrochemically recognise $H_2PO_4^-$, Cl^- and AcO^- through changes in the respective ferrocenyl oxidation waves.

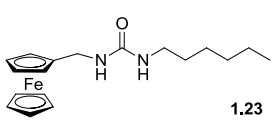

1.23

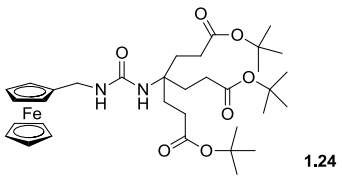

1.24

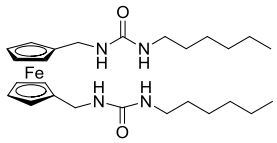

1.25

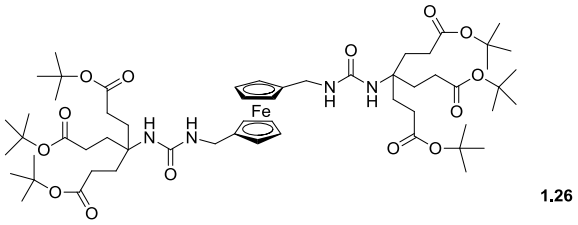

1.26

In the same year, Beer and coworkers reported the successful incorporation of a ferrocene unit onto the upper-rim of calix[4]arenes through either urea or amide hydrogen bonding units. The three novel receptors **1.27**-**1.29** synthesised could sense electrochemically the binding of anions.[47] ^{1}H NMR studies indicated that the receptors had a general preference for binding more basic anions and, in the case of the tetra-urea derivative, displayed a marked selectivity for dihydrogen phosphate.

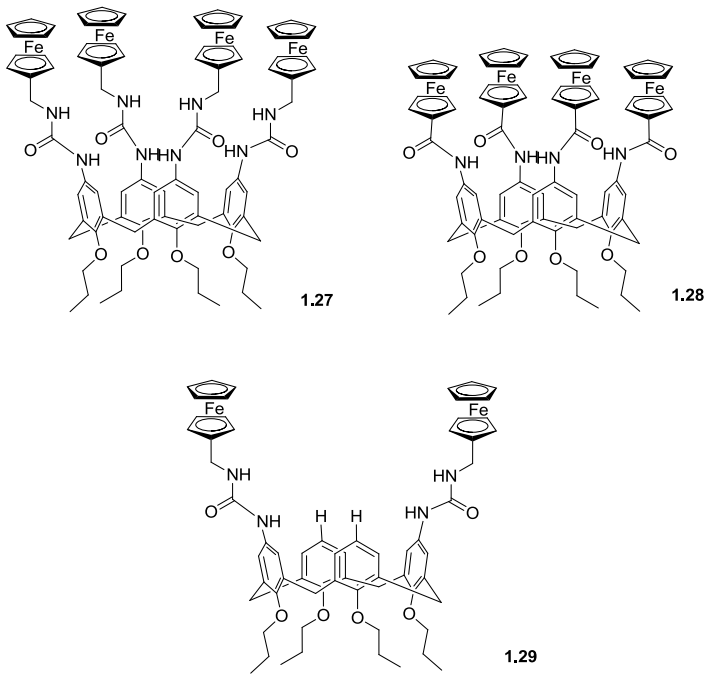

Cyclic and square wave voltammetric studies demonstrated that all receptors could electrochemically sense the binding of anions, with dihydrogen phosphate inducing the largest shifts (Figure 1.4).

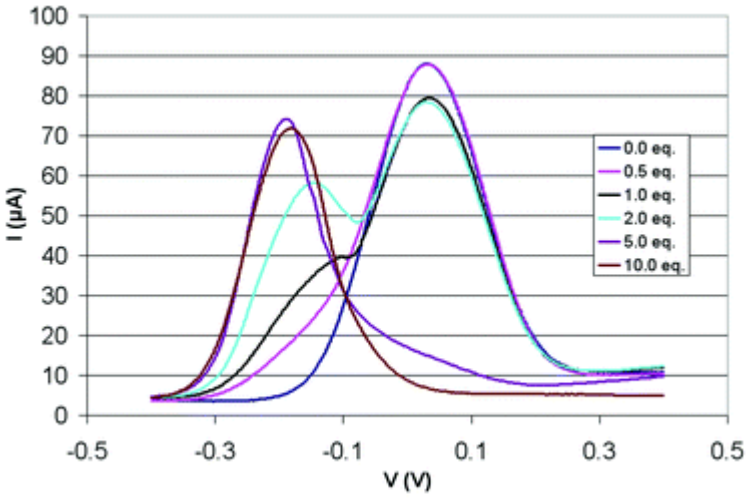

***Figure 1.4**: Square wave voltammogram of **1.27** in absence and presence of $H_2PO_4^-$ in 1:1 CH_2Cl_2/CH_3CN.*[47]

In one of their recent publications, Beer and coworkers published the synthesis of two novel ferrocene-containing macrocycles.[48] The amide-containing macrocycle **1.30** is able to sense

basic oxoanions such as $H_2PO_4^-$ and BzO^- although with weak binding strength. The urea-containing macrocycle **1.31**, is able to bind and sense a greater range of oxoanions, with a shift of –170 mV for the ferrocene/ferrocenium potential observed after addition of an excess of dihydrogen phosphate.

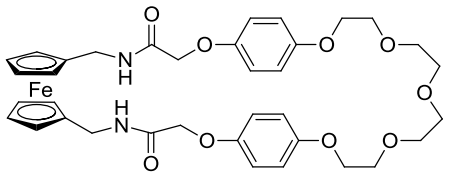

1.30

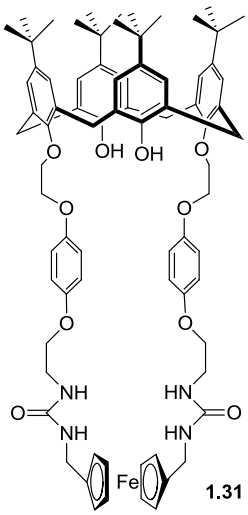

1.31

Molina and coworkers published a series of works on ferrocene-based ureas as receptors for anions.[49-53] One of the most recent is the synthesis of receptors **1.32** and **1.33**, included in work published in 2009, that was obtained in a one-flask preparation.[53]

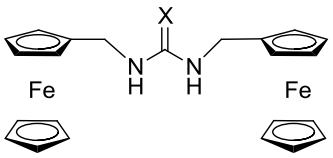

1.32 X=S
1.33 X=O

Electrochemical studies indicated that the peripheral ferrocenyl units were not in electronic communication, as only one wave was observed in the voltammograms. The electrochemical properties of compound **1.33** on its own and in the presence of Cl^-, F^-, AcO^-, NO_3^-, HSO_4^- and $H_2PO_4^-$ in variable concentration (added as tetrabutylammonium salts) as guest anions were studied using cyclic (CV) and differential pulse (DPV) voltammetry. Only one reversible wave

was observed, and upon addition of dihydrogenphosphate anion a remarkable cathodic shift occurred ($\Delta E^{0\prime} = -110$ mV).

1.5 Chiral recognition

The interactions common in supramolecular chemistry can be used for chiral recognition. The separation of enantiomers in chemistry is particularly important, together with the quantification of the enantiomeric excess of one enantiomer in a mixture of two, and the screening of asymmetric reactions. Enantiomers often differ in their biological properties, and one can be active and the other simply inactive. However, sometimes one of the enantiomers can have damaging activity, and its presence must be avoided. A good way to get a receptor able to discriminate between two enantiomers is to build a molecule with its own chiral properties, as described by Cram.[54]

In 1973 Cram described chiral recognition in molecular complexation with the synthesis of chiral cyclic ethers such as **1.34** containing binaphthyls.[55] These receptors were able to selectively complex (*R*)- and (*S*)- phenylethylammonium hexafluorophosphate in solution. The simple axial chirality provided by the binaphthyls could enable the receptors to discriminate between the enantiomers.

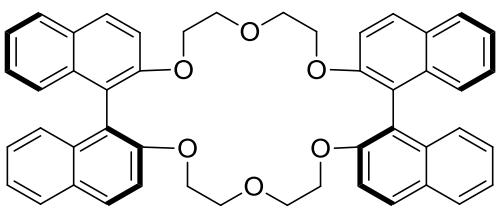

1.34

Many receptors designed following this strategy have been synthesised and used for sensing guest molecules with chiral centres, as summarised in the recent review published by Pu in 2012 about the use of fluorescence of organic molecules in chiral recognition.[56] Many groups have recently published work on the same subject.[57-62]

A relatively recent example of chiral recognition of carboxylic acids and amino acids is the work published by Wolf and coworkers, who synthesised a chiral 1,8-diacridylnaphthalene-derived sensor **1.35**. This exhibits a cleft designed specifically for stereoselective sensing through interactions with neutral guests containing hydrogen bond donor groups.[27] It was utilised for the determination of enantiomeric excess and concentration of carboxylic acids and of derivatised amino acid.

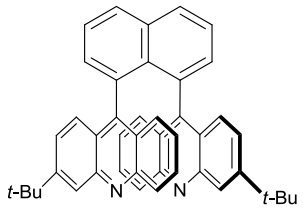

1.35

Effective hydrogen bonding interactions were expected to occur with chiral amino acids and carboxylic acids. The development of a fluorescence method made possible the gain of information about the enantiomeric excess of chiral compounds in MeCN. Guests of these studies were the amino acids and carboxylic acids shown in Figure 1.4.

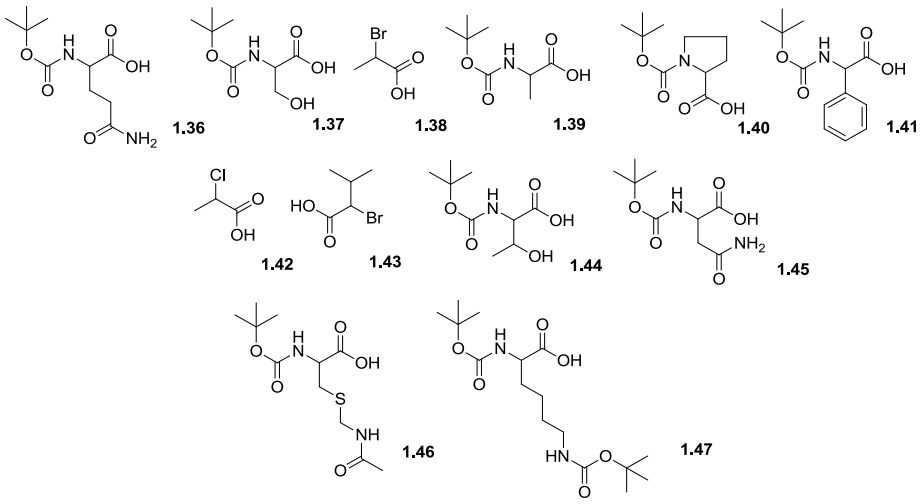

***Figure 1.4**: Structures of chiral carboxylic acids and amino acids used as guests.*[27]

The receptor **1.35** showed high enantioselectivity: for instance, the (*R*)-enantiomers of guest **1.43** showed little quenching, whilst the emission of (-)-**1.35** was quenched dramatically when the (*S*)-enantiomer was present in millimolar concentration (Figure 1.5).

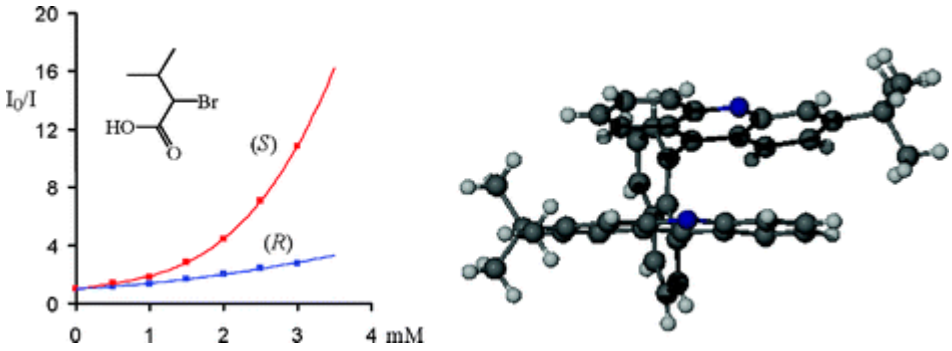

***Figure 1.5**: Plots showing enantioselective fluorescence quenching of (-)-**1.35** in the presence of **1.43**. Sensor conc.: 3.5 x 10^{-6} M in MeCN. Excitation (emission) wavelength: 360 nm (535 nm) On the right, single crystal structure of (-)-**1.35**.*[27]

Pu and coworkers synthesised a novel BINOL-amino alcohol receptor (*S*)-**1.48**,[63] which showed chiral fluorescent recognition of a protected serine derivative **Ser** with highly enantioselective emission enhancement (Figure 1.6). More examples are described in Section 4.1.

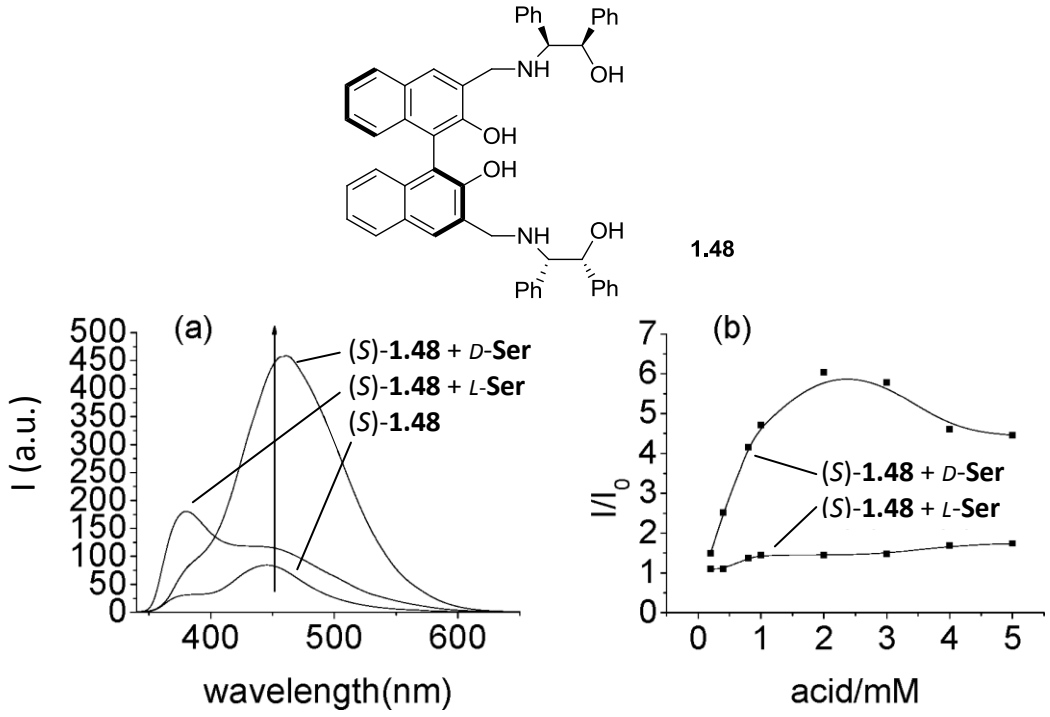

Figure 1.6: *(a) Fluorescence spectra of (S)-**1.48** (5.0×10^{-4} M) with* D- *and* L-***Ser*** *(2.0×10^{-3} M). (b) Fluorescence enhancement of (S)-**1.48** (5.0×10^{-4} M) with* D- *and* L-***Ser*** *at λ_{em} = 460 nm. (Solvent: benzene/2.5% DME. λ_{exc} = 341 nm, 5.0/5.0 nm).*[63]

1.6 Electrochemical chiral recognition

Despite the abundance of receptors containing ferrocene moieties that have been exploited for anion sensing, only a few examples of receptors that allow the chiral recognition by electrochemical techniques are reported in the literature.

One of the first examples was an article published in 1995 by Ori and Shinkai,[64] in which a chiral ferrocenylboronic acid **1.49** bound saccharides at around pH *7.* The complexation was investigated using electrochemical techniques, and it showed limited chiral discrimination for linear saccharides.

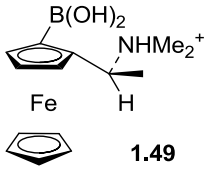

1.49

In 2006 Kim and coworkers published work on the enantiomeric determination of amines by voltammetry, using azophenolic crown ethers such as in the example **1.50**.[65]

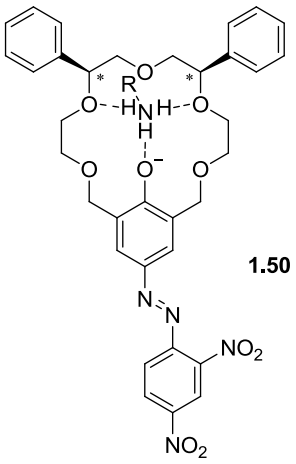

1.50

The redox potential of the receptor was affected by the structure of the alkyl amines that interacted with the binding sites. Enantiomeric amines could be selectively recognised, and even the R/S ratio in mixtures of enantiomers could be determined using the chiral receptor **1.50.** The ratio between the binding constants calculated by spectrophotometric titrations in the presence of (*S*)- or (*R*)-phenylglycinol showed a K_R/K_S value of 3.5. The peak separation of the square wave voltammograms of the two complexes showed a difference of 32 mV, with a linear variation of the peak potential against the enantiomeric ratio (Figure 1.7).

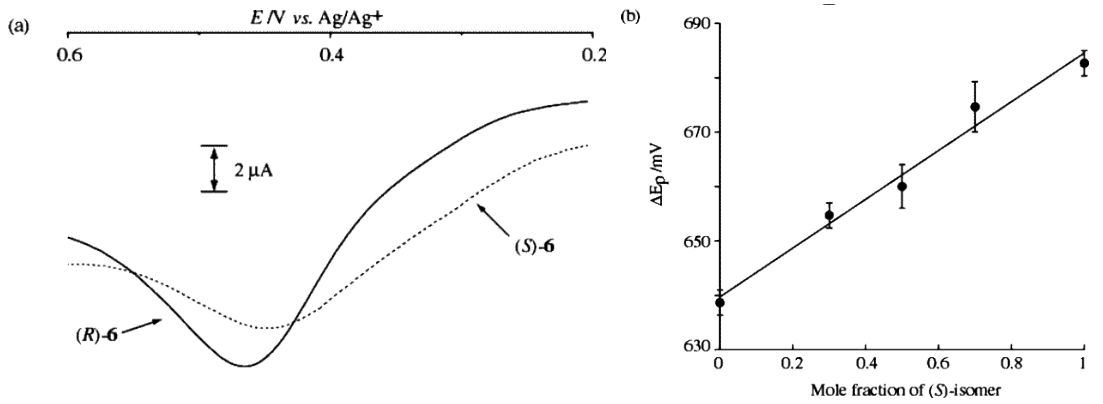

Figure 1.7: *a) SWV of 0.5 mM* ***1.50*** *in the presence of 0.25 mM (*R*)- (solid curve) and (*S*)-phenylglycinol (dotted curve); step potential, amplitude and frequency are 4 mV, 25 mV and 30 Hz, respectively; b) relationship between* E_p *and molar fraction of S isomer by SWV. Total concentration is 0.5 mM.*[65]

Previous work published by the Tucker group in 2002 described the asymmetric synthesis of redox-active ligands in good enantiomeric excess,[66] as a preliminary study towards chiral recognition. These were able to bind chiral carboxylate anions, and the complexation event was studied by monitoring the redox response in the presence of the guest.

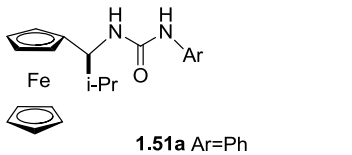

1.51a Ar=Ph
1.51b Ar=4-NO_2-C_6H_4

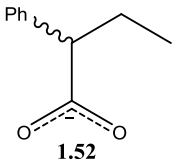

1.52

Upon addition of an excess of racemic **1.52** to a solution of receptor **1.51b**, a cathodic shift of -70 mV in the redox potential of **1.51b** was observed (Figure 1.8). However, no significant difference between the response to complexation of the enantiopure and racemic forms of **1.52** were observed.

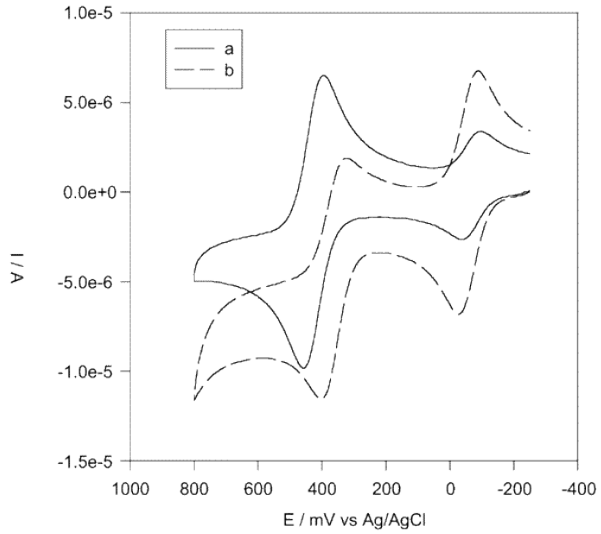

***Figure 1.10**: Cyclic voltammograms of (a) **1.51b** (0.5 mM) and (b) **1.51b** (0.5 mM) with 5 eq. of racemic **1.52**.*[66]

The Tucker group subsequently published in 2008 the synthesis of a series of chiral ureas **1.53-1.57** containing the ferrocene motif.[67]

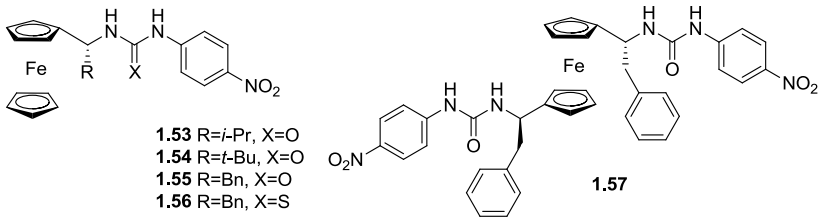

Each of these receptors was able to bind chiral carboxylates **1.58-1.60** in organic solvents such as MeCN and DMSO through hydrogen-bonding interactions, and the complexation was studied with spectroscopic and CV techniques. In particular, electrochemical sensing in solution was effective for discriminating between the different guests, and in one case also enantiomers of the same guest.

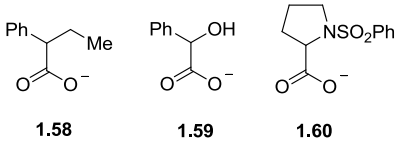

Indeed, the enantioselectivity in the complexation of the TBA salt of the amino acid derivative *N*-benzenesulfonylproline **1.60** with the ferrocenylbenzyl receptor **1.55** was high enough to be able to observe the difference in terms of chiral sensing using electrochemical measurements (Figure 1.9).

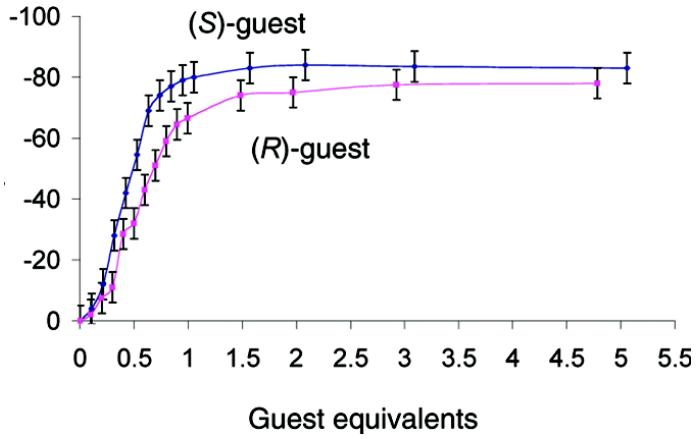

***Figure 1.9**: Titration of the ΔE_{obs} value in CH_3CN of the redox wave of receptor **1.55** against (a) molar equivalents of (S)-**1.60** (blue diamonds) and (R)-**1.60** (pink squares).*[67]

In one of the most recent publications, Tucker group described the synthesis of a novel chiral ferrocene-based boronic acid **1.61** that is able to interact with (*S*)- and (*R*)-BINOL to form specific complexes that can be easily distinguished due to their significant difference in the ferrocenyl redox potentials (Figure 1.10).[68]

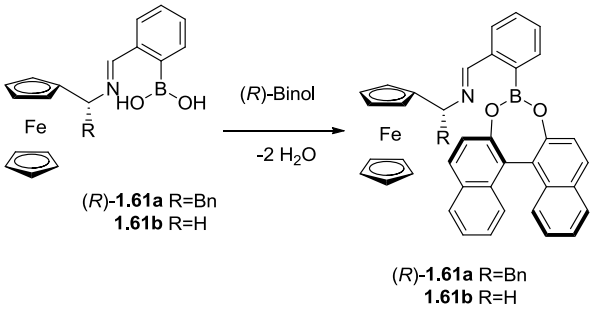

The differences observed in the redox behaviour can be conveniently exploited to assess what is the level of enantiomeric excess in mixtures of enantiomers that can be quantified using electrochemical methods.

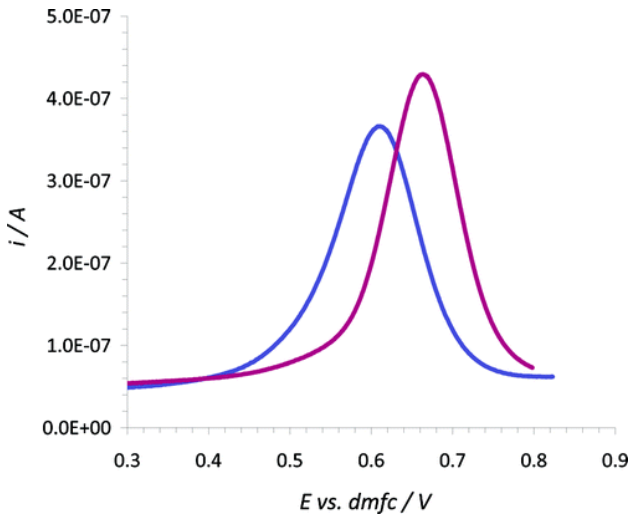

Figure 1.10: *Square wave voltammograms in CH_2Cl_2 of (R)-**1.61a**:(S) in blue and (*R*)-**1.61a**:(*R*) in purple (0.1 M $TBAPF_6$).*[68]

1.7 Receptors incorporated onto gold surfaces

Recognition in supramolecular chemistry may occur in different ways: in solution, at a liquid-liquid interface,[69] or on a surface - for example, on a Self-Assembled Monolayer (SAM).[70, 71] A SAM is formed after the adsorption of a layer of molecules on a surface. The molecules typically have an alkyl chain that ends in a functional group that strongly reacts with the surface used. The first reported example of a SAM on a metal surface was published by Nuzzo and Allara in 1983.[72] They employed solution adsorption of disulphides on gold surfaces, using spontaneous self-assembly for organisation of films. This technique is in

contrast to the Langmuir-Blodgett technique of deposition,[73] well studied and used at the time, but limiting in the type of molecules that could be used for the formation of films. The characterisation of these first examples of monolayers was obtained by ellipsometry, reflectance infrared spectroscopy, and calculating the contact angle of water.

SAMs on metal surfaces have been thoroughly investigated in subsequent years,[71, 73-75] and they have often been used for ion recognition.[70, 76] For gold surfaces the commonly chosen functional groups are thiols and disulphides, because of the strong affinity of sulphur for gold.[77, 78] The choice of this system is common because a gold surface is often used as the working electrode in redox-active systems.

One simple example is given by the functionalisation of crown ethers with alkyl chains terminating in thiols, designed by Flink and coworkers in 1998.[79] The receptors **1.62** and **1.63** formed SAMs on gold that were able to bind reversibly and selectively cations from aqueous solutions, respectively Na^+ and K^+.

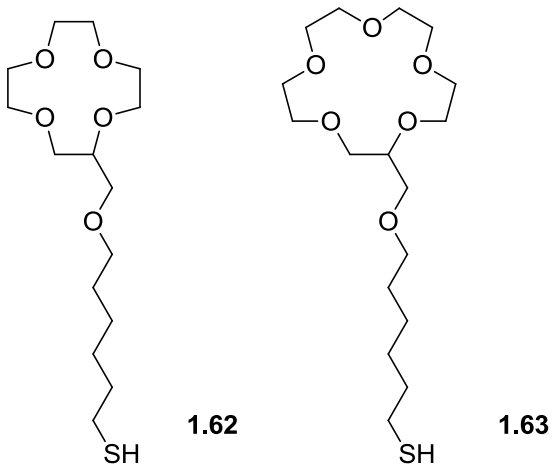

1.62 **1.63**

It is noteworthy that reducing the surface concentration of the receptors using heptanethiol to form mixed monolayers prevented sandwich complexation between two adjacent receptor molecules of bigger cations outside of the binding cavity, decreasing the selectivity of **1.63** for K^+ over Na^+.

Several examples on the use of SAMs for redox sensing have been reported in the literature over the last few years, using different redox active units such as metal complexes,[80] tetrathiofulvalene[81] or ferrocene.[82, 83]

An early example of anion binding with a ferrocene-containing SAM is the double armed amido-ferrocene thiol **1.64** reported by Beer and coworkers in 2002,[84] which was able to form a SAM on a gold electrode and sense $H_2PO_4^-$ in organic solvents, with a large cathodic shift in the formal potential of the Fc/Fc^+ couple of -300 mV. An amplification of the sensing was observed in comparison to that of the same receptor as a freely diffusing species in solution (-210 mV), due to surface pre-organisation and to the formation of pseudo-macrocyclic species.

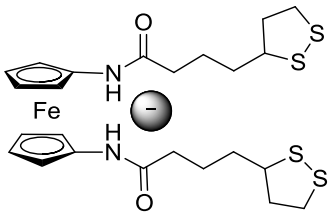

1.64

A recent example of anion binding was given by Beer and coworkers in 2010.[85] In their work they studied the properties of novel ureas and amides bearing ferrocene units and

calixarene, and functionalised with disulphides for incorporation onto gold surface to get redox-active anion sensors, such as **1.65**.

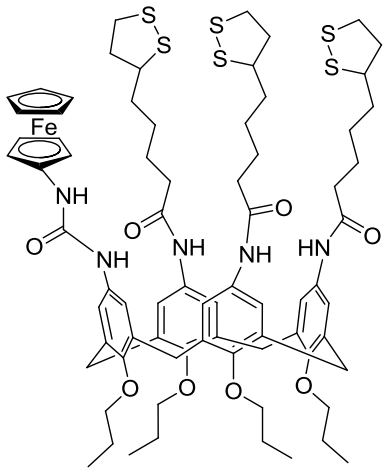

1.65

The SAM of the receptor was capable of electrochemically sensing anions with a significant shift in the redox potential of the ferrocene/ferrocenium redox couple. The magnitude of the cathodic response upon addition of suitable anions, such as chloride, was increased in comparison to what is observed using the same receptor free in solution. This is a demonstration of the so-called *surface enhancement effect* (Figure 1.11 and 1.12).

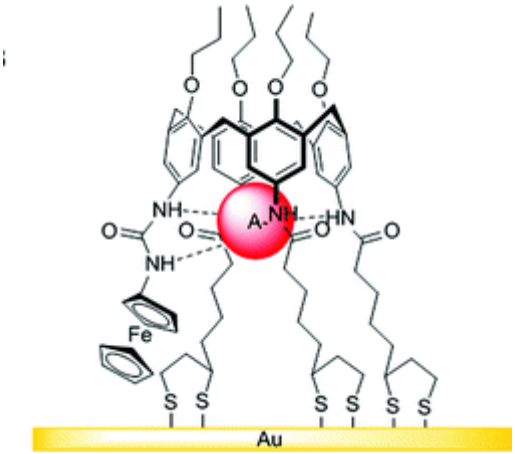

Figure 1.11: *Schematic of the preorganisation of* ***1.65*** *allowing enhanced anion binding.*[85]

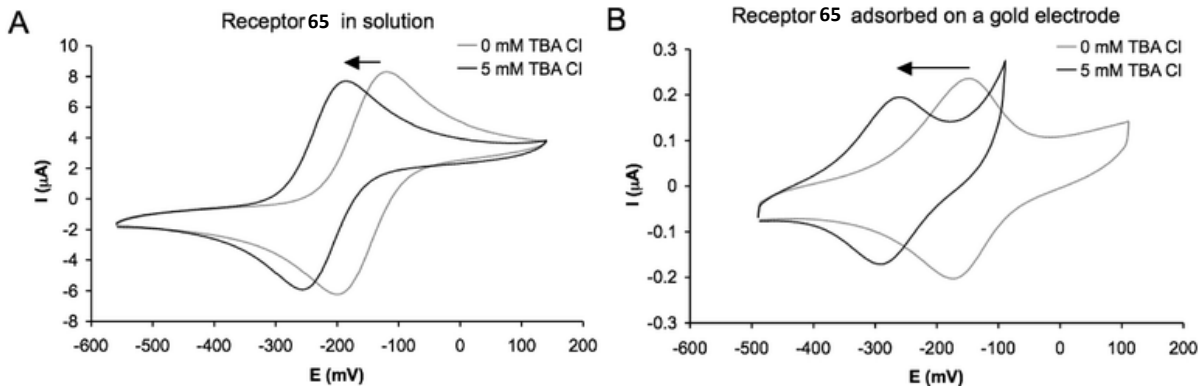

Figure 1.12: *The cathodic perturbations of ferrocene voltammetry observed with (A) receptor* ***1.65*** *in solution (0.1 M $TBABF_4$ in a 1:1 CH_3CN/CH_2Cl_2 solvent mixture) and (B) SAMs of receptor* ***1.65*** *in the same solvent system in the presence of 5 mM TBA chloride. An Ag/AgCl reference electrode was used.*[85]

1.8 Attempts at chiral recognition on surfaces

Despite the exponential increase in the use of SAMs for sensing of guest molecules in solution, there are only few examples of chiral recognition with receptors immobilised onto metal surfaces.[86-89] The first two examples below do not consist of electrochemical sensing, but they exploit the mass growth due to oxidation of the analyte on the gold electrode of a quartz crystal microbalance (QCM).

In 2002 Chan and coworkers showed the synthesis of mercaptyl functionalised β-cyclodextrins **1.66-1.68** and their self-assembly on the gold electrodes of a QCM to produce a sensor that shows chiral discrimination.[86]

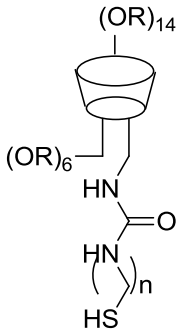

1.66a R=CH_3, n=2
1.66b R=CH_3, n=6
1.66c R=CH_3, n=11
1.67c R=n-C_5H_{11}, n=11
1.68c R=PhCO, n=11

Paolesse and coworkers then published work in which the porphyrin diad **1.69** was synthesised and its cobalt complex was studied as an enantioselective receptor for chiral sensing in solution and in solid state.[87]

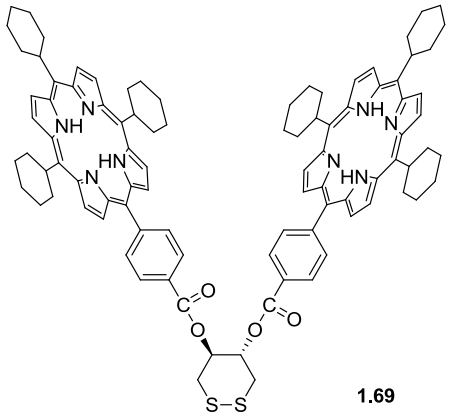

1.69

Self-assembled monolayers (SAMs) of [Co_2(**1.69**)] were formed on the surface of the gold electrodes of a QCM. These could then be used as nanogravimetric sensors in the gas phase. The chiral discrimination properties of the sensors towards opposite enantiomers of chiral guests were investigated, and a significant chiral discrimination was observed towards limonene, which was bound by coordination to the metal center.

The other two cited examples exploit the redox-activity of the guest, which is 3,4-dihydroxyphenylalanine (dopa). In the most recent, Fu and coworkers formed SAMs of the chiral protected amino acid N-isobutyryl-cysteine on gold surface,[89] and using these they were able to discriminate the opposite enantiomers of dopa. CV was used to analyse the behaviour of the enantiomers whilst sensing the guests (Figure 1.13).

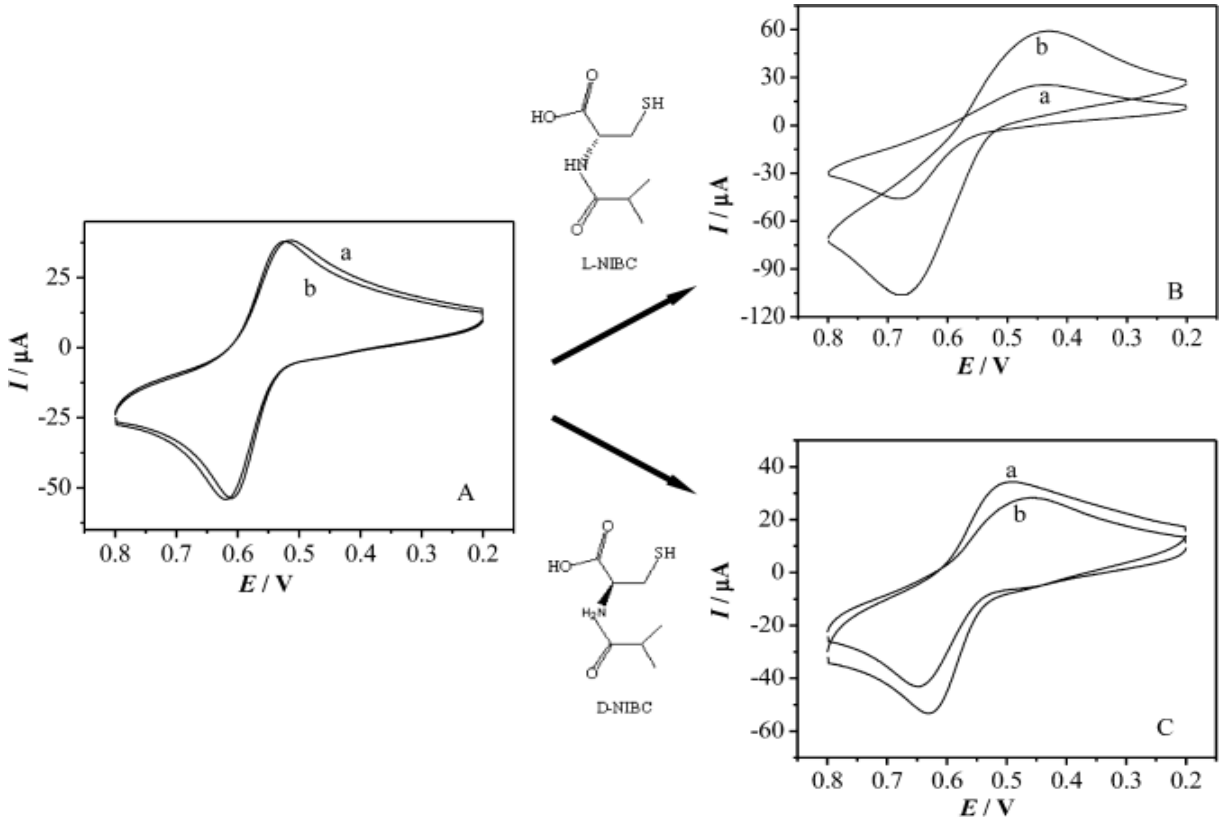

Figure 1.13: *CVs for redox reactions of 5 mM* L*-dopa (a) and* D*-dopa (b) in 0.25 M* H_2SO_4 *at 100 mV* s^{-1}*. (A) Bare gold electrode, (B)* L*-NIBC-Au, (C)* D*-NIBC-Au.*[89]

1.9 Electrochemical Techniques

The redox potential of an electro-active system can be assessed through techniques that measure the current as a function of the potential. A peak in the current intensity is

generated while applying the potential necessary to achieve a change in the redox state of the analyte. A three-electrode cell is used, consisting of a working electrode, a reference electrode and an auxiliary electrode immersed in an electrolyte solution. The cell is connected to a potentiostat that is able to vary the potential applied to the working electrode. This is measured relative to the reference electrode (usually the redox couple Ag/AgCl, which possesses a fixed potential at a constant composition), while the auxiliary electrode is placed in the electrolyte solution to prevent the flow of current through the reference electrode, which would affect the potential measured. In organic solvents the use of the aqueous solution based reference electrode mentioned above would cause an interphase potential that is not measurable but that affects the potential. For this reason an internal reference is used, in the form of a compound which is soluble in the organic solvent and possesses a formal redox potential distant from the one of the species under examination. Electrode potentials recorded are hence reported versus the internal reference.

1.9.1 Cyclic Voltammetry

In a cyclic voltammetry (CV) experiment, the potential is linearly scanned from an initial value $E_{initial}$ to a more positive switching value $E_{switching}$ and backwards to form a cycle (Figure 1.14).[90]

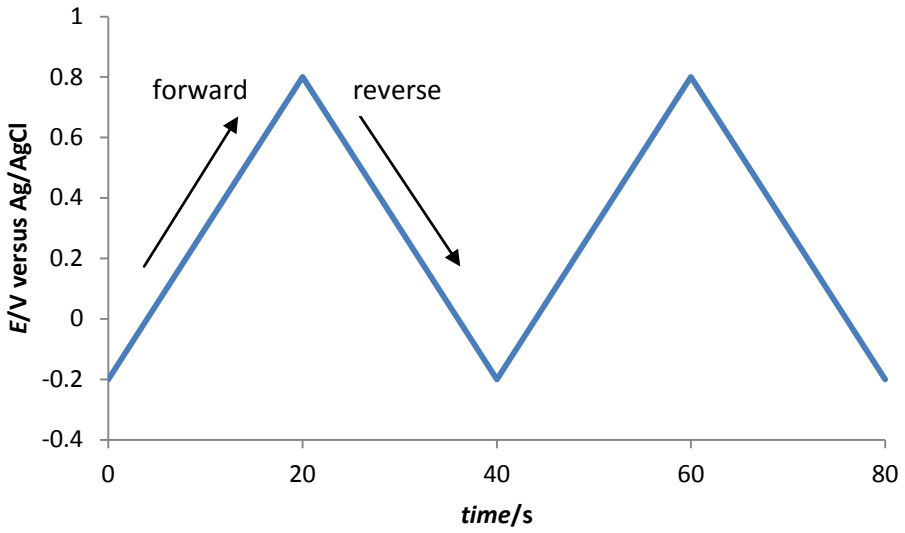

Figure 1.14: *Graph showing the potential E vs. time.*[90]

The current is recorded and plotted against the potential, and two peaks will form in the forward scan and reverse scan, respectively for the oxidation and the reduction of the analyte (Figure 1.15).

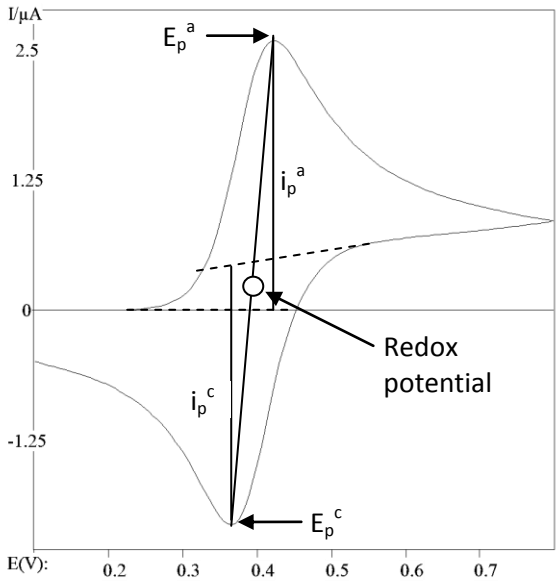

Figure 1.15: *Example of cyclic voltammogram of a reversible system.*[90]

The two peaks are not symmetrical because of the overpotential necessary for the electron transfer process to occur.

The overpotential appears in the Butler-Volmer equation,[91, 92] which describes mass transport and kinetics of the electron transfer:

$$k_{ET} = k^o e^{\frac{-\alpha n F}{RT}(E-E^{o'})} \qquad \textbf{\textit{Equation 1.2}}$$

where:

k^o = rate constant of the standard heterogeneous electron transfer

α = transfer coefficient

n = number of electrons transferred per molecule

F = Faraday constant

R = universal gas constant

T = temperature (K)

E-$E^{0'}$ = overpotential

The formal potential $E^{o'}$ is defined as ($E_p^a + E_p^c$)/2, as it is centered between the two peaks. Useful information on the reversibility of the reaction can be obtained from cyclic voltammograms: in a reversible process, i_p^a/i_p^c should be equal to 1 and $E_p^a - E_p^c$ should be close to 59 mV (at 25°C) for n = 1.[93] Slow electron transfer at the electrode surface could result in a larger peak separation. However, at high scan rates there is an increase in the peak separation that does not depend on a slow electron-transfer: this is due instead to the Ohmic drop caused by the uncompensated resistance of the solution, despite the use of the auxiliary electrode, as described by Nicholson.[94]

The peak current is dependent on the scan rate, as described by the Randles-Sevcik[95, 96] equation:

$$i_p = 2.69 \times 10^{-5} n^{3/2} A D^{1/2} C v^{1/2} \qquad \textit{Equation 1.3}$$

where:

i_p = peak current (A)

n = number of electrons transferred per molecule

A = electrode surface area (cm^2)

D = diffusion coefficient of solution species (cm^2/s)

C = bulk concentration (mol/cm^3)

v = sweep rate (V/s)

The peak current is directly proportional to the square root of the scan rate for free species in solution, and directly proportional to the scan rate for species adsorbed on the electrode surface.

1.9.2 Square Wave Voltammetry

Square wave voltammetry (SWV) was invented in 1969 by Ramaley and Krause[97] and further developed by Osteryoung and coworkers.[98, 99] It differs from cyclic voltammetry because the potential is regularly pulsed instead of linearly swept. The same time is spent at the potential of the increasing baseline and the superimposed pulse and the plot of the potential versus time consists in a square wave superimposed on a staircase (Figure 1.16).

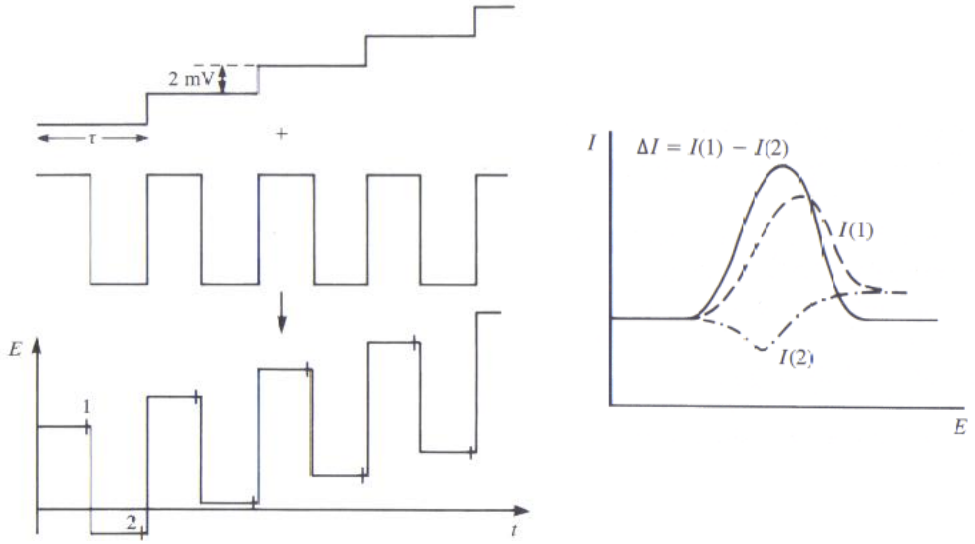

Figure 1.16: *Square wave voltammetry schematic waveform and profile of i vs. E.*[97]

The current is recorded before the pulse application and just before its end, leading to a symmetrical peak and reducing the effect of charging current, hence suppressing the background and increasing the sensitivity in comparison to cyclic voltammetry, with detection limit down to about 10^{-8} mol L^{-1}.[93]

1.10 Conclusions and aims of the project

Supramolecular interactions are used for the recognition of various guest molecules, which can be neutral, positively or negatively charged. Good selectivity can be achieved by designing the host molecule with an optimised complementarity towards the guest. Many receptors have been synthesised and functionalised with reporting groups that enable the sensing of guest molecules. The functioning of these sensors depends on the variation of a

property of the reporting group, such as a change in the redox potential, a quenching or an enhancement in the emission of a fluorophore or a shift of an absorption band.

Not many sensors for chiral recognition have been synthesised and studied, and only a few of them with electrochemical properties. The aim of this project is to broaden this field of supramolecular chemistry, with the synthesis of novel electrochemical sensors. These can be used for the recognition of small guests such as chiral carboxylates, carboxylic acids, amino acid derivatives, or amino acid anions, or macromolecules such as DNA or PNA. The properties of the sensors were studied in solution and upon incorporation onto gold surfaces. The latter leads to a useful improvement of the sensing process due to the possibility of reuse, and because the gold surface can act as a working electrode for direct sensing in a selective and efficient manner. To the best of our knowledge no example is present in the literature of a surface-bound redox-active receptor for chiral discrimination.

1.11 Thesis Outline

Chapter 2 discusses the synthesis of novel ferrocenylurea receptors to be used as chiral sensors for the enantiodiscrimination of chiral carboxylates in solution. The electrochemical behaviour of the novel receptors was studied with CV and SWV. ^{1}H NMR titrations *via* the software WinEQNMR[100, 101] and UV-Vis *via* the Benesi-Hildebrand equation are used to calculate the binding constants. The behaviour is then compared to previous work carried

out within the group, to give a better understanding of the phenomena observed with the aforementioned techniques.

Chapter 3 explores the incorporation of suitable disulphide based receptors on gold surfaces with the typical ferrocenylurea subunits of the receptors discussed in the previous chapters. The self-assembled monolayers (SAMs) formed are characterised by CV, ellipsometry and AFM. Electrochemistry is used to investigate the binding of chiral carboxylates and the possibility of usage of these systems as chiral sensors. The advantages and disadvantages of the sensing on the surface in comparison to sensing in solution are discussed.

Chapter 4 investigates the synthesis and study of novel chiral receptors containing both ferrocenyl units and BINOL as a fluorophore, to probe the effect of the presence of an electron-rich group such as ferrocene on the quenching of the BINOL emission. The studies explore the fluorescence enhancement obtained upon complexation of simple neutral molecules, such as carboxylic acids or amino acid derivatives, or amino acid anions, in the form of tetrabutylammonium salts. Moreover, the voltammetric behaviour of these systems is investigated, and the use of electrochemistry is compared to the use of emission experiments for chiral sensing.

Chapter 5 examines the study of a novel electrochemically active DNA analogue in which ferrocene is incorporated in the backbone of the nucleic acid.[102] This system is studied by CV to investigate its stability and interaction with complementary strands of DNA and PNA.

1.12 References

1. Lehn, J.-M., *Pure Appl. Chem.* **1978,** *50*, 871-892.
2. Lehn, J. M., *Angew. Chem. Int. Ed. Engl.* **1988,** *27*, 89-112.
3. Steed, J. W.; Turner, D. R.; Wallace, K. J., *Core Concepts in Supramolecular Chemistry and Nanochemistry*. Wiley: 2007.
4. Pedersen, C. J., *J. Am. Chem. Soc.* **1967,** *89*, 7017-7036.
5. Dietrich, B.; Lehn, J. M.; Sauvage, J. P., *Tetrahedron Lett.* **1969**, 2889-2892.
6. Gunnlaugsson, T.; Glynn, M.; Tocci, G. M.; Kruger, P. E.; Pfeffer, F. M., *Coord. Chem. Rev.* **2006**, 3094-3117.
7. Valeur, B., I. Leray, *Coord. Chem. Rev.* **2000**, 3-40.
8. Lehn, J.-M.; Sonveaux, E.; Willard, A. K., *J. Am. Chem. Soc.* **1978,** *100*, 4914-4916.
9. Yang, X.; Knobler, C. B.; Hawthorne, M. F., *Angew. Chem. Int. Ed. Engl.* **1991,** *30*, 1507-1508.
10. Kondo, S.; Hiraoka, Y.; Kurumatani, N.; Yano, Y., *Chem. Commun.* **2005**, 1720-1722.
11. Gale, P. A., R. Quesada *Coord. Chem. Rev.* **2006**, 3219-3244.
12. Sessler, J. L.; Sansom, P. I.; Andrievsky, A.; Král, V., Application Aspects Involving the Supramolecular Chemistry of Anions. In *Supramolecular Chemistry of Anions*, Bianchi, A.; Bowman-James, K.; Garcia-España, E., Eds. Wiley-VCH: New York, 1997.
13. Gale, P. A., S. E. Garcıa-Garrido, J. Garric, *Chem. Soc. Rev.* **2008,** *37*, 151-190.
14. Wenzel, M.; Hiscock, J. R.; Gale, P. A., *Chem. Soc. Rev.* **2010,** *41*, 480-520.
15. Park, C. H.; Simmons, H. E., *J. Am. Chem. Soc.* **1968,** *90*, 2431-2432.
16. Saeed, M. A.; Fronczek, F. R.; Huang, M.-J.; Hossain, M. A., *Chem. Commun.* **2010,** *46*, 404-406.
17. Garciatellado, F.; Goswami, S.; Chang, S. K.; Geib, S. J.; Hamilton, A. D., *J. Am. Chem. Soc.* **1990,** *112*, 7393-7394.
18. Fan, E.; Vanarman, S. A.; Kincaid, S.; Hamilton, A. D., *J. Am. Chem. Soc.* **1993,** *115*, 369-370.
19. Brooks, S. J.; Gale, P. A.; Light, M. E., *Chem. Commun* **2005**, 4696-4698.
20. Yin, Z.; Li, Z.; Yu, A.; He, J.; Cheng, J.-P., *Tetrahedron Letters* **2004,** *45*, 6803-6806.
21. Wu, L.; Liu, L.; Fang, R.; Deng, C.; Han, J.; Hu, H. W.; Lin, C.; Wang, L. Y., *Tetrahedron Lett.* **2012,** *53*, 3637-3641.
22. Gale, P. A., *Coord. Chem. Rev.* **2000,** *199*, 181-233.

23. Gale, P. A., *Coord. Chem. Rev.* **2001,** *213*, 79-128.
24. Gale, P. A., *Coord. Chem. Rev.* **2003,** *240*, 191-221.
25. Caltagirone, C., P. A. Gale, *Chem. Soc. Rev.* **2008,** *37*, 1-43.
26. Gale, P. A., *Chem. Soc. Rev.* **2010,** *39*, 3746-3771.
27. Wolf, C.; Liu, S.; Reinhardt, B. C., *Chem. Commun.* **2006**, 4242-4244.
28. Goulle, V.; Harriman, A.; Lehn, J. M., *J. Chem. Soc., Chem. Comm.* **1993,** 1034-1036.
29. Bissell, R. A.; Calle, E.; de Silva, A. P.; de Silva, S. A.; Gunaratne, H. Q. N.; Habib-Jiwan, J.-L.; Peiris, S. L. A.; Rupasinghe, R. A. D. D.; Shantha, T. K.; Samarasinghe, D.; Sandanayake, K. R. A. S.; Soumillion, J.-P., *J. Chem. Soc., Perkin Trans. 2* **1992,** *0*, 1559-1564.
30. Gunnlaugsson, T.; Davis, A. P.; Glynn, M., *Chem. Commun.* **2001**, 2556-2557.
31. Gunnlaugsson, T.; Davis, A. P.; Hussey, G. M.; Tierney, J.; Glynn, M., *Org. Biomol. Chem.* **2004,** *2*, 1856-1863.
32. Gunnlaugsson, T.; Davis, A. P.; O'Brien, J.; Glynn, M., *Org. Biomol. Chem.* **2005,** *3*, 48-56.
33. Camiolo, S.; Gale, P. A.; Hursthouse, M. B.; Light, M. E., *Org. Biomol. Chem.* **2003,** *1*, 741-744.
34. Beer, P. D., *Chem. Soc. Rev.* **1989,** *18*, 409-450.
35. Boulas, P. L.; Goméz-Kaifer, M.; Echegoyen, L., *Angew. Chem. Int. Ed.* **1998,** *37*, 216-247.
36. Beer, P. D., P. A. Gale, G. Z. Chen, *J. Chem. Soc., Dalton Trans.* **1999**, 1897-1909.
37. Beer, P. D.; Gale, P. A.; Chen, G. Z., *Adv. Phys. Org. Chem.* **1998,** *31*, 1-90.
38. Tucker, J. H. R.; Collinson, S. R., *Chem. Soc. Rev.* **2002,** *31*, 147-156.
39. Prins, R.; Korswagen, A. R.; Kortbeek, A. G. T. G., *J. Organomet. Chem.* **1972,** *39*, 335-344.
40. Han, S. W.; Seo, H.; Chung, Y. K.; Kim, K., *Langmuir* **2000,** *16*, 9493-9500.
41. Saji, T., *Chem. Lett.* **1986**, 275-276.
42. Beer, P. D.; Keefe, A. D., *J. Organomet. Chem.* **1989,** *375*, C40-C42.
43. Molina, P.; Tarraga, A.; Caballero, A., *Eur. J. Inorg. Chem.* **2008**, 3401-3417.
44. Beer, P. D., *Acc. Chem. Res.* **1998,** *31*, 71-80.
45. Alonso, B.; Casado, C. M.; Cuadrado, I.; Morán, M.; Kaifer, A., *Chem. Commun.* **2002**, 1778-1779.
46. Pratt, M. D.; Beer, P. D., *Polyhedron* **2003,** *22*, 649-653.
47. Evans, A. J.; Matthews, S. E.; Cowley, A. R.; Beer, P. D., *Dalton Trans.* **2003**, 4644-4650.
48. Evans, N. H.; Serpell, C. J.; Christensen, K. E.; Beer, P. D., *Eur. J. Inorg. Chem.* **2012**, 939-944.
49. Otón, F.; Tárraga, A.; Velasco, M. D.; Espinosa, A.; Molina, P., *Chem. Commun* **2004**, 1658-1659.
50. Oton, F.; Tarraga, A.; Velasco, M. D.; Molina, P., *Dalton Trans.* **2005**, 1159-1161.

51. Otón, F.; Tárraga, A.; Espinosa, A.; Velasco, M. D.; Molina, P., *J. Chem. Soc. Dalton Trans.* **2006**, 3685-3692.
52. Oton, F.; Tarraga, A.; Espinosa, A.; Velasco, M. D.; Molina, P., *J. Org. Chem.* **2006,** *71*, 4590-4598.
53. Lorenzo, A.; Aller, E.; Molina, P., *Tetrahedron* **2009,** *65*, 1397-1401.
54. Cram, D. J., *Science* **1988,** *240*, 760-767.
55. Kyba, E. B.; Koga, J.; Sousa, L. R.; Siegel, M. G.; Cram, D. J., *J. Am. Chem. Soc.* **1973,** *95*, 2692-2693.
56. Pu, L., *Acc. Chem. Res.* **2012,** *45*, 150-163.
57. Dhara, K.; Sarkar, K.; Roy, P.; Nandi, M.; Bhaumik, A.; Banerjee, P., *Tetrahedron* **2008,** *64*, 3153-3159.
58. Liu, S. L.; Pestano, J. P. C.; Wolf, C., *J. Org. Chem.* **2008,** *73*, 4267-4270.
59. Lu, Q. S.; Dong, L.; Zhang, J.; Li, J.; Jiang, L.; Huang, Y.; Qin, S.; Hu, C. W.; Yu, X. Q., *Org. Lett.* **2009,** *11*, 669-672.
60. Qing, G. Y.; Sun, T. L.; Chen, Z. H.; Yang, X.; Wu, X. J.; He, Y. B., *Chirality* **2009,** *21*, 363-373.
61. Costero, A. M.; Llaosa, U.; Gil, S.; Parra, M.; Colera, M., *Tetrahedron-Asymmetry* **2009,** *20*, 1468-1471.
62. Xu, K. X.; Qiu, Z.; Zhao, J. J.; Zhao, J.; Wang, C. J., *Tetrahedron-Asymmetry* **2009,** *20*, 1690-1696.
63. Liu, H. L.; Zhu, H. P.; Hou, X. L.; Pu, L., *Org. Lett.* **2010,** *12*, 4172-4175.
64. Ori, A.; Shinkai, S., *J. Chem. Soc., Chem. Commun.* **1995**, 1771 - 1772.
65. Chun, K. M.; Kim, T. H.; Lee, O. S.; Hirose, K.; Chung, T. D.; Chung, D. S.; Kim, H., *Anal. Chem.* **2006,** *78*, 7597-7600.
66. Laurent, P.; Miyaji, H.; Collinson, S. R.; Prokes, I.; Moody, C. J.; Tucker, J. H. R.; Slawin, A. M. Z., *Org. Lett.* **2002,** *4*, 4037-4040.
67. Willener, Y.; Joly, K. M.; Moody, C. J.; Tucker, J. H. R., *J. Org. Chem.* **2008,** *73*, 1225-1233.
68. Mirri, G.; Bull, S. D.; Horton, P. N.; James, T. D.; Male, L.; Tucker, J. H. R., *J. Am. Chem. Soc.* **2010,** *132*, 8903-8905.
69. Kataky, R.; Lopes, P., *Chem. Commun.* **2009**, 1490-1492.
70. Zhang, S.; Cardona, C. M.; Echegoyen, L., *Chem. Commun.* **2006**, 4461-4473.
71. Eckermann, A. L.; Feld, D. J.; Shaw, J. A.; Meade, T. J., *Coord. Chem. Rev.* **2010,** *254*, 1769-1802.
72. Nuzzo, R. G.; Allara, D. L., *J. Am. Chem. Soc.* **1983,** *105*, 4481-4483.
73. Ulman, A., *Chem. Rev.* **1996,** *96*, 1533-1554.
74. Love, J. C.; Estroff, L. A.; Kriebel, J. K.; Nuzzo, R. G.; Whitesides, G. M., *Chem. Rev.* **2005,** *105*, 1103-1169.
75. Porter, M. D.; Bright, T. B.; Allara, D. L.; Chidsey, C. E. D., *J. Am. Chem. Soc.* **1987,** *109*, 3559-3568.

76. Evans, N. H.; Rahman, H.; Davis, J. J.; Beer, P. D., *Anal. Bioanal. Chem.* **2010,** *402*, 1739-1748.
77. Nuzzo, R. G.; Zegarski, B. R.; Dubois, L. H., *J. Am. Chem. Soc.* **1987,** *109*, 733-740.
78. Vericat, C.; Vela, M. E.; Benitez, G.; Carro, P.; Salvarezza, R. C., *Chem. Soc. Rev.* **2010,** *39*, 1805-1834.
79. Flink, S.; Boukamp, B. A.; van den Berg, A.; van Veggel, F. C. J. M.; Reinhoudt, D. N., *J. Am. Chem. Soc.* **1998,** *120*, 4652-4657.
80. Gobi, K. V.; Ohsaka, T., *J. Electroanal. Chem.* **2000,** *485*, 61-70.
81. Jensen, L. G.; Nielsen, K. A.; Breton, T.; Sessler, J. L.; Jeppesen, J. O.; Levillain, E.; Sanguinet, L., *Chem.-Eur. J.* **2009,** *15*, 8128-8133.
82. Labande, A.; Ruiz, J.; Astruc, D., *J. Am. Chem. Soc.* **2002,** *124*, 1782-1789.
83. Astruc, D.; Daniel, M. C.; Ruiz, J., *Chem. Commun.* **2004**, 2637-2649.
84. Beer, P. D.; Davis, J. J.; Drillsma-Milgrom, D. A.; Szemes, F., *Chem. Commun.* **2002**, 1716-1717.
85. Cormode, D. P.; Evans, A. J.; Davis, J. J.; Beer, P. D., *Dalton Trans.* **2010,** *39*, 6532-6541.
86. Ng, S. C.; Sun, T.; Chan, H. S. O., *Tetrahedron Lett.* **2002,** *43*, 2863-2866.
87. Paolesse, R.; Monti, D.; Monica, L. L.; Venanzi, M.; Froiio, A.; Nardis, S.; Natale, C. D.; Martinelli, E.; D'Amico, A., *Chem. Eur. J.* **2002,** *11*, 2476-2483.
88. Matsunaga, M.; Nakanishi, T.; Asahi, T.; Osaka, T., *Chirality* **2007,** *19*, 295-299.
89. Han, Q.; Chen, Q.; Wang, Y.; Zhou, J.; Fu, Y., *Electroanal.* **2012,** *24*, 332-337.
90. Kissinger, P. T.; Heineman, W. R., *J. Chem. Educ.* **1983,** *60*, 702-706.
91. Butler, J. A. V., *Trans. Faraday Soc.* **1924,** *19*, 729-733.
92. Erdey-Gruz, T.; Volmer, M., *Z Phys. Chem A-Chem. Thermodyn. Kinet. Elektrochem. Eigensch.lehre* **1930,** *150*, 203-213.
93. Brett, C. M. A.; Oliveira, A. M., *Voltammetric Sensors in Electroanalysis*. Oxford University Press: 1998.
94. Nicholson, R. S., *Anal. Chem.* **1965,** *37*, 667-671.
95. Randles, J. E. B., *Trans. Faraday Soc.* **1948,** *44*, 327-338.
96. Sevcik, A., *Collect. Czech. Chem.Commun.* **1948,** *13*, 349-377.
97. Ramaley, L.; Krause, M. S., *Anal. Chem.* **1969,** *41*, 1362-1365.
98. Osteryoung, R. A.; Osteryoung, J., *Philos. Trans. R. Soc. A-Math. Phys. Eng. Sci.* **1981,** *302*, 315-326.
99. Osteryoung, J., *Acc. Chem. Res.* **1993,** *26*, 77-83.
100. Hynes, M. J., *J. Chem. Soc.-Dalton Trans.* **1993**, 311-312.
101. Molard, Y.; Bassani, D. M.; Desvergne, J. P.; Moran, N.; Tucker, J. H. R., *J. Org. Chem.* **2006,** *71*, 8523-8531.
102. Nguyen, H. V.; Zhao, Z.-y.; Sallustrau, A.; Horswell, S. L.; Male, L.; Mulas, A.; Tucker, J. H. R., *Chem. Commun.* **2012,** *48*, 12165-12167.

CHAPTER 2: Ferrocenyl-based centrally and planar chiral urea sensors in solution

2.1 Introduction and aims of the studies

As described in Section 1.6, only a few examples of electro-active sensors for chiral species are known in the literature. The Tucker group, in collaboration with the Moody group at the University of Nottingham, has previously worked on the subject and developed a new series of receptors that exploit the formation of hydrogen bonds with chiral carboxylates through urea binding sites.[1-2] The receptors contained a chiral centre in proximity to the binding site and the electrochemical signalling unit and in one case was able to electrochemically discriminate between enantiomers of the same carboxylate guest. Subsequently, the syntheses of novel receptors bearing both planar chirality and central chirality were developed.[3] Planar chiral ferrocene derivatives showed interesting properties in previous studies on asymmetric catalysis,[4-6] hence the idea to include this form of chirality in novel receptors and attempt to use them for chiral recognition. However, during the synthesis of receptor molecules bearing both elements of asymmetry, it was discovered that planar chirality overrode the stereocontrol caused by the chiral auxiliary used to determine the diastereoselectivity in the insertion of the chiral group on the receptor.[3] For this reason, only some combinations of the two elements of asymmetry could be obtained. The best result in terms of chiral sensing was found using receptor **2.1**,[2] but receptor **2.2** showed interesting properties when its interaction with guests **2.3**-**2.5** was investigated in preliminary unpublished studies.[7]

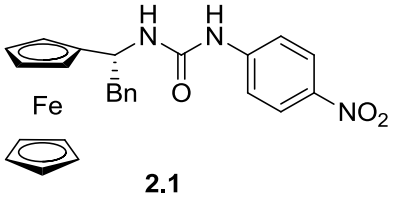

2.1

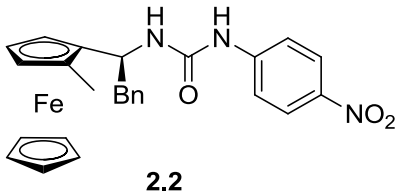

2.2

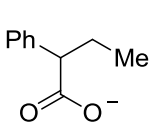

2.3

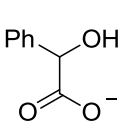

2.4

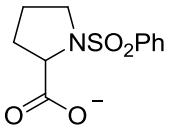

2.5

Subsequently, it was decided to synthesise a centrally chiral receptor **2.6** containing two peripheral ferrocene units, in order to achieve a higher electrochemical sensitivity due to the presence of two electroactive groups on the same receptor molecule. The chiral receptor **2.6** with benzyl groups was synthesised by the Moody group and was subjected to preliminary studies within the Tucker group.[7] It was therefore decided in this work to synthesise receptor **2.7** as an achiral control; the absence of chirality should verify any chiral discrimination observed with receptor **2.6**.

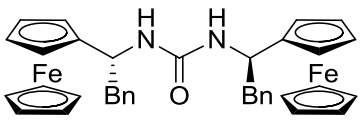

2.6

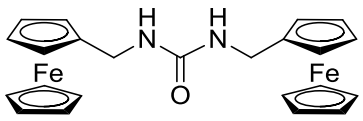

2.7

It was also decided to synthesise the planar chiral receptors **2.8** and **2.9** to investigate the role of planar chirality in directing the chiral recognition observed in the mono-ferrocenyl receptors, with the achiral receptor **2.10** also synthesised as a control.

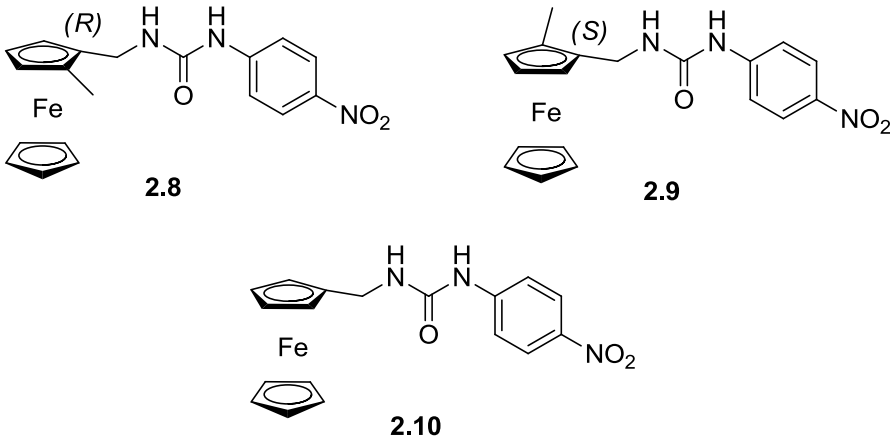

The interaction of the five different receptors **2.1**, **2.2** and **2.8-2.10** with guests **2.3-2.5** was compared by using UV-Vis spectroscopy and electrochemical techniques such as cyclic and square wave voltammetry. The binding of receptors **2.6** and **2.7** was investigated with guest **2.5** only, due to the large amount of compound needed for ^{1}H NMR titrations, which was necessary for the evaluation of the binding constants in the absence of any chromophore.

2.2 Synthesis of the receptors

The syntheses of receptors **2.1** and **2.2** were performed by Kevin Joly in the Moody group at the University of Nottingham. The synthesis of receptor **2.1** was published in 2008,[2] while the synthesis of **2.2**, containing both planar chirality and central chirality, was derived from the procedure used for the synthesis of thioureas previously published,[3] with the use of *p*-nitrophenylisocyanate to form the urea group.

The previously made receptor **2.10**[8] was synthesised by reaction[2] of the known ferrocenylmethanamine **2.12**[9] with the commercially available *p*-nitrophenylisocyanate

(Scheme 2.1). The amine was not synthesised by reductive amination of ferrocenecarboxaldehyde as done in the past in the group;[9] this choice was made in order to increase the yield and avoid the formation of byproducts such as bis-ferrocenyl secondary amine. Instead, a different synthetic route was designed: ferrocenecarboxaldehyde was reacted with hydroxylamine hydrochloride to give the oxime **2.11**,[10] which was then reduced to the desired amine using an excess of lithium aluminium hydride, added in portions with care due to hydrogen evolution (Scheme 2.1).[11]

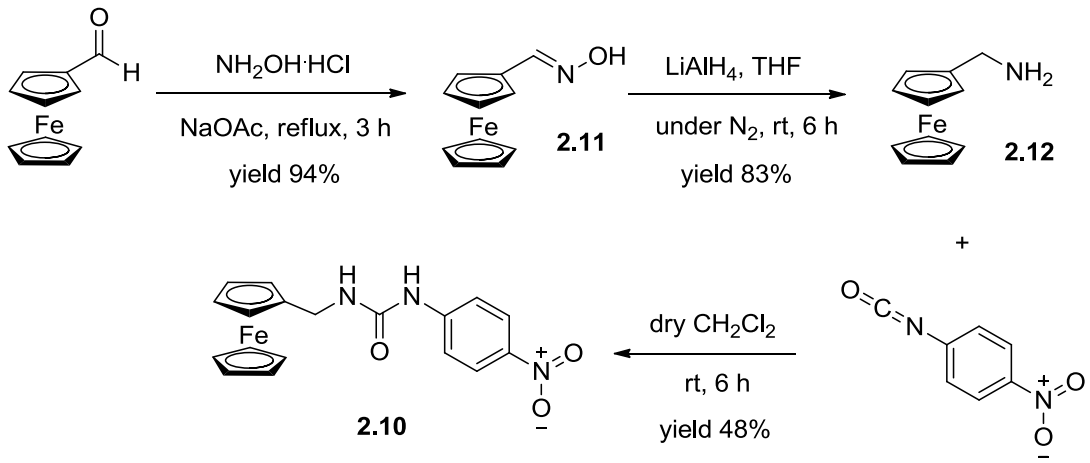

Scheme 2.1: *Synthesis of ferrocenylmethanamine* ***2.12*** *and of the achiral urea* N-*(4-nitrophenyl)*-N'-*(ferrocenemethyl)-urea* ***2.10.***

The achiral amine **2.12** was then reacted with *p*-nitrophenylisocyanate in dry CH_2Cl_2 to afford the achiral urea **2.10** (Scheme 2.1).[2]

Although already known in the literature,[12] receptor **2.7** was synthesised following a different route (Scheme 2.2) and subject to different binding studies. Receptor **2.7** was synthesised starting from the synthesis of ferrocenylmethanamine **2.12** (Scheme 2.1), which

was reacted with 1,1'-carbonyl diimidazole in anhydrous DMF and heated at 60 °C for 5 hours (Scheme 2.2).[13]

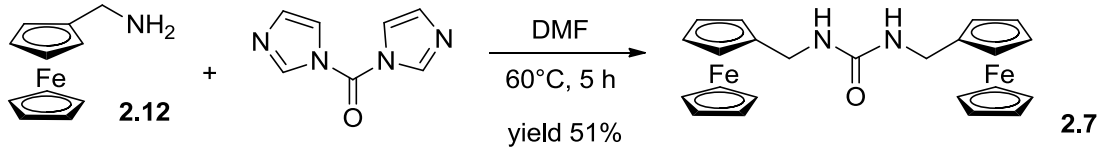

Scheme 2.2: *Synthesis of* N,N'-*bis(ferrocenylmethyl)urea* ***2.7.***

The yield of the reaction was lower than that obtained with the previously reported route. This is probably due to the efficiency of the extraction from DMF, given the high solubility of the compound in this solvent. However, the setup was easier as the streaming with a constant flow of CO_2(g) previously reported was avoided.[12]

The synthesis of receptor **2.6** was performed by Kevin Joly at the University of Nottingham following the same procedure, but using a central chiral ferrocenylamine obtained from a multistep reaction with use of the chiral auxiliary (*R*)-(-)-*O*-(1-phenylbutyl)hydroxylamine. The chiral auxiliary was reacted with ferrocenecarboxaldehyde to form an oxime ether. This was reacted with benzyl magnesium chloride in the presence of boron trifluoride diethyl etherate at -78 °C to give the corresponding hydroxylamine.[2] Cleavage of the N-O bond was achieved by reaction with zinc dust, after dissolution in a minimum amount of THF and addition of a mixture of 1:1 acetic acid/water. The reaction mixture was left in a sonic bath at 40 °C for 6 hours to obtain the chiral amine, which was then reacted with 1,1'-carbonyl diimidazole in anhydrous DMF at 60 °C for 5 h to give the urea **2.6** (Scheme 2.3).[13]

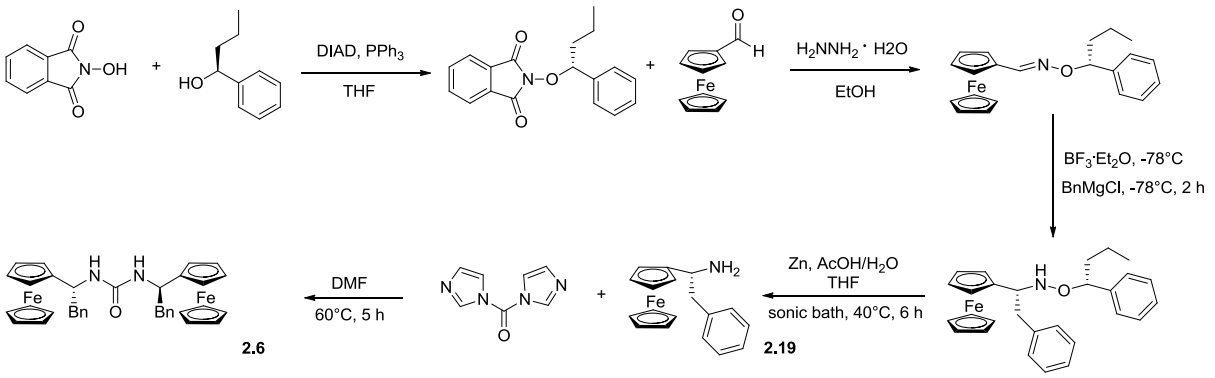

Scheme 2.3: *Synthesis of (R,R)-(-)-N,N'-[1-(1-Ferrocenyl-2-phenyl)-ethyl]-urea* ***2.6.***

Receptors **2.8** and **2.9** were obtained *via* a 5-step synthesis adapted from the literature.[14] To get mainly one enantiomer of the receptor, an asymmetric synthesis was performed, using the commercially available (*R*)- or (*S*)-1,2,4-butanetriol as chiral auxiliary. The triol was reacted with the acetal **2.13**, which was synthesised by reaction of the ferrocenecarboxaldehyde with trimethylorthoformate at 80 °C under acid catalysed conditions. The acetal reacted with two hydroxyl groups of the triol in the presence of activated molecular sieves to yield the chiral acetal **2.14** (Scheme 2.4).[14] The formation of the acetal **2.14** was favoured over the other possible isomers because of the formation of a six-membered ring, and its formation was verified by analysis of the position of the ^{13}C NMR peaks. For simplicity, only the synthesis of one enantiomer will be discussed in this section.

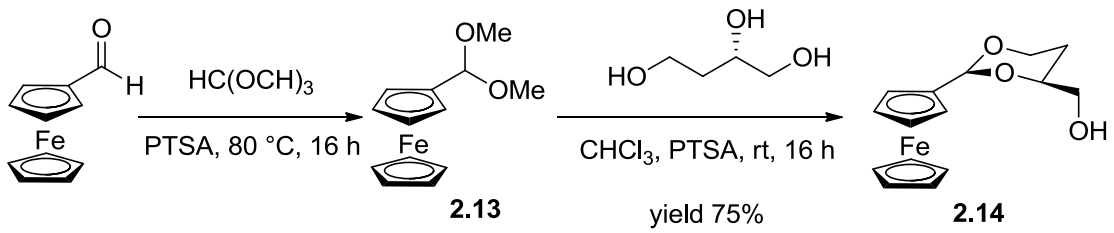

Scheme 2.4: *Synthesis of (2S,4S)-4-(hydroxymethyl)-2-ferrocenyl-1,3-dioxane* ***2.14.***

The chiral acetal was purified by flash chromatography and then protected at the hydroxyl group, to avoid its deprotonation in the next step. The protection was achieved by reaction with sodium hydride, followed by addition of methyl iodide to yield the known dioxane **2.15** (Scheme 2.5).[14]

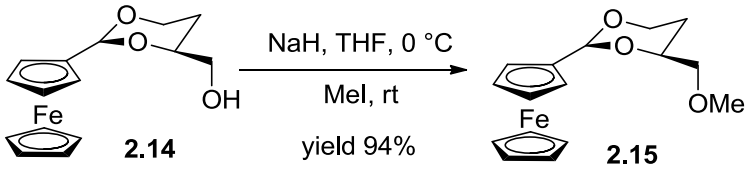

Scheme 2.5: *Synthesis of the (2S,4S)-4-(methoxymethyl)-2-ferrocenyl-1,3-dioxane* ***2.15.***

After purification by column chromatography, the protected acetal was reacted with *t*-butyl lithium to form a complex of lithium that directs the methylation reaction towards the formation of a single enantiomer. Then methyl iodide was added at -78 °C, to avoid polymethylation, reacted overnight at room temperature, and finally the auxiliary group was cleaved with HCl and MeOH to give the methylated aldehyde **2.16** in 61% yield (Scheme 2.6).[14] The methylated aldehyde was separated from byproducts and non-methylated aldehyde by column chromatography.

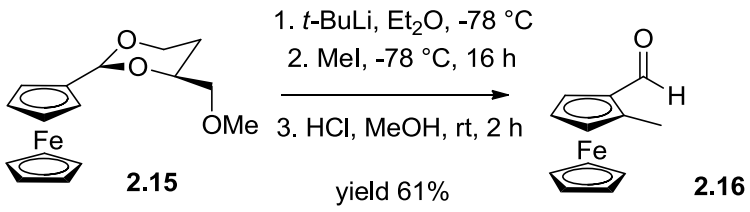

Scheme 2.6: *Synthesis of (*R*)-2-methyl-ferrocenecarboxaldehyde* ***2.16.***

The amines **2.17** and **2.18** were then synthesised *via* analogous reactions to those used to obtain the achiral amine (Scheme 2.1), and purified in the same way by column chromatography.

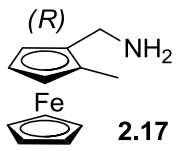

2.17

yield 42%

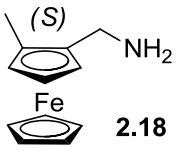

2.18

yield 65%

The planar chiral amines were then reacted with *p*-nitrophenylisocyanate in dry CH_2Cl_2 at 0 °C and then at room temperature for 6 hours using the same procedure shown in Scheme 2.3, to afford the target planar chiral ureas **2.8** and **2.9** in good enantiomeric excess, as calculated by analysis of chiral HPLC traces.

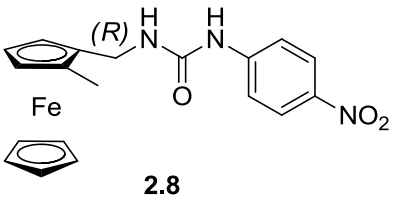

2.8

yield 70 %
%ee 97%

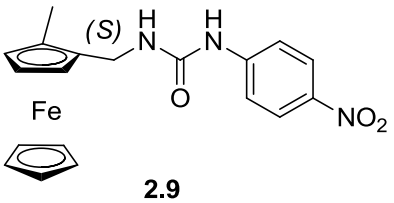

2.9

yield 75%
%ee 91%

Overall in the synthesis of **2.8** and **2.9**, the first steps showed a good yield, but the limiting step was the one involving lithiation and methylation of the acetal **2.15** (Scheme 2.6). The yield was not high and a significant amount of non-methylated aldehyde was recovered (yield 27%). However, if a separation were performed before the cleavage under acid conditions, the compound **2.15** could be reacted again in the lithiation and methylation step.

The chiral carboxylates **2.3-2.5** for the enantioselectivity studies were synthesised by reaction of the corresponding commercially available enantiopure acid with tetrabutylammonium hydroxide in MeOH (Scheme 2.7).[2]

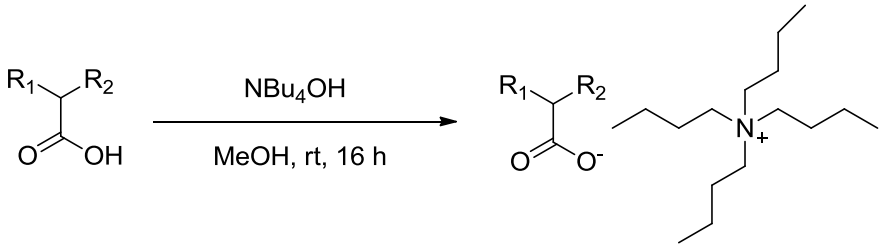

Scheme 2.7: *Synthesis of the tetrabutylammonium salts of the chiral carboxylates* ***2.3-2.5.***

2.3 Crystal structures

Attempts to grow crystals of **2.6** and **2.7** from slow evaporation of a solution in Et_2O were successful and the resulting crystals were found to be suitable for X-Ray diffraction experiments. The structures are presented in Figure 2.1 and Figure 2.2.

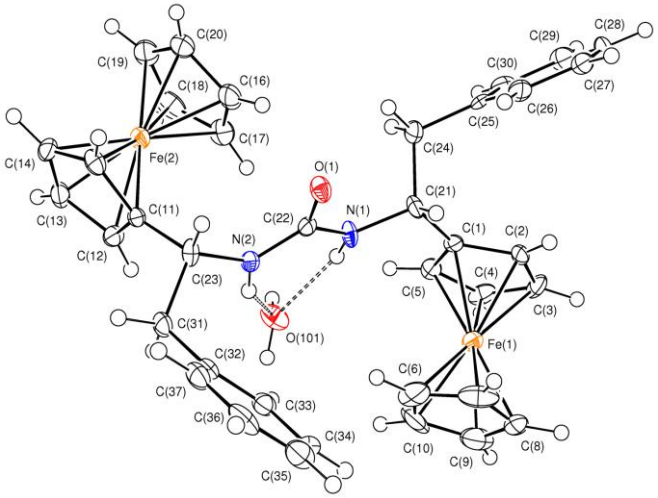

Figure 2.1*: Crystal structure of the chiral receptor* ***2.6*** *with ellipsoids drawn at 50% probability level. Dotted lines correspond to H-bonding. A water molecule is included in the crystal. All hydrogen atoms are reported.*

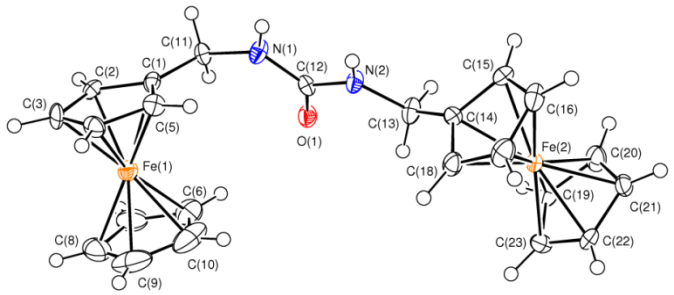

***Figure 2.2**: Crystal structure of the achiral receptor **2.7** with ellipsoids drawn at 50% probability level. All hydrogen atoms are reported.*

The crystal structure of **2.6** has the expected (*R*) configuration of the α-carbons and also shows the presence of the urea binding site inside a pseudo-cavity between the ferrocenyl and the benzyl groups. This spatial organization could be a factor in directing any chiral discrimination preferentially towards one enantiomer of a guest over the other. The binding site is occupied by one water molecule, which is interacting with the urea NH groups through two hydrogen bonds. The hydrogen bonding parameters are reported in Table 2.1.

***Table 2.1:** Hydrogen bonds for **2.6** [Å and °].*

D-H...*A*	d(*D*-H)	d(H...*A*)	d(*D*...*A*)	<(*DHA*)
N(1)-H(1)...O(101)	0.88	2.08	2.884(4)	151.8
N(2)-H(2A)...O(101)	0.88	2.06	2.860(4)	149.9
O(101)-H(01A)...O(1)#1	0.862(18)	1.787(19)	2.643(4)	172(4)

In the crystal structure of receptor **2.7** it is possible to see how the binding site is slightly more accessible in comparison to the hindered receptor **2.6**.

Crystals of the three mono-ferrocenyl receptors synthesised, **2.8**, **2.9** and **2.10**, were also successfully obtained. Crystals of **2.10** were produced by slow evaporation of a solution in a mixture of CH_2Cl_2 and Et_2O. The crystals were found suitable for X-Ray diffraction analysis and the resulting structure is presented in Figure 2.3.

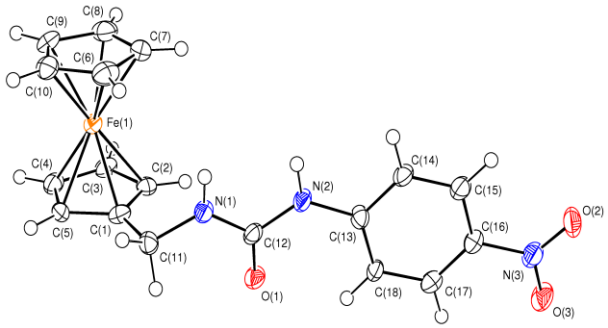

***Figure 2.3**: Crystal structure of the achiral receptor **2.10** with ellipsoids drawn at 50% probability level. All hydrogen atoms are reported.*

The crystal structure shows the urea binding site placed between the nitrophenyl and the ferrocenyl groups. This is in close proximity to both the functional motifs but it is not hindered by any of them and it would be easily accessible by suitable guests such as carboxylates.

Crystals of **2.8** and **2.9** were obtained by slow evaporation of a solution in chloroform and were found suitable for X-Ray diffraction analysis, with the resulting structures presented in Figure 2.4.

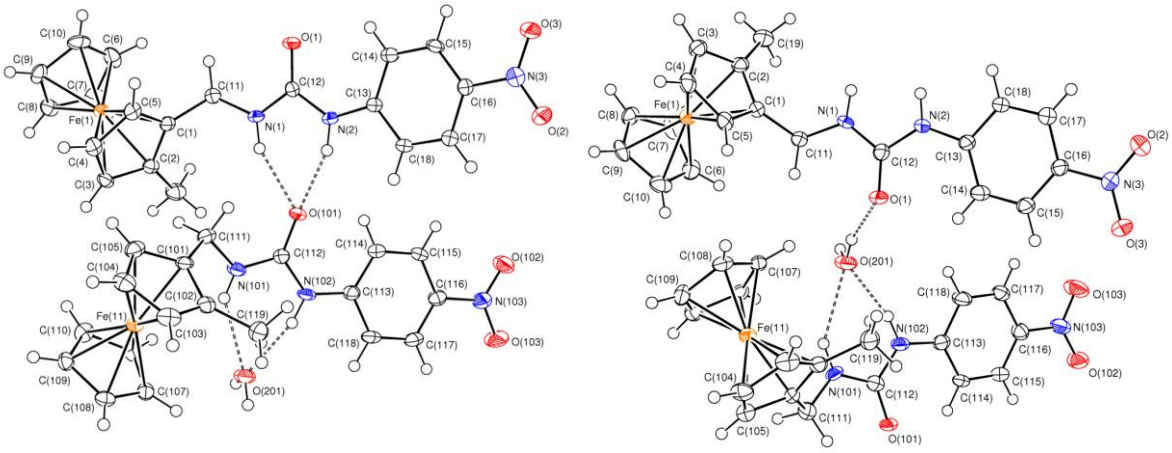

***Figure 2.4**: Crystal structures of the planar chiral receptors **2.8** (left) and **2.9** (right), with ellipsoids drawn at 50% probability level. Dotted lines correspond to H-bonding. A water molecule is included in each crystal structure, with 1:2 water/receptor stoichiometry. All hydrogen atoms are reported.*

The crystal of **2.9** contains a water molecule, which is interacting with the binding sites of two adjacent receptor molecules and acting as a hydrogen bond acceptor with the NH groups of one receptor and a hydrogen bond donor with the CO of another. The hydrogen bonding parameters are reported in Table 2.2.

***Table 2.2:** Hydrogen bonds for **2.9** [Å and °].*

D-H...*A*	d(*D*-H)	d(H...*A*)	d(*D*...*A*)	<(*D*H*A*)
N(1)-H(1)...O(101)#1	0.88	2.10	2.911	153.8
N(2)-H(2)...O(101)#1	0.88	1.98	2.827	161.5
N(101)-H(101)...O(201)	0.88	2.38	3.136	143.6
N(102)-H(102)...O(201)	0.88	1.96	2.818	166.0
O(201)-H(21A)...O(1)	0.871	1.87	2.720	164
O(201)-H(21B)...O(102)#2	0.876	2.42	3.122	137

The crystal of **2.8** contains a water molecule as well, but in this case it is interacting with only one receptor through hydrogen bonds to its NH groups. However in addition, the NH groups of another receptor are interacting with a carbonyl oxygen of the other receptor molecule showing how the receptors can interact directly with one another. The hydrogen bonding parameters are reported in Table 2.3.

Table 2.3: *Hydrogen bonds for* ***2.8*** *[Å and °].*

D-H...*A*	d(*D*-H)	d(H...*A*)	d(D...*A*)	<(DH*A*)
N(1)-H(1)...O(101)	0.88	2.09	2.907	153.4
N(2)-H(2)...O(101)	0.88	1.98	2.824	161.2
N(101)-H(101)...O(201)	0.88	2.38	3.133	144.0
N(102)-H(102)...O(201)	0.88	1.95	2.811	165.4
O(201)-H(21A)...O(102)#1	0.882	2.49	3.122	129
O(201)-H(21B)...O(1)#2	0.889	1.85	2.724	167

2.4 Anion Binding Studies

As described in the next sections, the receptors were studied in solution by UV-Vis spectroscopy and voltammetry measurements to monitor the enantioselectivity towards opposite enantiomers of the same guest, and the difference in binding strength between each chiral guest. In previous studies in the group,[7] ^{1}H NMR studies to assess the stoichiometry of the complexes had already been previously performed on receptor **2.2** and on similar molecules, following the downfield shift of the NH protons (Figure 2.5).

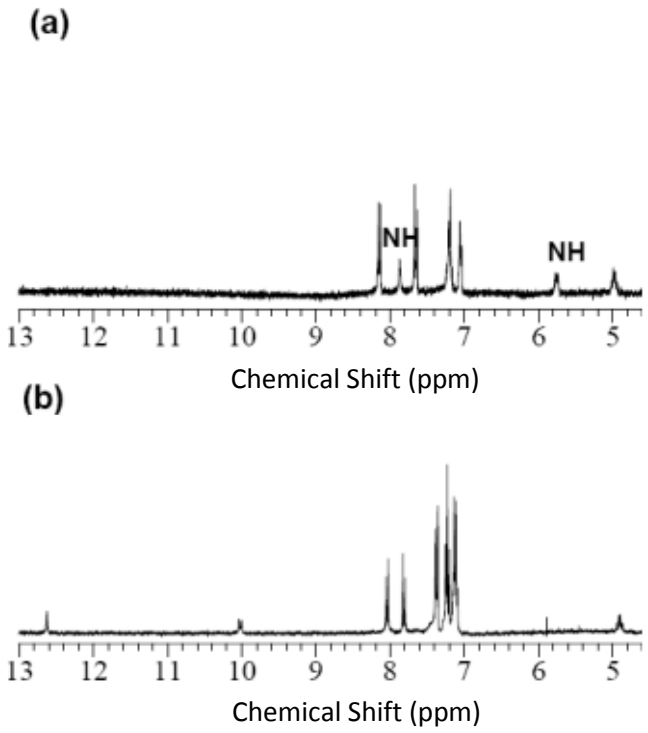

Figure 2.5. *^{1}H NMR in CD_3CN of (a)* ***2.2*** *(5 mM) and (b)* ***2.2*** *in the presence of one molar equivalent of (S)-****2.3*** *(5 mM total concentration).*[7]

These showed the expected 1:1 host/guest stoichiometry, with a complex structure exemplified in Figure 2.6.[7]

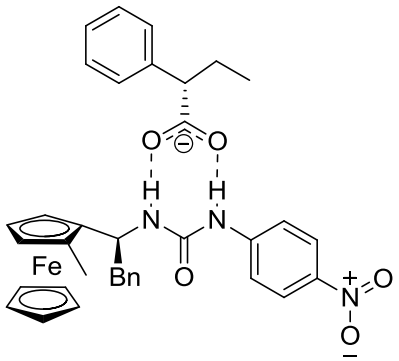

Figure 2.6: *Example of possible structure of a complex with 1:1 stoichiometry, between host* ***2.2*** *and guest (S)-****2.3.***

Also the bis-ferrocenyl receptors were found to bind in a 1:1 stoichiometry.[7] The possible structure of a complex with guest **2.5** is shown in Figure 2.7.

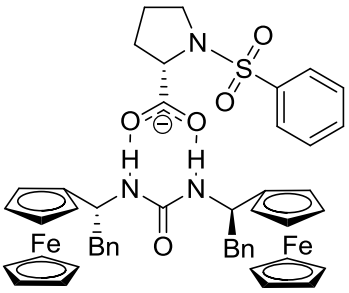

Figure 2.7: *Example of possible structure of a complex between the chiral host* ***2.6*** *and the guest (S)-****2.5****.*

The hydrogen bonding interaction in the mono-ferrocenyl receptors was too strong for ^{1}H NMR spectroscopy to be used to calculate the binding constants at NMR concentrations.[15] However, the interaction of the bis-ferrocenyl receptors with guest **2.5** was weak enough to allow these calculations to be performed, as described below.

2.4.1 ^{1}H NMR Titration Studies

^{1}H NMR titrations were carried out in CD_3CN using the chiral receptor **2.6** but, due to solubility issues, for receptor **2.7** a mixture of solvents (2:1 CD_3CN/CD_2Cl_2) was used. Nevertheless, the experiments with the achiral receptor **2.7** were performed in order to ensure that any result ascribable to chiral recognition with receptor **2.6** were due to the chirality of the host rather than systematic errors in the experiments. As expected, the addition of guest **2.5** (50 mM in a stock solution of the host) to each of the receptors (5 mM) caused a downfield shift of the urea NH protons from *ca.* 5.0 ppm to *ca.* 7.4 ppm (Figure 2.8 and Figure 2.9).

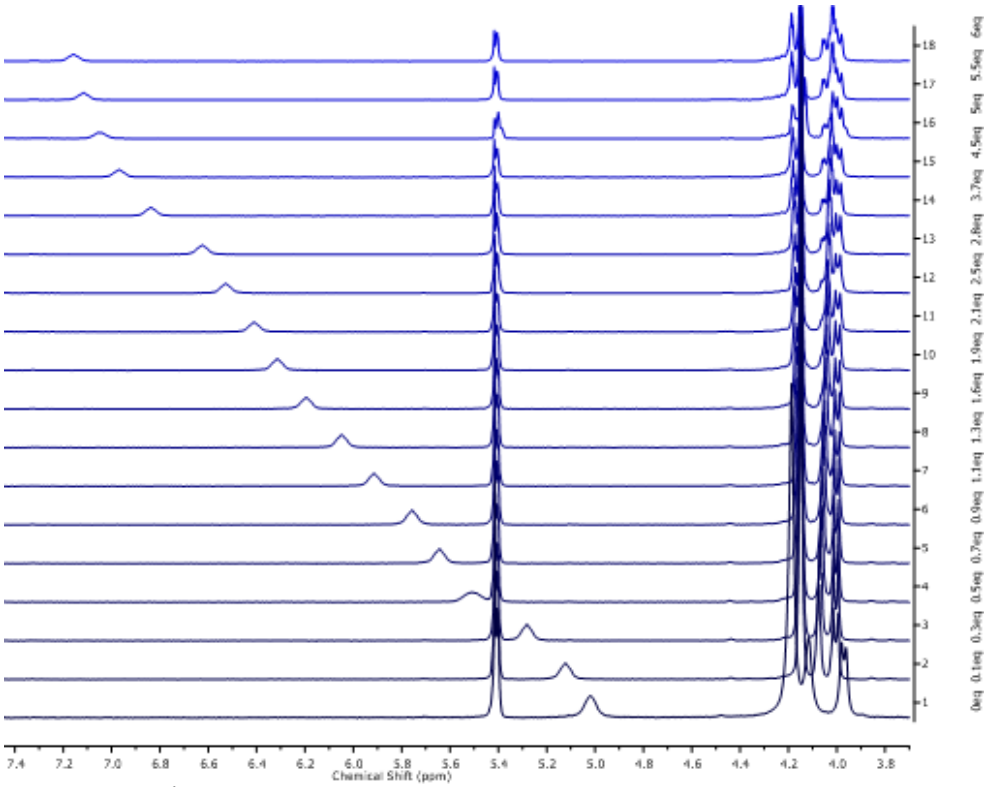

Figure 2.8: *Stacked ^{1}H NMR Spectra for the titration of* ***2.7*** *(5 mM) with (S)-****2.5*** *in 2:1 CD_3CN/CD_2Cl_2 at rt (guest 50 mM). Addition of up to 6 equivalents of guest going from bottom to top (guest aromatic signals > 7.4 ppm).*

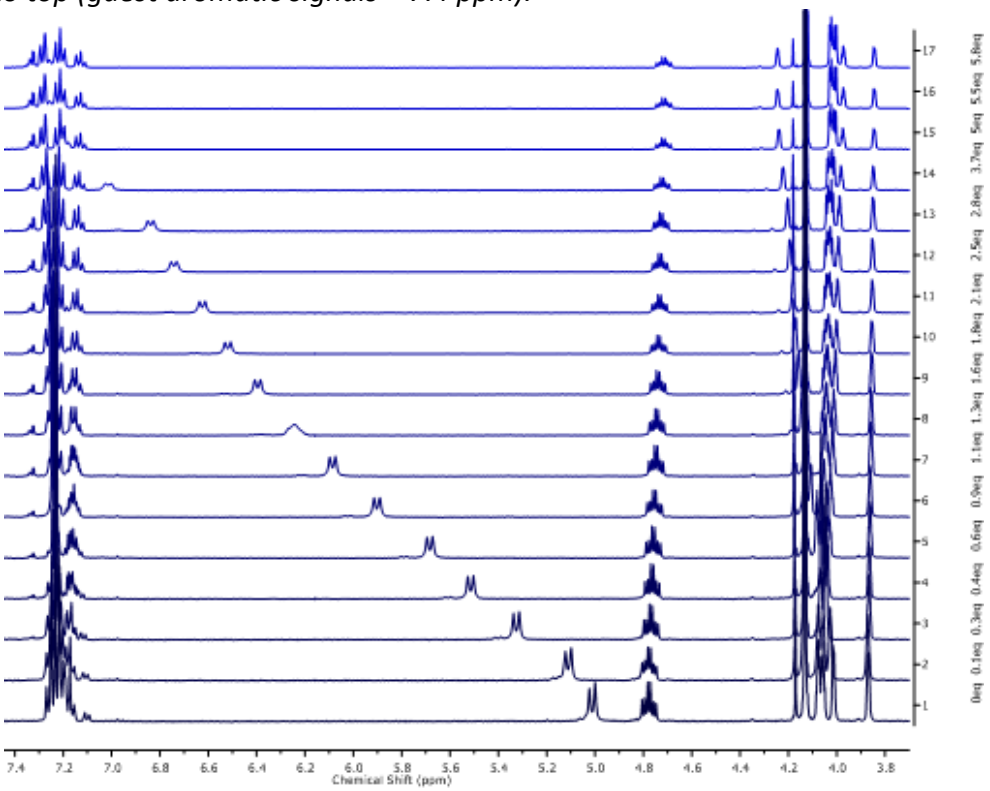

Figure 2.9: *Stacked ^{1}H NMR Spectra for the titration of* ***2.6*** *(5 mM) with (R)-****2.5*** *in CD_3CN at rt (guest 50 mM). Addition of up to 6 equivalents of guest going from bottom to top (guest aromatic signals > 7.4 ppm).*

For receptor **2.7** the same final value was obtained for both the enantiomers of the carboxylate guest, as expected for an achiral receptor (Figure 2.10).

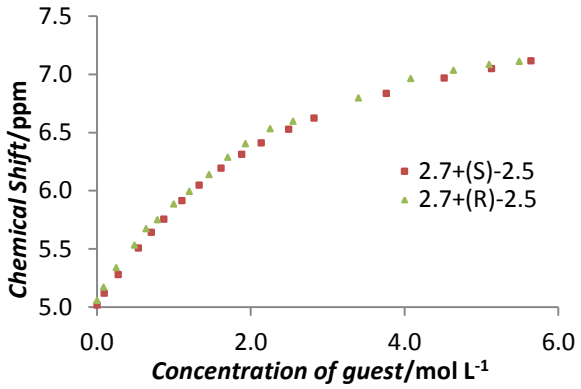

Figure 2.10: *Binding curves for the ^{1}H NMR titration of* ***2.7*** *with* ***2.5*** *2:1 CD_3CN/CD_2Cl_2 at rt (host 5 mM, guest 50 mM).*

On the contrary, for the titration with the chiral receptor **2.6** a different binding mode was observed when binding (*R*)-**2.5** or (*S*)-**2.5**, at the same concentration: the full shift reached upon addition of (*R*)-**2.5** was around 7.2 ppm, whilst after addition of (*S*)-**2.5** a shift around 7.5 ppm was reached. This difference is easily visualised by plotting the chemical shift of the NH of the urea of the host against the equivalents of anion added (Figure 2.11).

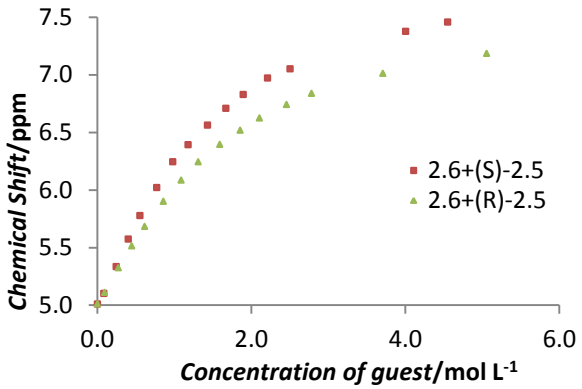

Figure 2.11: *Binding curves for the ^{1}H NMR titration of* ***2.6*** *with* ***2.5*** *in CD_3CN at rt (host 5 mM, guest 50 mM).*

As expected for an achiral receptor, the binding curves for the titrations of **2.7** are superimposable, as there is no major difference in the shift obtained upon addition of either enantiomer of guest **2.5**. On the contrary, the binding curves for the titrations of receptor **2.6** show a small difference that could be exploited for chiral discrimination in solution.

In the case of **2.6** the position of the NH signals could not be identified when it shifted underneath the aromatic signals between *ca.* 7.1 and 7.3 ppm. However, the calculation of binding constants was possible because the most important data points are situated in the first half of the titration, as they identify the slope of the binding curve.[15] The data obtained from the titrations were therefore fitted to a 1:1 binding model, as indicated by Job plot, using the software WinEQNMR[16-17] (Figure 2.12 and Figure 2.13). The corresponding binding constant values are reported in Table 2.4.

a) b)

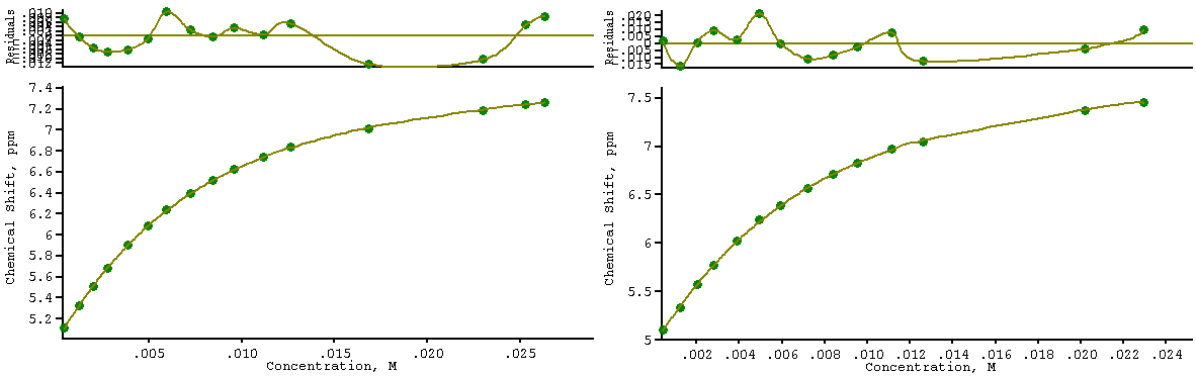

Figure 2.12: *Data fitting for the ^{1}H NMR titration of **2.6** (5 mM): a) with (R)-**2.5** and b) with (S)-**2.5** in CD_3CN at rt (guest 50 mM).*

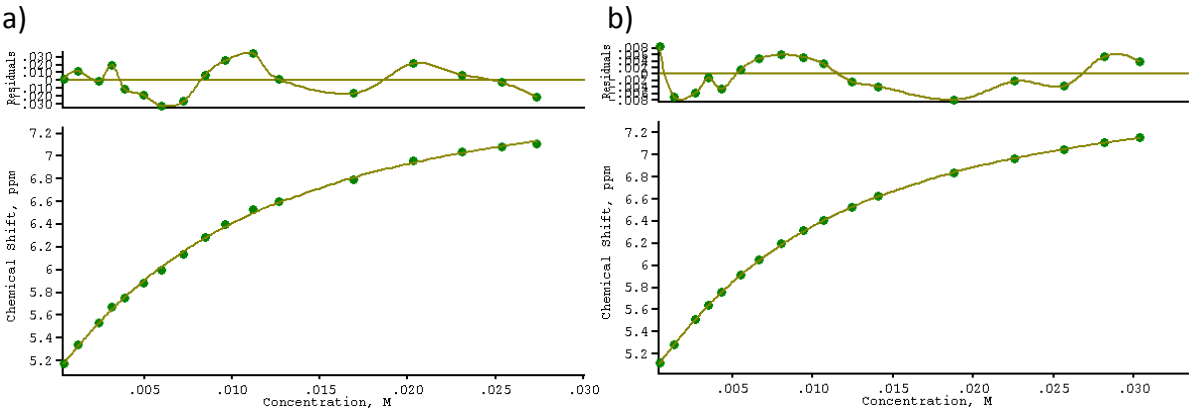

Figure 2.13: *Data fitting for the ^{1}H NMR titration of **2.7** (5 mM): a) with (R)-**2.5** and b) with (S)-**2.5** in 2:1 CD_3CN/CD_2Cl_2 at rt (guest 50 mM).*

Table 2.4: *Binding constants (M^{-1}) calculated for receptor **2.6** in CD_3CN (5 mM) and **2.7** in 2:1 CD_3CN/CD_2Cl_2 (5 mM) with (R)-**2.5** and with (S)-**2.5** at rt; errors below ± 6%.*

DESCRIPTION	PARAMETER
$K_{2.6+(R)\text{-}2.5}$	217
$K_{2.6+(S)\text{-}2.5}$	258
$K_{2.7+(R)\text{-}2.5}$	121
$K_{2.7+(S)\text{-}2.5}$	120

The binding constant calculated for the complex between **2.6** and *(S)*-***2.5*** is *ca.* 1.2 times bigger than the one for the complex between **2.6** and *(R)*-**2.5** (Table 2.4). This is an expected trend, given the slight preference of receptor **2.1** with the same (*R*) configuration for the (*S*) enantiomer of guest **2.5**.[2] On the contrary, the binding constants calculated for the achiral receptors have the same value, within experimental error, for the formation of a complex with either enantiomer of the same guest.

2.4.2 UV-Vis Studies

Having the nitrobenzene chromophore present on the mono-ferrocenyl molecules meant it was possible to determine the binding constants *via* UV-Vis spectroscopy using the Benesi-Hildebrand method.[18]

This method is based on the following equation:

$$\frac{1}{Abs} = \left(\frac{1}{[G]}\right)\left(\frac{1}{K\varepsilon}\right) + \frac{1}{\varepsilon} \qquad \textbf{\textit{Equation 2.1}}$$

Where:

Abs = (A-A_0) where A_0 is the initial absorbance and A the absorbance after each addition

[G] = concentration of the guest after each addition

K = binding constant

ε = molar absorptivity

Using this equation it is possible to draw a double reciprocal plot of 1/Abs against 1/[G], to obtain a line in which the slope is 1/*K*ε and the intercept is 1/ε. The results are plotted at different wavelengths and an average value of the binding constant calculated from each wavelength is taken as the final value (presented as a log*K* value). Nitrobenzene possesses an absorption band with a maximum at *ca.* 350 nm. It is possible to follow a bathochromic shift in this absorption band upon complexation of the guest in solution. This shift is high in MeCN[7] but the Benesi-Hildebrand method is valid only if a significant amount of complexation is achieved after addition of a large excess of guest.[1, 18] Therefore, in order to accurately calculate the binding constant *via* the Benesi-Hildebrand method, it is necessary to perform the UV-Vis titration experiments in a more competitive solvent such as DMSO. In this solvent, the shift observed was lower (Figure 2.14), but the changes were large enough for an analysis to be made.

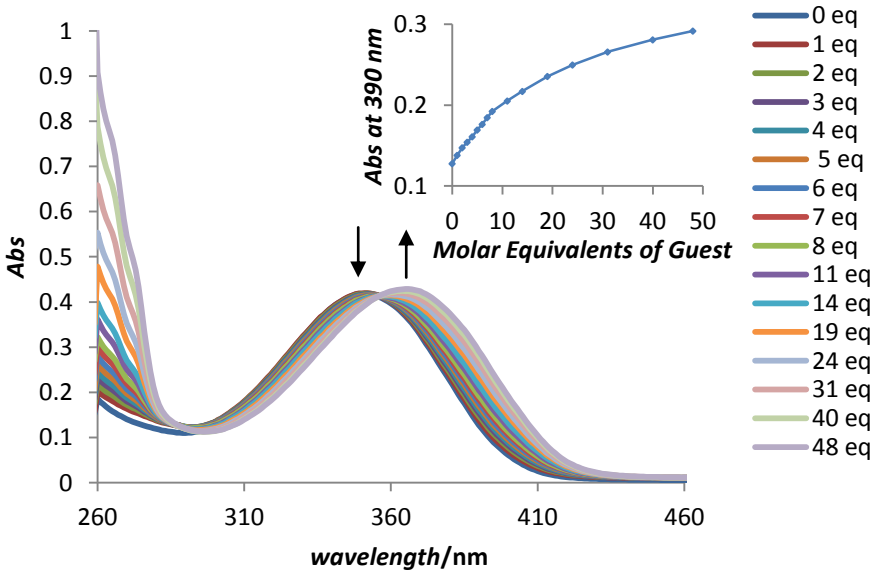

Figure 2.14: *UV-Vis titration of* ***2.10*** *(0.025 mM) in DMSO upon addition of (S)-****2.3*** *at rt, showing the band at 350 nm decreasing and the band at 370 nm increasing as the complex forms. The inset shows the increase of absorption at 390 mV upon addition of (S)-****2.3.***

As expected, the experiments in DMSO (host 0.025 mM and guest 6.25 mM) with the achiral receptor **2.10** gave similar binding constants (presented as log*K* values in Table 2.5) for either enantiomer of the same guest, within experimental error (± 0.05). However, different values and shifts in the absorption band for the different guests **2.3-2.5** (Figure 2.15) were observed. Guest **2.4** was bound more weakly and **2.3** formed the strongest H-bonds with this host. This is possibly due to differences in the pK_a value of the conjugate acids of the guests, which is lower for mandelic acid than for the conjugate acids of the other guests.[7]

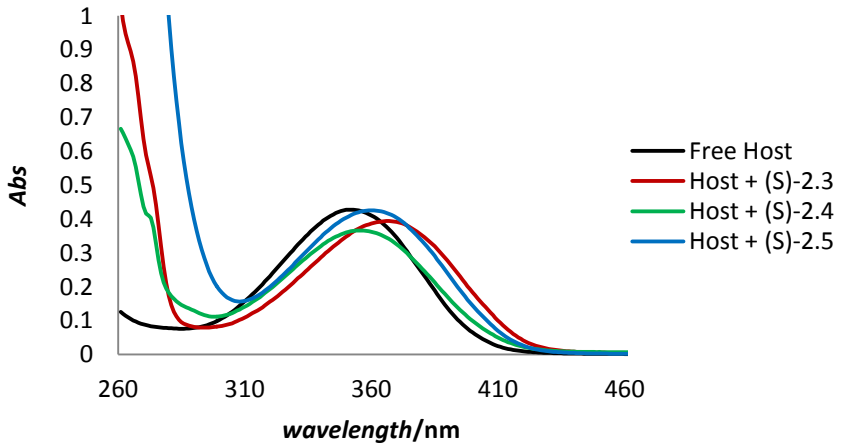

Figure 2.15: *UV-Vis spectra of* ***2.10*** *(0.025 mM) in DMSO upon addition of (S)-****2.3****, (S)-****2.4*** *and (S)-****2.5****, showing the difference in the bathochromic shift for the different guests.*

This can be also seen from analysis of the Benesi-Hildebrand plots, taken at a specific wavelength (370 nm). The binding constants were calculated from the division of the intercept by the gradient in the plots of 1/Abs against 1/[G]. By inspection with the naked

eye it is possible to determine the relative binding strength of the three different guests (Figure 2.16), which is **2.3** > **2.5** > **2.4**.

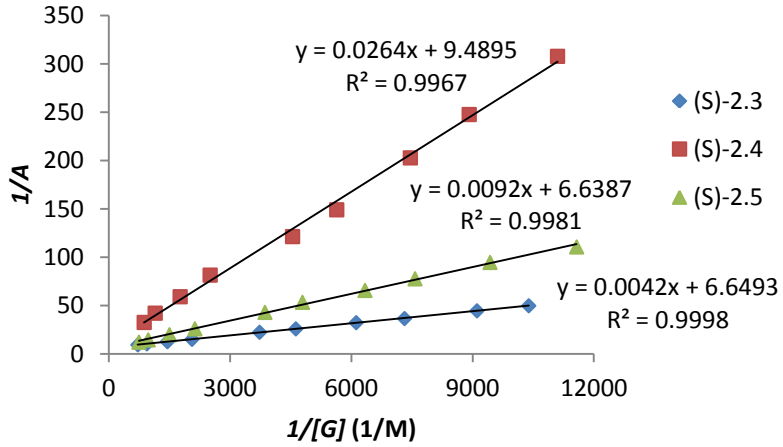

Figure 2.16: *Benesi-Hildebrand plots of* ***2.10*** *(0.025 mM) in DMSO at rt upon addition of (S)-* ***2.3****, (S)-* ***2.4*** *and (S)-* ***2.5****. A steeper slope corresponds to a lower binding constant.*

Unfortunately, the experiments in DMSO (host 0.025 mM and guest 6.25 mM) with the planar chiral receptors **2.8** and **2.9** did not show any chiral selectivity towards enantiomers of the guests under investigation (Table 2.3), but they followed the same binding strength trend for the different guests as observed for host **2.10**. For an effective comparison, the binding constant values calculated for receptors **2.8-2.10** are reported in Table 2.5 together with the values observed for receptors **2.1**[2] and **2.2**.[7]

Table 2.5: *Binding constant values for the five hosts with both enantiomers of the three guests, expressed as log*K *(± 0.05) in dry DMSO at rt. a) data obtained from ref.*[7] *Data in italics are used in Section 2.4.3. Data in bold are used in Section 2.4.4.*

	(S)-**2.3**	*(R)*-**2.3**	*(S)*-**2.4**	*(R)*-**2.4**	*(S)*-**2.5**	*(R)*-**2.5**
2.1[a]	3.42	3.33	2.98	2.93	**3.25**	**3.03**
2.2[a]	3.38	3.39	**2.47**	2.52	**3.06**	**2.82**
2.8	3.37	3.37	*2.53*	*2.56*	2.93	2.93
2.9	3.36	3.35	*2.54*	*2.52*	2.93	2.93
2.10	3.23	3.24	2.58	2.59	2.96	2.98

The only host/guest combination in which chiral recognition is observed (*i.e.* outside of experimental error) is for receptors **2.1** and **2.2** towards guest **2.5**. This is likely to be associated with a combination of π-stacking interactions and steric effects. Surprisingly, receptor **2.2** shows selectivity towards the same (*S*) guest as receptor **2.1**, despite the opposite central chirality. Consequently, it appears that planar chirality plays an important role in directing the selectivity of the receptor, although only in combination with central chirality. Furthermore, the data indicate that planar chirality does not relay chiral discrimination properties to these receptors in the same way that central chirality does in the case of guest **2.5**. The experiments with UV-Vis spectroscopy were unsuccessful in explaining the peculiar behaviour towards guest **2.5** of receptor **2.2** in comparison to **2.1**. The different behaviour might be due to the structural difference caused by the presence of the methyl substituent on the Cp ring of receptor **2.2**. Electrochemical experiments were next performed in order to further investigate the properties of the hosts, as described below.

2.4.3 Electrochemical Sensing

As described in Section 1.4, the presence of ferrocene as a reporting redox-active group in a receptor makes it possible to use it as an electrochemical sensor, if a shift in the formal electrode potential is observed upon addition of guests. In these studies, the receptors and their interaction with chiral carboxylate guests were investigated by cyclic voltammetry and also square wave voltammetry. Initially, the formal electrode potentials of receptors **2.6-2.10** were recorded at room temperature *versus* decamethylferrocene (dmfc) and compared with the potentials recorded for receptors **2.1** and **2.2**.[7] The values are reported in Table 2.6.

Table 2.6: *Formal electrode potentials E°′ (mV ± 2 mV) of the receptors in MeCN at rt.*

Receptor	*E°′* vs. dmfc /mV
2.1	523
2.2	473
2.6	495
2.7	503
2.8	470
2.9	470
2.10	517

As expected, the formal electrode potentials are less positive for receptors **2.2**, **2.8** and **2.9** than for **2.1** and **2.10**. This is due to the presence of an electron donating methyl substituent on one of the cyclopentadienyl rings, which increases the electron density in proximity of the iron centre, stabilising the higher oxidation state and reducing the thermodynamic driving force required for its oxidation.[19-20] The formal electrode potentials of the two bis-ferrocenyl receptors are not too dissimilar from each other. The reversibility of the oxidation of the receptors was verified by cyclic voltammetry varying the scan rate between 50 and 1000 mV s^{-1} (Figure 2.17, Figure 2.18 and Figure 2.19). The intensity of current of the cathodic peak was found to be similar to that of the anodic peak.[21] The hosts displayed a linear relationship between i_p and the square root of the scan rate, in accord with the Randles-Sevcik[22-23] equation (Equation 1.3, see Section 1.9.1).

$$i_p = 2.69 \times 10^{-5} n^{3/2} A D^{1/2} C \nu^{1/2} \qquad \textbf{\textit{Equation 1.3}}$$

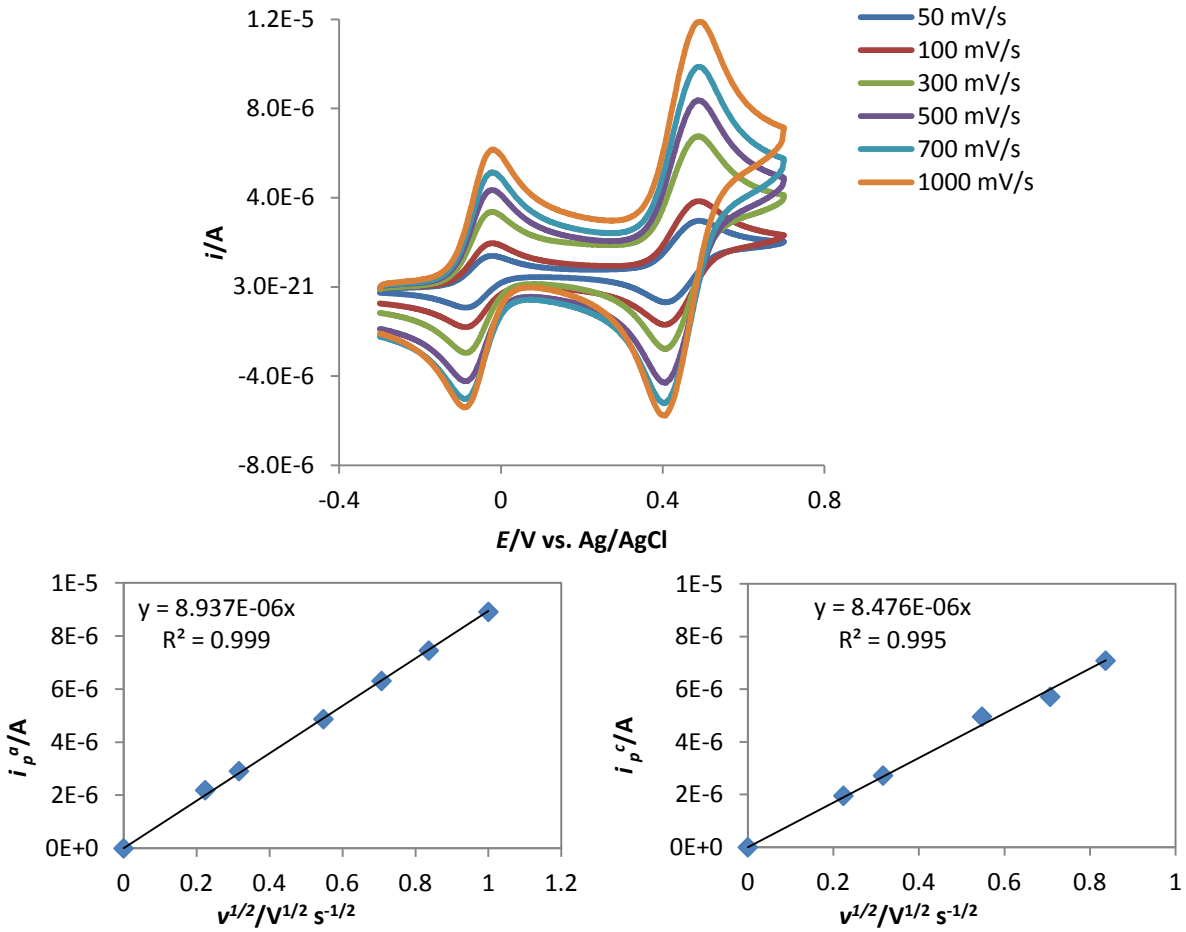

Figure 2.17: *Cyclic voltammograms at various scan rates and plot of the current intensity vs. the square root of the scan rate for* ***2.7*** *(2.5 x 10^{-4} M in MeCN, $TBAPF_6$ 0.1 M, with dmfc at rt.)*

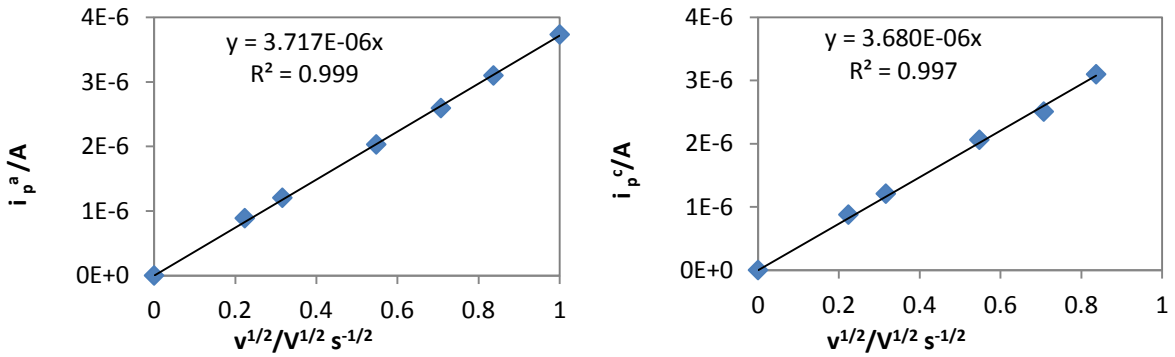

Figure 2.18*: Plot of the current intensity vs. the square root of the scan rate for* ***2.6*** *(1.85x10^{-4} M in MeCN, $TBAPF_6$ 0.1 M, with dmfc at rt).*

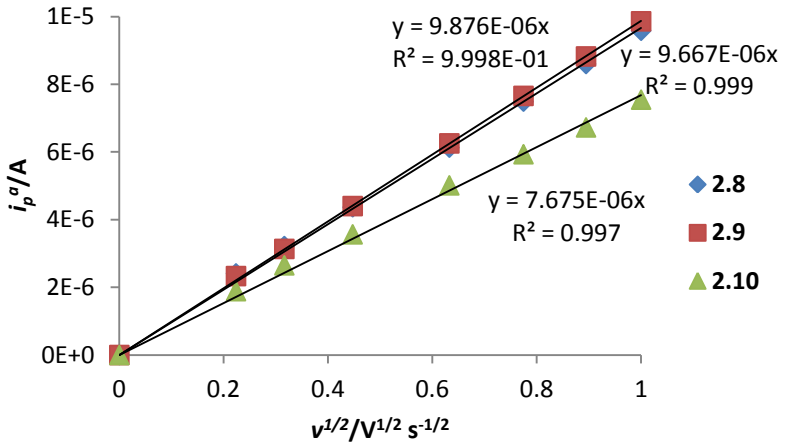

Figure 2.19: *Plot of the current intensity vs. the square root of the scan rate for the mono-ferrocenyl receptors (5 x 10^{-4} M in MeCN, $TBAPF_6$ 0.1 M, with dmfc at rt.) (legend + axis)*

The peak separation $E_p{}^a$ - $E_p{}^c$ was *ca.* 80 mV, consistent with a one-electron process considering that the slightly wide peak separation, larger than 59 mV, is a result of uncompensated Ohmic drop. The waves were considered reversible as the intensity of current of the cathodic peak is similar to that of the anodic peak[21] and there was no loss of electroactivity over a number of consecutive scans (up to 20). The bis-ferrocenyl receptors showed one single redox wave, as the two peripheral ferrocene moieties of the molecules are equivalent and not communicating with each other.[24]

Using square wave voltammetry in order to minimise the error in the potential shift (see Section 1.9.2), titration experiments *via* consecutive additions of small volumes of carboxylate guest (15 mM to 0.75 M in dry MeCN) to a solution of receptor (0.2 to 0.5 mM in dry MeCN) were performed at room temperature (an example of a set of SWVs is provided in Figure 2.20).

dmfc

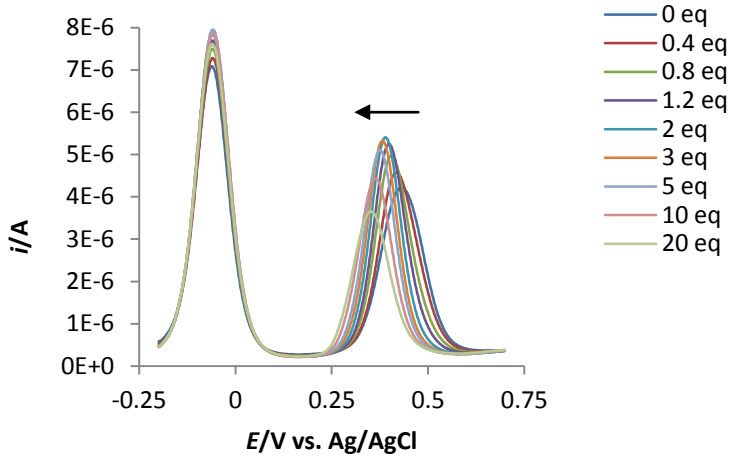

Figure 2.20: *Typical series of square wave voltammograms for the addition of* (R)-***2.5*** *as* TBA^+ *salt (0.75 M) to* ***2.6*** *(0.18 mM), with dmfc (0.3 mM) in MeCN with* $TBAPF_6$ *0.1 M at rt.*

In every experiment, a less positive potential was observed upon complexation, which is consistent with anion binding pushing electron density onto the ferrocene unit, making it thermodynamically easier to oxidise. In most cases, one-wave behaviour was observed (described more in section 2.4.4). The extent of these potential shifts depends on the guest: the shifts are generally smaller for **2.4**, which may be explained by the lower basicity of this guest. After addition of up to 20 equivalents of guest, no more changes were observed and therefore complexation was considered complete. The values recorded by SWV agreed with those recorded by CV, but they were preferred when possible due to the smaller error associated with the technique (see Section 1.9.2). The differences between opposite enantiomers of the same guest were also considered and the values at full shift are reported in Table 2.7.

Table 2.7: *Shift in the formal electrode potentials* ΔE_{obs} *(where* $\Delta E_{obs} = E_{obs} - E°'_{host}$*) obtained from SWV experiments (mV ± 4 mV) of the receptors (0.2 to 0.5 mM) upon addition of the*

*guests **2.3-2.5** in dry MeCN at rt. * from CV experiments (± 10 mV) obtained from ref.*[7] ¤ two-wave behaviour. *Data in bold are used in Section 2.4.4.*

	(S)-**2.3**	*(R)*-**2.3**	*(S)*-**2.4**	*(R)*-**2.4**	*(S)*-**2.5**	*(R)*-**2.5**
2.1	-81*	-82*	-59*	-63*	**-83***	**-78***
2.2	-89*¤	-91*¤	**-74***	-68*	**-91¤**	**-84¤**
2.6	-82*	-86*	---	---	-85	-87
2.7	---	---	---	---	-76	-73
2.8	-75	-78	-60	-63	-76	-73
2.9	-79	-77	-63	-61	-76	-74
2.10	-73	-74	-59	-58	-72	-73

For the bis-ferrocenyl receptors, the number of equivalents of guest needed to achieve full complexation (20 equivalents) was larger than for the mono-ferrocenyl receptors (5 equivalents), which indicates that weaker complexes are formed, as indicated by the ^{1}H NMR studies. Unfortunately, the final shift observed for all the complexes was the same for both the enantiomers, within experimental error. This means that these values alone cannot be used as an indicator of chiral sensing. However, for the systems showing one-wave behaviour, a difference in the binding constant is reflected by the equivalents of guest needed to reach the full shift in the potential. For a stronger binding system, the latter should be achieved by the addition of one equivalent of guest to the receptor but, for the formation of a complex with a weaker binding constant, more of an excess of guest would be needed to reach full complexation and a full shift. Analysis of the binding curve obtained by plotting ΔE_{obs} *vs.* equivalents of guest (where $\Delta E_{obs} = E_{obs} - E°'_{host}$) can, therefore, be another way of indicating the chiral sensing properties of these receptors.[2] However, unfortunately, for the new systems studied (*i.e.* receptors **2.6, 2.8** and **2.9**) no chiral discrimination could be observed using this approach.

The achiral control **2.10** displayed as expected superimposable binding curves with guests **2.3-2.5**, and chiral discrimination was absent. (Examples for **2.6**, **2.7** and **2.10** are given in Figure 2.21).

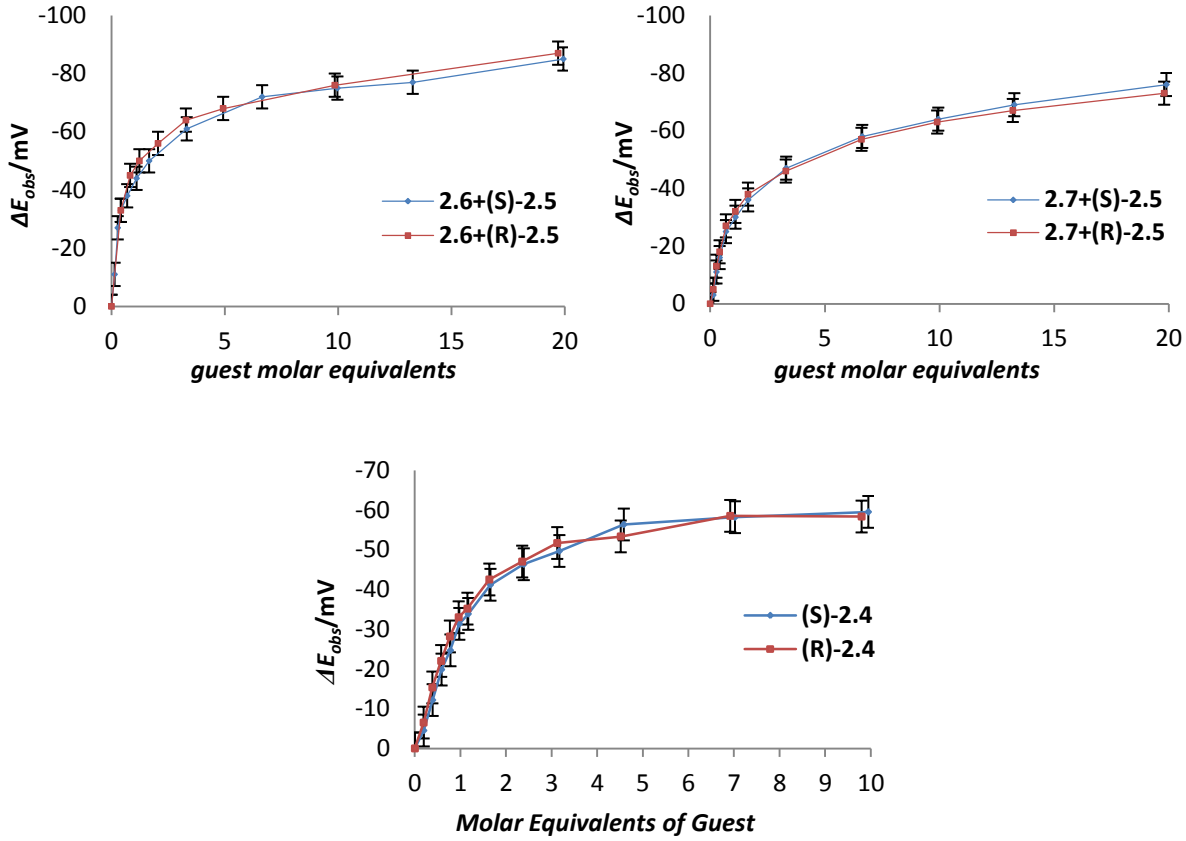

Figure 2.21: *Values of ΔE_{obs} (mV ± 4 mV) for **2.6**, **2.7** and **2.10** upon addition of guests **2.5** or **2.4** as TBA^+ salts. (Host 0.02 mM and guest 0.75 M in MeCN with $TBAPF_6$ 0.1 M and dmfc at rt.) (bold legend)*

For the planar chiral receptors **2.8** and **2.9**, the binding curves also generally showed no difference for opposite enantiomers of the same guest. However, despite the values recorded being within experimental error, repetition of the experiments confirmed that the binding curves always displayed mirrored behaviour for these two receptors when titrated with guest **2.4**: *i.e.* receptor **2.8** gives the higher curve for (*R*)-**2.4** while, on the contrary, its opposite enantiomer **2.9** gives the higher curve for (*S*)-**2.4** (Figure 2.22).

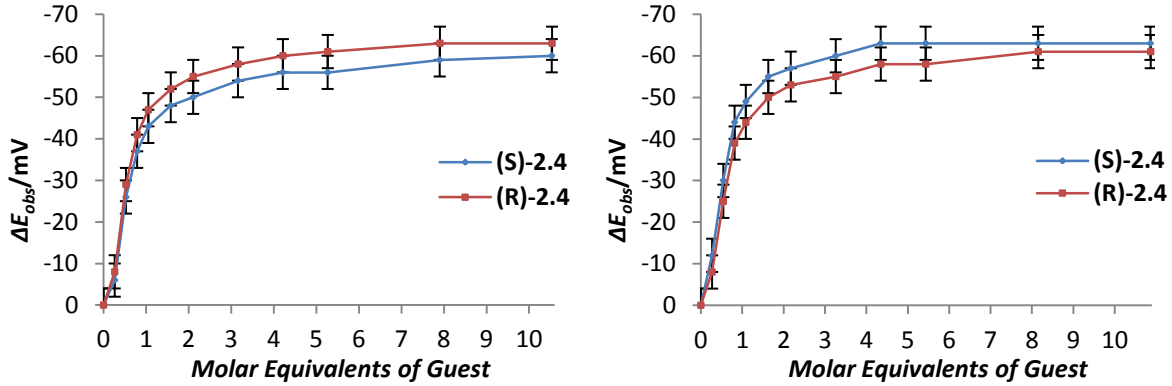

Figure 2.22: *Values of ΔE_{obs} (mV ± 4 mV) for **2.8** upon addition of **2.4** (left) and **2.9** upon addition of **2.4** (right); (Host 0.025 mM in MeCN with $TBAPF_6$ 0.1 M and dmfc at rt).*

If there is indeed any chiral sensing, it could be because of the difference in the binding constants, although they were calculated in DMSO and in fact they show a very small difference that is within experimental error (Table 2.5 in italics). It would appear that unlike the system for **2.1** with guest **2.5**,[2] in which larger differences in binding constants were observed, chiral sensing could not be revealed through electrochemical titrations.

2.4.4 Two-wave behaviour *versus* one-wave behaviour[25-26]

Interestingly, another feature emerged by comparing the voltammetric behaviour of receptors **2.1** and **2.2**. For receptor **2.2**, the redox wave for the free host gradually disappears while a new wave at less positive potential appears upon complexation (two-wave behaviour), but only when the binding is stronger (*i.e.*, either enantiomer of guest **2.5** and **2.3** but not for **2.4**). This can be seen in Figures 2.23b and 2.24b. For receptor **2.1** with

any guest, or **2.2** with guest **2.4**, the redox wave instead shifts gradually to less positive potential (one-wave behaviour). This can be seen in Figures 2.23a and 2.24a.

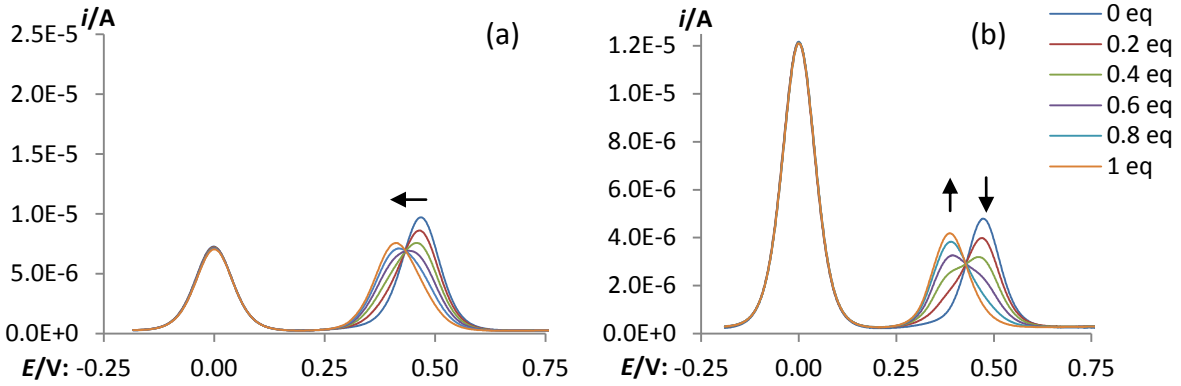

Figure 2.23: *Square wave voltammetric behaviour differences for a)* ***2.2*** *upon addition of* (*S*)-**2.4** *(one-wave behaviour) and b)* (*S*)-**2.5** *(two-wave behaviour); guests added* as TBA^+ *salts, potential reported vs. dmfc (c = 3.5 x* 10^{-4} *M, 0.1 M* $TBAPF_6$ *in MeCN at rt).*

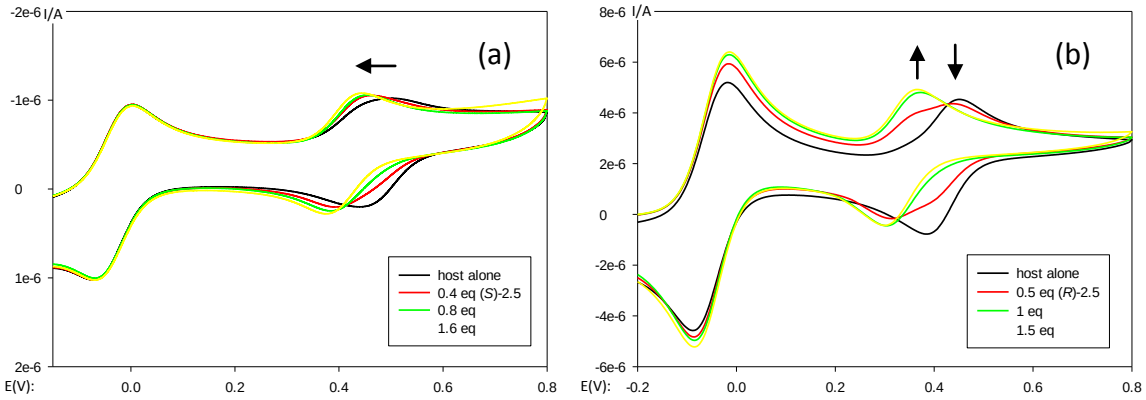

Figure 2.24: *Cyclic voltammetric behaviour differences for a)* ***2.1*** *(0.9 x* 10^{-4} *M, 0.1 M* $TBAPF_6$ *in MeCN at rt) upon addition of* (*S*)-**2.5** *(one-wave behaviour) and b)* ***2.2*** *(5.0 x* 10^{-4} *M, 0.1 M* $TBAPF_6$ *in MeCN at rt) upon addition of* (*R*)-**2.5** *(right, two-wave behaviour).*

As described in Section 1.4, the ΔE_{obs} values depend on K_{ox}/K_{red}, following equation 1.1:

$$\frac{(E^{o\prime}{}_{H} - E^{o\prime}{}_{HG})nF}{RT} = \ln\left(\frac{K_{ox}}{K_{red}}\right) \qquad \textbf{\textit{Equation 1.1}}$$

Kaifer and coworkers stated that the observation of two-wave or one-wave behaviour is dependent on the strength of the host-guest binding and the magnitude of the ΔE_{obs} value.[25] In the case of weaker binding one-wave behaviour was always observed, even if the ΔE_{obs} value was large, which was confirmed by digital simulations. This is consistent in our studies

for receptor **2.2** with guest **2.4** and **2.5** (Table 2.5 and 2.7 in bold) since ΔE_{obs} values and binding constants are lower with **2.4** than with **2.5**. However, from analysis of the data in this table, it appears that the binding strength and ΔE_{obs} are not the only features that influence the voltammetric behaviour: receptor **2.1** always shows one-wave behaviour in the interactions with any guest, despite in comparison with **2.2**, having similar binding constants and ΔE_{obs} values for the interaction with guests **2.3** and **2.5**. The most striking example is the interaction of **2.2** with (*R*)-**2.5** compared to that of **2.1** with (*S*)-**2.5**. In this case, despite the lower binding constant in the former, two-wave behaviour is observed. Therefore, the reason for different voltammetric behaviour lies in another property of these complexes.

It was decided to perform digital simulations of cyclic voltammograms with the software DigiSim in order to collect more information and explain the differences in the voltammetric behaviour. The data used for the simulations were found in the literature or collected experimentally. The concentration (0.5 mM), initial potential (Table 2.6), final potential (Table 2.7), scan rate (0.1 V s^{-1}), WE radius (0.08 cm) and temperature (293 K) were the same as in the voltammetric experiments. The binding constants in MeCN for the reduced form were assumed multiplying by 100 the corresponding binding constants in DMSO, as calculated from UV-Vis spectroscopy (Table 2.5). This value was chosen to fit the experimental data obtaining a nearly complete shift upon addition of one equivalent of guest. The binding constants for the oxidised form were calculated by the software using Equation 1.1. The viscosity of the solvent was reported in literature[27] but it was approximated to the value for the solvent in absence of electrolyte (0.00522 cm^2 s^{-1}). The

diffusion coefficients, *D*, which are an indication of the movement of the species under the influence of a chemical potential or concentration gradient,[21] were calculated using the Randles-Sevcik[22-23] Equation 1.3, knowing that only one electron is exchanged in the Fc/Fc^+ redox couple.

i_p values for the oxidised and reduced forms were plotted against the square root of the scan rate, whose linearity is a sign of the chemical reversibility of the redox reaction (Figure 2.25 and Figure 2.26). The values of *D* obtained are reported in Table 2.8.

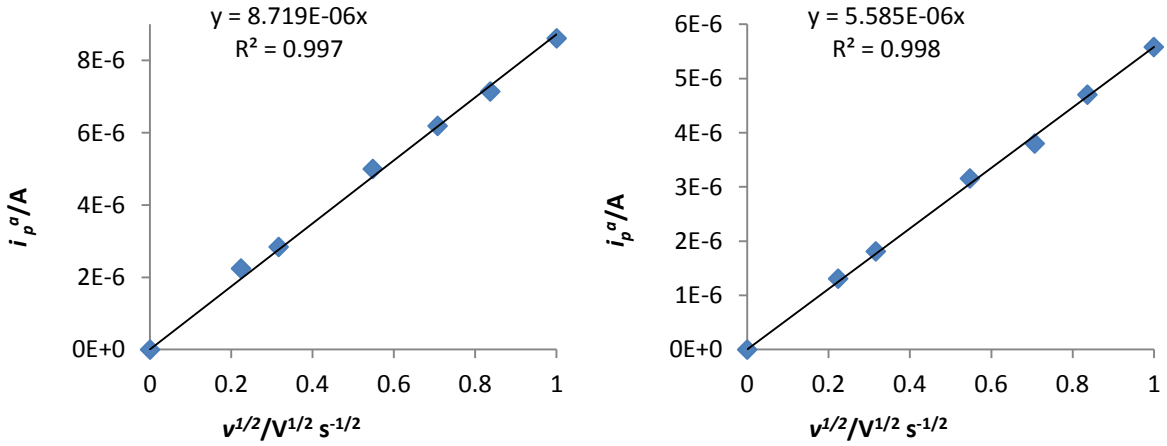

Figure 2.25: *Dependence of anodic peak height (i_p) on scan rate (v) for* ***2.1*** *(left) and for* ***2.1*** *with* (R)-**2.5** *(right). R^2 is the deviation from linearity, ideal for $R^2 = 1$.*

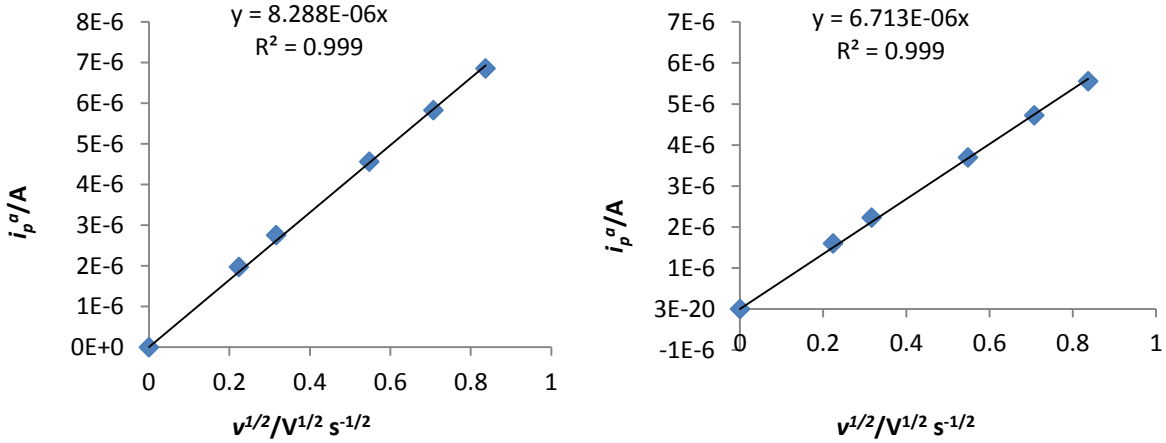

Figure 2.26: *Dependence of anodic peak height (i_p) on scan rate (v) for* ***2.2*** *(left) and for* ***2.2*** *with* (S)-**2.5** *(right). R^2 is the deviation from linearity, ideal for $R^2 = 1$.*

Table 2.8: *Diffusion coefficients calculated for* ***2.1*** *and* ***2.2*** *in their free form and upon addition of* (R)-**2.5**, (S)-**2.5** *and* (S)-**2.4**, *together with the values of $D(H_{ox}) - D(HG_{ox})$. (in MeCN with 0.1 M $TBAPF_6$, host 0.5 mM at rt.) *In the simulations this values were adjusted by adding the experimental error.*

$D/cm^2\ s^{-1}$	H_{red}	H_{ox}	HG_{red}	HG_{ox}	$H_{ox} - HG_{ox}$
2.1 + (S)-**2.5**	1.11×10^{-5}	9.71×10^{-6}	6.08×10^{-6}*	3.98×10^{-6}	5.73×10^{-6}
2.1 + (*R*)-**2.5**	1.20×10^{-5}	1.16×10^{-5}	6.25×10^{-6}*	5.99×10^{-6}	5.61×10^{-6}
2.2 + (*S*)-**2.5**	9.07×10^{-6}	8.22×10^{-6}	8.02×10^{-6}	6.22×10^{-6}	2.00×10^{-6}
2.2 + (*R*)-**2.5**	1.04×10^{-5}	9.12×10^{-6}	9.37×10^{-6}*	8.52×10^{-6}	0.60×10^{-6}
2.2 + (*S*)-**2.4**	1.13×10^{-5}	1.09×10^{-5}	1.03×10^{-5}	9.26×10^{-6}	1.64×10^{-6}

An error of ± 1.5×10^{-6} was estimated from the experimental data for the free host and used to correct the values of HG_{red}, which were observed to influence the equilibrium rather than the voltammetric behaviour (*i.e.* one-wave or two wave). What is clear from the simulations is that the observation of two-wave *versus* one-wave behaviour is very sensitive to changes in the diffusion coefficient parameters for the oxidised species H_{ox} and HG_{ox}. By analysis of the values of diffusion coefficient in Table 2.8, it is possible to infer how the difference in voltammetric behaviour could be related to the variation in diffusion coefficient in the oxidised form going from the free receptor to the complex $D(H_{ox}) - D(HG_{ox})$.

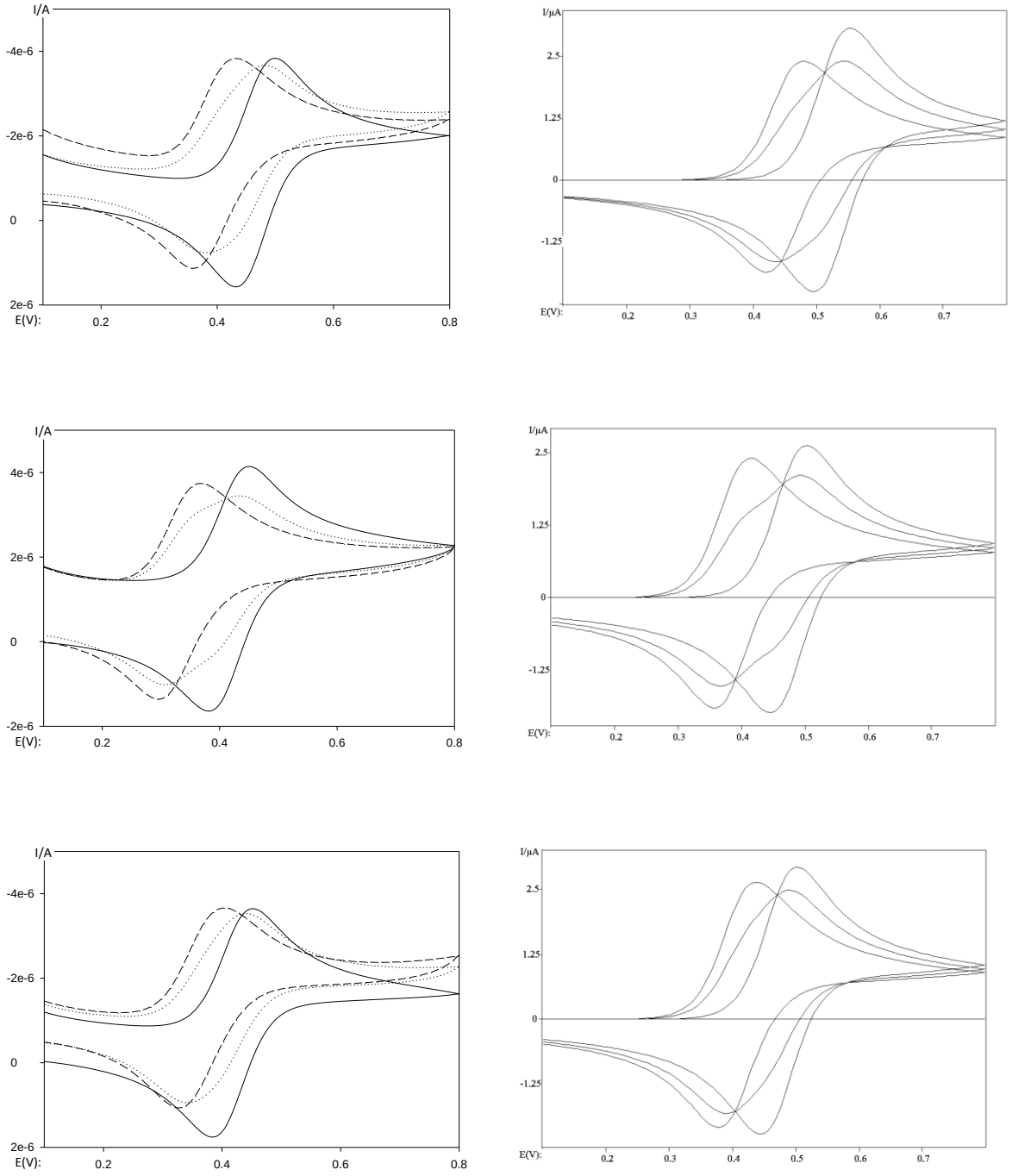

Figure 2.27: *Experimental data (left) and digital simulation (right) of the cyclic voltammograms of* ***2.1*** *+* (R)-**2.5**, ***2.2*** *+* (S)-**2.5** and ***2.2*** *+* (S)-**2.4** *(top to bottom) at rt. Solid line: free host; dotted line: 0.5 eq. of guest; dashed line: 1 eq. of guest.*

When this change is smaller, as in the case of **2.2** + (*S*)-**2.5** and **2.2** + (*R*)-**2.5,** two-wave behaviour (Figure 2.27, centre) rather than one-wave behaviour is observed. However, in the case of guest **2.4**, a small change in diffusion coefficient is alone not enough to give two-wave behaviour (Figure 2.27, bottom), presumably because the ΔE_{obs} value is not large enough. On the contrary, in the case of **2.1** + (*S*)-**2.5** and **2.1** + (*R*)-**2.5,** the difference $D(H_{ox})$ – $D(HG_{ox})$ is larger and one-wave behaviour is observed (Figure 2.27, top). This hypothesis is confirmed by the digital simulations, which fit particularly well with the experimental data (Figure 2.27). Control simulations for **2.2** + (*S*)-**2.4** and for **2.1** + (*R*)-**2.5** in which the data were kept the same but ΔE_{obs} was increased, gave two-wave voltammetric behaviour, as expected. Moreover, by cross-comparison, it appears that in these cases the voltammetric behaviour is not related to $E^{o\prime}{}_{H}$, but only to ΔE_{obs}. Control simulations verified this hypothesis.

Having collected more information on the behaviour of the systems, the only remaining issue was the use of receptor **2.2** as an electrochemical chiral sensor. From analysis of the final shift achieved with full complexation of the opposite enantiomers of guest **2.5** (Table 2.7), it is possible to identify a small difference in the voltammograms through the different ΔE_{obs} values (Figure 2.28). This difference is in fact just within the experimental error (± 4 mV) but repeating at least twice the experiments confirmed that the full shift was always larger upon addition of guest (*S*)-**2.5** than (*R*)-**2.5.** However, for typical two-wave voltammetric behaviour, it is of course not possible to plot a titration of ΔE_{obs} *versus* molar equivalents of guest added as in the previous systems.

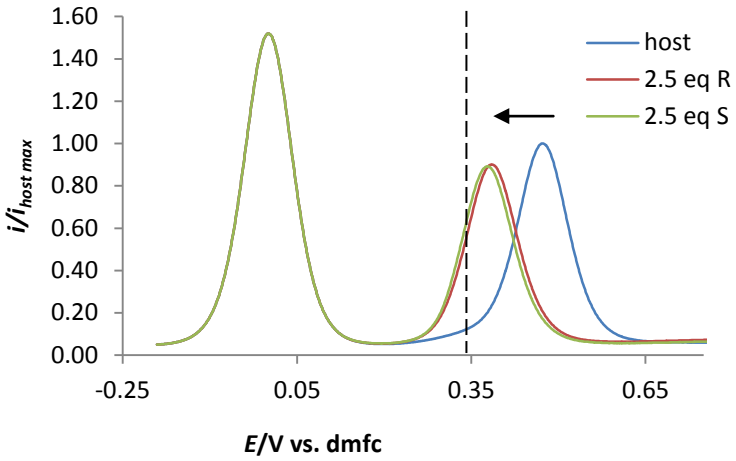

Figure 2.28: *Square Wave Voltammograms of* ***2.2*** *in its free form and upon addition of 2.5 eq. of guest* ***2.5****. (Host conc. 0.5 mM, TBAPF$_6$ 0.1 M, in MeCN at rt.) Current values are normalised with the peak intensity of the free host. The dashed line indicates the potential where the largest difference in current intensity between the SWVs of the different complexes is observed.*

Instead, the observed two-wave behaviour can be exploited by plotting the variation in the intensity of current at a specific potential *versus* the equivalents of guest added. For this reason the values of intensity were normalised for the peak intensity of the host in its free form, in order to be able to compare the intensity at a convenient potential after addition of either enantiomer of the guest. The potential chosen was 340 mV in order to maximise the difference in the variation of intensity of current between the different enantiomers (dashed line in Figure 2.28). Values of the current intensity are plotted as a function of molar equivalents of guest in Figure 2.29.

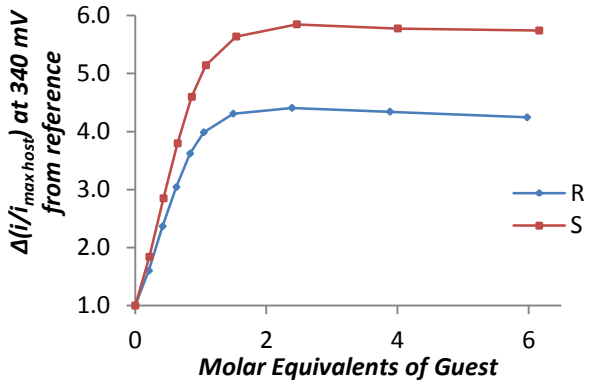

Figure 2.29: *Values of Δ(i/i$_{max\ host}$) at 340 mV from ref. against molar equivalents of guest added for* ***2.2*** *upon addition of guest* ***2.5****. (Host conc. 0.5 mM, TBAPF$_6$ 0.1 M, in MeCN at rt). Current values are corrected against the peak intensity of the free host.*

This type of plot appears to be an effective method for visualising the difference in response upon binding with opposite enantiomers of the same guest, for which large enough differences in ΔE_{obs} are observed.

2.5 Conclusions and Future Work

A new series of chiral ureas containing two redox-active ferrocene groups, or one ferrocene group and the chromophore *p*-nitrobenzene, was successfully synthesised and studied. The two peripheral ferrocene groups in the bis-ferrocenyl ureas did not show any electronic communication. Binding of carboxylate anions caused a negative shift in the redox potential of the ferrocene groups, which indicates that these receptors can be effectively used as electrochemical sensors for these anions in solution. In the case of the bis-ferrocenyl receptors, ^{1}H NMR could differentiate between the two enantiomers of the guest **2.5**, although with a small ratio of K_S/K_R = 1.2. The poor chiral discrimination showed by this system could be related to the weak binding, possibly caused by the presence of two ferrocene groups on the same receptor, which influence the binding site electronically and

sterically. In the mono-ferrocenyl receptors, the chromophore enabled the calculation of the binding constants of the complexes formed between ureas and carboxylates in DMSO, with the possibility to evaluate the extent of the enantioselectivity from differences in binding strength in competitive solvents. From the studies carried out, it emerged that the inclusion of central chirality in the receptors is the most effective way to achieve chiral recognition, although this was too small to be followed by electrochemical techniques in the bis-ferrocenyl receptors. Electrochemistry can give an immediate response. Subtle differences in the binding constants and potential are reflected, in some cases, in the different slopes of curves plotting the shift in observed potential against the equivalents of guest added. Planar chirality alone is not effective for the enantioselective recognition properties bestowed on the sensor but it gives interesting properties when central chirality is already present on the receptor: planar chirality does not enhance the sensing properties given by the central chiral group in an additive manner but modifies the property of the receptor, reverting its enantioselectivity, as well as changing its voltammetric behaviour, which is switched between one-wave and two-wave behaviour. Future work on this class of receptors could move towards the synthesis of a macrocyclic receptor by linking the two ferrocene units on the unsubstituted cyclopentadienyl rings. This should theoretically increase the binding strength, due to the macrocyclic effect.[28-29] Moreover, the selectivity towards one enantiomer could be increased by changing the substituents on the cyclopentadienyl with some bulkier groups such as isopropyl or benzyl. A useful addition could be an extra functionality on the same cyclopentadienyl ring where the binding site is attached. This could be introduced with the same procedure of lithiation and subsequent electrophile

addition and could present a hydrogen bond donor or a hydrogen bond acceptor, such as the nitrogen of a pyridine group (Scheme 2.8).

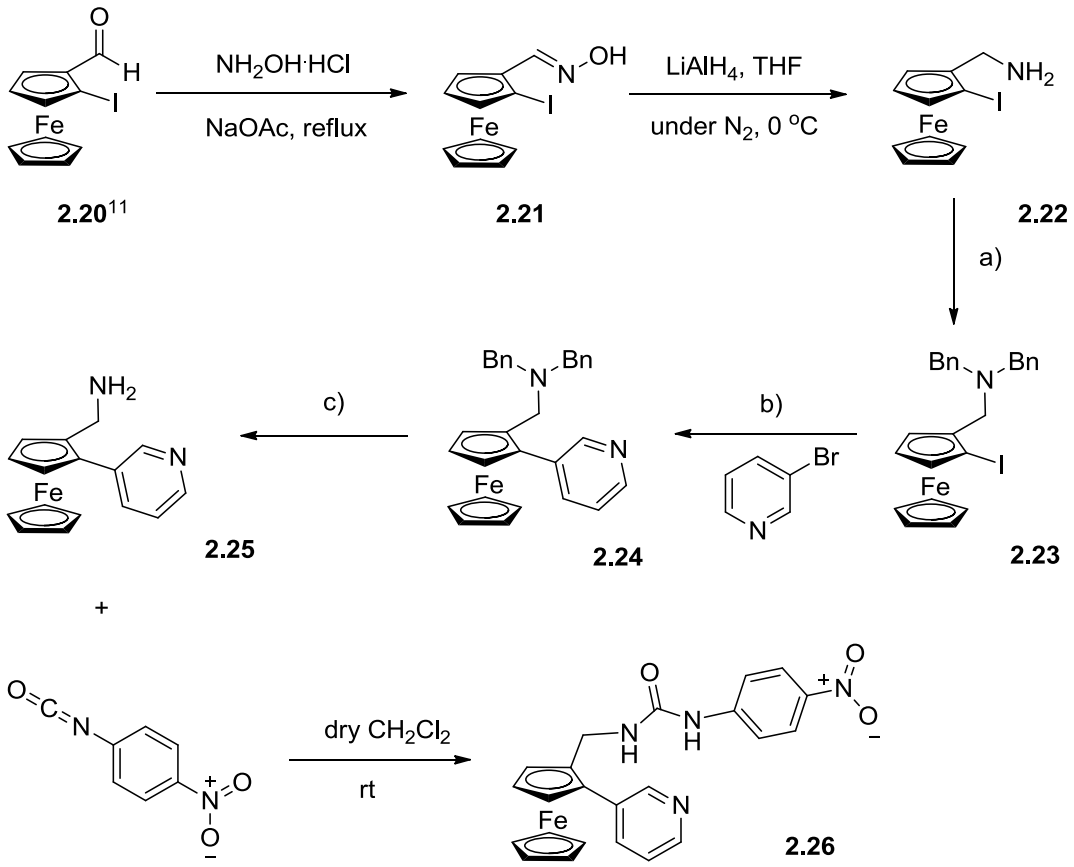

Scheme 2.8: *Synthesis of a urea derivative with a bulkier substituent on the Cp ring and an extra hydrogen bond acceptor. a)[30] BnBr, Et_3N, CH_3CN; b)[31] $PdCl_2(PPh_3)_2$ (5 mol%), DIBAH (10 mol%), under N_2, rt; c)[30] Pd/C, HCOOH, CH_3OH, 25 °C.*

The above-mentioned extra functionality in a rigid conformation could modify the binding properties towards guests such as mandelate, which possesses an –OH group on the side chain that would possibly interact by hydrogen bond formation. If the binding of one enantiomer is favoured over the other, the chiral recognition properties would be enhanced.

2.6 References

1. Laurent, P.; Miyaji, H.; Collinson, S. R.; Prokes, I.; Moody, C. J.; Tucker, J. H. R.; Slawin, A. M. Z., *Org. Lett.* **2002,** *4*, 4037-4040.
2. Willener, Y.; Joly, K. M.; Moody, C. J.; Tucker, J. H. R., *J. Org. Chem.* **2008,** *73*, 1225-1233.
3. Joly, K. M.; Wilson, C.; Blake, A. J.; Tucker, J. H. R.; Moody, C. J., *Chem. Commun.* **2008**, 5191-5193.
4. Richards, C. J.; Locke, A. J., *Tetrahedron Asymmetry* **1998,** *9*, 2377-2407.
5. Schwink, L.; Knochel, P., *Chem.-Eur. J.* **1998,** *4*, 950-968.
6. Colacot, T. J., *Chem. Rev.* **2003,** *103*, 3101-3118.
7. Willener, Y. S. I. Organometallic Receptors and Sensors for Chiral Carboxylates and Other Anions. The University of Birmingham, Birmingham, 2009.
8. Miyaji, H.; Collinson, S. R.; Prokes, I.; Tucker, J. H. R., *Chem. Commun* **2003**, 64-65.
9. Kraatz, H. B., *J. Organomet. Chem.* **1999,** *579*, 222-226.
10. Huikai, S.; Qingmin, W.; Runqiu, H.; Heng, L.; Yonghong, L., *J. Organomet. Chem.* **2002,** *655*, 182-185.
11. Beer, P. D.; Smith, D. K., *J. Chem. Soc. Dalton Trans.* **1998**, 417-423.
12. Lorenzo, A.; Aller, E.; Molina, P., *Tetrahedron* **2009,** *65*, 1397-1401.
13. Rannard, S. P.; Davis, N. J.; Herbert, I., *Macromolecules* **2004,** *37*, 9418-9430.
14. Riant, O.; Samuel, O.; Flessner, T.; Taudien, S.; Kagan, H. B., *J. Org. Chem.* **1997,** *62*, 6733-6745.
15. Hirose, K., *J. Inclusion Phenom.* **2001,** *39*, 193-209.
16. Hynes, M. J., *J. Chem. Soc. Dalton Trans.* **1993**, 311-312.
17. Molard, Y.; Bassani, D. M.; Desvergne, J. P.; Moran, N.; Tucker, J. H. R., *J. Org. Chem.* **2006,** *71*, 8523-8531.
18. Benesi, H. A.; Hildebrand, J. H., *J. Am. Chem. Soc.* **1949,** *71*, 2703-2707.
19. Silva, M.; Pombeiro, A. J. L.; Dasilva, J.; Herrmann, R.; Deus, N.; Castilho, T. J.; Silva, M., *J. Organomet. Chem.* **1991,** *421*, 75-90.
20. Emilia, M.; Silva, N.; Pombeiro, A. J. L.; Dasilva, J.; Herrmann, R.; Deus, N.; Bozak, R. E., *J. Organomet. Chem.* **1994,** *480*, 81-90.
21. Bard, A. J.; Faulkner, L. R., *Electrochemical Methods, Fundamentals and Applications*. Wiley, New York, 2001.
22. Randles, J. E. B., *Trans. Faraday Soc.* **1948,** *44*, 327-338.
23. Sevcik, A., *Collect. Czech. Chem.Commun.* **1948,** *13*, 349-377.
24. Ferguson, G.; Glidewell, C.; Opromolla, G.; Zakaria, C. M.; Zanello, P., *J. Organomet. Chem.* **1996,** *517*, 183-190.
25. Miller, S. R.; Gustowski, D. A.; Chen, Z. H.; Gokel, G. W.; Echegoyen, L.; Kaifer, A. E., *Anal. Chem.* **1988,** *60*, 2021-2024.

26. Amendola, V.; Boiocchi, M.; Colasson, B.; Fabbrizzi, L.; Monzani, E.; Douton-Rodriguez, M. J.; Spadini, C., *Inorg. Chem.* **2008,** *47*, 4808-4816.
27. Garcia, B.; Ortega, J. C., *J. Chem. Eng. Data* **1988,** *33*, 200-204.
28. Kyba, E. B.; Koga, J.; Sousa, L. R.; Siegel, M. G.; Cram, D. J., *J. Am. Chem. Soc.* **1973,** *95*, 2692-2693.
29. Cram, D. J., *Angew. Chem. Int. Ed. Engl.* **1986,** *25*, 1039-1057.
30. Greene, T. W.; Wuts, P. G. M., *Protective Groups in Organic Synthesis*. Wiley, New York, 1999.
31. Negishi, E.; King, A. O.; Okukado, N., *J. Org. Chem.* **1977,** *42*, 1821-1823.

CHAPTER 3: Ferrocenyl-based urea sensors onto gold surfaces

3.1 Introduction and aims of the studies

Redox active molecules can be functionalised with thiols or disulphides for assembly on the surface of gold electrodes, due to the strong affinity of sulphur for gold (homolytic bond strength of 44 kcal/mol).[1-2] They can spontaneously adsorb onto gold from solution to form a monolayer in which the tail groups point out of the surface.[3] The surface organisation of the monolayer is influenced by the anchoring group used: the angle between the surface and an alkyl chain terminating in a thiol tends to be different from that observed for an alkyl chain terminating in a chiral disulphide,[4] as shown in Figure 3.1.

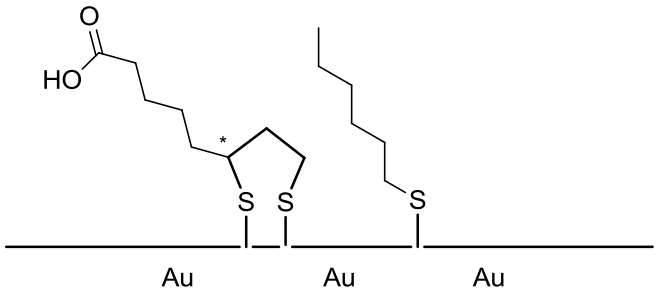

Figure 3.1: *Surface organisation of a chiral disulphide and a thiol anchored onto a surface.*

The packing can be governed by the length of the alkyl chain; every methylene group of the chain contributes to the stabilisation of the SAM by interacting through dispersion forces with the neighbouring molecules (1.4-1.8 kcal/mol for each methylene group).[5] However, if the chain is too long, the distance from the redox-active unit to the electrode surface would be too big for efficient electron transfer and the process would show irreversible behaviour due to slow electron transfer kinetics.[6] On the other hand, if the chain is short the formation of a well ordered monolayer would take a long time, due to the absence of the above mentioned interactions.[5, 7]

The time needed for the formation of well-packed monolayers varies between a few minutes[8] to many hours.[5] The self-assembled monolayer forms very rapidly on the surface but its reorganisation to a well-ordered structure usually needs long adsorption times.[9] However, the presence of extra functionalities on the molecules, such as groups that can form hydrogen bonds, can increase the interaction between neighbouring chains and form more compact monolayers with shorter adsorption times.[10]

The surface organisation can be characterised by cyclic voltammetry in the presence of a redox-active group at the end of the alkyl chain, after formation of a SAM on the surface of a gold electrode. Previous work in the Tucker group described the preparation and characterisation of SAMs on polycrystalline gold electrode using the isolipoic acid derivative **3.2**, obtained by reaction of the isolipoic acid **3.1** with the chiral ferrocenylamine **2.19**.[11] Isolipoic acid **3.1** was synthesised by Kevin Joly in the Moody Group at the University of Nottingham and it was chosen instead of the commercially available lipoic acid because of the absence of chirality, due to the prospect of future chiral sensing applications.

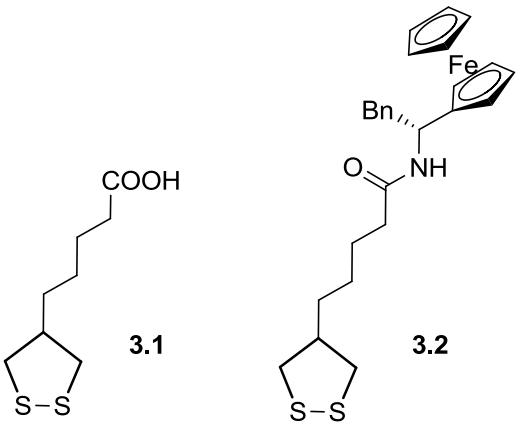

3.1 **3.2**

Scheme 3.1: *Structure of isolipoic acid* ***3.1*** *and the isolipoic acid derivative* ***3.2****.*[11]

Figure 3.2 shows CVs of the modified surface; the peak separation observed for oxidation and reduction peaks was 45 mV at 100 mV s^{-1}, therefore indicative of surface-bound species being lower than 59 mV.

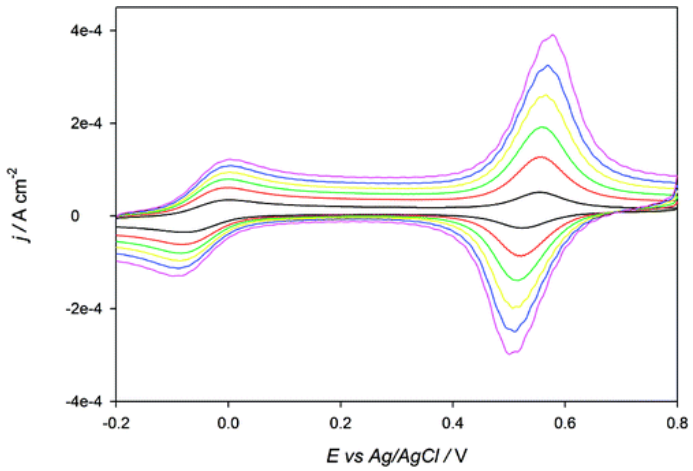

Figure 3.2: *CVs of disulphide* ***3.2*** *recorded in dichloromethane (0.1 M $TBAPF_6$ as the supporting electrolyte and dmfc as an internal reference) at various scan rates. (100, 300, 500, 704, 909, and 1111 mV s^{-1}, respectively black, red, green, yellow, blue, and pink.)*[11]

The sharp peaks observed were typical of attractive interactions between the neighbouring chains,[12-13] possibly due to dispersion interactions and formation of hydrogen bonds. Figure 3.3 shows that, as expected for surface-bound species, a direct proportionality between the peak current intensity and the scan rate was observed, rather than between the peak current and the root of the scan rate, which would be observed for free species in solution.

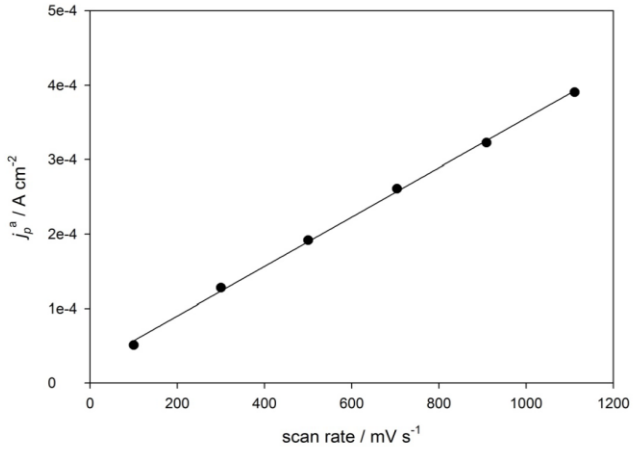

Figure 3.3*: Linear dependence of the peak current i_p^a on the scan rate for SAM of* ***3.2****.*[11]

This is because surface-bound molecules display diffusionless voltammetric behaviour, which does not follow the Randles-Sevcik[14-15] equation but instead equation 3.1:[16]

$$i_p = \frac{n^2F^2}{4RT}\nu A\Gamma \qquad \textbf{\textit{Equation 3.1}}$$

where:

i_p = peak current (A)

n = number of electrons transferred per molecule

F = Faraday constant

R = universal gas constant

T = temperature (K)

v = sweep rate (V/s)

A = electrode surface area (cm^2)

Γ = surface excess before the sweep

Ideally, due to the absence of diffusion, the peak potential for oxidation and reduction process should be the same and the voltammogram should be symmetrical, as shown in Figure 3.4, in which the voltammogram is depicted assuming no charging current is present.[17-18]

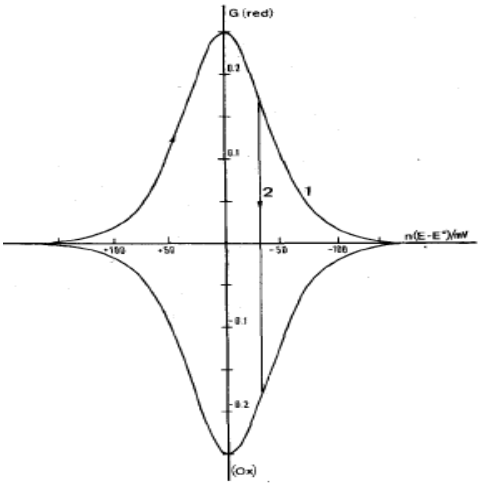

Figure 3.4: *Theoretical adsorption peaks. (1) The potential is reversed after the current has practically dropped to zero; (2) the potential is reversed along the peak.*[17]

However, a peak separation is observed as the scan rate increases, due to uncompensated Ohmic drop or slow electron transfer kinetics.[13, 19-20] A well-packed monolayer shows blocking properties towards ion penetration, which could account for this observation. In addition, diffusing redox-active species such as the internal reference dmfc give a peak separation larger than 59 mV.

The surface coverage of the monolayer can be calculated from the area under the oxidation wave of the cyclic voltammogram, which corresponds to the quantity of charge transfer occurring during the oxidation (expressed in Coulombs),[21] using equation 3.2:

$$\Gamma = \frac{Q}{nFA} \qquad \textbf{\textit{Equation 3.2}}$$

where:

Q = charge transfer (C)

n = number of electrons transferred per molecule

F = Faraday constant (96485.34 C mol^{-1})

A = electrode surface area (cm^2)

The theoretical value for a close-packed monolayer of molecules containing ferrocene can be calculated as 4.9 x 10^{-10} mol cm^{-2}, from the space occupied by the ferrocene groups (considered as spheres of diameter 0.66 nm).[22] If a higher value is observed this is not necessarily related to the formation of multilayers, but it can be ascribed to the roughness of the electrode surface, often higher than what an ideal perfectly smooth polycrystalline gold surface would be. The roughness of the surface can be evaluated *in situ* prior to any

experiment. This is done by analysis of the cyclic voltammogram obtained during the pre-treatment of the electrode by determination of the Au_2O_3 monolayer formed during the oxidation in aqueous solution of sulphuric acid 0.1 M (Figure 3.5).[23]

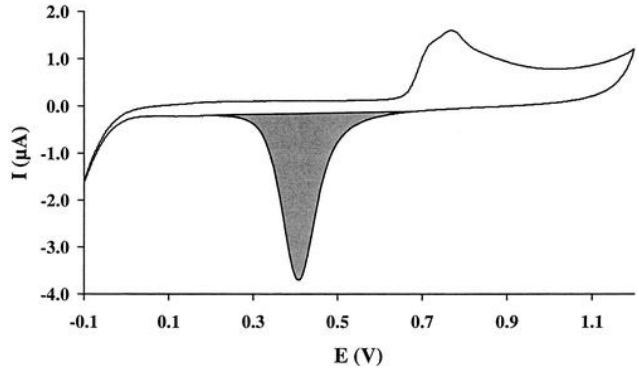

Figure 3.5: *Determination of the surface roughness of a gold electrode by integration of the gold oxide reduction peak in the cyclic voltammogram. (phosphate buffer pH 7.4; volume flow rate 0.1 mL min^{-1}; potential scan rate 50 mV s^{-1}).*[23]

It was calculated that the oxidation of the gold surface required a quantity of current of 482 µC cm^{-2}.[23] From this value it is possible to calculate the real surface area if the area under the sharp reduction peak observed in the voltammogram is known, as well as the geometrical area of the electrode. The ratio between the real area and the geometrical area is the roughness factor, which is usually higher than 1, and it is considered to be acceptable for the gold electrode surface when less than 2.[24]

As mentioned earlier, the shape of the voltammograms depends on the interactions between adjacent redox-active groups: attractive interactions are reflected in sharp, narrow peaks, whilst repulsive interactions generate broader and flatter peaks. If a spacer is added to separate the redox-active groups, different patterns may arise and this may affect the

shape of the voltammograms as well as the potential observed.[19, 25] Other than separating the electroactive units, the co-adsorption of spacers could give more accessibility to the binding sites of molecules designed for sensing purposes. These so-called mixed SAMs can be prepared by mixing the active molecule with a different terminated thiol or disulphide in the preparation solution[26-27] or by using two separate solutions and functionalising the electrode consecutively in both solutions (exchange method).[28] In the first case, several parameters need to be taken into account to choose the stoichiometry of the two molecules in the preparation solution: alkyl chains length,[29] mixing ratio in solution,[30] solubility in the chosen solvent[31] and the properties of the functional groups.[7] In the second case, the soaking time in each solution of the components is crucial, if they are prepared with the same concentration.[30] The displacement of the previously adsorbed component can happen if the replacing component has a stronger interaction with gold and if the kinetics of the displacement is favourable. In the case of thiols and disulphides the free energy of the interaction is about -6 and -14 kcal per S-Au bond, respectively.[32-33] Either way, the control over the formation of dispersed monolayers rather than domains of aggregation of the electroactive species is hard to obtain. Nevertheless, the formation of domains can be distinguished from well-dispersed organisation from the cyclic voltammograms: aggregations of redox-active species results in shoulder peaks, peak asymmetry or peak-broadening.[34-35] An example is given in Figure 3.6.

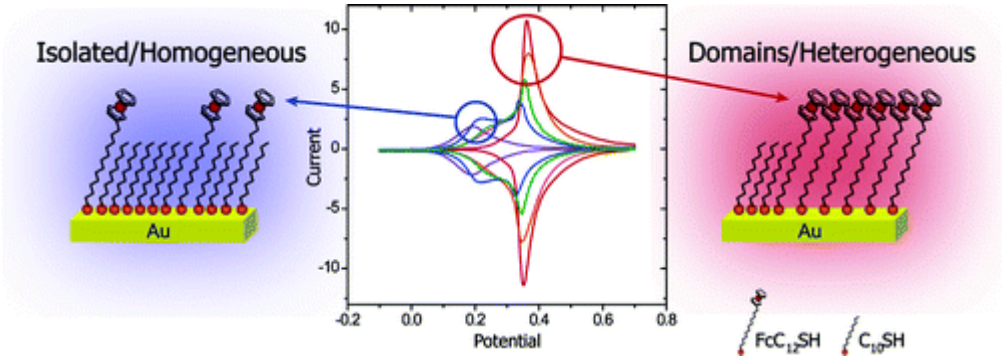

***Figure 3.6**: Cyclic voltammograms of binary SAMs formed from 2 mM ethanolic solutions containing various ratios of $C_{10}SH$ and $FcC_{12}SH$. Electrodes were incubated for at least 9 h at room temperature. CVs are measured in 1.0 M $HClO_4$, and the scan rate is 20 $mV \cdot s^{-1}$.*[35]

To avoid the formation of domains, a small molar fraction of the electroactive species is needed;[35] an alternative approach is to use a short soaking time in the case of sequential surface functionalisation.

The aim of the work described in this chapter is the development of a methodology to obtain reproducible formation of self-assembled monolayers on gold working electrode, for sensing applications. Chiral sensing was investigated, *via* SAMs of ferrocenyl functionalised disulphides, or mixed SAMs of the same disulphides with hexanethiol as a spacer. The isolipoic acid **3.1** was used in the synthesis of the disulphides **3.3-3.7**, in order to avoid an additional chiral centre respect to the one already present in proximity to the binding site. The behaviour of the resulting receptors was compared to that observed with the corresponding chiral lipoic acid derivatives **3.8** and **3.9**. The same chiral groups incorporated in some of the sensors studied in Chapter 2 were incorporated in the receptors, as shown in Figure 3.7.

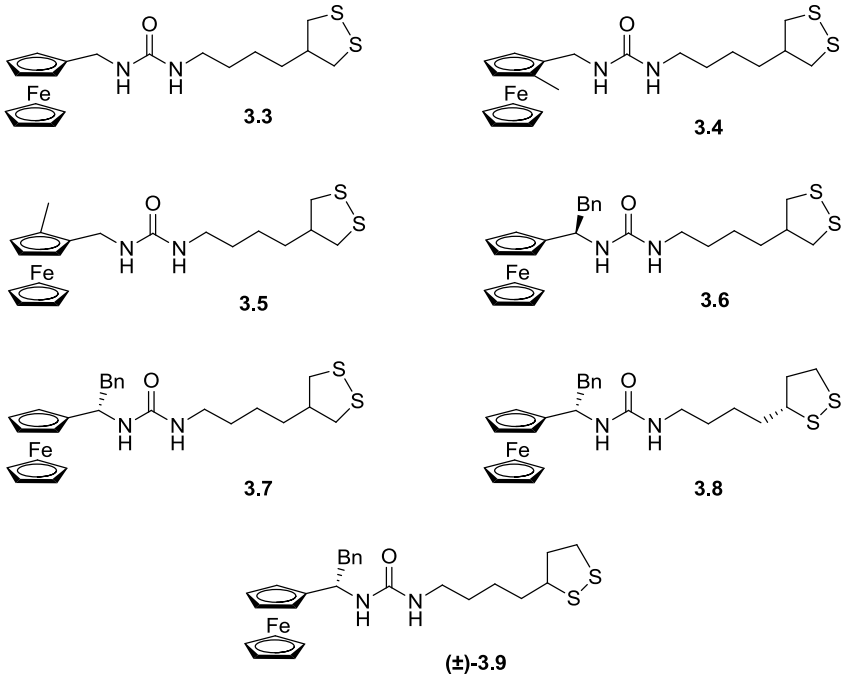

***Figure 3.7**: Redox-active receptors for self-assembled monolayers on gold surfaces. Receptors 3.7-3.9 were synthesised by Kevin Joly in the Moody group at the University of Nottingham.*

The binding affinities were investigated using the same carboxylate anions (**2.3**-**2.5**) used in the studies described in Chapter 2, in order to compare the results in solution with those on functionalised surfaces. The interactions were studied by cyclic voltammetry and square wave voltammetry and the surface organisation was investigated by ellipsometry and atomic force microscopy (AFM).

3.2 Synthesis of the receptors

The synthesis of the isolipoic acid **3.1** was performed by Kevin Joly in the Moody group at the University of Nottingham. The synthesis of this molecule had been previously published but it appeared to be long and troublesome.[36] Therefore, Joly altered the synthetic route to the multi-step procedure shown in Scheme 3.2.[11]

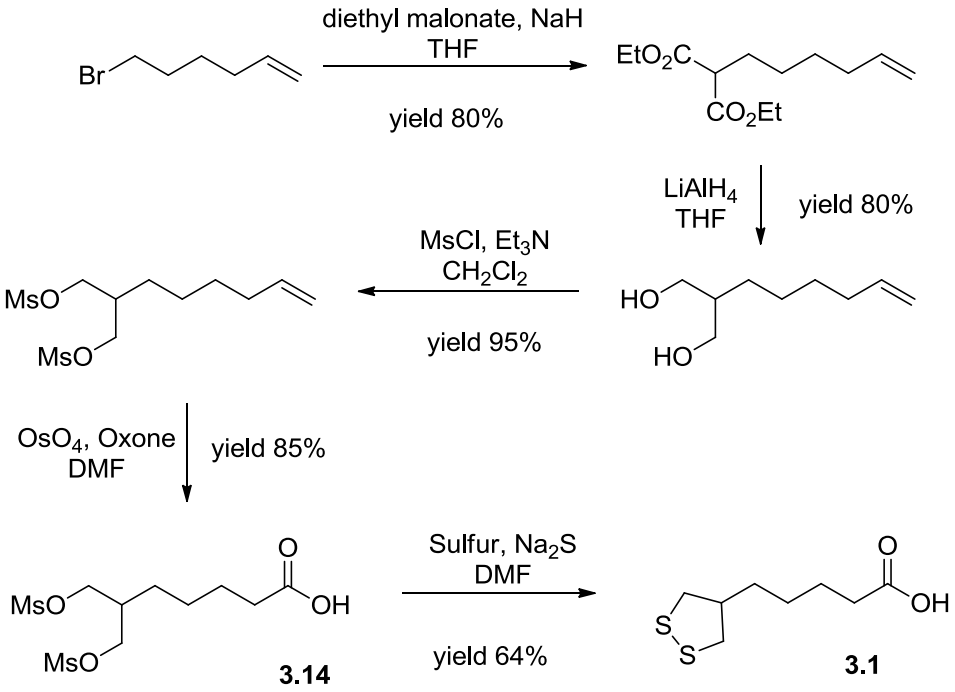

Scheme 3.2: *Synthesis of isolipoic acid* ***3.1.***

The synthesis involved a nucleophilic substitution on 6-bromo-1-hexene by diethyl malonate in the presence of sodium hydride. The resulting malonate was reduced to the corresponding diol using lithium aluminium hydride. The diol was then protected as a mesylate and the double bond was oxidised to a carboxylic acid using oxone and osmium tetraoxide. The intermediate **3.14** obtained was stored before being converted to disulphide, given the poor stability of **3.1**. The synthesis of **3.1** was then performed by reaction of the mesylated diol **3.14** with sulphur and sodium sulphide hydrate in DMF to obtain the disulphide functionality. The limiting factor in the yield of the reaction was found in the extraction from DMF, given the high solubility of the compound in this solvent.

The central chiral amine was synthesised following the multi-step synthesis described below. The chiral auxiliary (*S*)-*N*-(1-phenylbutoxy)-phtalimide **3.10** was obtained *via* Mitsunobu reaction between *N*-hydroxyphthalimide and (*R*)-1-phenylbutanol (Scheme 3.3).[37]

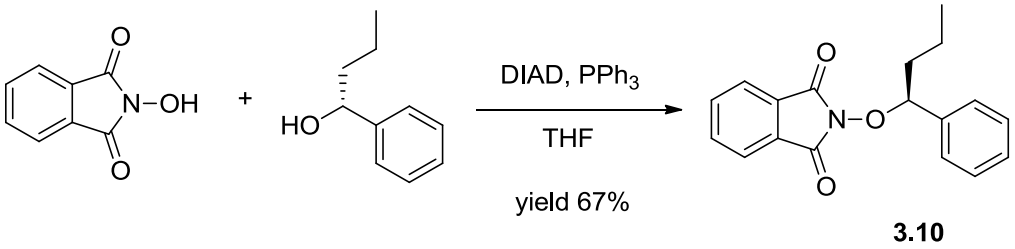

Scheme 3.3: *Synthesis of the chiral auxiliary* ***3.10****.*

This reaction proceeded with inversion of configuration of the alcohol. The chiral auxiliary was then reacted with hydrazine, forming *in situ* the activated (*S*)-1-phenyl-butanoxyamine, which was subsequently reacted with ferrocenecarboxaldehyde to give the chiral oxime ether **3.11** (Scheme 3.4).[38]

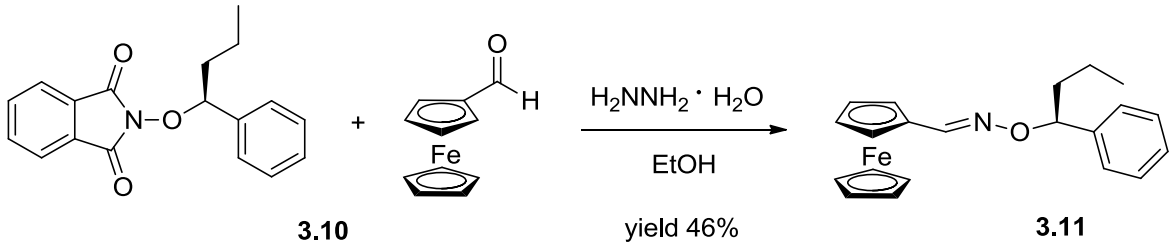

Scheme 3.4: *Synthesis of the chiral oxime* ***3.11****.*

The chiral oxime was reacted with benzyl magnesium chloride in the presence of boron trifluoride diethyl etherate at -78°C to obtain the *N*-alkoxylamine **3.12** *via* stereoselective

nucleophilic addition of the Grignard reagent (scheme 3.5).[39] The diastereomeric excess was calculated by integration of the ^{1}H NMR peaks.

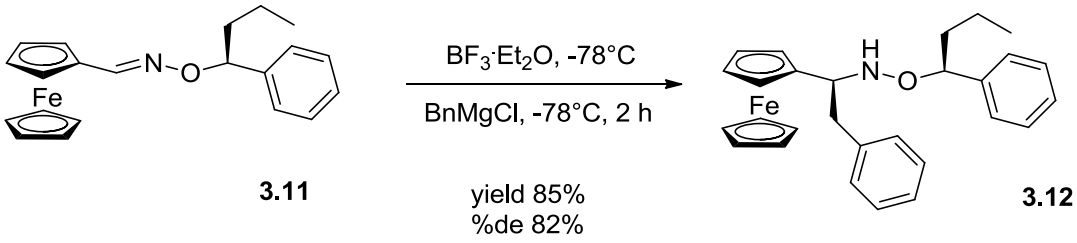

Scheme 3.5: *Synthesis of the chiral* N-*alkoxyamine* ***3.12****.*

Cleavage of the N-O bond was obtained by reduction with zinc dust, after dissolution in a minimum amount of THF and addition of a mixture of 1:1 acetic acid/water. The reaction mixture was left in a sonic bath at 40°C for 6 hours to obtain the crude amine **3.13**, which was purified by column chromatography (Scheme 3.6).[39]

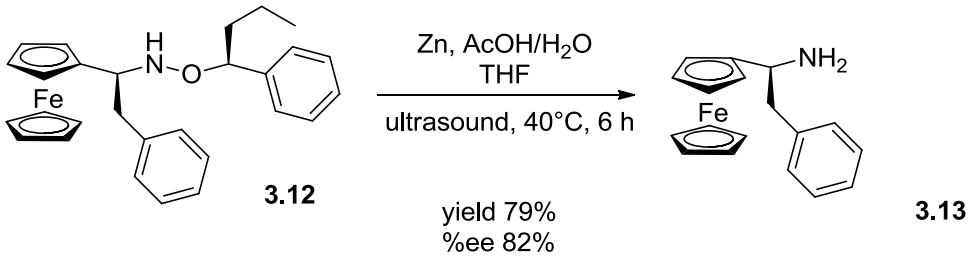

Scheme 3.6*: Synthesis of (S)-1-ferrocenyl-2-phenyl-ethylamine* ***3.13****.*

3.1 was then assembled with the achiral amine **2.12**, planar chiral amine synthons **2.17** and **2.18** and with the central chiral amine **3.13**, to prepare receptors **3.3-3.6**. Receptors **3.7-3.9** were synthesised in Nottingham using the central chiral amine of opposite chirality and reacting it with, respectively, **3.1**, (*R*)-lipoic acid and (±)-lipoic acid. All these reactions were performed by introduction of a nitrogen atom through a Curtius rearrangement strategy,[40]

to obtain a highly reactive isocyanate, which was reacted *in situ* with the desired amine *via* the same reaction described in Scheme 2.1, to obtain the ferrocenyl urea (the example for the synthesis of **3.3** is shown in Scheme 3.7).

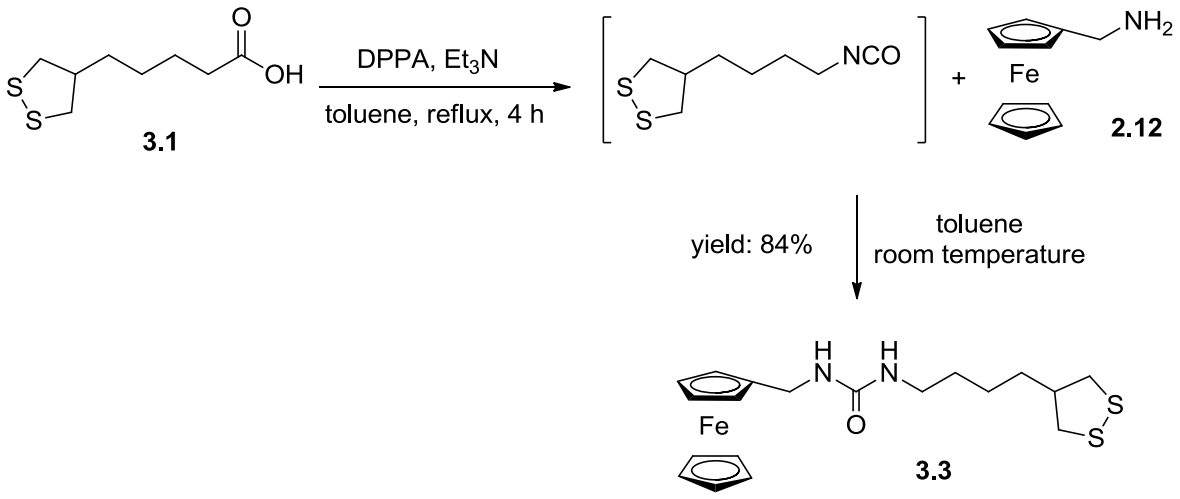

Scheme 3.7: *Synthesis of the ferrocenyl-urea disulphide derivative* ***3.3****.*

The desired receptors were obtained in acceptable yield (49-84%) and good enantiomeric excess (≈94% for the planar chiral receptors, 82-89% for the centrally chiral receptors, as shown by chiral HPLC). The centrally chiral receptors gave lower enantiomeric excesses than the planar chiral receptors but they were used nonetheless for attempts at chiral sensing. If any chiral sensing was observed, it would be considered as a less than optimum result than that obtained with an enantiopure receptor.

3.3 SAM preparation

Only one polycrystalline gold electrode was used, in order to avoid the complication of having different surfaces to deal with. Before monolayer formation, the gold electrode was polished following the procedure described in Section 6.4.2. The use of abrasive microcloth pad and diamond solution was used only if the roughness factor calculated was above 2 and the roughness of the surface needed to be decreased. The SAMs were prepared by soaking the electrode in the dark and at room temperature in a 1.5 mM solution of the receptor in dry CH_2Cl_2 for a variable time of 5 minutes for the achiral receptor, 30 minutes for the planar chiral receptors and 2 hours for the centrally chiral receptors.

For the preparation of mixed monolayers it was decided to opt for an exchange method in order to have more accurate control over the surface coverage of the electroactive species. Moreover, this procedure is less explored than the one with a single preparation solution and, to the best of our knowledge, relatively few examples of mixed SAMs formed with this method are present in the literature.[28, 41-42] Mixed monolayers were prepared by soaking the electrode in a 1.5 mM solution of hexanethiol in dry CH_2Cl_2 overnight, rinsing the electrode with dry CH_2Cl_2 to wash away the excess of unbound thiol and then soaking it in a 1.5 mM solution of the receptor in dry CH_2Cl_2 for a variable time of 5 minutes for the achiral receptor, 20 minutes for the planar chiral receptors and 30 minutes for the centrally chiral receptors. Upon removal from the preparation solution, the electrode was thoroughly rinsed with CH_2Cl_2 to remove any excess unbound receptor.

The samples for ellipsometry and AFM were prepared using commercially available plates of approximately 1 cm^2 area of 100 nm thick gold on silicon wafer. These were washed with EtOH, dried with a stream of nitrogen and cleaned by treatment with UV/ozone, and then immersed in the same 1.5 mM solutions for the same times as for the functionalisation of the gold electrode used in the electrochemical studies. Upon removal from the preparation solution, the plates were thoroughly rinsed with CH_2Cl_2 to remove the excess of unbound molecules.

3.4 Electrochemical Studies

3.4.1 Single component SAMs

At first, single component SAMs, *i.e.* those containing no other thiol diluent, were prepared and studied, as described below.

3.4.1.1 SAMs of free receptors

The voltammetric behaviour of SAMs of the free receptors was investigated by cyclic voltammetry in dry dichloromethane with tetrabutylammonium hexafluorophosphate ($TBAPF_6$) at room temperature with addition of decamethylferrocene (dmfc).

The scan rate dependence was studied varying the scan rate between 100 and 1100 mV s^{-1} and the reversibility of the systems was investigated by plotting the peak current intensity observed against the scan rate. The results for **3.3** are shown in Figure 3.8.

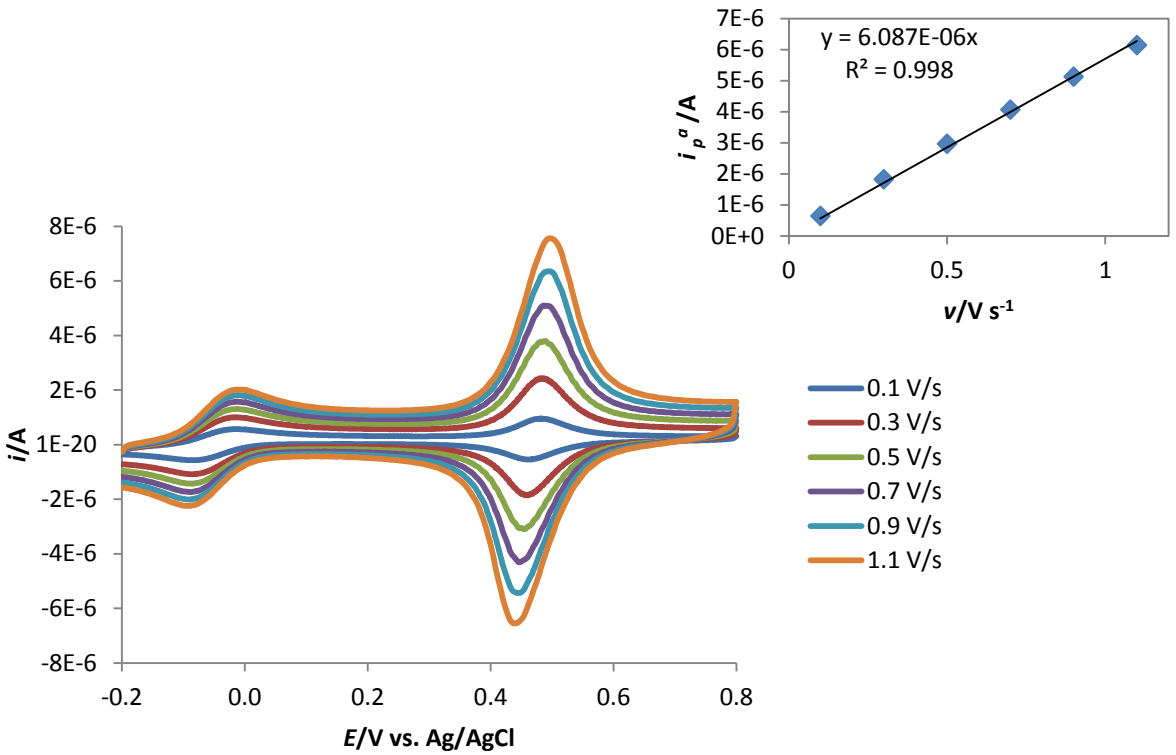

Figure 3.8: *CVs at various scan rates for* ***3.3*** *in dry CH_2Cl_2, 0.1 M $TBAPF_6$ with dmfc at rt. Inset: plot of anodic peak height against scan rate.*

It was verified that the peak current intensity was directly proportional to the scan rate, typical for surface-bound species, rather than the square root of the scan rate, typical for diffusive species in solution. The oxidation peak and the reduction peak are symmetrical and the separation between the two is smaller than 59 mV, as expected for surface-bound species. This peak separation increases together with the scan rate, due to slow electron transfer kinetics. The separation between oxidation and reduction peak of the decamethylferrocene internal reference is also bigger than 59 mV: this suggests the formation of a well-packed SAM with good blocking properties towards the migration of species in solution towards the electrode surface.[16] The regular shape of the redox waves suggests that the surface organisation is uniform and the SAM is structured as a uniform

phase on the gold surface. The value of i_p^a/i_p^c was close to 1, a sign of reversible redox behaviour.[16]

The surface coverage was calculated from the area below the oxidation peak of the voltammogram, as described in Section 3.1. The typical values observed using the different receptors are reported in Table 3.1, together with the formal electrode potentials recorded for the SAMs and the standard deviation associated, at room temperature in dry CH_2Cl_2. Values with standard deviation are reported, recorded over an average of 20 experiments.

Table 3.1: *Formal electrode potentials (mV ± σ) versus dmfc and surface coverage of SAMs of the different receptors (± σ) in CH_2Cl_2 at rt in the presence of $TBAPF_6$ 0.1 M. The potential of* ***3.9*** *in solution is reported vs. dmfc using a Pt WE. (2.2 – 3.1 x 10^{-4} M in dry CH_2Cl_2 in the presence of 0.1 M $TBAPF_6$ at rt.)*

Receptor	$E^{o'}$/mV vs. dmfc	Γ/ x 10^{-10} mol cm^{-2}
3.3	468 ± 5	4.2 ± 0.6
3.4	426 ± 4	4.3 ± 0.5
3.5	423 ± 4	4.1 ± 0.4
3.6	519 ± 5	4.4 ± 0.3
3.7	517 ± 7	4.6 ± 0.3
3.8	512 ± 9	4.4 ± 0.4
3.9	515 ± 2	4.3 ± 0.6
3.9 in solution	491 ± 2	---

Depending on the experiment, the surface coverage obtained is near the ideal value for a closely packed self-assembled monolayer (4.90 x 10^{-10} mol cm^{-2}),[43] although this was hard to reproduce under the same experimental conditions, given the large range of coverages observed. Also the range of formal electrode potentials observed for each receptor varied significantly in each experiment, most likely because of the different extent of the

interactions between neighbouring electroactive molecules. The formal electrode potentials were similar for receptors **3.3** and **3.6-3.9**, but they were significantly lower for receptors **3.4-3.5**. This is because of the effect of the methyl substituent on the cyclopentadienyl ring, which pushes electron density onto the redox centre, stabilising the higher oxidation state and making the molecule thermodynamically easier to oxidise.[44-45] The same trend was observed for the solution studies described in Chapter 2. However, there is also the influence of a surface effect to be taken into account and although the trend is the same, the potentials of **3.3-3.5** are lower than those observed for comparable species in solution (see Table 2.6). On the other hand, this effect is almost negligible for the hosts **3.6-3.9**, which in fact show slightly more positive values when incorporated on the surface than when studied in solution in the same solvent, although with a different working electrode. This could be related to a proximity effect of nearby ionisable units.[46] The lower values for **3.3**-**3.5** are possibly due to the formation of hydrogen bonding between neighbouring molecules in the SAM,[22] (Figure 3.9) which may be less effective in the presence of bulky groups such as benzyl.

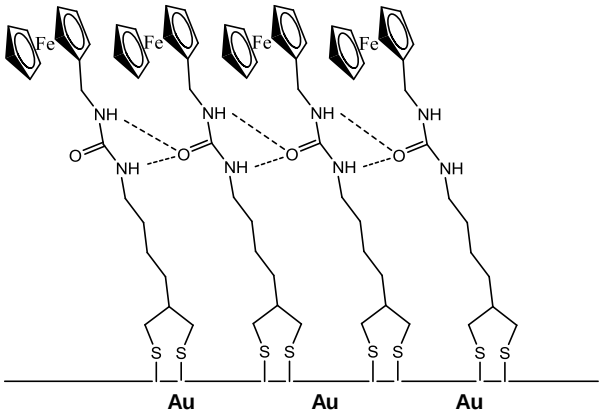

Figure 3.9: *Proposed formation of extensive hydrogen bonding in a SAM of* ***3.3****.*

3.4.1.2 Addition of guests to the SAMs

The receptors were titrated with aliquots from a solution of each guest **2.3-2.5** (0.02 M) and the shift in the ferrocene-centred redox wave of the receptor monitored. Typical results are provided in Figure 3.10.

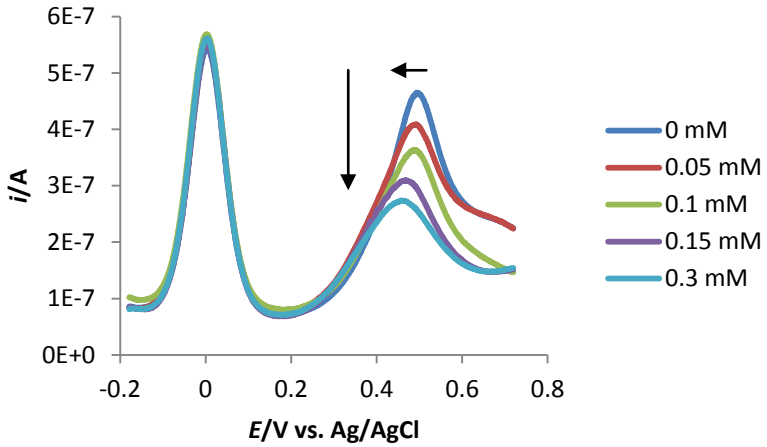

Figure 3.10: *Typical series of square wave voltammograms, for the addition of* (R)-***2.5*** *(0.02 M) to* ***3.6*** *in dry CH_2Cl_2 with 0.1 M $TBAPF_6$ in the presence of dmfc at rt.*

In each case, two effects were observed: firstly, the peak shifted towards less positive potentials because of the negative charge of the anions pushing electron density towards the redox centre and making it thermodynamically easier to oxidise; secondly, the current intensity decreased significantly upon each guest addition because of a loss of electroactivity. This last phenomenon is possibly due to the nucleophilicity of the anions in solution; other examples are present in literature of a decrease in the electroactivity of the ferrocene units after addition of anions such as chloride, benzoate and dihydrogen phosphate.[22, 47-48] Control studies in the absence of the receptors revealed that the guests displayed no redox activity in regions where complexation-induced shifts in potential were

observed. Additions were continued until a near-limiting value of potential shift was observed. This choice was made in order to avoid the addition of too large an excess of anions, which would cause a large decrease in the electroactivity of the SAM. The values observed for a concentration of guest of 0.3 mM by SWV are reported in Table 3.2, together with the standard deviation associated. The values were recorded over typically 3 experiments. If deviations are not reported only a single experiment was performed, as a control. In all cases, one-wave behaviour was observed.

Table 3.2: *Shift in the formal electrode potentials $\Delta E^{\circ\prime}$ (mV ± σ) of the receptors upon addition of the guests* ***2.3-2.5*** *(0.3 mM) in dry CH_2Cl_2 in the presence of dmfc at rt.*

Receptor	*(S)*-**2.3**	*(R)*-**2.3**	*(S)*-**2.4**	*(R)*-**2.4**	*(S)*-**2.5**	*(R)*-**2.5**
3.3	-37 ± 7	-38 ± 9	-37 ± 3	-39 ± 5	-46 ± 4	-47 ± 5
3.4	-32 ± 3	-28 ± 4	-29 ± 11	-27 ± 7	-34 ± 7	-30 ± 5
3.5	-22	-24	-19	-20	-30	-26
3.6	-41 ± 10	-39 ± 9	-34 ± 9	-36 ± 8	-55 ± 18	-48 ± 16
3.7	-37 ± 4	-42 ± 2	-34 ± 10	-28 ± 4	-51 ± 14	-52 ± 10
3.8	-38 ± 2	-38 ± 12	-28 ± 7	-34 ± 6	-46 ± 10	-37 ± 12
3.9	-28	-30	-24	-25	-42	-36

From analysis of the values in Table 3.2 it can be inferred how the variation in the shift is too large to draw conclusions about the sensing. However, it is evident how the $\Delta E^{\circ\prime}$ values are generally smaller than those recorded for similar receptors in solution (see Table 2.7). Most likely this is due to the poor accessibility of the binding site when the receptors are closely packed in the self-assembled monolayer, which would prevent full occupation of the binding sites (Figure 3.11) in the case of the achiral and planar chiral receptors, or to the presence of the bulky groups blocking the access to the binding sites in the case of the centrally chiral receptors.

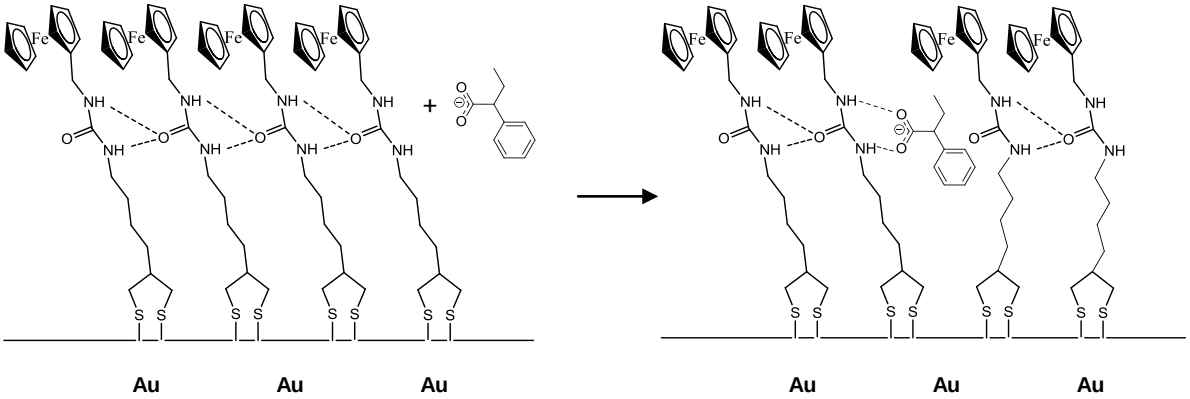

Figure 3.11: *Proposed binding of guest* ***2.3*** *to a SAM of* ***3.3****.*

Moreover, from the proposed binding in Figure 3.11 it is possible to imagine how the binding of the guest would disrupt the organisation of the SAM. This could give an explanation for the wide potential shift ranges observed upon addition of the guests, which is largely affected by structural differences in the organisation of the SAMs, which also relates to how the initial potential is affected by the surface organisation (Table 3.1).

Titrations were used in an attempt to determine any chiral sensing effects. The observed shift in electrode potential was evaluated for the addition of each aliquot of enantiomer and plotted against guest concentration. An example for **3.9** is provided in Figure 3.12.

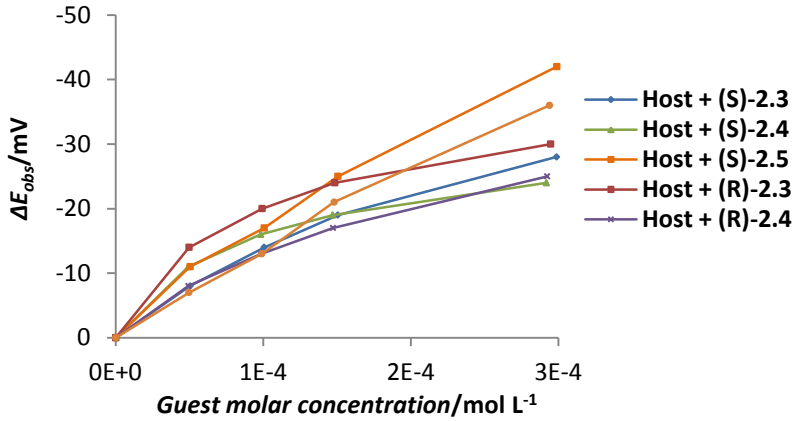

Figure 3.12: *Values of* ΔE_{obs} *for* ***3.9*** *upon addition of the different guests (guests 0.02 M in* CH_2Cl_2*, with* $TBAPF_6$ *0.1 M and dmfc at rt).*

From analysis of Figure 3.12 and given the large variation in the observed shifts (Table 3.2), it is clear that the receptors on the surface are not able to discriminate between different enantiomers of the same guest, or even different guests, which was possible at least for the receptors in solution (see Chapter 2). This second aspect can be seen in Figure 3.13. The reason is likely to be the difficulty in reproducing exactly the same surface organisation in each experiment. This overrides any small differences in effects due to complexation previously observed for receptors in solution.

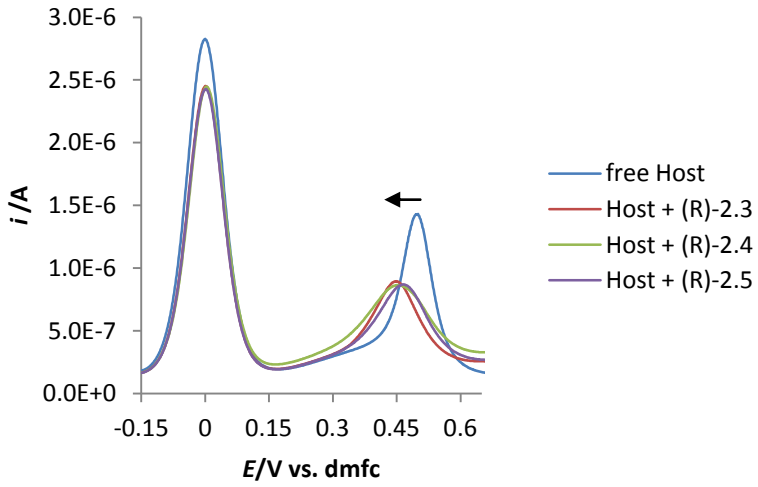

Figure 3.13: *SWVs of a SAM of* ***3.7*** *before and after addition of guests* ***2.3-2.5*** *(added as* TBA^+ *salts in dry* CH_2Cl_2*, 3 x* 10^{-4} *M, with 0.1 M* $TBAPF_6$ *and dmfc at rt.)*

This issue was further investigated by examining the different shape of voltammograms observed in repeated experiments; it was found that peaks could be narrow and tall or broad and short and still correspond to the same surface coverage (Figure 3.14).

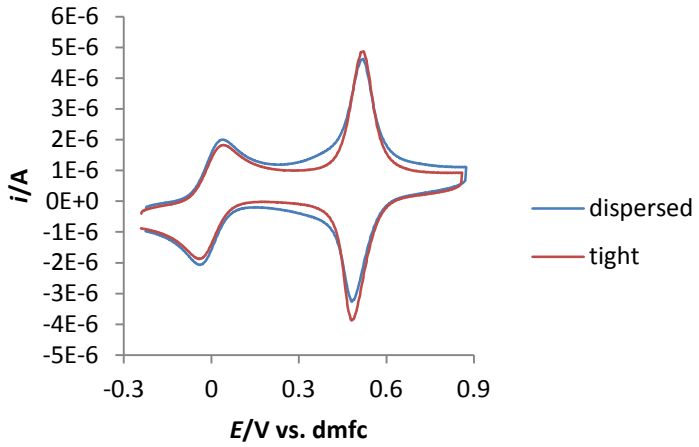

Figure 3.14: *Cyclic voltammograms of SAMs of* ***3.3*** *with the same surface coverage but with different wave shapes, corresponding to different surface organisation (in dry CH_2Cl_2, 0.1 M $TBAPF_6$, in the presence of dmfc at rt.)*

As described earlier, the shape of the peaks is determined by interactions between neighbouring electroactive units.[11] The disulphide receptors can be assembled in domains rather than in a more dispersed and homogenous structure.[49] The latter corresponds to a situation in which the interaction between neighbouring ferrocene moieties is weak, and the peaks in the voltammogram are broad. The former is reflected in sharper peaks but with a certain degree of asymmetry because two different situations are present at the same time: the ferrocene groups within the domain are strongly interacting with each other but the ones in the edges will be lacking such interaction and will possess different voltammetric behaviour.[35, 43] This hypothesis was supported by the images recorded with AFM (see Section 3.5). When the SAM is organised in domains, presumably only the binding sites on the edges of the domain will preferentially bind the guest and the shift in the redox potential of the ferrocene will be minimal. However, when the SAM is organised in a more dispersed way, more of the receptors on the surface might be expected to more readily bind the guests and therefore the shift in the redox potential would be considerably larger.

The difficulties in obtaining reproducibility in the organisation of the SAMs under the same preparation conditions (*i.e.* same electrode and same soaking time in the same receptor solution) can be related to the changes in the atomic scale defects on the surface of the polycrystalline gold electrode upon polishing between each experiment. This is usually overcome by good packing homogeneity in SAMs formed by simple molecules such as alkylthiols. In more complex molecules, with bulky groups protruding from the alkylic chain, reproducibility would appear to be harder to obtain.

3.4.1.3 Receptors stability and SAMs re-usage

The receptors showed good stability in CH_2Cl_2 solution. The CVs of SAMs formed from a fresh preparation solution or from the same solution 2 months after preparation showed no significant difference (an example for receptor **3.7** is provided in Figure 3.15).

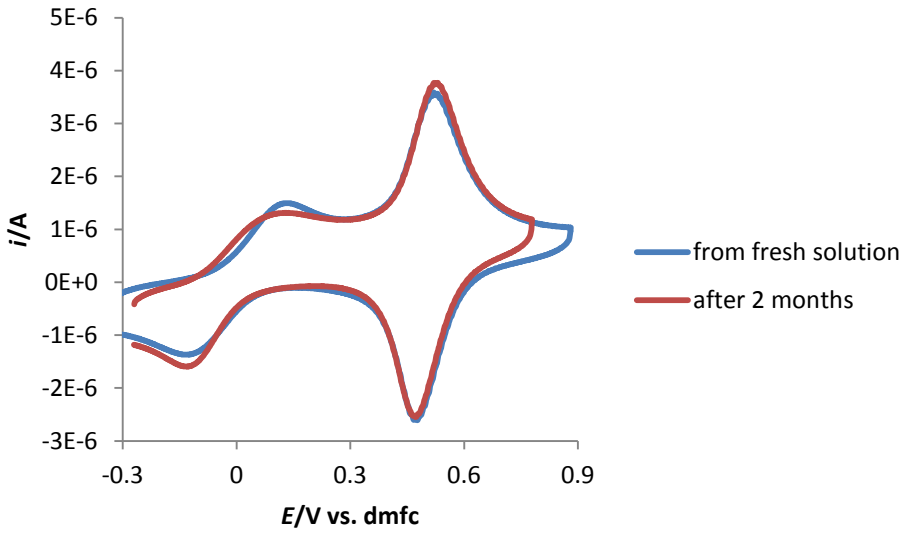

Figure 3.15: *Cyclic voltammograms of SAMs of* ***3.7*** *formed from a fresh solution or from the same solution 2 months after preparation (in dry CH_2Cl_2, 0.1 M $TBAPF_6$, in the presence of dmfc at rt.)*

It was decided to test the re-usage of the SAMs of the receptors. After washing the working electrode surface with a gentle stream of CH_2Cl_2, CV and SWV scans revealed that the potential recorded in a fresh solution in the absence of guest was the same as before the binding experiment, although with a significantly reduced current intensity. However, upon re-addition of the same guest under the same conditions, the negative potential shift observed was not reproducible and so the same functionalised electrode could not be re-used. Attempts to re-functionalise the same electrode without polishing were unsuccessful: this phenomenon could be explained by the absence of free gold surface for the disulphide molecules to self-assemble. Therefore, the decreased current intensity could be explained by degradation of individual molecules within the SAM through loss of electroactive species, as described in Section 3.4.1.2.[22, 47-48]

3.4.2 Mixed SAMs

3.4.2.1 SAMs of free receptors

As described above, the lack of discrimination due to the surface effects overriding the sensing effects made it difficult to use single component SAMs as sensors. Therefore attention was focused on the formation of mixed monolayers, with the idea of improving the dispersion of the receptors on the surface by minimising the intermolecular hydrogen-bonding and thus making the binding sites more accessible, for a more reproducible sensing platform. Hexanethiol was used to dilute the disulphide receptors, as in several examples already present in the literature.[28, 50-54] However, for sensing purposes, it was also chosen with the idea that the chain was short enough to avoid hindrance to the binding sites of the

receptors so that the binding event would not have a big influence on the SAM organisation, as depicted schematically in Figure 3.16.

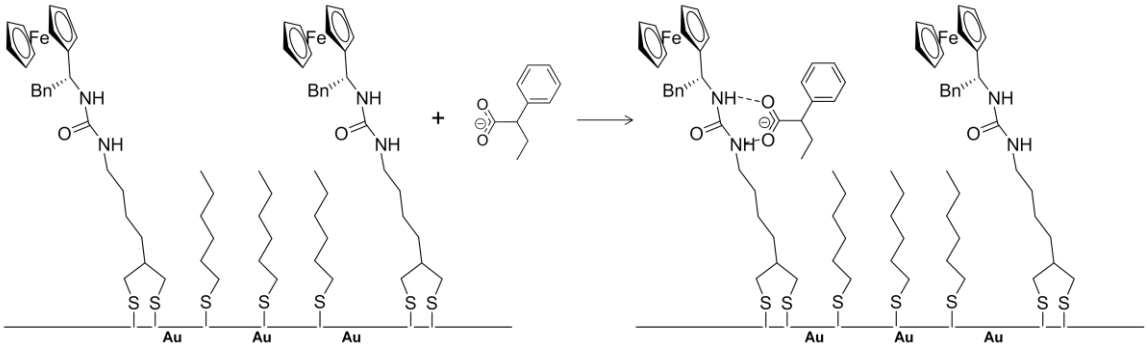

Figure 3.16: *Proposed binding of guest **2.3** in a mixed SAM of hexanethiol and **3.7**.*

Moreover, the adsorption of thiols is thermodynamically unfavoured in comparison with the adsorption of disulphides,[32] which would make possible the use of an exchange method for the formation of the mixed monolayers. Thus, a monolayer of thiol was formed during a long soaking time, in order to obtain a uniform SAM, and then a small part of it was replaced with the disulphides by soaking the electrode in the receptor solution for a short time. The voltammetric behaviour of mixed SAMs of the free receptors was investigated by cyclic voltammetry in dry CH_2Cl_2 with $TBAPF_6$ at room temperature in the presence of dmfc. The scan rate dependence was studied, varying the scan rate between 50 and 1100 mV s^{-1} and the reversibility of the systems was investigated by plotting the peak current intensity observed against the scan rate. An example for **3.3** is given in Figure 3.17.

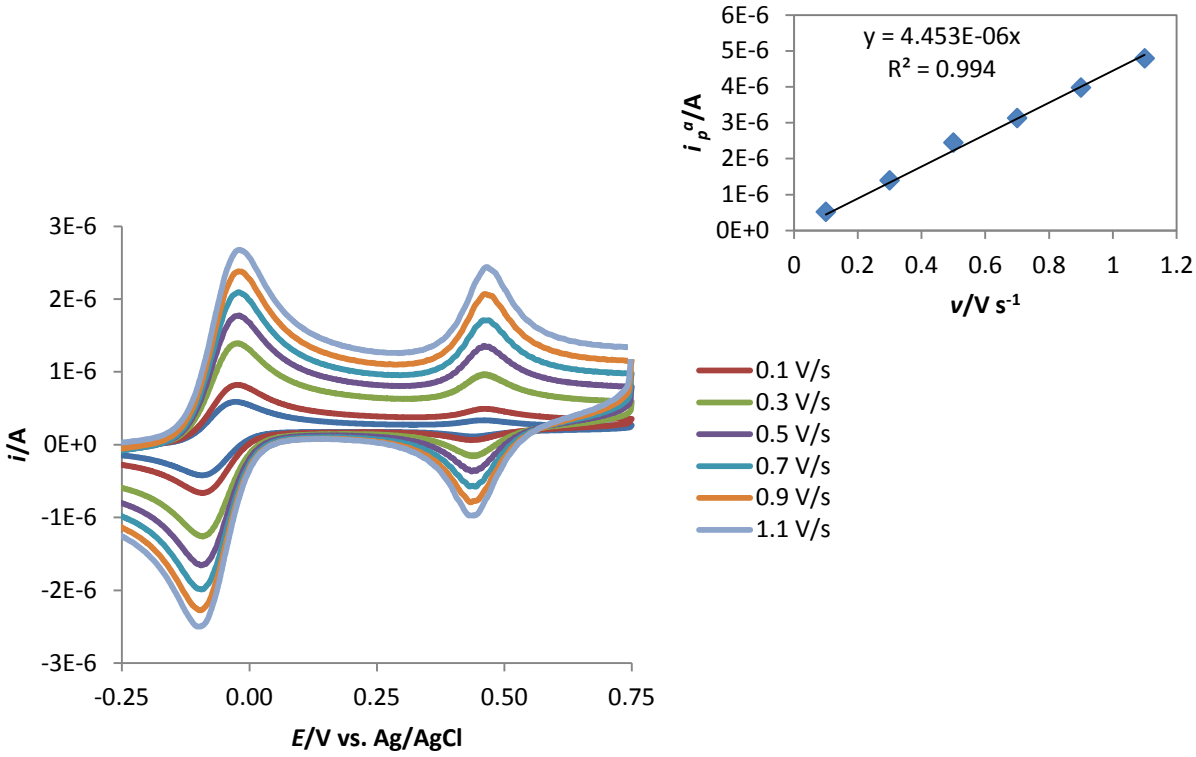

Figure 3.17: *CVs at various scan rates for a mixed SAM of* ***3.3*** *in dry CH_2Cl_2, 0.1 M $TBAPF_6$ with dmfc at rt. Inset: plot of anodic peak height against scan rate.*

It was verified that the peak current intensity was directly proportional to the scan rate. The capacitance observed was similar to that observed for single component SAMs (Figure 3.8), as expected for a closely packed monolayer. However, the peak intensity relative to the electroactive surface-bound species was smaller, as was the surface coverage calculated using the area below the oxidation peak and reported in Table 3.3. Moreover, the peaks were short and broad, as expected for a system with low interaction between neighbouring electroactive species and with a good dispersion of the receptors. The separation between oxidation and reduction peaks was less than 59 mV at all scan rates (24 to 29 mV), as expected for surface-bound species, and the peak separation for the dmfc was as large as in the more packed single component SAM shown in Figure 3.8, as expected for a fully covered electrode surface. The value of i_p^a/i_p^c was close to 1, a sign of reversible redox behaviour.[16]

The formal electrode potentials recorded for the mixed SAMs at room temperature in dry CH_2Cl_2 are reported in Table 3.3, together with the surface coverage obtained in the different experiments and the formal potential observed for the single component SAMs, with the standard deviation associated. Ranges were recorded over an average of 20 experiments.

Table 3.3: *Formal electrode potentials (mV ± σ) versus dmfc and range of surface coverage of mixed SAMs of the different receptors (± σ) in CH_2Cl_2 at rt in the presence of $TBAPF_6$ 0.1 M.*

Receptor	$E^{o'}$ single component /mV vs. dmfc	$E^{o'}$ mixed SAM /mV vs. dmfc	Γ/ x 10^{-10} mol cm^{-2}
3.3	468 ± 5	505 ± 4	1.2 ± 0.6
3.4	426 ± 4	468 ± 4	1.3 ± 0.3
3.5	423 ± 4	460 ± 7	1.9 ± 0.4
3.6	519 ± 5	517 ± 3	1.3 ± 0.6
3.7	517 ± 7	511 ± 3	1.2 ± 0.5
3.8	512 ± 9	512 ± 7	1.9 ± 0.3
3.9	515 ± 2	512 ± 10	1.7 ± 0.6

The surface coverage of the electroactive molecules was lower than for the single component SAMs whose values are reported in Table 3.1. This is because a short soaking time was chosen for the replacement of the hexanethiol with the disulphide receptors. This soaking time was varied between 5 and 30 minutes, depending on the receptor (see Section 3.3), in order to get an optimum surface coverage of *ca.* 1 x 10^{-10}, which corresponds to 1/5 of the surface coverage for a closely packed monolayer of ferrocenyl receptors. The formal electrode potentials are similar for receptors **3.3** and **3.6-3.9** but lower for receptors **3.4-3.5**, as also observed for the single component systems. However, for the mixed SAMs of receptors **3.3-3.5** the values are higher than those for the single component systems and are also more similar to the ones observed in comparable species in solution (see Table 2.6). This

is because the surface influence on the formal electrode potential is negligible, most likely due to the absence of hydrogen bonding between neighbouring urea units in the SAMs,[22] due to the spacing effect of the hexanthiol molecules.

3.4.2.2 Addition of guests to the SAMs

The receptors were titrated with aliquots of a solution of each guest **2.3-2.5** (0.02 M) and the shift in the ferrocene-centred redox wave of the receptor monitored. Shifts occurred towards less positive potentials, as previously described (Figure 3.10), and the shifts at a guest concentration of 0.03 mM are reported in Table 3.4, together with the associated standard deviation. Ranges were recorded over an average of 3 experiments. If deviations are not reported only a single experiment was performed.

Table 3.4: *Shift in the formal electrode potentials $\Delta E^{\circ\prime}$ (mV ± σ) of the mixed SAMs of the receptors upon addition of guests* ***2.3-2.5*** *(0.3 mM) in CH_2Cl_2 at rt in the presence of dmfc.*

Receptor	*(S)*-**2.3**	*(R)*-**2.3**	*(S)*-**2.4**	*(R)*-**2.4**	*(S)*-**2.5**	*(R)*-**2.5**
3.3	-58 ± 6	-67 ± 7	-28 ± 5	-26 ± 4	-58 ± 5	-52 ± 3
3.5	-109	-114	-59	-68	-81	-76
3.7	-134 ± 5	-126 ± 8	-29 ± 6	-32 ± 9	-85 ± 9	-87 ± 6
3.8	-139	-148	-62	-64	-73	-65

It was observed that, despite differences in the surface coverage, the reproducibility of the sensing was better than that achieved with single component SAMs: this is most likely due to a more uniform and more reproducible surface organisation, with a good dispersion of the receptors on the electrode surface. This hypothesis was supported by the images recorded with AFM (see Section 3.5). The values reported in the table above are representative of the

full shift for the formation of the host/guest complexes. This can be assumed from analysis of the plots of the observed shift against guest concentration, in which the curves start to tail off before the guest concentration reaches a value of 0.03 mmol L^{-1}, shown in Figure 3.18.

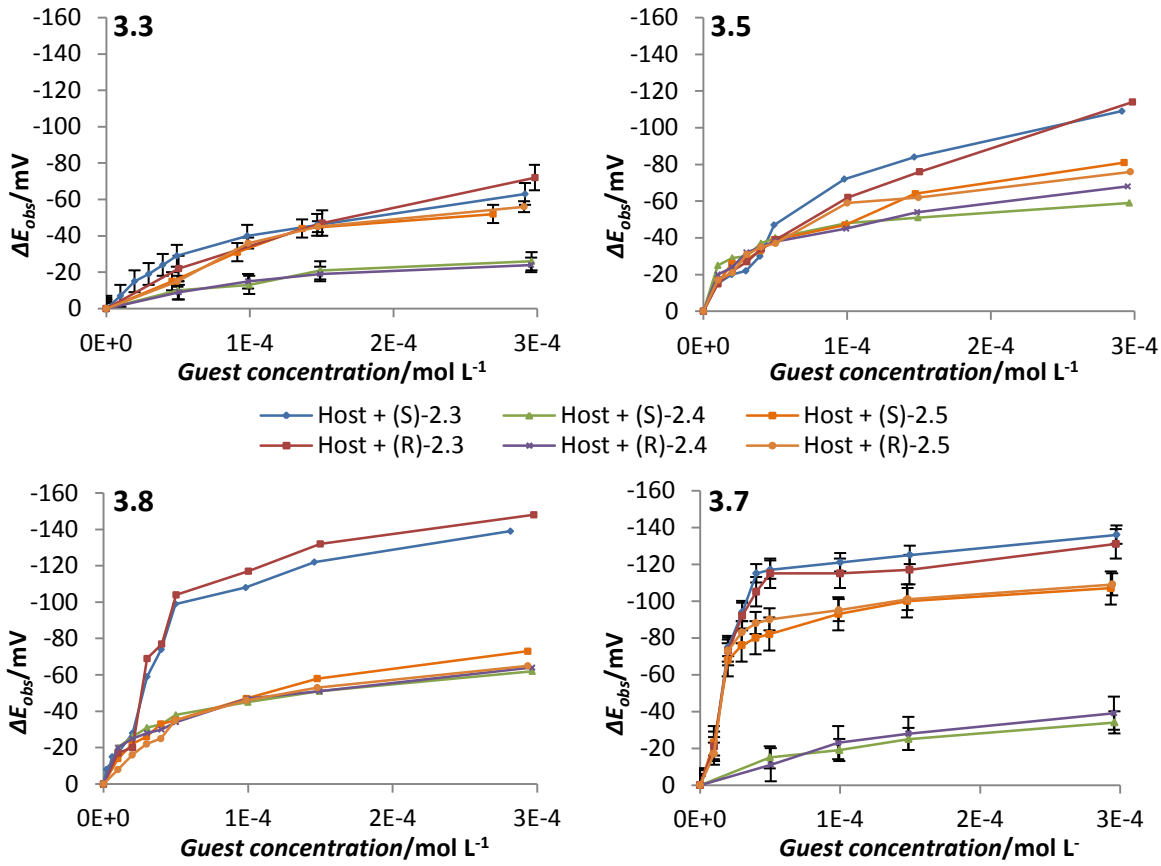

Figure 3.18: *Values of ΔE_{obs} for the receptors upon addition of the different guests (guests 0.02 M in dry CH_2Cl_2, with 0.1 M $TBAPF_6$ and dmfc at rt). Error bars are associated with standard deviations where possible.*

By analysis of the data in Table 3.4 and Figure 3.17 it appears that the receptors in the mixed SAMs are not able to provide chiral discrimination between the guests **2.3-2.5**. However, the shifts observed are significantly larger than in the single component SAMs (Table 3.2) and in many cases larger than those recorded for similar receptors in solution (Table 2.7). For

receptor **3.3** and **3.5**, despite the larger shifts, the differences between the different guests are minimal and cannot be exploited for effective sensing. However, for receptor **3.7** and **3.8** the shifts are larger, especially with guest **2.3**, making these receptors able to discriminate between different guests. In the case of receptor **3.8**, only **2.3** can be discriminated from the other guests but receptor **3.7** is able to discriminate between each guest under the same conditions, following the trend in ΔE_{obs} of **2.3** > **2.5** > **2.4**, as shown in Figure 3.19. This follows the trend found in the solution studies with similar receptors.

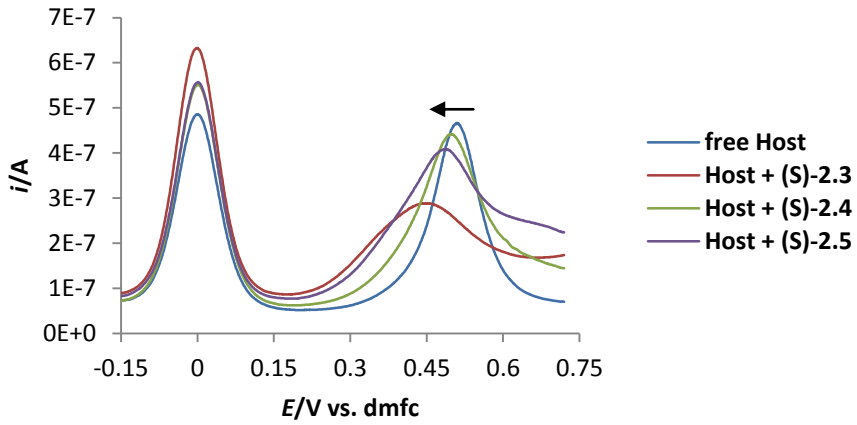

Figure 3.19: *SWVs of a mixed SAM of **3.7** and hexanethiol before and after addition of guests **2.3-2.5** (added as TBA^+ salts in dry CH_2Cl_2, 5 x 10^{-5} M, with 0.1 M $TBAPF_6$ and dmfc at rt.)*

The effectiveness of **3.7** is possibly due to the difference in the tethering group, which orients the receptor in a different way with respect to the surface and the neighbouring hexanethiol molecules, with consequently more distinct interactions, depending on the guest. To gain further information, the behaviour of the centrally chiral receptors with the achiral tethering group was compared on a SAM and in solution (Figure 3.20). Because of a larger availability of receptor **3.6** this was chosen for the studies in solution, knowing that the receptors do not show chiral discrimination.

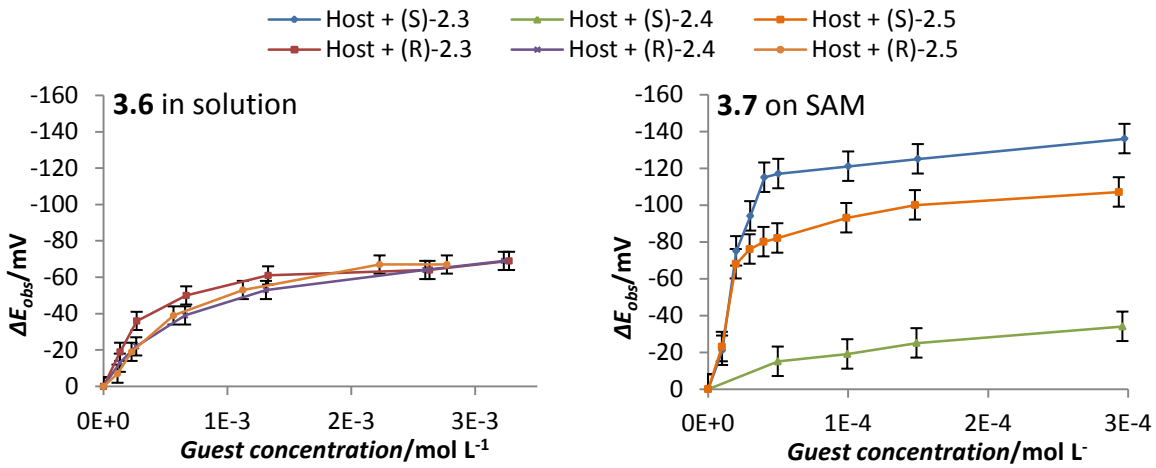

Figure 3.20: *Values of ΔE_{obs} for **3.6** in solution or **3.7** on a SAM upon addition of the different guests (Host ≈2.5 x 10^{-4} M in dry CH_2Cl_2, with 0.1 M $TBAPF_6$ and dmfc at rt).*

Figure 3.19 shows different sensing properties. Comparing the different behaviours it appears that, when on the surface, receptor **3.7** experiences a favoured interaction with guest **2.3** and a disfavoured interaction with guest **2.4**, hence the discrimination properties of **3.7** are enhanced. By comparing Figure 3.19 with Figure 3.13 it appears that the mixed SAMs are more efficient in discriminating between different guests and have a higher sensitivity. In fact, a different response with different guests can be achieved at concentrations as low as 5 x 10^{-5} M. Furthermore, a shift in the potential can be recorded at concentrations as low as 10^{-6} M, as seen in Figure 3.21. In contrast, the single component SAMs are less effective at discriminating, even at a concentration of 3 x 10^{-4} M.

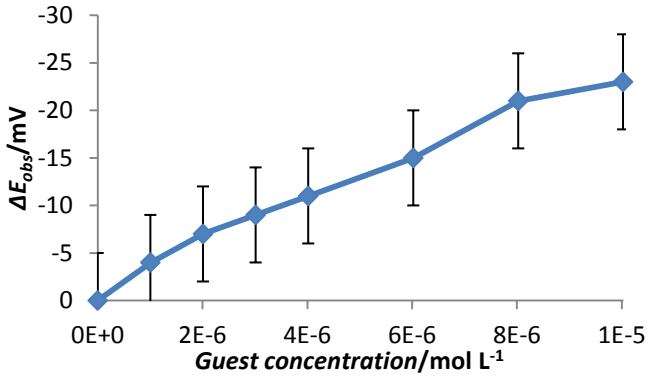

Figure 3.21: *Values of ΔE_{obs} for host **3.7** upon addition of guest (S)-**2.3** (Surface coverage of the host 1.37 x 10^{-10} mol cm^{-2}, guest 3 mM, in dry CH_2Cl_2, with 0.1 M $TBAPF_6$ and dmfc at rt).*

3.4.2.3 SAMs stability and re-usage

As with the single component SAMs, it was decided to test the reusability of the mixed SAMs. These results are presented in Figure 3.22.

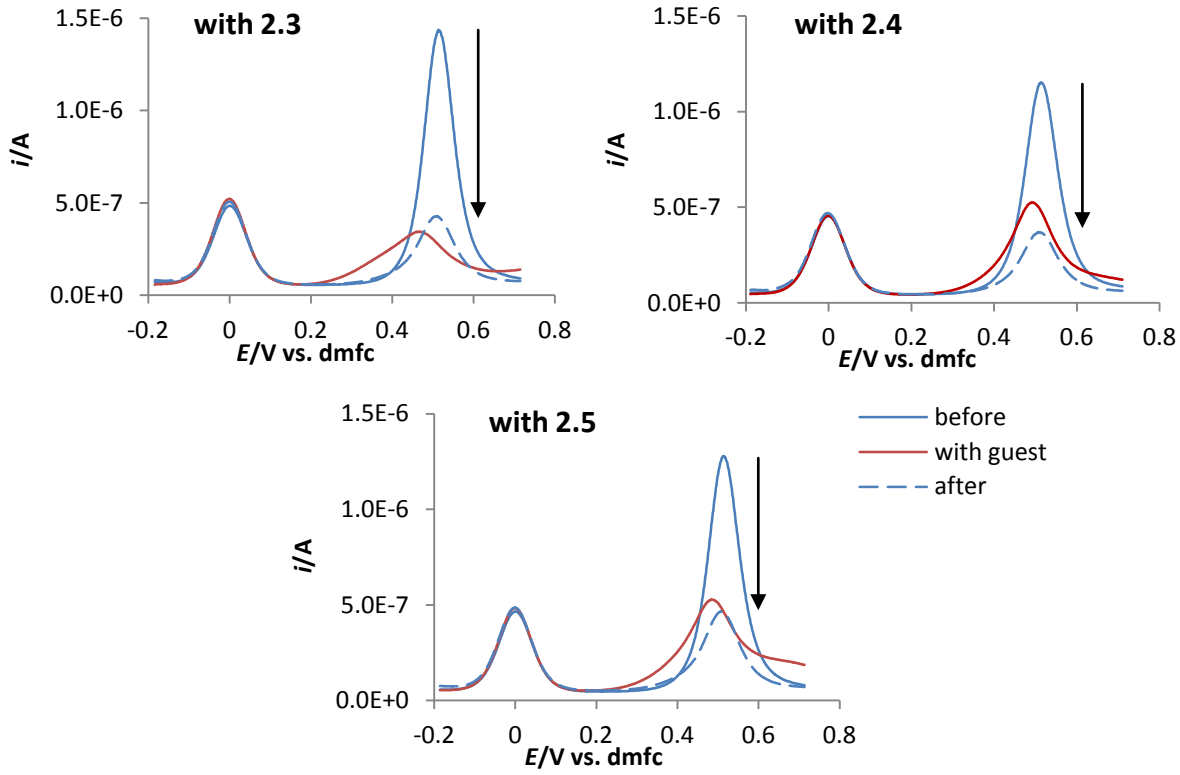

Figure 3.22: *SWVs of a mixed SAM of host **3.7** in 0.1 M $TBAPF_6$ supporting electrolyte solution in dry CH_2Cl_2, in the presence of 0.05 mM guest, and after removal of the guest and immersion in the initial electrolyte solution, at rt.*

The formal potential of the ferrocene groups on a functionalised electrode was recorded in a solution of 0.1 M supporting electrolyte only, then in a solution containing supporting electrolyte and guest at a concentration of 5 x 10^{-5} M, then again in the first solution (Figure 3.22). The electrode surface was gently washed with a stream of dry CH_2Cl_2 before being immersed in each different solution. A loss of activity was observed, but the formal potential of the receptors shifted back to the original values. Despite the loss of active receptor the electrode could still be reused several times, or simply immersed in the preparation solution of the receptor for a short time (3 to 5 minutes) to allow the initial coverage to be reobtained without needing to functionalise the surface again for long periods of time. An example is given in Figure 3.23.

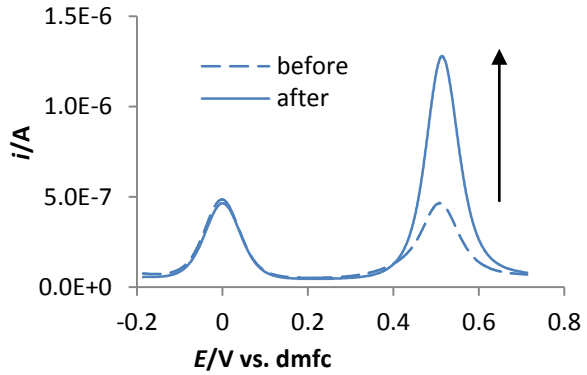

Figure 3.23: *SWVs of a mixed SAM of host **3.7**, before and after re-functionalisation, in 0.1 M $TBAPF_6$ solution in dry CH_2Cl_2 in the presence of dmfc at rt.*

To understand what causes the loss of electroactivity on the functionalised electrode surface, the stability of the SAMs of the receptors was tested while immersed in the 0.1 M supporting electrolyte solution in dry CH_2Cl_2 for a long period of time. Receptor **3.7** was chosen due to the good results achieved in the previous experiments. The data obtained are shown in Figure 3.24.

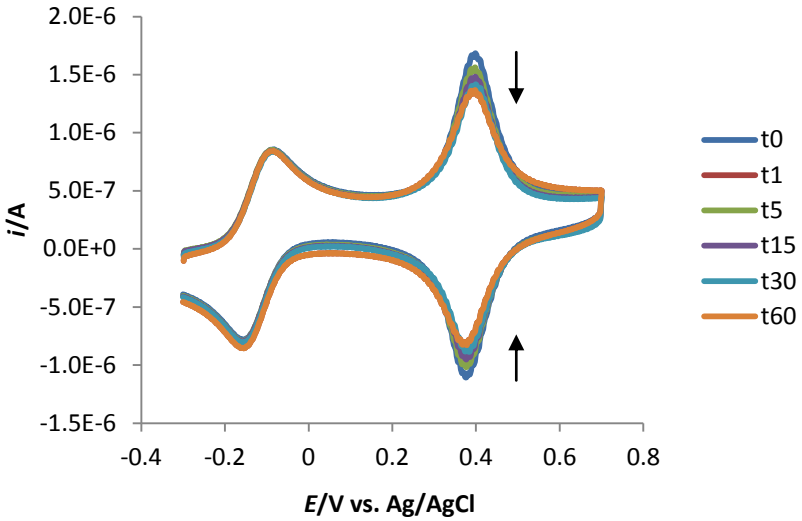

Figure 3.24: *Stability over time of a mixed SAM of host* ***3.7*** *in the 0.1 $TBAPF_6$ supporting electrolyte solution in dry CH_2Cl_2, in the presence of dmfc at rt.*

The potential was scanned at time intervals while leaving the working electrode immersed in the electrolyte solution. The SAM displayed good stability in solution, with a small loss of electroactive species (27%) over a period of one hour. The values of surface coverage recorded are given in Table 3.5.

Table 3.5: *Loss of electroactivity in the surface coverage over time of a mixed SAM of host* ***3.7*** *in the 0.1 $TBAPF_6$ supporting electrolyte solution in dry CH_2Cl_2 at rt.*

Time/m	Q/C	Γ/x 10^{-10} mol cm^{-2}
0	0.3373	1.74
1	0.3208	1.65
5	0.2901	1.49
15	0.2665	1.37
30	0.2535	1.31
60	0.2450	1.26

An alternative test was performed, by immersing the functionalised electrode in the same electrolyte solution and recording the starting cyclic voltammogram, then after 10 minutes

and finally after applying a constant potential of 0.8 V for 10 minutes. The data from this experiment are shown in Figure 3.25.

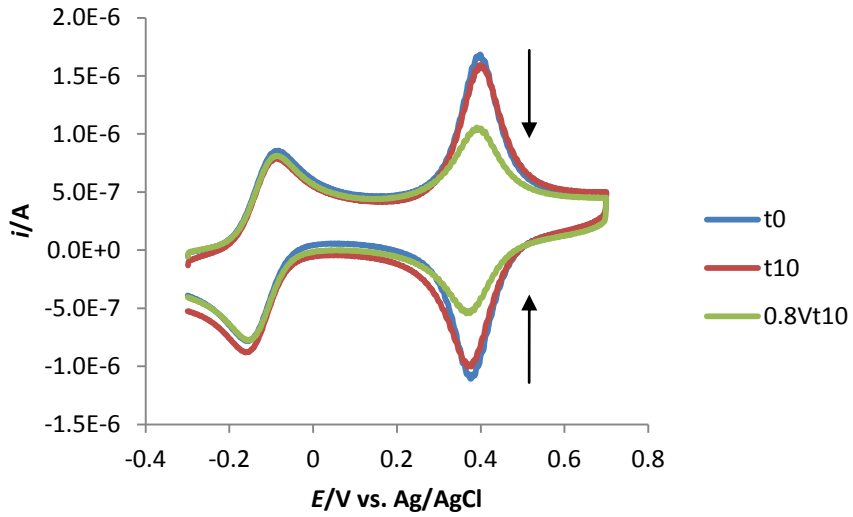

Figure 3.25: *SWVs of a mixed SAM of host* ***3.7*** *in the 0.1 M $TBAPF_6$ supporting electrolyte solution in dry CH_2Cl_2 at rt showing the stability over time and after application for 10 minutes of a potential of 0.8 V.*

After 10 minutes the loss of electroactive species from the electrode surface was <5%. The application of the potential of 0.8 V caused instead a loss of electroactive species of 46%. This is most likely due to the oxidation of the disulphide to sulphonate at this potential, as previously observed for SAMs of similar molecules in different solvents.[2]

3.5 Atomic Force Microscopy (AFM)

3.5.1 Introduction to the technique

Atomic Force Microscopy (AFM) is a technique first developed in 1986 by Gerber and coworkers.[55] Since then it has been increasingly exploited for the visualisation of surfaces and their characterisation through studies of intermolecular interactions. AFM was invented

as a combination of the principles of stylus profilometry (SP)[56-59] and of scanning tunnelling microscopy (STM).[60] The new microscope was able to investigate surfaces on the atomic scale, penetrating the regime of interatomic forces, with lateral resolution of 30 Å and vertical resolution of less than 1 Å (much higher than the 1000 Å and 10 Å, respectively, achieved with SP). The major advantage in comparison with STM is the incorporation of a probe that does not damage the surface. This is derived from the stylus used in the SP, which is mounted on a cantilever spring and is able to plastically deform rough surfaces while scanning. AFM experiments are performed by keeping the force between the sharp tip and the surface of the sample constant, through a feedback mechanism. This force is created by the proximity to the surface, so when the tip is moved along the surface, it will follow its contours without causing any damage. The principle is depicted schematically in Figure 3.26.

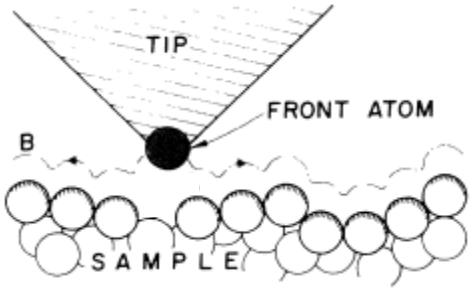

Figure 3.26: *Diagram of the principle operation of an AFM. The tip follows contour* B *to maintain constant force between tip and sample (sample and tip either insulating or conducting).*[55]

The cantilever is fixed to a piezoelectric element which drives the cantilever beam, connected to a feedback loop which maintains the force acting on the tip at a constant level. This can be achieved operating the setup in different modes: examples are the tapping mode, in which the lever is modulated along the *z* direction at its resonating frequency and it

is deflected by the force generated with the sample surface, and the contact mode, which maintains the tunnelling gap constant by changing the force on the tip. This mode proved to be the most reproducible.[55] The deflection of the cantilever is caused by the overlap of the electron orbitals of tip and sample (Born repulsion).[61] The deflection is recorded through an optical laser beam apparatus and optical images of the sample surface are obtained by plotting the deflection of the cantilever against its position on the sample.[61] The typical set-up of an atomic force microscope is shown in Figure 3.27.

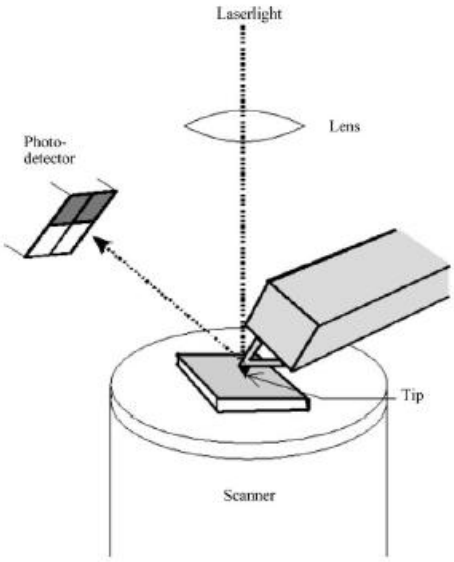

Figure 3.27: *Schematic of an atomic force microscope.*[61]

Atomic Force Microscopy has been increasingly exploited to investigate functionalised surfaces with adsorbed monolayers of organic molecules.[62-71] Another method to use this technique is the functionalization of the AFM tip with functional groups that have a specific interaction with the sample surface, inducing a deflection of the cantilever,[72] as described in the review published by Voyer *et al.*[73] This technique is known as chemical force microscopy, often obtained by gold-thiol coating.[74-75] Additionally, mixed SAM formation and

morphology has been investigated to confirm the influence of the interaction between neighbouring chains in the monolayers.[76] In these studies the problem of the deformation of surfaces by scanning[77] was solved by adjusting the height of the cantilever in order to minimise the forces and avoid crushing against the surface,[76] which could also cause destruction of formed monolayers.[61]

3.5.2 AFM imaging of SAMs

Contact AFM imaging experiments were performed on SAMs of the receptors **3.3**, **3.7** and **3.9** on gold surfaces. The set-point was chosen at 0.8 V in order to generate a force large enough to give an acceptable intensity of the laser beam deflected on the detector, but also to avoid having the tip too close to the sample surface, which might cause damage to the self-assembled monolayer. 10 µm x 10 µm images for single-component SAMs were recorded (Figure 3.28).

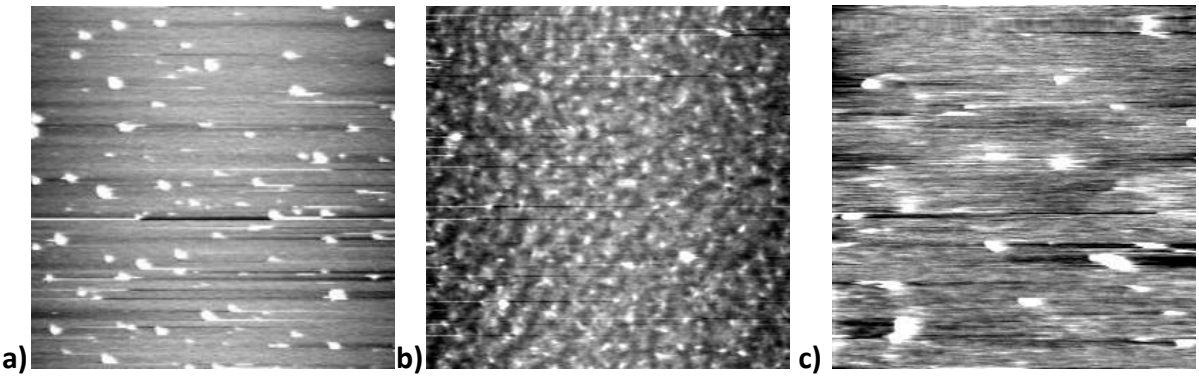

Figure 3.28: *Contact AFM topography of: a) a SAM of host **3.3**; b) a SAM of host **3.7**; c) a SAM of host **3.9.** Size of images is 10 µm x 10 µm*.

Imaging on the single component monolayers of receptor **3.3** displayed an organisation in domains over the gold surface. Single component monolayers of receptor **3.7** showed

instead a more dispersed organisation, although the resulting surface appeared rough and not homogeneous. Finally, the single component monolayers of racemic receptor **3.9** showed a fairly dispersed organisation as found with receptor **3.7** but some large domains were also present on the surface. It is possible that receptor **3.7** is slightly better organised on the surface than receptor **3.9** because of the tethering group, which is symmetrical for the first receptor and asymmetric for the second receptor. On the other hand, receptor **3.3** does not have a bulky group, such as the benzyl, to disfavour intermolecular hydrogen-bonding interactions, hence the formation of domains are easier than for receptor **3.7**. Although SAMs of receptor **3.7** display a more dispersed structure, smaller domains that are consistent with some intermolecular interactions are distributed more or less evenly along the sample surface.

Mixed monolayers of each receptor and hexanethiol were then analysed in the same way, with the resulting images presented in Figure 3.29.

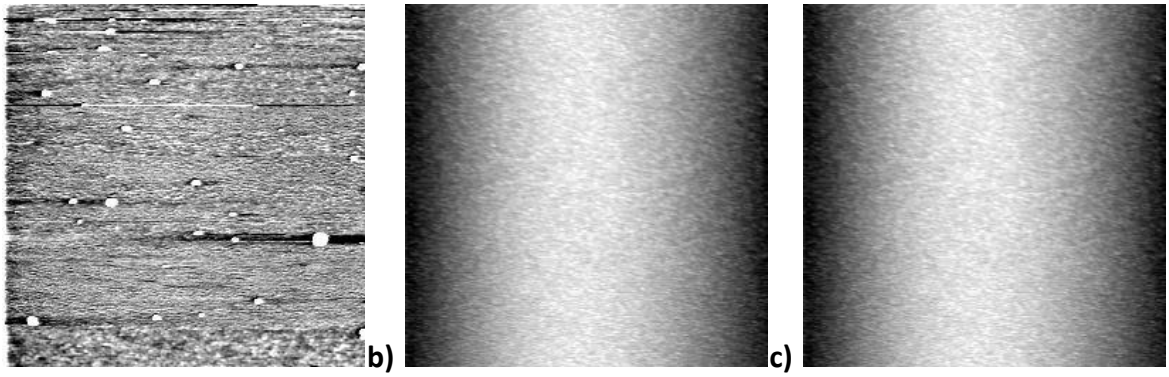

Figure 3.29: *Contact AFM topography of: a) a mixed SAM of hexanethiol and host **3.3**; b) a mixed SAM of hexanethiol and host **3.7**; c) a mixed SAM of hexanethiol and host **3.9.** Size of images is 10 µm x 10 µm.*

In the case of receptor **3.3**, AFM revealed a fairly homogenous surface coverage of thiol and a more dispersed organisation of the receptors than the corresponding single component monolayers, but with some small domains of receptors still present. For both **3.7** and **3.9**, uniform and dispersed monolayers were observed, clearly an improvement on the corresponding single component monolayers. This is most likely due to the effect of the hexanethiol, which limits the interaction between neighbouring molecules of receptor and the formation of intermolecular hydrogen-bonding, which would result in the formation of domains. This is not completely avoided in the case of receptor **3.3**, because the formation of intermolecular hydrogen-bonding is easier than in the more sterically hindered receptors **3.7** and **3.9**. In the case of these two receptors the surface organisation is similar, because the distance between each neighbouring receptor molecule is large enough to override the structural differences caused by the chirality of the anchoring group.

These AFM results indicate that the higher sensitivity and selectivity towards the different carboxylates displayed by the mixed SAMs is associated with the higher dispersion of the receptor molecules on the surface. This causes a higher and more reproducible accessibility of the guests to the binding sites, with a significant enhancement of the sensing properties.

3.6 Ellipsometry

3.6.1 Introduction to the technique[78]

Ellipsometry is a widely used investigation technique, developed by Drude in 1889,[79-80] which allows the estimation of the thickness of adsorbed films on opaque substrates.[81] This is done by determining the refractive index of the film using elliptically polarised light, which is

polarised in two directions: parallel and perpendicular to the plane of incidence. The technique measures the ratio between the two components after they have travelled across the film under study and been reflected by the surface (*complex reflectance ratio,* ρ). The ratio can be parametrised, but the parameters are known only by fitting of the results with a layer model, which varies depending on the nature of the substrate, the anchoring groups and the layer under investigation. A typical ellipsometer setup, shown in Figure 3.30, comprises a light source, a rotating polariser, an analyser and a detector connected to a computer.

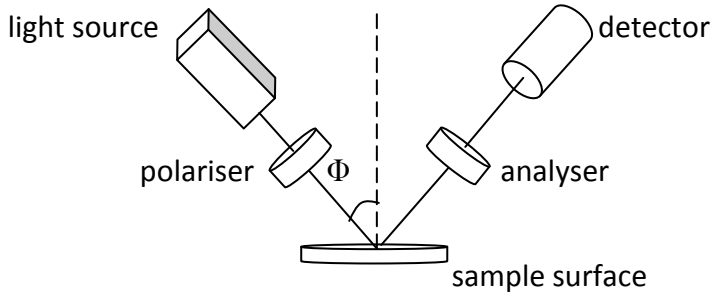

Figure 3.30*: Schematic diagram of an ellipsometer.*[78]

When the polarised light hits the surface of the film layer, part of it is reflected but another part goes through (refracted by the layer) and hits the support surface, from which it is then reflected with the same angle and finally refracted again when it exits the layer. This process is depicted schematically in Figure 3.31. The angle of reflection of the different components that reach the analyser is the same but the polarisation parameters are different and the ellipsometer uses them to give information about the thickness of the layer.

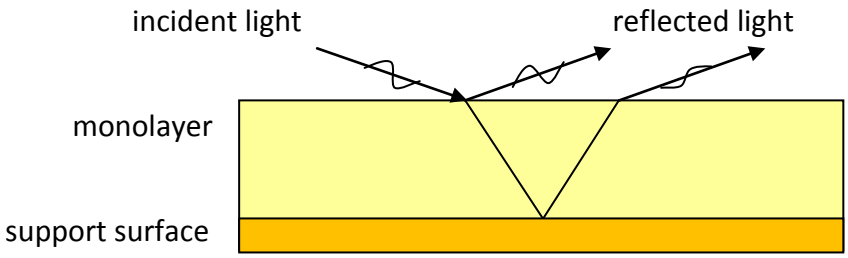

Figure 3.31: *Schematic representation of the path of light through a thin monolayer.*[78]

The benefits of ellipsometry in surface characterisation are that it is a non-destructive analysis and it possesses a thickness resolution of 0.01 nm, therefore it is suitable to study layers of molecular dimensions.[82] It can be used to investigate the thickness of self-assembled monolayer of electroactive molecules on metal or semiconductor surfaces,[83] as described in publications on the subject.[29-30] In particular, different examples are known in which ellipsometry has been used for measuring the thickness of alkanethiols on gold surfaces.[7, 84-87] From the ellipsometry data, and knowing the length of the alkyl chain, it is possible to calculate the average molecular orientation of the molecules with respect to the gold surface.[88]

3.6.2 Assessment of the SAM thickness

Ellipsometry was used to calculate the thickness of the single-component self-assembled monolayers formed by receptors **3.3-3.8**, using a model which was included in the software and which takes into account the nature of the substrate used, the tethering group and the presence of functional groups such as ferrocene. Before the experiments, measurement of

the thickness of the blank gold plates was carried out. The values were then subtracted from the observed thickness by the software, to obtain the thickness of the monolayer, reported in Table 3.6.

ArgusLab with UFF optimisation[89] was used to calculate the length of the receptor molecules (Figure 3.32) to which the typical length of the Au-S bond in a disulphide (0.250 nm)[90] was added to get the theoretical thickness of the monolayer, and the angle formed with respect to the normal to the surface was thus calculated, as reported in Table 3.6.

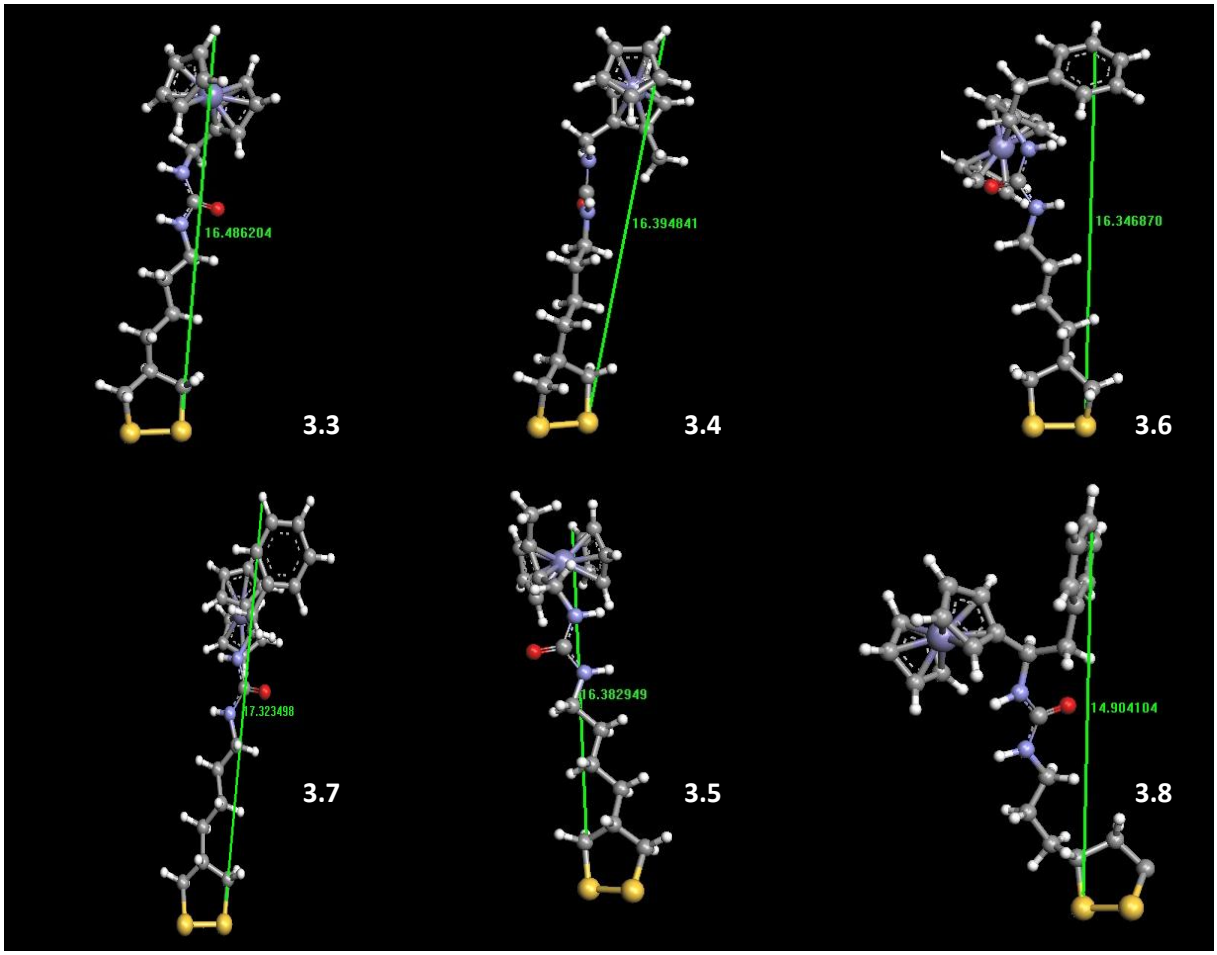

Figure 3.32: Ab initio *molecular modelling with the software ArgusLab,*[89] *with reported calculation of the length of the molecules.*

Table 3.6: *Range of thickness of the SAMs over at least 3 measures in comparison to the calculated thickness and range of angles between molecules and normal to the surface.*

Receptor	Experimental thickness/nm	Calculated thickness /nm	Angle /° from normal
3.3	1.005-1.248	1.899	49.0-58.0
3.4	0.923-0.957	1.889	59.6-60.1
3.6	0.814-1.001	1.982	59.7-65.8
3.7	0.818-1.154	1.885	52.3-64.3
3.8	0.839-1.089	1.740	51.3-61.2

All SAMs show similar thickness and similar angle from the normal to the surface, within the range observed over at least 3 measurements. In each case, the thickness recorded is small enough to exclude the formation of multilayers, which could be identified from higher experimental values than those obtained from the calculations.

3.7 Conclusions and Future Work

Redox active receptors for carboxylate anions have been functionalised with disulphides to be effectively assembled on the surface of gold electrodes to perform selective recognition, with a number of advantages compared with sensing using receptors in solution. One clear advantage is the quantity of material required for the experiments. A solution of a receptor can be used only for a single experiment, if used for sensing in solution; however, the same solution can be used many times for the preparation of SAMs, with minimal changes to its concentration. The receptors showed good stability in CH_2Cl_2 solution, and could be kept and used for months without loss of the ability to form SAMs in a fairly reproducible way. A second advantage that is often showed by receptors on a surface compared to those in

solution is a sensing enhancement, through larger ΔE_{obs} values and in some cases an improved ability to discriminate between different guests. This is especially valid in the mixed SAMs, in which the binding sites of the receptors are easily accessible to the guest molecules due to the presence of the hexanethiol spacer. A third advantage is the detection limit, with detection of guest at concentrations as low as 10^{-6} M. One of the drawbacks was the reusability of the functionalised electrodes due to the low stability of the SAMs. However, in the mixed SAMs, shortly re-soaking the electrodes in the preparation solution added some fresh receptor to the electrode surface and therefore the original monolayer could be reused. Moreover, the formation of mixed monolayers could provide more homogeneous surfaces and more reproducible sensing than the single component analogues. Looking at differences between the properties and the behaviour of the different receptors it is possible to justify the long synthesis required for the achiral disulphide rather than the commercially available but expensive chiral disulphide. For similar reasons, the choice of the receptor with central chirality rather than the simple achiral receptor with no bulky group and the use of mixed SAMs rather than single component SAMs can be justified. The achiral disulphide with a centrally chiral urea moiety was able to form monolayers with the most uniform and dispersed organisation. Moreover, it was able to distinguish between each of the different guests used in the study, with the possibility of a broad range of applications. Unfortunately, chiral recognition was not achieved: the difference in the variation of potential shift is too small in the sensing of enantiomers with systems of this sort, smaller than the differences coming from the organisation of the SAMs. Future work on this class of receptors should move towards the improvement of the chiral recognition of the receptors. Clearly at present, the variation in the response at a surface from one experiment

to the next is too big to have reliable and reproducible chiral sensing. The research could move towards increasing the difference in the response upon addition of one enantiomer of guest rather than the other, obtainable by an increase in the preorganisation and selectivity of the host. Nevertheless, a change in the anchoring group to obtain an organised SAM in a reproducible way could improve the sensing properties. This could be achieved by changing the surface functionalization approach, for example using electrografting instead of self-assembly, with consequently highly stable monolayers.[91-92] Another interesting use of this class of receptors could be the formation of self-assembled monolayers on gold nanoparticles, with the possibility to follow the binding towards chiral carboxylates using different spectroscopic techniques in solution.

3.8 References

1. Nuzzo, R. G.; Zegarski, B. R.; Dubois, L. H., *J. Am. Chem. Soc.* **1987,** *109*, 733-740.
2. Vericat, C.; Vela, M. E.; Benitez, G.; Carro, P.; Salvarezza, R. C., *Chem. Soc. Rev.* **2010,** *39*, 1805-1834.
3. Ulman, A., *Chem. Rev.* **1996,** *96*, 1533-1554.
4. Fabianowski, W.; Coyle, L. C.; Weber, B. A.; Granata, R. D.; Castner, D. G.; Sadownik, A.; Regen, S. L., *Langmuir* **1989,** *5*, 35-41.
5. Dubois, L. H.; Nuzzo, R. G., *Annu. Rev. Phys. Chem.* **1992,** *43*, 437-463.
6. Finklea, H. O.; Hanshew, D. D., *J. Am. Chem. Soc.* **1992,** *114*, 3173-3181.
7. Bain, C. D.; Troughton, E. B.; Tao, Y. T.; Evall, J.; Whitesides, G. M.; Nuzzo, R. G., *J. Am. Chem. Soc.* **1989,** *111*, 321-335.
8. Bandyopadhyay, K.; Patil, V.; Sastry, M.; Vijayamohanan, K., *Langmuir* **1998,** *14*, 3808-3814.
9. Lee, L. Y. S.; Lennox, R. B., *Phys. Chem. Chem. Phys.* **2007,** *9*, 1013-1020.
10. Sek, S.; Misicka, A.; Bilewicz, R., *J. Phys. Chem. B* **2000,** *104*, 5399-5402.
11. Joly, K. M.; Mirri, G.; Willener, Y.; Horswell, S. L.; Moody, C. J.; Tucker, J. H. R., *J. Org. Chem.* **2010,** *75*, 2395-2398.
12. Laviron, E., *J. Electroanal. Chem.* **1974,** *52*, 395-402.

13. Laviron, E.; Roullier, L., *J. Electroanal. Chem.* **1980,** *115*, 65-74.
14. Randles, J. E. B., *Trans. Faraday Soc.* **1948,** *44*, 327-338.
15. Sevcik, A., *Collect. Czech. Chem.Commun.* **1948,** *13*, 349-377.
16. Bard, A. J.; Faulkner, L. R., *Electrochemical Methods, Fundamentals and Applications*. Wiley, New York, 2001.
17. Laviron, E., *J. Electroanal. Chem.* **1974,** *52*, 355-393.
18. Laviron, E., *J. Electroanal. Chem.* **1975,** *63*, 245-261.
19. Laviron, E., *J. Electroanal. Chem.* **1979,** *100*, 263-270.
20. Roullier, L.; Laviron, E., *J. Electroanal. Chem.* **1983,** *157*, 193-203.
21. Eckermann, A. L.; Feld, D. J.; Shaw, J. A.; Meade, T. J., *Coord. Chem. Rev.* **2010,** *254*, 1769-1802.
22. Cormode, D. P.; Evans, A. J.; Davis, J. J.; Beer, P. D., *Dalton Trans.* **2010,** *39*, 6532-6541.
23. Hoogvliet, J. C.; Dijksma, M.; Kamp, B.; van Bennekom, W. P., *Anal. Chem.* **2000,** *72*, 2016-2021.
24. Mirri, G. Ferrocene-based Electrochemical Chiral Sensors. The University of Birmingham, Birmingham, 2011.
25. Seo, K.; Jeon, I. C.; Yoo, D. J., *Langmuir* **2004,** *20*, 4147-4154.
26. Atre, S. V.; Liedberg, B.; Allara, D. L., *Langmuir* **1995,** *11*, 3882-3893.
27. Guiomar, A. J.; Guthrie, J. T.; Evans, S. D., *Langmuir* **1999,** *15*, 1198-1207.
28. Fujii, S.; Kurokawa, S.; Murase, K.; Lee, K.-H.; Sakai, A.; Sugimura, H., *Electrochim. Acta* **2007,** *52*, 4436-4442.
29. Bain, C. D.; Whitesides, G. M., *J. Am. Chem. Soc.* **1989,** *111*, 7164-7175.
30. Bain, C. D.; Evall, J.; Whitesides, G. M., *J. Am. Chem. Soc.* **1989,** *111*, 7155-7164.
31. Bain, C. D.; Whitesides, G. M., *J. Am. Chem. Soc.* **1988,** *110*, 6560-6561.
32. Rouhana, L. L.; Moussallem, M. D.; Schlenoff, J. B., *J. Am. Chem. Soc.* **2011,** *133*, 16080-16091.
33. Gronbeck, H.; Curioni, A.; Andreoni, W., *J. Am. Chem. Soc.* **2000,** *122*, 3839-3842.
34. Guo, Y.; Zhao, J. W.; Zhu, J. J., *Thin Solid Films* **2008,** *516*, 3051-3057.
35. Lee, L. Y. S.; Sutherland, T. C.; Rucareanu, S.; Lennox, R. B., *Langmuir* **2006,** *22*, 4438-4444.
36. Bergson, G.; Frisell, C., *Acta Chem. Scand.* **1964,** *18*, 2000-2001.
37. Moody, C. J.; Lightfoot, A. P.; Gallagher, P. T., *J. Org. Chem.* **1997,** *62*, 746-748.
38. Laurent, P.; Miyaji, H.; Collinson, S. R.; Prokes, I.; Moody, C. J.; Tucker, J. H. R.; Slawin, A. M. Z., *Org. Lett.* **2002,** *4*, 4037-4040.
39. Willener, Y.; Joly, K. M.; Moody, C. J.; Tucker, J. H. R., *J. Org. Chem.* **2008,** *73*, 1225-1233.
40. Curtius, T., *Journal Fur Praktische Chemie-Leipzig* **1917,** *95*, 168-256.
41. Fujii, S.; Murase, K.; Sugimura, H., *Electrochemistry* **2007,** *75*, 523-527.

42. Fontaine, O.; Trippe, G.; Fave, C.; Lacroix, J. C.; Randriamahazaka, H. N., *J. Electroanal. Chem.* **2009,** *632*, 1-7.
43. Uosaki, K.; Sato, Y.; Kita, H., *Langmuir* **1991,** *7*, 1510-1514.
44. Silva, M.; Pombeiro, A. J. L.; Dasilva, J.; Herrmann, R.; Deus, N.; Castilho, T. J.; Silva, M., *J. Organomet. Chem.* **1991,** *421*, 75-90.
45. Emilia, M.; Silva, N.; Pombeiro, A. J. L.; Dasilva, J.; Herrmann, R.; Deus, N.; Bozak, R. E., *J. Organomet. Chem.* **1994,** *480*, 81-90.
46. Leopold, M. C.; Black, J. A.; Bowden, E. F., *Langmuir* **2002,** *18*, 978-980.
47. Ye, S.; Haba, T.; Sato, Y.; Shimazu, K.; Uosaki, K., *Phys. Chem. Chem. Phys.* **1999,** *1*, 3653-3659.
48. Han, S. W.; Seo, H.; Chung, Y. K.; Kim, K., *Langmuir* **2000,** *16*, 9493-9500.
49. Rowe, G. K.; Creager, S. E., *Langmuir* **1991,** *7*, 2307-2312.
50. Willicut, R. J.; McCarley, R. L., *Anal. Chim. Acta* **1995,** *307*, 269-276.
51. Azehara, H.; Mizutani, W.; Suzuki, Y.; Ishida, T.; Nagawa, Y.; Tokumoto, H.; Hiratani, K., *Langmuir* **2003,** *19*, 2115-2123.
52. Viana, A. S.; Leupold, S.; Eberle, C.; Shokati, T.; Montforts, F. P.; Abrantes, L. M., *Surf. Sci.* **2007,** *601*, 5062-5068.
53. Wawrzyniak, U. E.; Wozny, M.; Kowalski, J.; Domagala, S.; Maicka, E.; Bilewicz, R.; Wozniak, K.; Korybut-Daszkiewicz, B., *Chem.-Eur. J.* **2009,** *15*, 149-157.
54. Hayashi, T.; Makiuchi, N.; Hara, M., *Jpn. J. Appl. Phys.* **2009,** *48, 095503*.
55. Binnig, G.; Quate, C. F.; Gerber, C., *Phys. Rev. Lett.* **1986,** *56*, 930-933.
56. Williamson, J. B. P., *Proc., Inst. Mech. Eng., London* **1967-1968,** *182*, 21-30.
57. Kubo, M.; Peklenik, J., *Ann. CIRP* **1968,** *16*, 257-265.
58. Peklenik, J.; Kubo, M., *Ann. CIRP* **1968,** *16*, 257-265.
59. Teague, E. C.; Scire, F. E.; Baker, S. M.; Jensen, S. W., *Wear* **1982,** *83*, 1-12.
60. Binnig, G.; Rohrer, H., *Helv. Phys. Acta* **1982,** *55*, 726-735.
61. Butt, H. J.; Cappella, B.; Kappl, M., *Surf. Sci. Rep.* **2005,** *59*, 1-152.
62. Alves, C. A.; Smith, E. L.; Porter, M. D., *J. Am. Chem. Soc.* **1992,** *114*, 1222-1227.
63. Alves, C. A.; Porter, M. D., *Abstr. Pap. Am. Chem. S.* **1993,** *205*, 122.
64. Alves, C. A.; Porter, M. D., *Langmuir* **1993,** *9*, 3507-3512.
65. McDermott, M. T.; Green, J. B. D.; Porter, M. D., *Abstr. Pap. Am. Chem. S.* **1994,** *208*, 217.
66. McDermott, C. A.; McDermott, M. T.; Green, J. B.; Porter, M. D., *J. Phys. Chem.* **1995,** *99*, 13257-13267.
67. Green, J. B. D.; McDermott, M. T.; Porter, M. D., *J. Phys. Chem.* **1996,** *100*, 13342-13345.
68. Caldwell, W. B.; Campbell, D. J.; Chen, K. M.; Herr, B. R.; Mirkin, C. A.; Malik, A.; Durbin, M. K.; Dutta, P.; Huang, K. G., *J. Am. Chem. Soc.* **1995,** *117*, 6071-6082.
69. Jaschke, M.; Schonherr, H.; Wolf, H.; Butt, H. J.; Bamberg, E.; Besocke, M. K.; Ringsdorf, H., *J. Phys. Chem.* **1996,** *100*, 2290-2301.

70. Woodward, J. T.; Schwartz, D. K., *J. Am. Chem. Soc.* **1996,** *118*, 7861-7862.
71. Fang, L.; Park, J. Y.; Ma, H.; Jen, A. K. Y.; Salmeron, M., *Langmuir* **2007,** *23*, 11522-11525.
72. Han, T.; Williams, J. M.; Beebe, T. P., *Anal. Chim. Acta* **1995,** *307*, 365-376.
73. Barattin, R.; Voyer, N., *Chem. Commun.* **2008**, 1513-1532.
74. Noy, A.; Vezenov, D. V.; Lieber, C. M., *Annu. Rev. Mater. Sci.* **1997,** *27*, 381-421.
75. Smith, D. A.; Connell, S. D.; Robinson, C.; Kirkham, J., *Anal. Chim. Acta* **2003,** *479*, 39-57.
76. Tamada, K.; Hara, M.; Sasabe, H.; Knoll, W., *Langmuir* **1997,** *13*, 1558-1566.
77. Liu, G. Y.; Salmeron, M. B., *Langmuir* **1994,** *10*, 367-370.
78. Tompkins, H. G., *A User's Guide to Ellipsometry*. Academic Press Inc., London, 1993.
79. Drude, P., *Ann. Physik and Chem.* **1889,** *36*, 865-897.
80. Drude, P., *Ann. Physik and Chem.* **1890,** *39*, 481-554.
81. Bartell, L. S., *J. Chem. Phys.* **1956,** *24*, 1108-1108.
82. Arwin, H., *Thin Solid Films* **1998,** *313*, 764-774.
83. Tran, T. K.; Qcafrain, M.; Karpe, S.; Blanchard, P.; Roncali, J.; Lenfant, S.; Godey, S.; Vuillaume, D., *Chem.-Eur. J.* **2008,** *14*, 6237-6246.
84. Nuzzo, R. G.; Allara, D. L., *J. Am. Chem. Soc.* **1983,** *105*, 4481-4483.
85. Porter, M. D.; Bright, T. B.; Allara, D. L.; Chidsey, C. E. D., *J. Am. Chem. Soc.* **1987,** *109*, 3559-3568.
86. Ohtsuka, T.; Sato, Y.; Uosaki, K., *Langmuir* **1994,** *10*, 3658-3662.
87. Viana, A. S.; Abrantes, L. M.; Jin, G.; Floate, S.; Nichols, R. J.; Kalaji, M., *Phys. Chem. Chem. Phys.* **2001,** *3*, 3411-3419.
88. Laibinis, P. E.; Whitesides, G. M.; Allara, D. L.; Tao, Y. T.; Parikh, A. N.; Nuzzo, R. G., *J. Am. Chem. Soc.* **1991,** *113*, 7152-7167.
89. Rappe, A. K.; Casewit, C. J.; Colwell, K. S.; Goddard, W. A.; Skiff, W. M., *J. Am. Chem. Soc.* **1992,** *114*, 10024-10035.
90. Hayashi, T.; Morikawa, Y.; Nozoye, H., *J. Chem. Phys.* **2001,** *114*, 7615-7621.
91. Marshall, N.; Locklin, J., *Langmuir* **2011,** *27*, 13367-13373.
92. Mattiuzzi, A.; Jabin, I.; Mangeney, C.; Roux, C.; Reinaud, O.; Santos, L.; Bergamini, J.-F.; Hapiot, P.; Lagrost, C., *Nat. Commun.* **2012,** *3,* 1-8.

CHAPTER 4: Ferrocenyl derivatised BINOL sensors

4.1 Introduction and aims of the studies

As described in Chapter 1, many receptors have been designed and used for sensing chiral guest molecules through exploitation of their fluorescence properties.[1-6] The field of fluorescent chiral recognition has been growing particularly in the past decade due to the ease of detection of either enantiomeric excess or of the larger presence of an enantiomer over the other with immediate response. The idea behind the studies described in this chapter derived from a collaboration between the Tucker group and Professor Lin Pu, University of Virginia.

In 2004 Pu and coworkers first described the synthesis of simple BINOL based enantiomers of novel receptor **4.2** from the easily accessible compound **4.1**. This molecule possesses side chains containing bulky groups and -OH and –NH as binding sites for the complexation of small carboxylic acids such as mandelic acid, or protected amino acids such as *N*-benzyloxycarbonylphenylglycine **4.3**.[7]

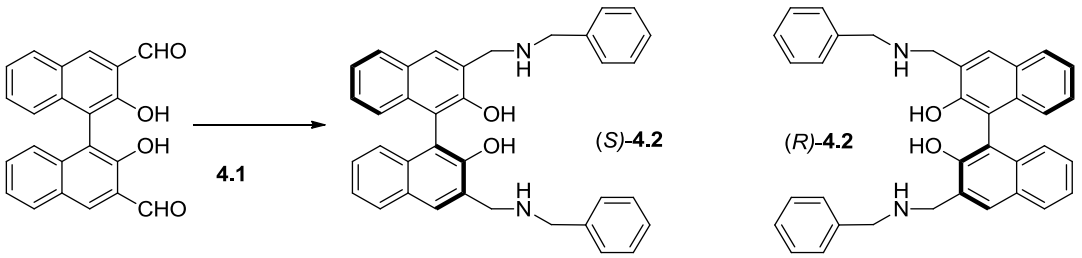

The presence of the axial chirality provided by the BINOL scaffold alone was able to give chiral discrimination between the opposite enantiomers of the guest when this was bound within the chiral cleft formed by the receptor where the binding sites are located.

The differences in the responses upon binding of the analytes were monitored using fluorescence spectroscopy (Figure 4.1).

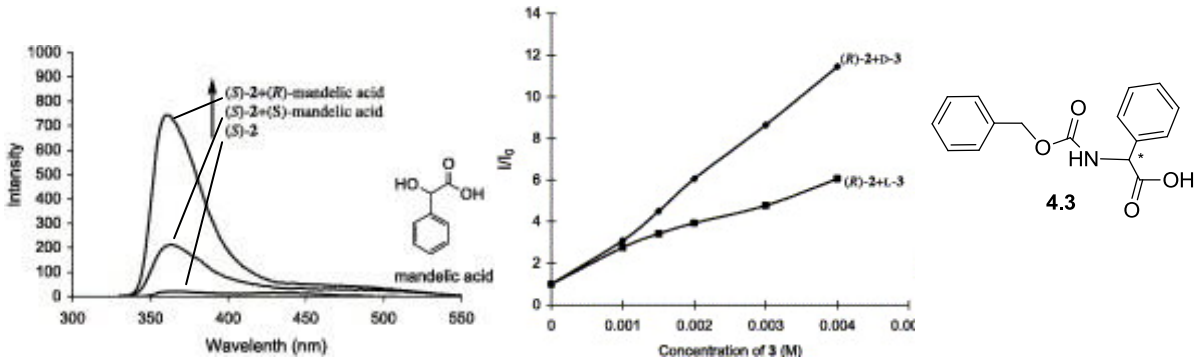

Figure 4.1: *(left) Fluorescence spectra of (*S*)-**4.2** with/without (*R*)- and (*S*)-mandelic acid (2.0 x 10^{-2} M); (right) Fluorescence enhancement of (*R*)-**4.2** versus concentration of* D/L-***4.3****. (host 1.0 x 10^{-4} M in benzene containing 2% DME, λ_{exc}=320 nm.)*[7]

The fluorescent emission of the BINOL groups was nearly completely quenched in the free host, but it was significantly enhanced in the presence of the guests mandelic acid and **4.3** and exhibited a different magnitude for the different enantiomers of the same guest. The addition of an extra chiral centre on the side chains to give receptor **4.4** increased the differentiation between the opposite enantiomers of **4.3** (Figure 4.2).[7]

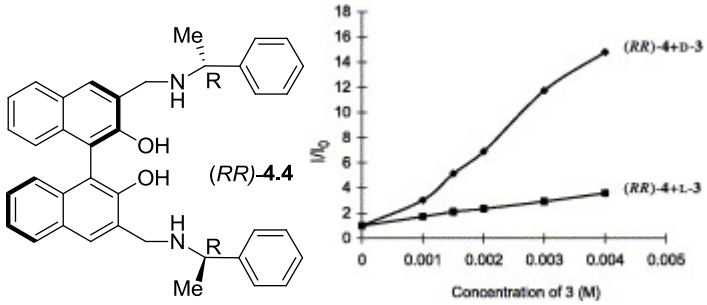

Figure 4.2*: Fluorescence enhancement of (*RR*)-**4.4** (1.0 x 10^{-4} M in benzene/2% DME) versus concentration of* D/L-***4.3****(λ_{exc} = 320 nm).*[7]

The insertion of additional chiral centres and bulkier groups on the side chains further increased the discrimination of opposite enantiomers of chiral α-hydroxycarboxylic acids, as in the example reported in 2009 with receptor **4.5** and mandelic acid (Figure 4.3)[8] or in 2010 with receptor **4.6** and guest **4.7** (Figure 4.4).[9]

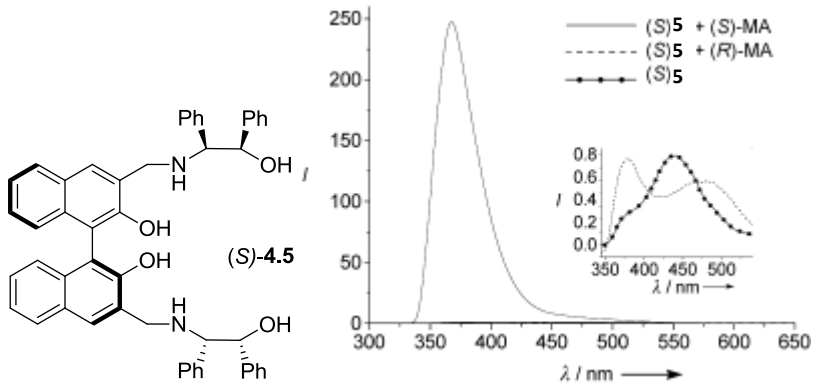

***Figure 4.3**: Fluorescence spectra of (S)-**4.5** (5.0 × 10^{-4} M) with (R)- and (S)-MA (4.0 × 10^{-3} M) in benzene/0.4 vol % DME (λ_{exc} = 341 nm, slit width = 5.0/5.0 nm).[8]*

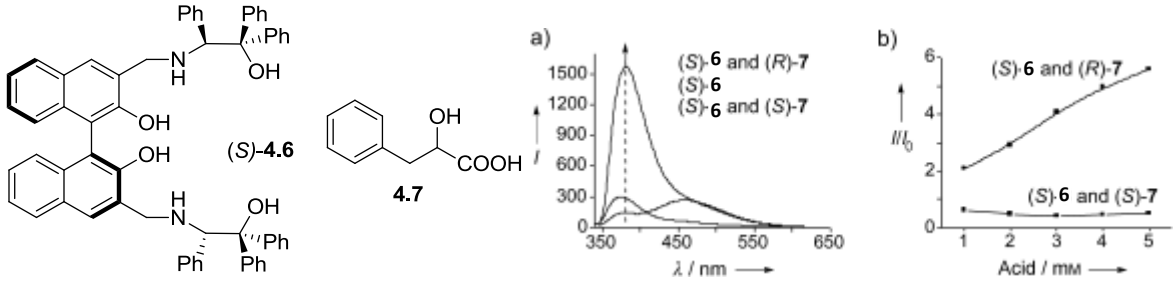

***Figure 4.4**: a) Fluorescence spectra of (S)-**4.6** (2.0 × 10^{-4} mol L^{-1} in benzene, 0.4 %v/v DME) with (R)-**4.7** or (S)-**4.7** (5.0 × 10^{-3} mol L^{-1}). b) Fluorescence enhancement of (S)-**4.6** at various concentrations of (R)-**4.7** or (S)-**4.7** at λ_{em} = 382 nm (λ_{exc} = 334 nm, slit = 5.0/5.0 nm).[9]*

It is noteworthy that the receptors tend to form 1:1 complexes with carboxylic acids, as reported in 2010[9] and shown in Figure 4.5 but, for complexes with amino acids, both host/guest stoichiometries of 1:1 and 1:2 were observed[10] (Figure 4.6).

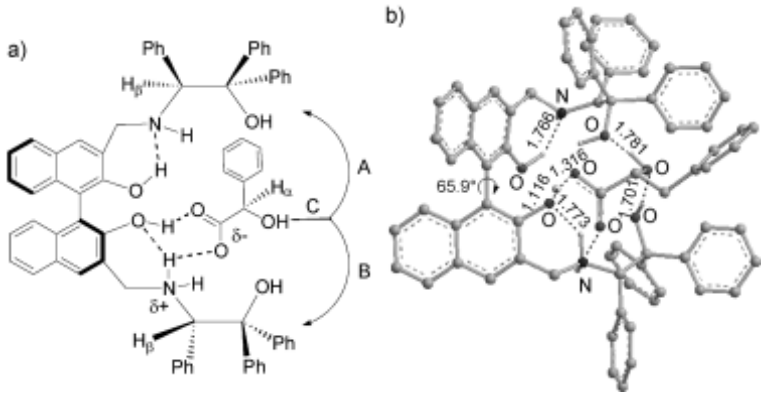

***Figure 4.5**: a) The modes, A–C of the proposed 1:1 complexation of (S)-**4.6** + (R)-**4.7**; b) Calculated structures of mode C. For clarity, most hydrogen atoms are omitted.*[9]

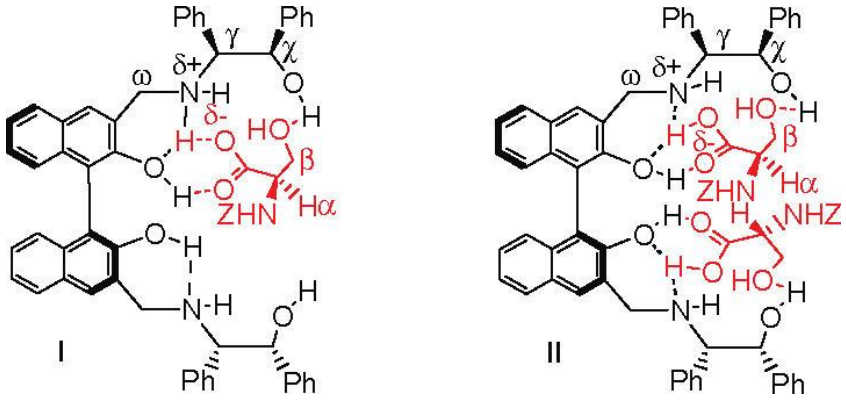

***Figure 4.6:** The Job plot obtained on the basis of the ^{1}H NMR data indicated the formation of a mixture of 1:1 and 1:2 complexes of (S)-**4.5** versus* N-*Z*-D-*Ser*-OH. *Structures **I** and **II** represent the possible structures of the ground state 1:1 and 1:2 complexes, respectively.*[10]

Receptor **4.5** gave good chiral sensing towards *N*-Z-Ser-OH, as described in the example reported in Section 1.5 (Figure 1.8).

The aim of the studies described in this chapter is the investigation of a new series of receptors based on the BINOL receptors developed by Prof. Pu, with the addition of ferrocene groups on the side chains to obtain bifunctional photo-active and electrochemical sensors.

Luminescent sensors can often achieve a higher sensitivity than electrochemical sensors, in terms of concentration of guest that can be detected (e.g. 10^{-5} M *vs.* 10^{-4} M respectively).[11] On the other hand, the latter have advantages in terms of versatility and applicability.[12] A number of receptors have been previously synthesised for the recognition of cations or ion pairs, with both electrochemical and optical reporting properties.[11, 13-14] However, despite the abundance of supramolecular receptors with the mentioned properties, there is no reported design of multifunctional molecules for chiral recognition.

It was anticipated that the addition of the ferrocene groups would modify the emission properties of the BINOL receptors,[15] as well as adding redox-active functionality to the sensors. Furthermore, the functionalisation of the side chains with chiral centres and planar chiral ferrocene groups would give the opportunity to study the effect of the different kinds of chirality on the enantioselective discrimination.

4.2 Synthesis of the receptors

Several receptors **4.8-4.15** were synthesised, containing different combinations of planar, central and axial chirality. They were obtained from the assembly of synthons obtained separately from adaptations of multi-step synthetic routes previously published. The ferrocenylmethanamine synthon **2.12** and the planar chiral amine **2.17** were obtained *via* the syntheses described in Section 2.2. The central chiral amines **2.19** and **3.13** were obtained using the three-step synthesis described in Section 3.2. The bis-carboxaldehyde BINOL derivatives were obtained from a three-step synthesis[16] involving protection of the hydroxy groups of either enantiomer of BINOL with methoxymethoxy groups, reaction with

n-BuLi and DMF to insert the carboxaldehyde groups at the α positions, and deprotection of the methoxymethoxy groups with HCl (Scheme 4.1).

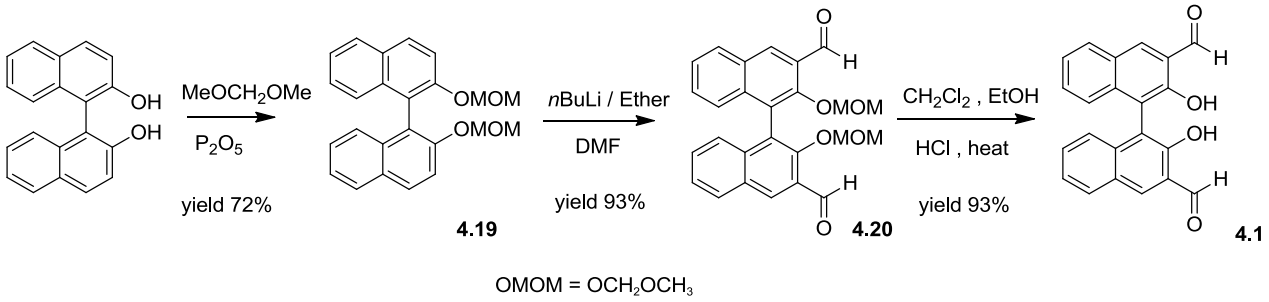

Scheme 4.1: *Synthesis of 3,3'-diformyl-2,2'-dihydroxy-1,1'-binaphthyl* ***4.1****.*[16]

The protecting groups direct the *ortho* lithiation by complexation with the oxygens of the methoxymethoxy groups. The deprotection consists of a simple and high yielding acid hydrolysis.

Receptors **4.8-4.15** were then obtained by reaction of the BINOL derivative, in its (*R)* or (*S)* form, with each of the different ferrocenyl amines, through condensation of the aldehyde groups with the amino groups (Scheme 4.2).[7, 17]

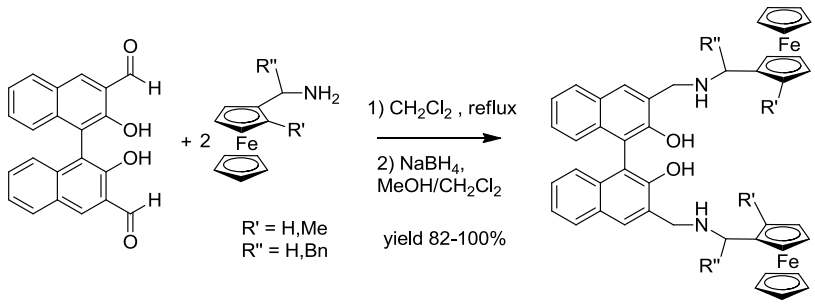

Scheme 4.2: *Synthesis of a generic BINOL receptor.*[7, 17]

Initially the Schiff base was formed, but it was not isolated and the crude was reacted with sodium borohydride to reduce it to the corresponding secondary amine in a high yield and with an enantiomeric excess derived from the enantiopurity of the synthons, to give receptors **4.8**-**4.15** (Scheme 4.3).

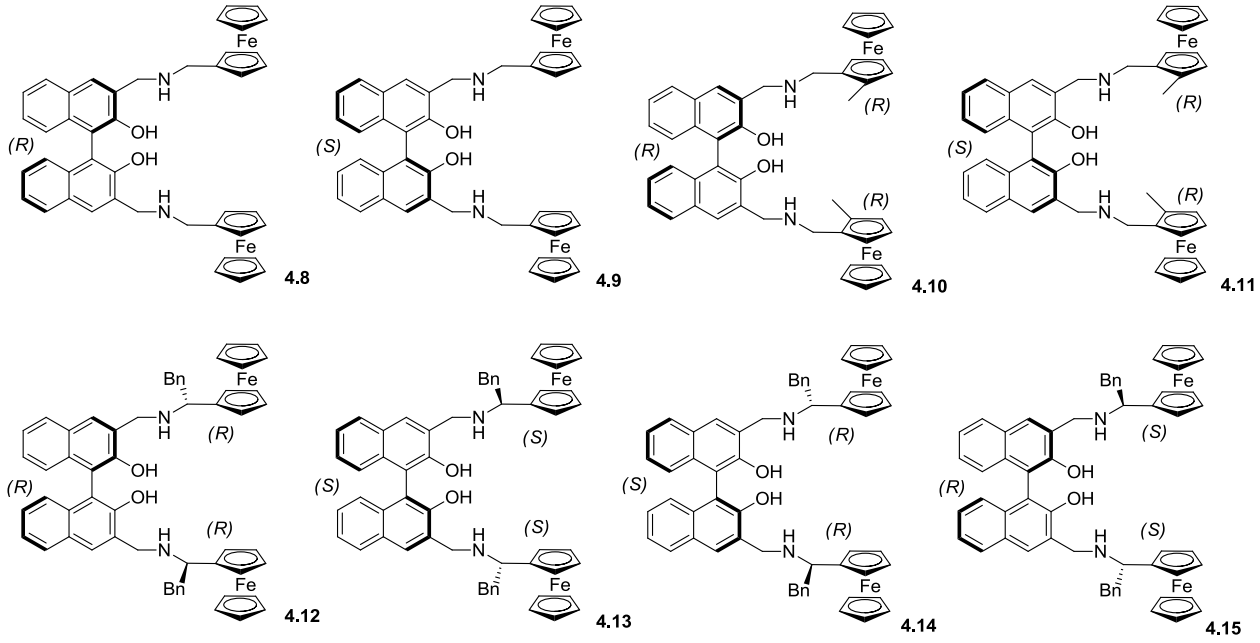

Scheme 4.3: *Receptors investigated in the studies.*

The receptors obtained were defined by the presence on the molecule of axial chirality only (**4.8** and **4.9**), axial chirality together with planar chirality on the ferrocene group (**4.10** and **4.11**) and the four different combinations coming from opposite axial chirality on the binol side and opposite central chirality on the ferrocenyl side of the receptors (**4.12** to **4.15**).

From analysis of the chiral HPLC traces of the receptors (reported in Appendix), it appears that all receptors with (*S*)-axial chirality had a slightly higher enantiopurity than the ones

with (*R*)-axial chirality, despite both BINOL starting materials being enantiopure (as assessed by chiral HPLC). Most likely, due to the high temperature, during the synthesis in Scheme 4.1 a partial conversion of (*R*) to (S) enantiomer occurred whilst the conversion of (*S*) to (*R*) enantiomer was smaller. For the receptors with only axial chirality **4.8** and **4.9**, the absence of any other stereochemistry simplifies the product distribution, with only two peaks observed: a major one for the desired product and a minor one for the opposite enantiomer. For receptors **4.10** and **4.11** the situation was the same, as the good enantiopurity of the planar chiral amine (ee% = 97% as deduced from the chiral purity of the ureas described in Chapter 2) hardly affected the purity of the final product. However, the situation was more complicated for receptors **4.12** to **4.15.** The centrally chiral amines used as synthons showed lower enantiopurity (ee% 82-89%) and upon reaction with the BINOL synthon, three products were formed, as indicated by chiral HPLC (see Appendix): the desired receptor as the major product, the diastereoisomer from the reaction with the opposite ferrocenyl enantiomer as the minor product and a third product in which both centrally chiral configurations were present in the same molecule (Scheme 4.4). Each receptor was purified using semi-prep HPLC, but unfortunately receptors **4.12** to **4.15** could not be successfully separated from the other two diastereoisomers described above and so they were used in the subsequent experiments without further purification, but nevertheless with a reasonable diastereomeric purity of ca. 83%.

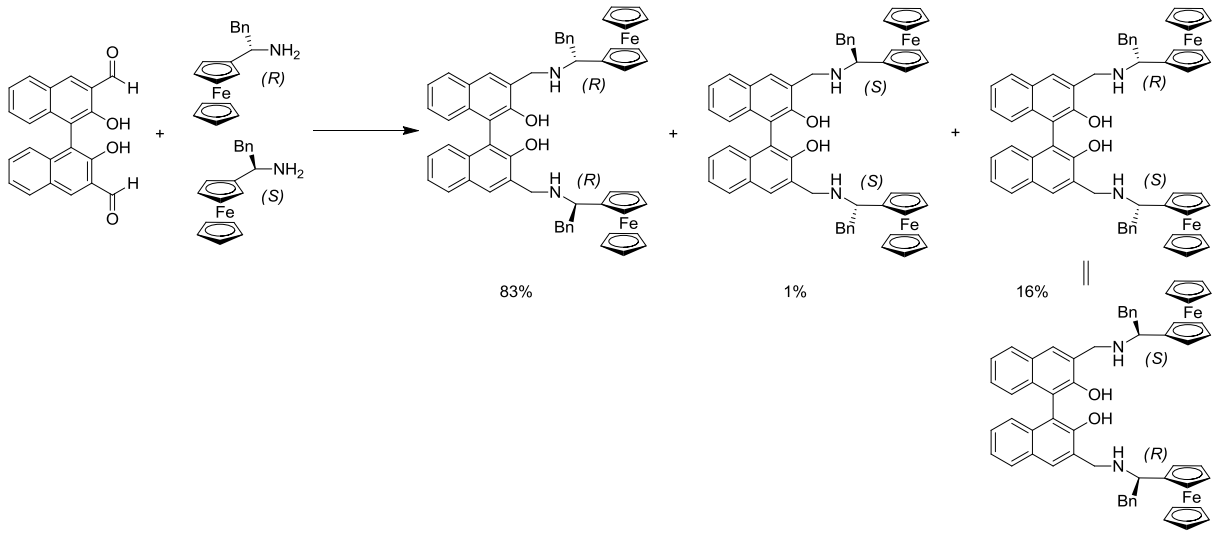

Scheme 4.4: *Possible diastereomeric products obtained using not enantiopure amines as synthons for the synthesis of the receptors with central chirality.*

Binding studies were performed with a variety of guests: initially the binding of mandelic acid **4.16** was explored as well as protected amino acids *N*-Cbz-Ser-OH **4.17** and *N*-Cbz-Ala-OH **4.18**. Given the poor solubility of the cheaper unprotected amino acids in a range of solvents, the binding of the TBA salts of Alanine **Ala**, Serine **Ser** and Proline **Pro** were also undertaken.

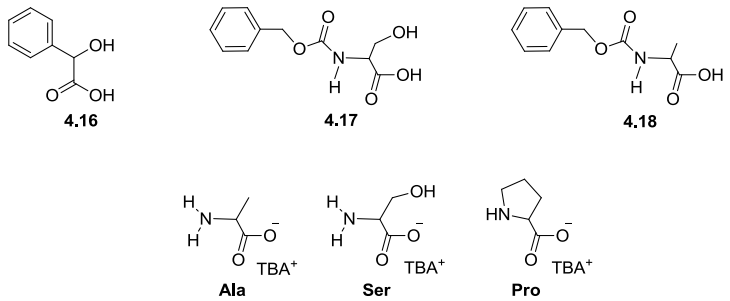

4.3 Binding Studies: ^{1}H NMR Studies and modeling

Unfortunately, no crystals suitable for X-Ray diffraction analysis were obtained from the class of receptors synthesised. To get information about the binding processes, ^{1}H NMR titrations were performed and Job plots calculated for receptors **4.17** and **4.18**. In addition, some semiempirical modelling of the structures of the receptors was performed to evaluate the possible structure of the complexes and explain binding affinities. A Job plot experiment[18] involving receptor **4.11** in the presence of guest **4.17** was performed. The receptor was dissolved in CD_2Cl_2 to prepare a solution of 5 mM concentration, and an equimolar solution of *L*-**4.17** was prepared in the same way. The two solutions were then mixed in different ratios, to obtain 11 samples of increasing molar fraction of the guest. These samples were then analysed by ^{1}H NMR spectroscopy, and the resulting spectra are shown in the stack in Figure 4.7.

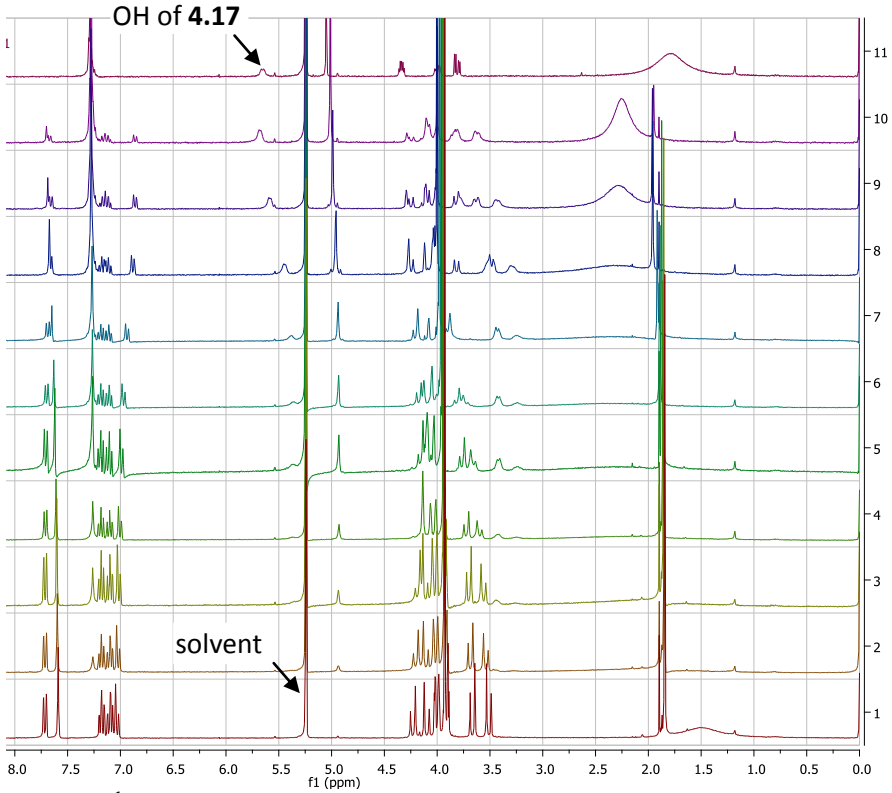

Figure 4.7: *Stack of ^{1}H NMR spectra of **4.11** with **4.17** with increasing molar fraction of guest: from 0 to 1 increasing 0.1 in each sample, 5 mM total conc. in CD_2Cl_2 at rt.*

From the spectra it was possible to observe an upfield shift in the OH signal of the guest, which indicated its participation in binding. Shifts in the CH_2 signal next to the binding sites were also observed, in the area between 3.5 and 4.5 ppm, but they overlap with the signals of the CH of the Cp rings and were not easy to follow, therefore the Job plot was obtained by following the shift of the aromatic CH signal from 7.04 to 6.86 (Figure 4.8).

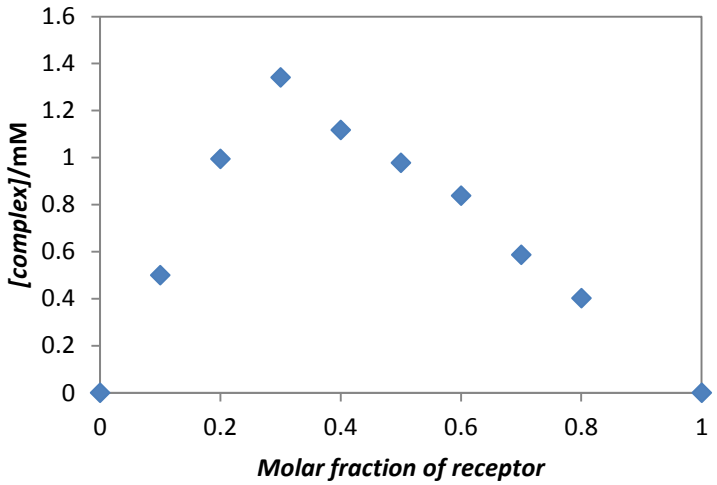

Figure 4.8: *^{1}H NMR Job plot of **4.11** with L-**4.17** in CD_2Cl_2 at rt (5 mM total concentration).*

A maximum at a host mole fraction of 0.33 indicates a 2:1 guest/host complex. However, a small shoulder at around 0.5 indicates that a 1:1 guest/host complex can also form, although in a smaller concentration.

Analogous experiments were performed with *L*-**4.18** and the same receptor **4.11**. The stacked ^{1}H NMR spectra are shown on the next page in Figure 4.9.

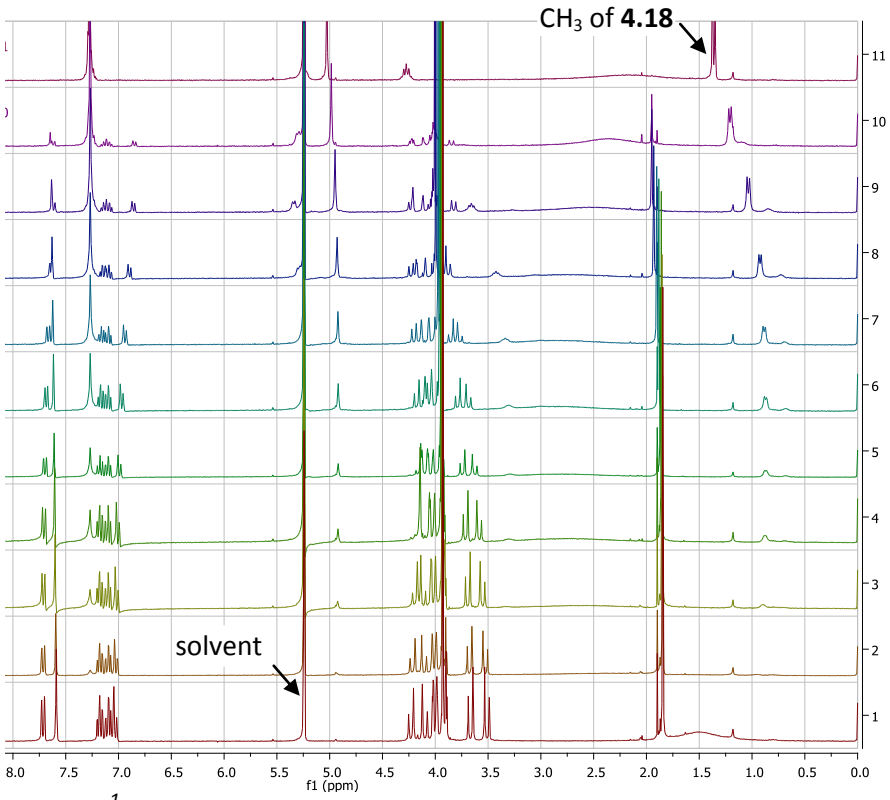

Figure 4.9: *Stack of ^{1}H NMR spectra of **4.11** with **4.18** with increasing molar fraction of guest: from 0 to 1 increasing 0.1 in each sample, 5 mM total conc. in CD_2Cl_2 at rt.*

In this guest the OH is not present; nevertheless, a small shift of the CH_3 is observed, as this could reside close to the binding sites. As in the previous experiment, the shifts of the CH_2 could not be followed, and the shift of the aromatic proton signals from 7.03 to 6.85 ppm was followed instead. The Job plot experiment showed analogous stoichiometry to the previous experiment (Figure 4.10).

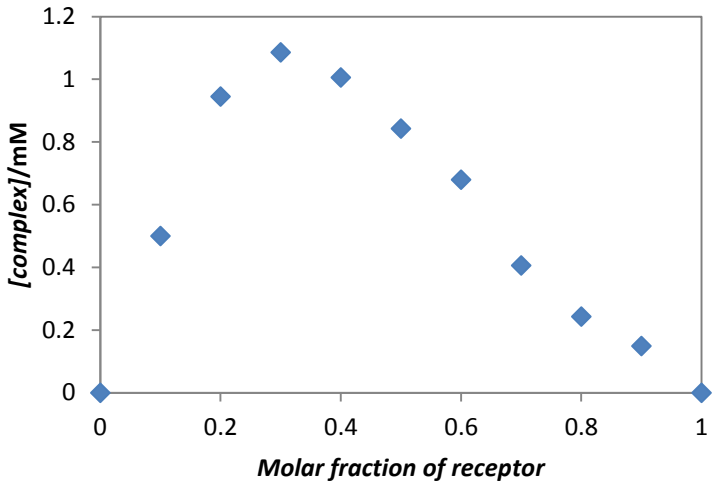

Figure 4.10: *^{1}H NMR Job plot of **4.11** with L-**4.18** in CD_2Cl_2 at rt (5 mM total concentration).*

Semi empirical modelling of the receptor **4.11** was then performed using ArgusLab software and UFF optimisation,[19] in order to understand how the binding sites can be oriented in the receptor and to obtain more information concerning possible structures of the complexes formed (Figure 4.11).

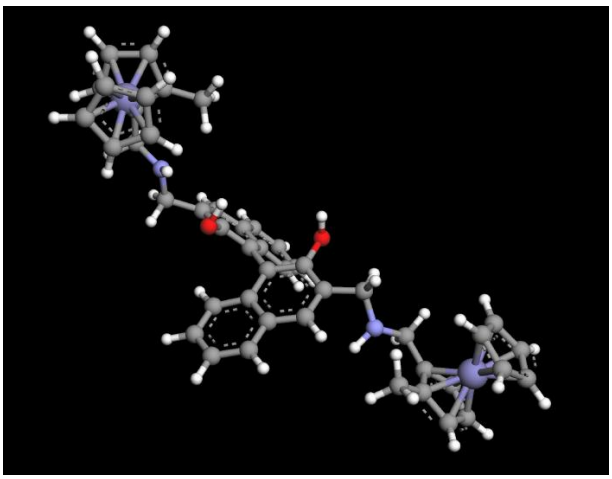

Figure 4.11: *Semi empirical model of the structure of **4.11.***

From evaluation of the structure it is possible that, while the OH groups are inside the cleft formed by the side chains of the receptor, the NH groups are pointing outside due to the ability of the side chains to twist. Thus, the cleft opens up and it is able to accommodate 2 guest molecules, which are bound perching sideways, as shown in Figure 4.12. Moreover, the π-stacking would explain the significant upfield shift observed for the aromatic protons.[20]

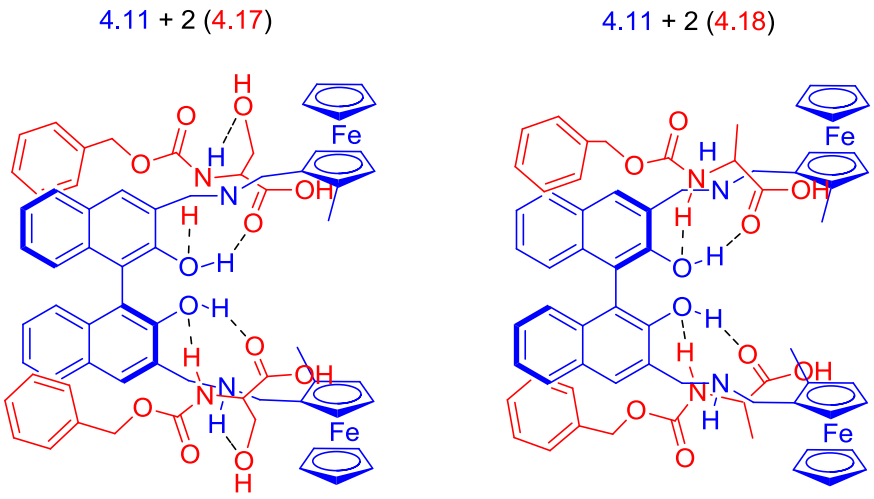

Figure 4.12: *Proposed structure of the complex of* ***4.11*** *with 2 molecules of* ***4.17*** *(left) and with 2 molecules of* ***4.18*** *(right).*

More ^{1}H NMR experiments were performed using guests **4.16** and **Ala**, **Ser** and **Pro**. Ten molar equivalents of each guest were added to the host **4.11** in CD_2Cl_2, in order to identify the interactions typical of the binding of these classes of molecules (Figure 4.13). Attention has been focused on the signals in the aromatic area, to investigate the effect of π-stacking on the binding, and for convenience the area of the spectra containing the signals relative to the tetrabutylammonium cations has been omitted.

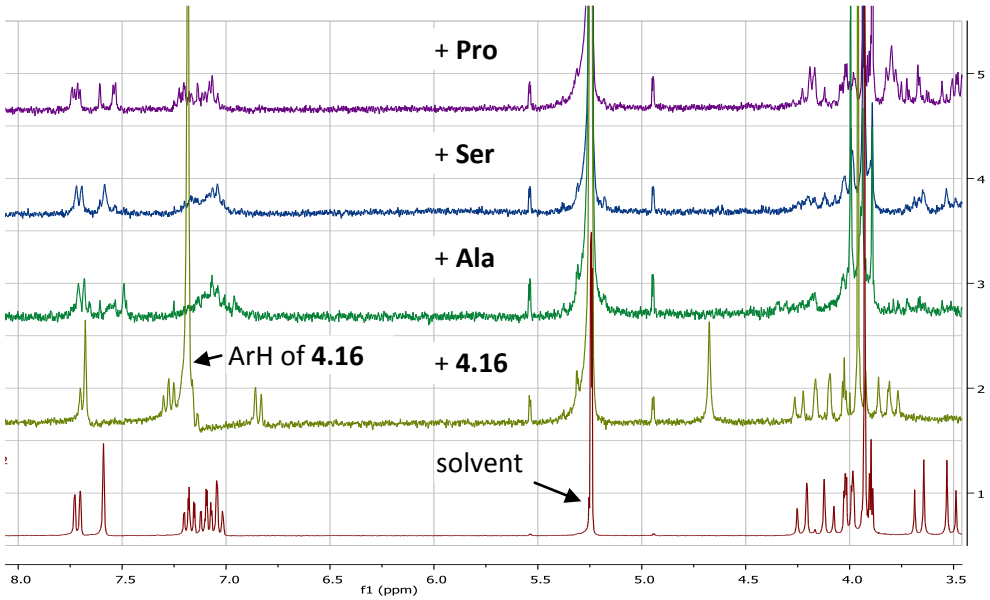

Figure 4.13: *Stack of ^{1}H NMR spectra of (bottom to top)* ***4.11*** *and* ***4.11*** *with* ***4.16***, ***Ala***, ***Ser*** *and* ***Pro.*** *(10 molar equivalents of guest, 5 mM total conc. in CD_2Cl_2 at rt.)*

The signals of some of the aromatic protons of **4.11** were shifted upfield after addition of **4.16**, as an effect of the π-stacking, but this shift did not occur for the addition of **Ala**, **Ser** and **Pro**, because of the absence of aromatic groups in the guest molecules. The CH_2 signals of the host molecule, which are situated in proximity of the NH groups, experienced a shift in each experiment (although with some differences). This is an indication that binding between the host and each of the guest molecules involved the NH binding sites.

4.4 Binding Studies: UV-Vis and Fluorescence Spectroscopy

The absorption spectra of the receptors were recorded in various solvents (MeCN, CH_2Cl_2, and toluene) in order to find an appropriate solvent for monitoring binding events. Preliminary experiments were performed by adding an excess amount of the various guests to all the receptors, but the changes in the adsorption spectra were generally minimal,

which would give an error too large in the calculation of the binding constants using the Benesi-Hildebrand method[21] (see Section 2.4.2). However, a peak at 340 nm was observed in every solvent. After confirmation from excitation spectra, this peak was chosen for the excitation wavelength in the emission experiments. For simplicity, only the absorption spectrum of one receptor in one solvent is reported, as they all showed the same absorption properties (Figure 4.14).

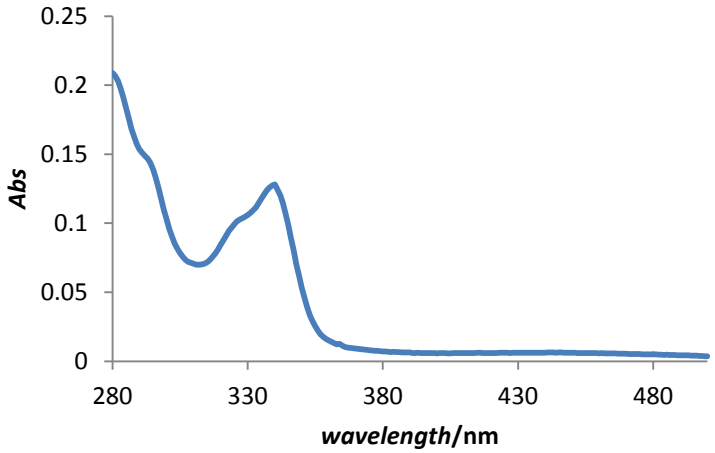

Figure 4.14: *UV-Vis of* ***4.12*** *in CH_2Cl_2 ($c = 2.0 \times 10^{-5}$ M; $Abs_{340nm} = 0.128$; $\varepsilon_{340nm} = 6384$).*

As described in Section 4.1, whereas BINOL is fluorescent itself, its emission is often quenched by functionalisation. This can be restored by the binding of guest molecules that disrupt the intramolecular hydrogen bonding and the communication with the side chains of the receptors. When this interaction is stronger with one enantiomer, it is possible to have chiral recognition through a larger emission enhancement for the guest that binds more strongly.[22-23] The emission experiments were performed with a concentration of host at 1.0×10^{-5} M, excitation at 340 nm, slit width 4.0 nm x 4.0 nm, scanning from 360 nm to 550 nm and subtraction of the solvent peak, unless stated otherwise. Initial tests in CH_2Cl_2 did not

show any emission enhancement upon addition of up to 50 equivalents of **4.16**. Thus, a less competitive solvent such as toluene was chosen, but a small percentage (1%) of dimethoxyethane (DME) had to be used to solubilise the guest, which was otherwise insoluble in toluene. Unfortunately, the receptors showed low stability in this solvent mixture, as the emission intensity increased with each scan: this is most likely due to degradation of the receptor upon irradiation with powerful UV light (150 W) in the presence of a high percentage of DME, with loss of the ferrocene moieties from the side chains and the subsequent gradual removal of the quenching. By reducing the amount of DME to 0.03 %, good stability of the emission signal was observed for the free host, but the same instability occurred in the presence of the guest **4.16**, possibly because of its acidic nature. However, the first scan showed significant differences in the emission enhancement upon complexation of opposite enantiomers. These were confirmed by mirrored results with opposite enantiomers of the receptors (Figure 4.15). Unfortuantely it was not possible to perform titrations with subsequent addition of this guest: for this reason the interaction with different types of guests was investigated.

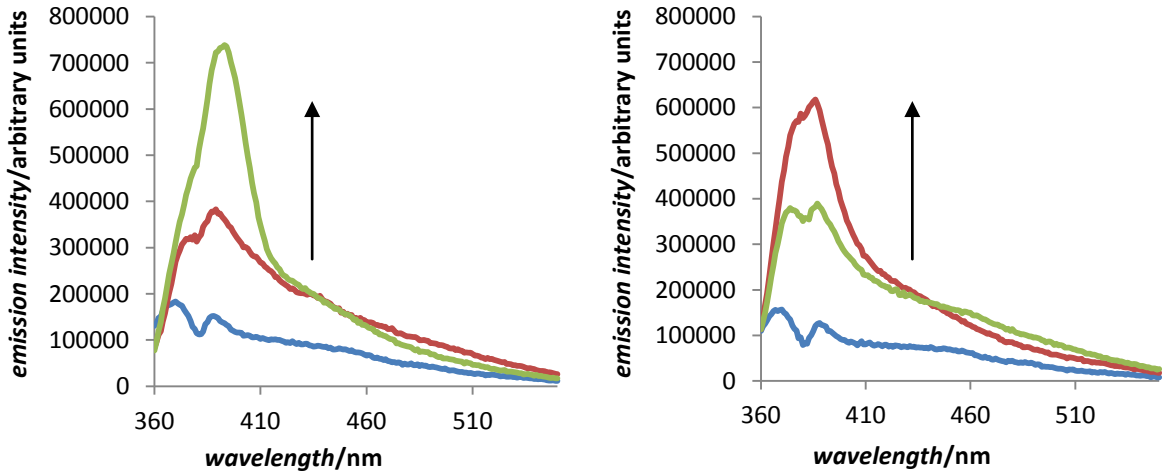

Figure 4.15: *Emission enhancement of* ***4.12*** *(left) and* ***4.13*** *(right) in toluene/DME 0.03%, host conc. 1.0 x* 10^{-5}*M,* λ_{exc} *= 340 nm, slit 4.0 nm x 4.0 nm at rt; blue) free host; red) with 10 eq. of (R)-****4.16****; green) with 10 eq. of (S)-****4.16****.*

Preliminary studies with less acidic guests such as diols [*cis*-cyclopentanediol, (2*S*,4*S*)-pentanediol and (2*R*,4*R*)-pentanediol] were performed, but no emission enhancement was observed upon addition of up to 100 equivalents in toluene, presumably due to a lack of binding. Protected amino acids were then selected: they are less acidic than mandelic acid, they can be important analytes and the protecting group on the amino functionality ensures a good solubility in organic solvents, unachievable with unprotected amino acids.[10, 24]

N-Cbz-Serine-OH **4.17**, in its *L* and *D* forms, was tested with addition of 100 equivalents to hosts **4.8** and **4.12** in toluene/DME 1%. The emission signal in the free host was variable upon irradiation with UV light because of the high percentage of DME, as described previously. However, the receptors showed significant change in emission in the first scan upon complexation, and receptor **4.12** was able to give chiral recognition (Figure 4.16).

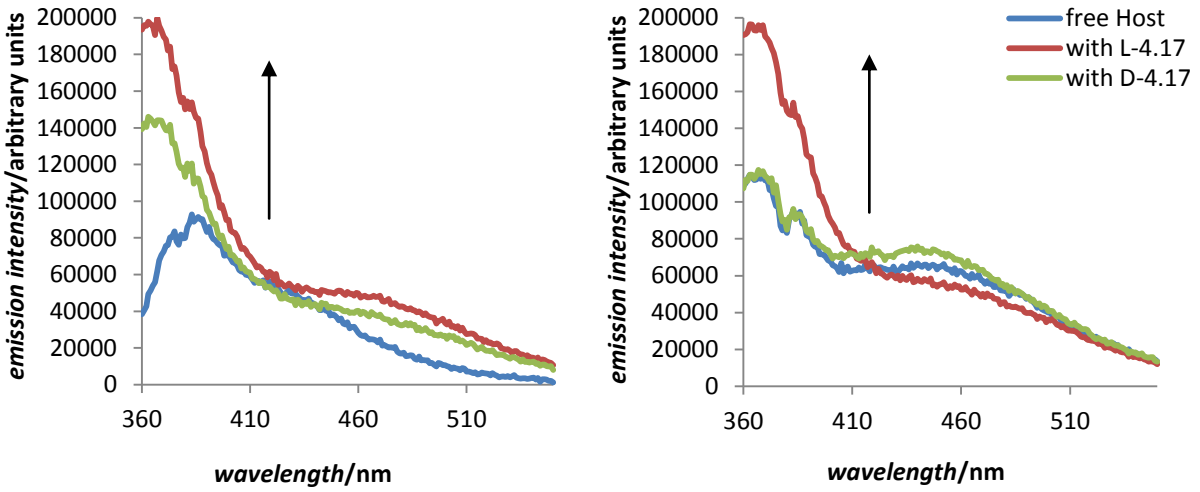

Figure 4.16: *Emission enhancement of of* ***4.8*** *(left) and* ***4.12*** *(right) in toluene/DME 1%, host conc. 1.0 x 10^{-5}M, λ_{exc} = 340 nm, slit 4.0 nm x 4.0 nm, with 100 equivalents of* ***4.17*** *at rt.*

To try to avoid the instability in the emission signals, the same experiment was repeated in different solvents (dichloromethane and toluene/THF 2%). In dichloromethane, the compounds were stable over time as shown by constant fluorescence emission levels, but chiral discrimination of opposite enantiomers of the same guest **4.17** was fairly poor (Figure 4.17).

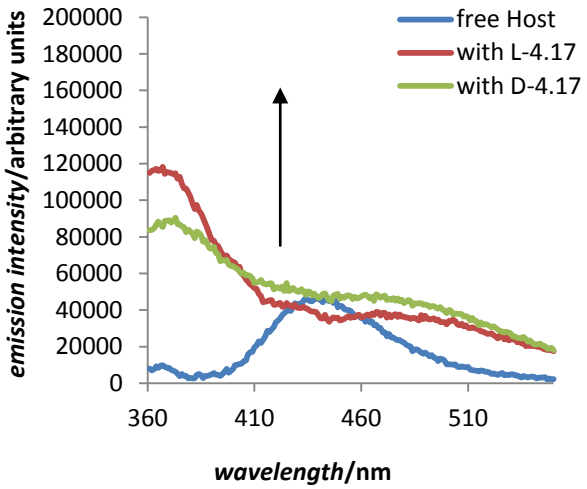

Figure 4.17: *Emission enhancement of* ***4.12*** *in CH_2Cl_2, host conc. 1.0 x 10^{-5}M, λ_{exc} = 340 nm, slit 4.0 nm x 4.0 nm, with 100 equivalents of* ***4.17*** *at rt.*

It was thought that the high solubility of both receptors and guest **4.17** in THF could make of this solvent a good alternative to DME. However, THF also caused instability in the fluorescent emission by causing degradation of the receptors. Nevertheless, the emission intensity was significantly different in the first scan for the free host and for the host in the presence of 100 equivalents of guest, and receptor **4.12** could be used for chiral recognition. This was confirmed by experiments with the host **4.13** with opposite chirality (Figure 4.18).

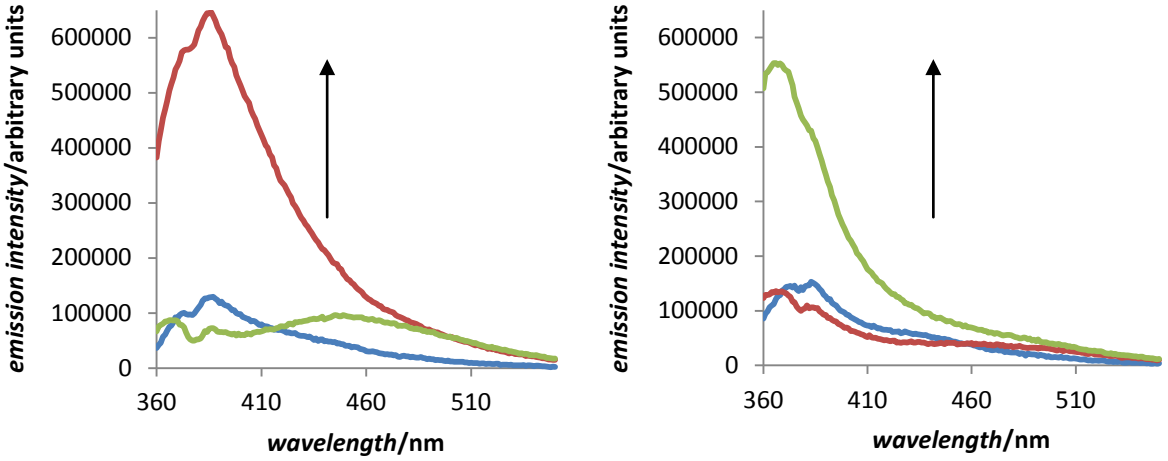

Figure 4.18: *Emission enhancement of* ***4.12*** *(left) and* ***4.13*** *(right) in toluene/THF 2%; host conc. 1.0 x* 10^{-5}*M, slit 4.0 nm x 4.0 nm; blue) free host; red) with 100 eq. of* L-***4.17****; green) with 100 eq. of* D-***4.17****.*

The experiments were also repeated at different concentrations, but it appears that the concentration of 10^{-5} mol/L was optimum to obtain the best results in terms of sensitivity and selectivity. This is likely to be consistent with an aggregation effect at higher concentration,[25-26] which would decrease the selectivity of the receptors.

With an interest in exploring the binding of smaller guests than the bulky protected amino acids, tetrabutylammonium salts of Alanine (**Ala**), Serine (**Ser**) and Proline (**Pro**) were prepared following the procedure described in Section 6.1.45. Fluorescence studies in CH_2Cl_2 were performed using receptor **4.12** and **4.13** and testing the addition of 50 equivalents of both the enantiomers of the amino acid salts (Figure 4.19). Whilst the receptors were not able to discriminate between the enantiomers of the same guest, giving approximately the same fluorescence enhancement response upon formation of the complex, they showed a good selectivity towards **Pro** over the other amino acid salts.

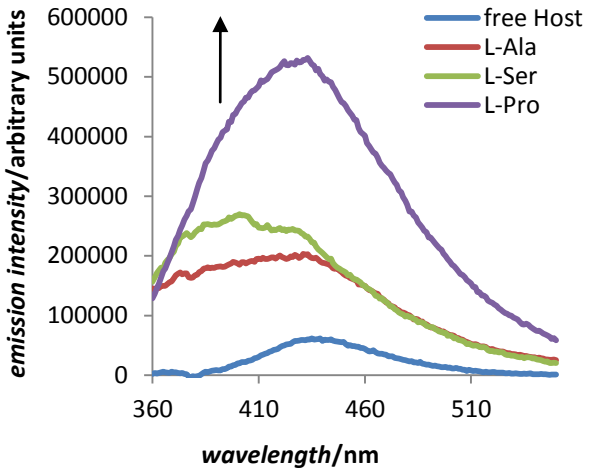

Figure 4.19: *Emission of* ***4.12*** *as a free host, and upon addition of 50 equivalents of the* L-*enantiomers of* ***Ala***, ***Ser*** *and* ***Pro*** *(Host conc. 1.0 x* 10^{-5} *M, slit 4.0 nm x 4.0 nm, in* CH_2Cl_2 *at rt.)*

To assess if the selectivity towards **Pro** was caused only by a stronger quenching effect of the primary amine groups[27] of **Ala** and **Ser** or by a stronger binding of **Pro** to the receptors, competition experiments followed by UV-Vis spectroscopy were performed (Figure 4.20).

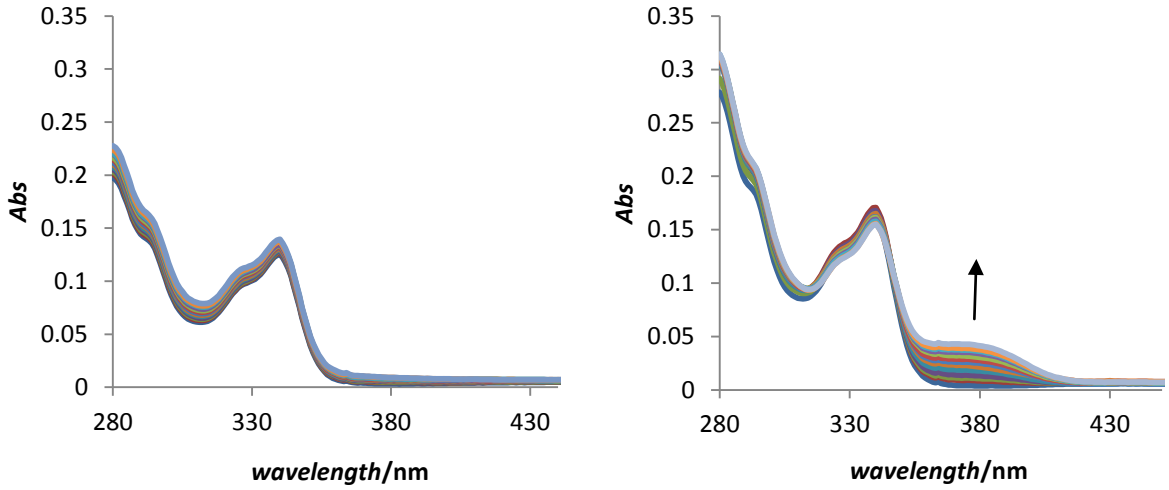

Figure 4.20: *Change in the absorption spectrum of* ***4.12*** *with addition of (left)* L-***Pro*** *or (right)* L-***Ala*** *in* CH_2Cl_2 *at rt, host 2.0 x* 10^{-5} *M, up to 50 equivalents of guest added.*

In contrast to the fluorescence results, the addition of **Pro** as well as **Ser** did not cause any significant changes in the absorption spectrum in CH_2Cl_2, whereas the addition of **Ala** did generate a new absorption band around 380 nm. This interesting effect was exploited to

understand the relative difference in binding strength between these two guests. A solution of **4.12** with 70 equivalents of **Ala** already present was prepared, giving the band at 380 nm. To this solution the competing guest **Pro** was then slowly added as in a normal titration, in aliquots of *ca.* 5 equivalents each (Figure 4.21).

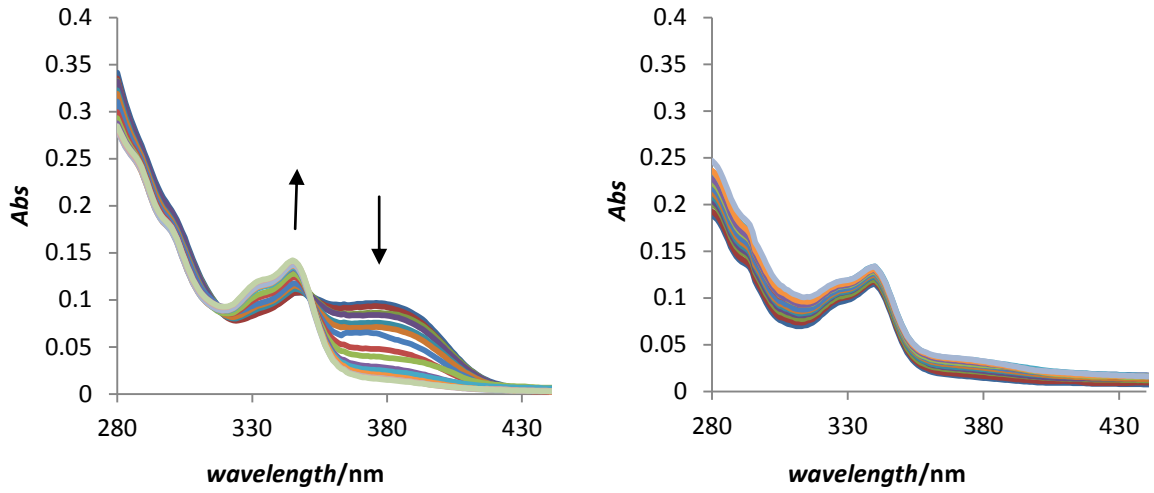

Figure 4.21: *Change in the absorption spectrum of (left)* ***4.12*** *with 70 eq. of* L-***Ala*** *and addition of* L-***Pro****, and (right)* ***4.12*** *with 70 eq. of* L-***Pro*** *and addition of* L-***Ala****, in* CH_2Cl_2 *at rt, host 2.0 x* 10^{-5} *M, up to 70 equivalents of competing guest added.*

This resulted in the absorption band at 380 nm completely disappearing, while the absorption at 340 nm increased slightly, and an isosbestic point at 350 nm was observed. Therefore, **Pro** is able to displace **Ala** from the binding sites of the receptor. A control experiment under the same conditions, in which **Ala** was added to a prepared solution of **4.12** with **Pro**, confirmed that **Pro** binds more strongly than **Ala** to the receptor, since the band at 380 nm did not appear and **Ala** was not able to displace **Pro** from the binding sites of the receptor (Figure 4.21). This is possibly due to the structural difference in the guests, with **Ala** and **Ser** possessing primary amine groups, whereas **Pro** possesses a secondary amine group, which could be less effective in destabilising the complex formation.

4.5 Electrochemical Studies

4.5.1 Studies on the free receptors

Initially, cyclic voltammetry was used to assess whether the free receptors showed electrochemical reversibility in organic solvents such as MeCN. The potential was swept at different scan rate, varying from 100 to 1100 mV s^{-1} (CVs are provided in Figure 4.22).

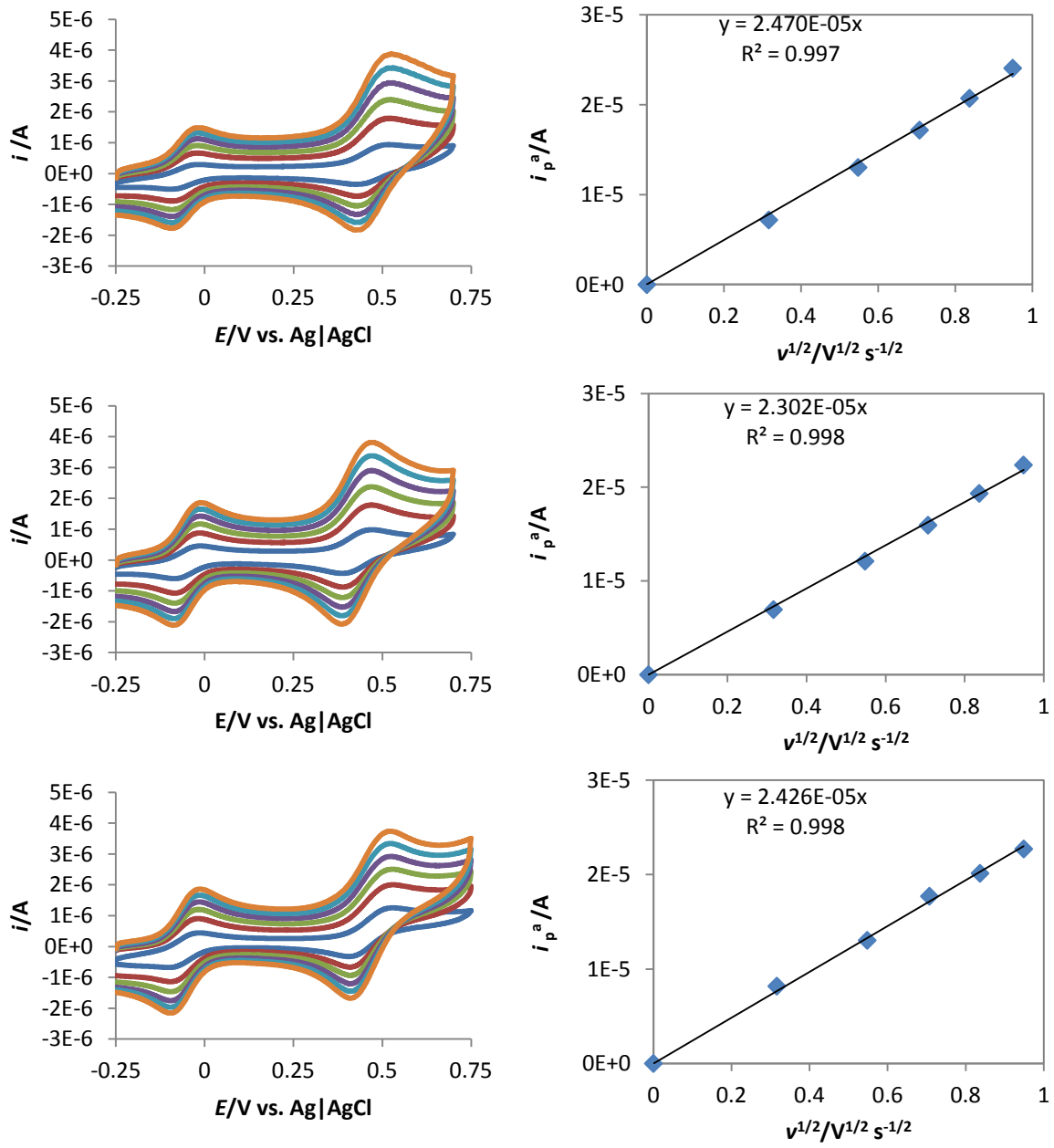

Figure 4.22: *CVs at various scan rates and plots of current intensity vs. the square root of the scan rate for a)* ***4.9*** *b)* ***4.10*** *c)* ***4.12*** *(≈7 x 10^{-5} M in MeCN at rt, $TBAPF_6$ 0.1 M, with dmfc; scan rate analysed: 100 mV s^{-1}, 300 mV s^{-1}, 500 mV s^{-1}, 700 mV s^{-1}, 900 mV s^{-1}, 1100 mV s^{-1}).*

All the receptors exhibited one single redox wave, as the two ferrocene moieties on the side chains of the molecules are equivalent and not communicating with each other.[28] The waves are reversible as the intensity of current of the cathodic peak is similar to that of the anodic peak[29] and there was no loss of electroactivity over several consecutive scans (up to 20).

As expected (Table 4.1), the receptors **4.8** and **4.9** with no substituents on the ferrocene gave more positive formal electrode potentials than the planar chiral ferrocene compounds **4.10** and **4.11** because of the electron donating properties of the methyl group on the cyclopentadienyl.[30-31] These make the Fc groups thermodynamically easier to oxidise by stabilising the higher oxidation state.

Table 4.1: *Formal electrode potentials (mV ± 5 mV) versus dmfc of receptors* ***4.8*** *to* ***4.15****. (≈7 x* 10^{-5} *M,* $TBAPF_6$ *0.1 M in MeCN at rt.)*

Receptor	*E*/V vs. dmfc
4.8	529
4.9	528
4.10	479
4.11	476
4.12	514
4.13	522
4.14	520
4.15	516

4.5.2 Binding Studies with Mandelic Acid

Square wave voltammetry was used to minimise the error in the position of the peaks and consequently in the binding curves. Binding curves were obtained by plotting the shift in the potential from the initial value for the free receptor against the equivalents of guest added. All the receptors exhibited a peak shift towards more positive potentials (example in Figure 4.23) of approximately the same magnitude (between 60 and 70 mV) upon addition of a large excess of guest (approximately 100 equivalents).

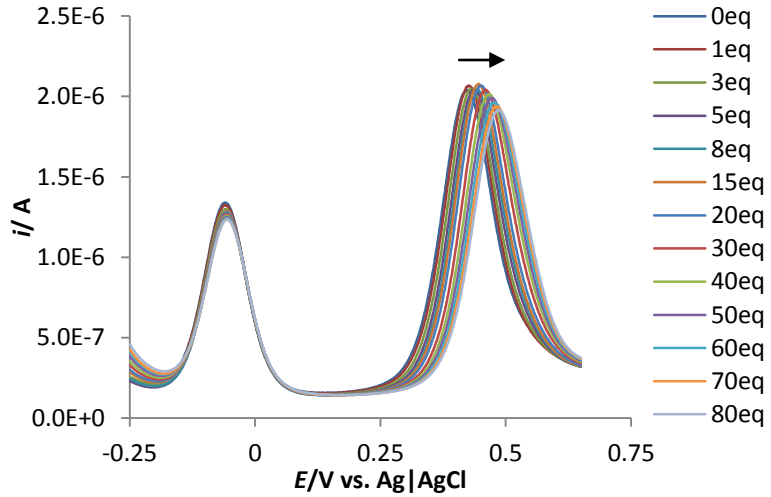

Figure 4.23: *Formal electrode potential shift observed for* ***4.10*** *upon addition of (S)-****4.16.*** *(Host 6.8 x 10^{-5} M in MeCN, $TBAPF_6$ 0.1 M, with dmfc, guest 7.6 x 10^{-2} M at rt.)*

The positive shift indicates that complexation of the guest induces an electron withdrawing effect, gradually destabilising the higher oxidation state of the ferrocenyl redox active units. This is consistent with the NH groups on the receptors acting as H-bond donors to the guests. However, the shifts are relatively smaller than those observed with the receptors discussed in the previous chapters. This could be due to the use of a neutral guest rather than a charged guest. Some differences between enantiomers were observed, but many

were within experimental error, apart from the results with receptor **4.10**, as shown in Figure 4.24 and Table 4.2.

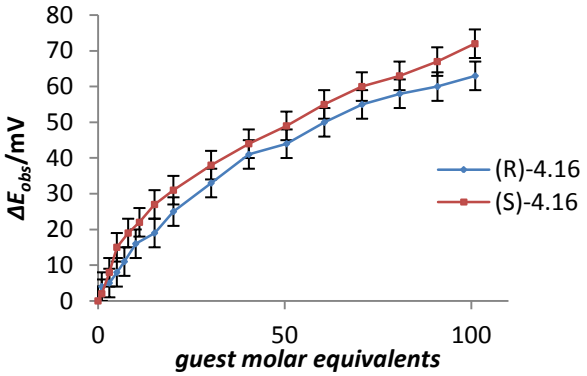

Figure 4.24: *Potential shift observed (mV ± 4 mV) for* ***4.10*** *plotted against the equivalents of (S)-****4.16*** *and (R)-****4.16*** *added. (Host 6.7 x 10^{-5} M in MeCN, $TBAPF_6$ 0.1 M, with dmfc at rt.)*

Table 4.2: *Potential shift (mV ± 4 mV) observed for receptors* ***4.8*** *to* ***4.15*** *upon addition of 100 equivalents of (S)-****4.16*** *and (R)-****4.16.*** *(≈7 x 10^{-5} M, $TBAPF_6$ 0.1 M in MeCN at rt.)*

Receptor	(*S*)-**4.16**	(*R*)-**4.16**
4.8	+62	+62
4.9	+61	+61
4.10	+72	+63
4.11	+67	+71
4.12	+36	+35
4.13	+36	+35
4.14	+35	+30
4.15	+38	+33

This could be due to the combined effect of (*R*)-planar chirality with (*R*)-axial chirality being slightly more effective in chiral discrimination than (*R*)-planar chirality with (*S*)-axial chirality. The receptors with central chirality gave a smaller potential shift upon addition of the same number of equivalents of guest. This was possibly due to the bulkier groups present on the receptors, which obstruct the complementarity towards the guests under examination.

4.5.3 Binding studies with protected amino acids

Electrochemical studies using square wave voltammetry were performed to study the behaviour of receptors **4.12** and **4.13** in the presence of *L*-**4.17**, *D*-**4.17** and *L*-**4.18**. Once again, the addition of guests caused a shift towards a more positive potential of the wave relative to the ferrocene/ferrocenium couple (example in Figure 4.25). The shifts are reported in Table 4.3.

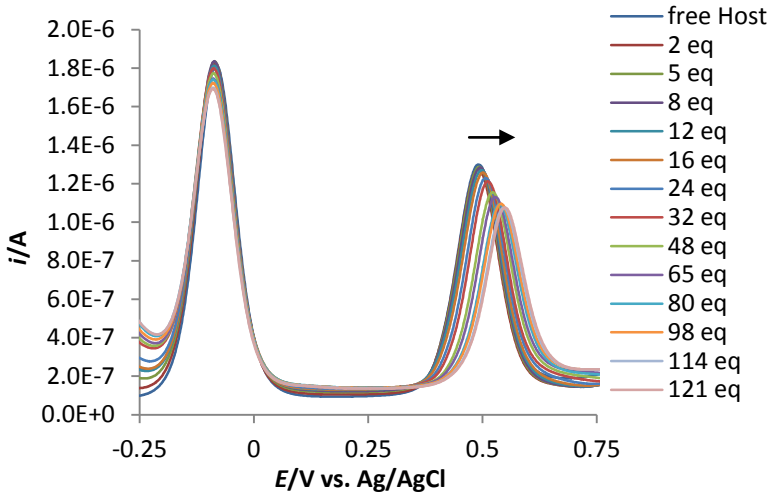

Figure 4.25: *Potential shift observed for* ***4.12*** *upon addition of* L-***4.18.*** *(Host 5.9 x* 10^{-5} *M in* CH_2Cl_2 *at rt,* $TBAPF_6$ *0.1 M, with dmfc, guest 9.6 x* 10^{-2} *M.)*

Table 4.3: *Potential shift (mV ± 4 mV) observed for receptors* ***4.12*** *and* ***4.13*** *upon addition of 30 equivalents of* L-***4.17****,* D-***4.17****, and 120 equivalents of* L-**4.18.** *(≈7 x* 10^{-5} *M,* $TBAPF_6$ *0.1 M in* CH_2Cl_2 *at rt.)*

	4.12	**4.13**
L-**4.17**	+85	+83
D-**4.17**	+77	+93
L-**4.18**	+64	+65

The potential shift $\Delta E^{o\prime}$ was higher with 30 equivalents of **4.17** than with 100 equivalents of **4.16** (Table 4.2) and 120 equivalents of **4.18**. The differences between the responses

obtained with the opposite enantiomers are small in CH_2Cl_2; the solubility of analytes and supporting electrolytes in toluene are poor, thus it was not possible to perform the electrochemistry experiments and reproduce the results obtained in the fluorescence experiments. Also, in CH_2Cl_2 the solubility of the guests was limited and for this reason the addition of guest **4.17** was stopped at 30 equivalents. However, limited chiral discrimination was observed with **4.17**, as shown in Figure 4.26 and confirmed by opposite results obtained with receptors of opposite chirality.

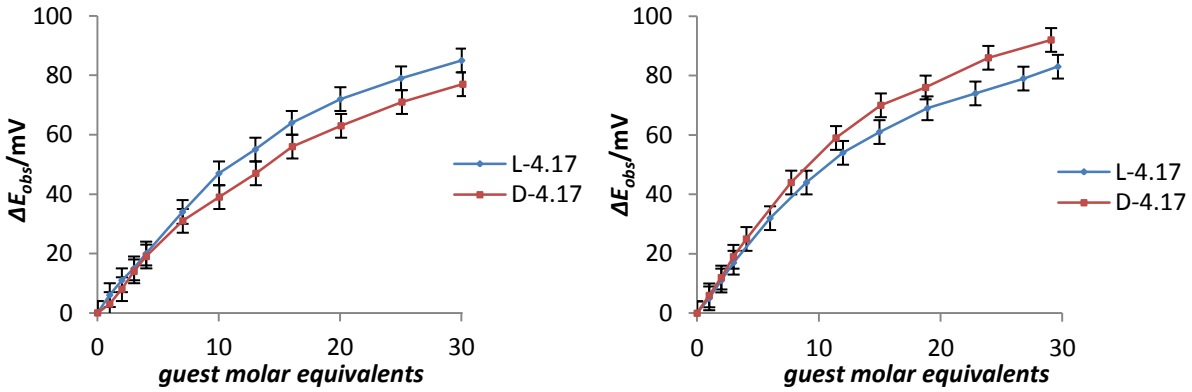

Figure 4.26: *Potential shift observed for* ***4.12*** *(left) and* ***4.13*** *(right) against the equivalents of* L-***4.17*** *and* D-***4.17*** *added. (Host 5.4 x* 10^{-5} *M in* CH_2Cl_2*,* $TBAPF_6$ *0.1 M, with dmfc at rt.)*

The relatively large shift compared to mandelic acid could be caused by a greater tendency to form the 1:2 complex rather than 1:1, as suggested by the previous studies described in Section 4.1 and by the Job plot[18] results obtained by ^{1}H NMR and described in Section 4.3. However, this is not the only cause because control experiments with *L*-**4.18** showed a much weaker binding and the total absence of chiral discrimination (Figure 4.27).

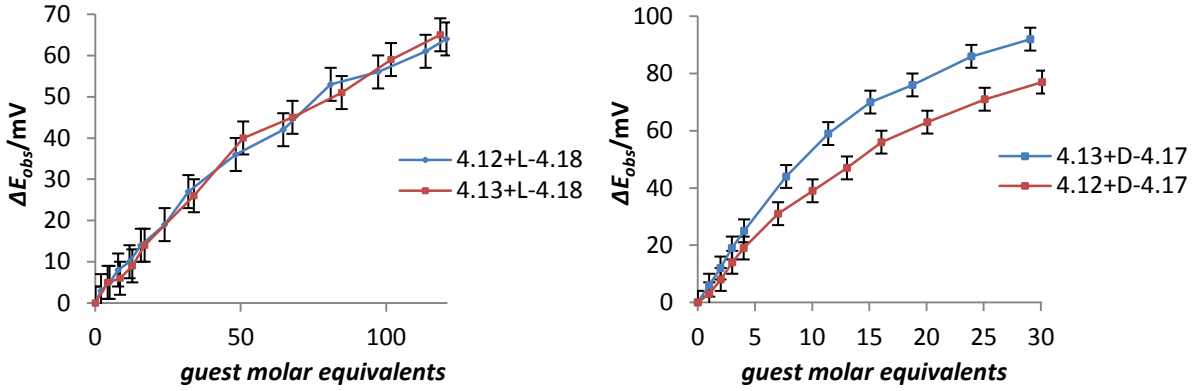

Figure 4.27: *Formal electrode potential shift (mV ± 4 mV) observed for* ***4.12*** *and* ***4.13*** *plotted against the equivalents of* L-***4.18*** *(left) and* D-***4.17*** *(right) added. (Host 5.7 x* 10^{-5} *M in* CH_2Cl_2*,* $TBAPF_6$ *0.1 M, with dmfc at rt.)*

This can be explained by the absence on **4.18** of the hydroxyl group present on **4.17**, which is the only difference between the two substrates. This hydroxyl group can interact with the receptor (as shown in Section 4.3) strengthening the binding, as confirmed using the software Letagrop,* which is a non-linear regression program capable of fitting the voltammograms and calculate the binding constants (Table 4.4). The binding constants showed smaller values for **4.18** than **4.17**. However, they are too similar to explain any chiral discrimination, as this effect is possibly not due to enantioselective binding, but to differences in the redox response to complexation.[32]

Table 4.4: *Binding constants calculated for receptors* ***4.12*** *and* ***4.13*** *with addition of* L-***4.17***, D-***4.17*** *and* L-***4.18***. *(≈5.5 x* 10^{-5} *M,* $TBAPF_6$ *0.1 M in* CH_2Cl_2 *at rt.)*

		L-**4.17**	*D*-**4.17**	*L*-**4.18**
4.12	**logK_1**	3.65 ± 0.15	3.23 ± 0.07	2.16 ± 0.16
	logβ	7.26 ± 0.14	6.86 ± 0.60	5.19 ± 0.08
4.13	**logK_1**	3.65 ± 0.16	3.24 ± 0.18	2.00 ± 0.13
	logβ	7.25 ± 0.14	7.15 ± 0.10	5.38 ± 0.06

* Fitting and calculations performed by Dr. Nathan D. McClenaghan at the University of Bordeaux 1

4.5.4 Binding studies with amino acid salts

Cyclic Voltammetry experiments were performed on the complexes formed between the BINOL receptors and the amino acid salts by adding an excess of guest to a solution of the host (Figure 4.28).

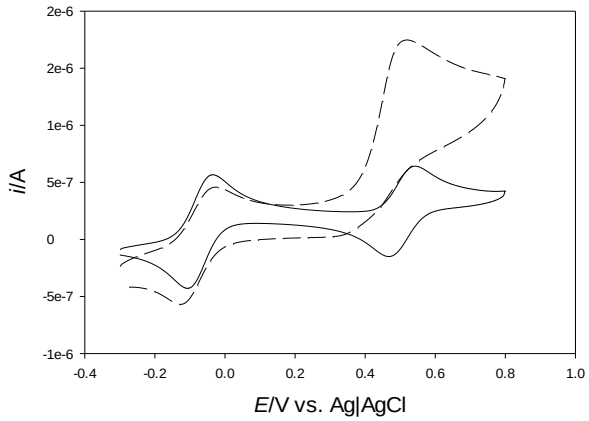

Figure 4.28: *Cyclic voltammograms of* ***4.12*** *(solid line) and* ***4.12*** *upon addition of 25 equivalents of* L-***Pro*** *(dashed line). Host 5.32 x* 10^{-5} *M in* CH_2Cl_2, $TBAPF_6$ *0.1 M, with dmfc at rt.*

Unlike the guests previously studied, these guests caused a shift towards less positive potential in the waves relative to the ferrocene/ferrocenium redox couple, in CH_2Cl_2. This is consistent with the results reported in the previous chapters and in previous work of the group,[32-33] as the negative charge of the anions pushes electron density towards the ferrocene units, making them thermodynamically easier to oxidise. However, when the complex is formed there is a loss in chemical reversibility, with complete disappearance of the reduction peak of the analyte. This is because the oxidised form decomposes upon formation of the complex on the timescale of the experiment. Therefore, it was not possible to perform a titration as described previously for the other guests.

4.6 Conclusions and Future Work

A novel class of receptors based on BINOL and ferrocenyl units with –OH and –NH binding sites was synthesised successfully and in high yield. The only weak point found was in the less than optimum chiral purity of the central chiral amines, which caused the formation of diastereoisomers that were hard to separate from the desired receptors. However, given that the desired product was present as the major component of the mixture, the receptors could still be used for chiral recognition. The best chiral recognition was obtained in toluene, a solvent that is not as competitive as CH_2Cl_2 or MeCN. However, experiments in toluene could only be performed using fluorescence techniques rather than electrochemistry, due to the low polarity of this solvent. The guests by themselves were not soluble in toluene, so the addition of an auxiliary solvent was needed. 2% of THF in toluene was the optimum solvent mixture to obtain a good enantioselectivity for the system of the central chiral receptors with *N*-Cbz-Ser-OH. The presence of THF decreased the stability of the analytes upon irradiation with UV light; therefore, titration experiments could not be performed. Nevertheless, the initial scan of free host and host/guest complexes were reproducible and they showed mirrored behaviour for opposite enantiomers of the receptors. Therefore, they could be exploited for chiral discrimination. Electrochemistry experiments were performed on these systems in CH_2Cl_2: in general low or no enantioselectivities were observed in this more competitive solvent, but the potential shift was quite large. This was in line with the proposed formation of a 2:1 guest/host complex, confirmed by a ^{1}H Job plot. One application of these receptors could also be the discrimination between different amino acids in their anionic form: proline could be distinguished by fluorescence spectroscopy and

this effect could be related to the absence of quenching from primary amine groups, or to its superior binding strength, as indicated by UV-Vis spectroscopy.

Future work on this class of receptors could start with attempts to increase the stability of the molecules under irradiation with UV light, by replacing the secondary amino groups with amide or urea functionalities. An interesting advancement in this research could also include the closure of the cleft to form a cavity by synthesising a series of macrocycles, thus increasing the complementarity towards the guests. An alkyl chain terminating in a thiol or disulfide could also be appended to the receptors to immobilise them on a surface and exploit the surface enhancement described in Chapter 3, with all the advantages in terms of reusability and amount of material used for the experiments.

4.7 References

1. Dhara, K.; Sarkar, K.; Roy, P.; Nandi, M.; Bhaumik, A.; Banerjee, P., *Tetrahedron* **2008,** *64*, 3153-3159.
2. Liu, S. L.; Pestano, J. P. C.; Wolf, C., *J. Org. Chem.* **2008,** *73*, 4267-4270.
3. Lu, Q. S.; Dong, L.; Zhang, J.; Li, J.; Jiang, L.; Huang, Y.; Qin, S.; Hu, C. W.; Yu, X. Q., *Org. Lett.* **2009,** *11*, 669-672.
4. Qing, G. Y.; Sun, T. L.; Chen, Z. H.; Yang, X.; Wu, X. J.; He, Y. B., *Chirality* **2009,** *21*, 363-373.
5. Costero, A. M.; Llaosa, U.; Gil, S.; Parra, M.; Colera, M., *Tetrahedron-Asymmetry* **2009,** *20*, 1468-1471.
6. Xu, K. X.; Qiu, Z.; Zhao, J. J.; Zhao, J.; Wang, C. J., *Tetrahedron-Asymmetry* **2009,** *20*, 1690-1696.
7. Lin, J.; Rajararn, A. R.; Pu, L., *Tetrahedron* **2004,** *60*, 11277-11281.
8. Liu, H. L.; Hou, X. L.; Pu, L., *Angew. Chem.-Int. Edit.* **2009,** *48*, 382-385.
9. Liu, H. L.; Peng, Q.; Wu, Y. D.; Chen, D.; Hou, X. L.; Sabat, M.; Pu, L., *Angew. Chem.-Int. Edit.* **2010,** *49*, 602-606.
10. Liu, H. L.; Zhu, H. P.; Hou, X. L.; Pu, L., *Org. Lett.* **2010,** *12*, 4172-4175.

11. Alfonso, M.; Contreras-Garcia, J.; Espinosa, A.; Tarraga, A.; Molina, P., *Dalton Trans.* **2012,** *41*, 4437-4444.
12. Boulas, P. L.; Goméz-Kaifer, M.; Echegoyen, L., *Angew. Chem. Int. Ed.* **1998,** *37*, 216-247.
13. Alfonso, M.; Espinosa, A.; Tarraga, A.; Molina, P., *Org. Lett.* **2011,** *13*, 2078-2081.
14. Zapata, F.; Caballero, A.; Espinosa, A.; Tarraga, A.; Molina, P., *Dalton Trans.* **2010,** *39*, 5429-5431.
15. Fery-Forgues, S.; Delavaux-Nicot, B., *J. Photochem. Photobiol. A-Chem.* **2000,** *132*, 137-159.
16. Zhang, H. C.; Huang, W. S.; Pu, L., *J. Org. Chem.* **2001,** *66*, 481-487.
17. Yu, S. S.; DeBerardinis, A. M.; Turlington, M.; Pu, L., *J. Org. Chem.* **2011,** *76*, 2814-2819.
18. Job, P., *Ann Chim.* **1928,** *9*, 113-203.
19. Rappe, A. K.; Casewit, C. J.; Colwell, K. S.; Goddard, W. A.; Skiff, W. M., *J. Am. Chem. Soc.* **1992,** *114*, 10024-10035.
20. Majumder, M.; Sathyamurthy, N., *Theor. Chem. Acc.* **2012,** *131,* 1092.
21. Benesi, H. A.; Hildebrand, J. H., *J. Am. Chem. Soc.* **1949,** *71*, 2703-2707.
22. Pu, L., *Chem. Rev.* **2004,** *104*, 1687-1716.
23. Pu, L., *Acc. Chem. Res.* **2012,** *45*, 150-163.
24. Lin, J.; Li, Z. B.; Zhang, H. C.; Pu, L., *Tetrahedron Lett.* **2004,** *45*, 103-106.
25. Li, Z. B.; Lin, J.; Zhang, H. C.; Sabat, M.; Hyacinth, M.; Pu, L., *J. Org. Chem.* **2004,** *69*, 6284-6293.
26. Li, Z. B.; Lin, J.; Pu, L., *Angew. Chem.-Int. Edit.* **2005,** *44*, 1690-1693.
27. Iwanek, W.; Mattay, J., *J. Photochem. Photobiol. A-Chem.* **1992,** *67*, 209-226.
28. Ferguson, G.; Glidewell, C.; Opromolla, G.; Zakaria, C. M.; Zanello, P., *J. Organomet. Chem.* **1996,** *517*, 183-190.
29. Bard, A. J.; Faulkner, L. R., *Electrochemical Methods, Fundamentals and Applications*. Wiley, New York, 2001.
30. Silva, M.; Pombeiro, A. J. L.; Dasilva, J.; Herrmann, R.; Deus, N.; Castilho, T. J.; Silva, M., *J. Organomet. Chem.* **1991,** *421*, 75-90.
31. Emilia, M.; Silva, N.; Pombeiro, A. J. L.; Dasilva, J.; Herrmann, R.; Deus, N.; Bozak, R. E., *J. Organomet. Chem.* **1994,** *480*, 81-90.
32. Willener, Y.; Joly, K. M.; Moody, C. J.; Tucker, J. H. R., *J. Org. Chem.* **2008,** *73*, 1225-1233.
33. Laurent, P.; Miyaji, H.; Collinson, S. R.; Prokes, I.; Moody, C. J.; Tucker, J. H. R.; Slawin, A. M. Z., *Org. Lett.* **2002,** *4*, 4037-4040.

CHAPTER 5: Ferrocene Nucleic Acid as a structural DNA mimic

5.1 Introduction and aims of the studies

The modification and mimicry of natural nucleic acid to add functionalities and complement the properties of what is found in nature has been an important topic of chemical research for several decades.[1-3] A structural mimic of a nucleic acid can be obtained by replacing at least one of the three typical units of the nucleic acid polymer (nucleobase, phosphate linker and sugar) with suitable alternatives.

Within the field of metallopolymers,[4] novel metal-containing analogues of nucleic acids have been developed. Progress in this field has led to the replacement of the nucleobase itself with metal-coordinating groups,[5-6] where metal coordination is able to trigger the formation of duplexes and triplexes. However, a metal-containing analogue of DNA could be obtained through an alternative approach, in which the metal becomes a component of the backbone. The nucleobases would be still present, but the backbone itself would be formed by repeating metal-based unit. An obvious candidate for this replacement is ferrocene: the distance between its Cp rings (3.3 Å)[7] is very similar to the one between consecutive base pairs in B-DNA (3.4 Å).[8] Furthermore, ferrocene is used in various areas of biomolecular sensing and bioorganometallic chemistry.[9] However, the creation of a strand of this ferrocene nucleic acid (FcNA) would need the replacement of an important structural component of the backbone of the DNA with ferrocene, rather than the use that has been done in the past as a linker group within,[9] or a tag to,[10-11] an existing DNA structure.

An example of DNA analogue where ferrocene is used as a linker group within the DNA strand is the work of Brisset and coworkers,[12] who recently synthesised novel electrochemically active probes for detecting nucleic acids. A ferrocenyl based phosphoramidate synthon (Fc) was incorporated into stem-looped oligodeoxyribonucleotides (ODNs) (Figure 5.1). The ferrocene groups gave only a small destabilization in the structure of the DNA analogue.

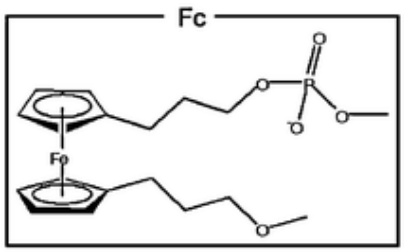

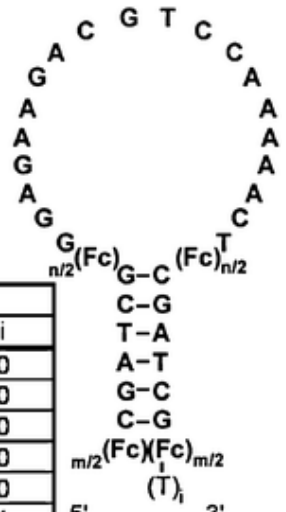

Hairpin	Modifications		
	n	m	i
unmodified	0	0	0
A	2	0	0
B	4	0	0
C	6	0	0
D	8	0	0
E	0	2	1
F	0	4	1

Figure 5.1: *Structure of the ferrocene (Fc) incorporated in the ODN sequences (top left) and general design of the stem-loop Fc oligonucleotides (Fc-ODNs); table refers to the different combination of modifications introduced to produce different hairpins.*[12]

These hairpins were then spotted on a gold electrode microarray, and a self-structuring phenomenon occurred on the surface. When hybridization with a complementary strand of nucleic acid target occurred, the hairpin opened and a variation in potential and current intensity of the ferrocenes was observed by CV (Figure 5.2).[12]

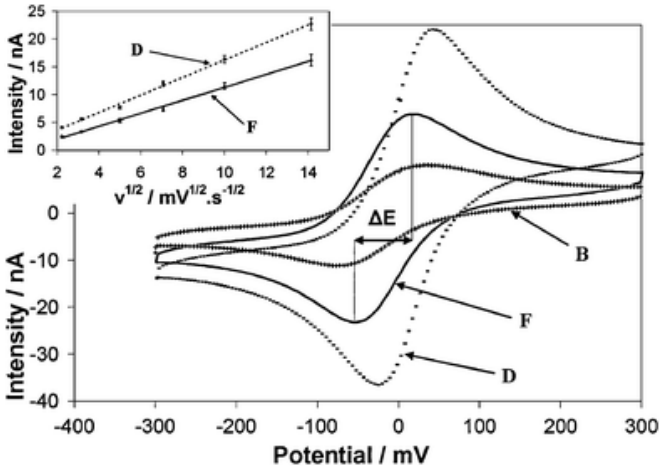

***Figure 5.2**: Electrochemical response of hairpin B, D and F by CV, at 80 min after the deposition of probe solution (50 mM) on the gold electrode microarray (scan rate = 100 mV/s); inlay shows oxidative current variation (I_{ox}) as a function of the scan rate square root for hairpins D and F ($I_{ox} = f(v^{1/2})$).* [12]

Recently the Tucker group has been investigating what structural properties a ferrocenyl nucleobase derivative should have to mimic the phosphate-sugar backbone in natural DNA. Initial computational studies suggested that the optimum structure should consist of a three-carbon linkage between the Cp rings and the phosphate, and two-carbon linkage between the Cp rings and the nucleobase, achieved using the monomer shown in Figure 5.3.[13]

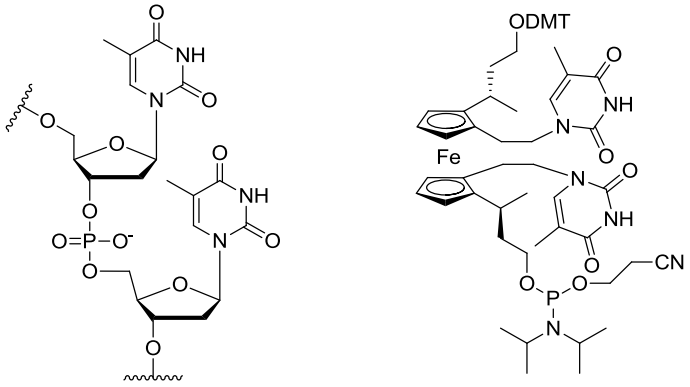

***Figure 5.3:** Structure of the DNA dinucleotide (left) and the monomer used for the synthesis of the DNA analogue (right).*[13]

Initially, coupling of nucleobases to ferrocene *via* a two-carbon linker was studied in bis-substituted systems.[14] Then, using a similar route, an enantiopure (R,R,R_p,R_p)-tetra-substituted monomer of the thymine system was synthesised and successfully oligomerised within the group via automated oligonucleotide synthesis to form a ferrocene nucleic acid (FcNA) oligomer of 8 units called $(FcTT)_8$ (Figure 5.4).[13]

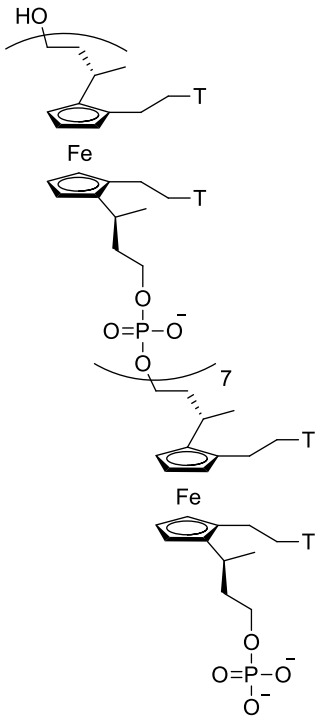

Figure 5.4: *Structure of the oligomer* $(FcTT)_8$ *with (*S,S,S_p,S_p*) chirality.*[13]

This oligomer of FcNA was purified by reversed-phase HPLC and characterised by HPLC and mass spectrometry to confirm its purity and identity.[13] The molecule showed good solubility in aqueous phosphate buffer at pH 7. This chapter describes the electrochemical studies performed on the $(FcTT)_8$ oligomer as a single strand and preliminary studies in its interaction with complementary DNA and PNA[15-16] strands.

5.2 Electrochemistry of $(FcTT)_8$

It was decided to investigate the electrochemical properties of $(FcTT)_8$ using cyclic voltammetry. A 100 µL aqueous solution was prepared using a concentrated solution of the oligomer and adding sodium phosphate buffer and NaCl, and adjusting the volume with ultrapure water, resulting in a 100 µM solution in 10 mM sodium phosphate and 100 mM NaCl aqueous buffer at pH 7.0. The solution was then transferred into a glass bridge tube for the working electrode, which was immersed in a buffer solution of the same concentration (10 mM sodium phosphate and 100 mM NaCl) but without the analyte. In this solution were also placed a platinum wire auxiliary electrode and an Ag/AgCl reference electrode.

The potential was then swept between -0.2 and 0.7 V at different scan rates, between 10 and 200 mV s^{-1}. A single quasi-reversible wave was observed in each scan, centred at 212 mV ± 5 mV vs. Ag/AgCl (Figure 5.5).

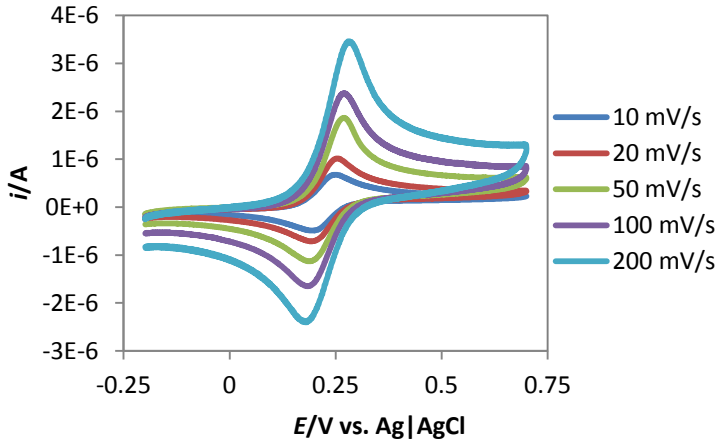

Figure 5.5: *Cyclic voltammograms of $(FcTT)_8$ at various scan rates (100 µM, 10 mM sodium phosphate buffer, 100 mM NaCl) at rt.*

Unlike previous studies of ferrocene derivatives in aqueous media[17-18], $(FcTT)_8$ showed good stability in the absence of complementary DNA (there was no loss of electroactivity over 20 consecutive scans). This is possibly caused by stabilisation of the Fc^+ ion by the positive inductive effect from the side chains on the Cp rings, often labile otherwise in the presence of Cl^- anions as described in Section 1.4.[19] Such an effect would make the ferrocene oxidation potential lower[20-21] and the stability of the functionalised ferrocenium cation ($FeCp_2^+$) higher, therefore making the Cp^- less exchangeable with Cl^-.

Table 5.1: *Data obtained from the cyclic voltammograms in Figure 5.5.*

Scan Rate/mV s^{-1}	i_p^a/A	i_p^c/A	i_p^a/i_p^c	E_p^a/mV	E_p^c/mV	E_p^a-E_p^c/mV	$E^{0'}$/mV
10	6.73×10^{-7}	-5.09×10^{-7}	1.32	236	181	55	208
20	1.00×10^{-6}	-7.31×10^{-7}	1.37	241	179	62	210
50	1.46×10^{-6}	-1.15×10^{-6}	1.27	255	174	81	214
100	2.27×10^{-6}	-1.65×10^{-6}	1.37	255	170	85	212
200	3.20×10^{-6}	-2.32×10^{-6}	1.38	269	164	105	216

The formal electrode potential ($E^{o'}$) of 212 mV is similar to the potentials observed for related oligomers in previous publications in the literature,[9, 12] and its more positive value can be explained by the influence of the neighbouring ferrocene units on each other: when one Fc^+ ion is formed it withdraws electrons from the adjacent ferrocene groups, making them thermodynamically harder to oxidise.

The separation between the oxidation peak and the reduction peak varies quite significantly with the scan rate, and at high scan rate it is quite large due to the presence of the glass frit that separates the solution containing the working electrode from the solution containing the reference and auxiliary electrodes. The glass frit constitutes an obstacle to the electric

conduction, therefore a large Ohmic drop is observed. However, it is noteworthy how the value for the 10 mV s^{-1} scan rate is close to 59 mV, the ideal value for a one-electron process.[22] From these observations, it can be deduced that distinct electron transfer processes take place within the strand of FcTT units, as would be expected for a redox-active oligomer such as this.

To help understand how the electron transfer occurs under the conditions used, digital simulations of the cyclic voltammograms were performed using DigiSim software. At first, a simulation of the behaviour of a control species **2.12** with one ferrocene unit and a single electron transfer process was compared with the experimental data measured in the same conditions (Figure 5.6).

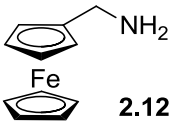

2.12

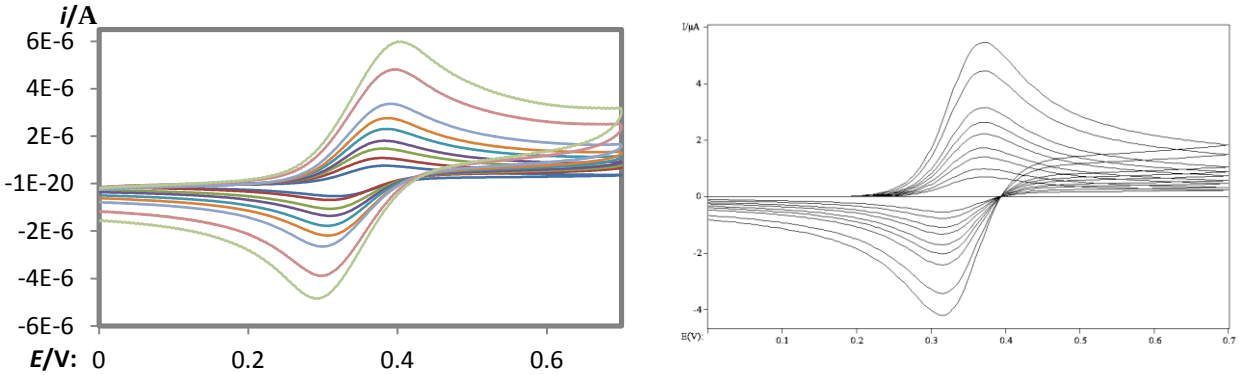

Figure 5.6: *Experimental data (left) and digital simulation (right) of the cyclic voltammograms of* $FcCH_2NH_2$ *(100 µM, 10 mM sodium phosphate buffer, 100 mM NaCl) at room temperature, between 5 mV* s^{-1} *and 300 mV* s^{-1}*.*

Given the good fitting of the simulation with the experimental data, simulations of the $(FcTT)_8$ system described above were performed. The diffusion coefficients were calculated

using the Randles-Sevcik[23-24] equation (see Section 1.9.1 and below), from the assumption that a known number of electrons *n* where transferred, which should be 8 in this case.

$$i_p = 2.69\times10^{-5} n^{3/2} A D^{1/2} C v^{1/2} \qquad \textbf{Equation 1.3}$$

The current peak values, i_p, for the oxidised and reduced forms were plotted against the sweep rate, whose linearity is a sign of the chemical reversibility of the redox reaction (Figure 5.7).

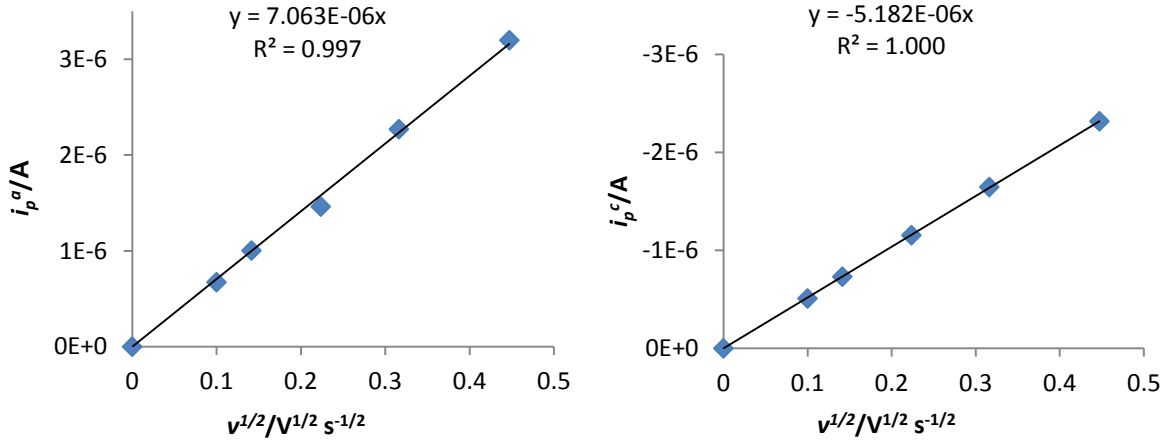

Figure 5.7: *Dependence of anodic (left) and cathodic (right) peak height (i_p) on scan rate (v). R^2 is the deviation from linearity, ideal for R^2=1.*

The conditions tested were that the 8 electrons of the ferrocene units were either transferred in separate steps or in one single step, as in the equations shown in Scheme 5.1.

$(FcTT)_8 \rightarrow (FcTT)_8^{+} + 1\ e^-$
$(FcTT)_8^{+} \rightarrow (FcTT)_8^{2+} + 1\ e^-$
$(FcTT)_8^{2+} \rightarrow (FcTT)_8^{3+} + 1\ e^-$
$(FcTT)_8^{3+} \rightarrow (FcTT)_8^{4+} + 1\ e^-$
$(FcTT)_8^{4+} \rightarrow (FcTT)_8^{5+} + 1\ e^-$
$(FcTT)_8^{5+} \rightarrow (FcTT)_8^{6+} + 1\ e^-$
$(FcTT)_8^{6+} \rightarrow (FcTT)_8^{7+} + 1\ e^-$
$(FcTT)_8^{7+} \rightarrow (FcTT)_8^{8+} + 1\ e^-$

$(FcTT)_8 \rightarrow (FcTT)_8^{8+} + 8\ e^-$

Scheme 5.1: *Equations defining the electron transfer in $(FcTT)_8$ in the assumption of eight separate steps (left) or one single step (right).*

If the electrons are transferred in eight separate steps, it is hard to tell if this happens at the same potential or in steps at different potential. Initially, a simulation of eight steps in which each electron is transferred separately at the same potential was performed, to have a simpler comparison with the case in which the 8 electrons are transferred in one single step. A simulation in which only 1 electron is transferred was performed as a control (Figure 5.8).

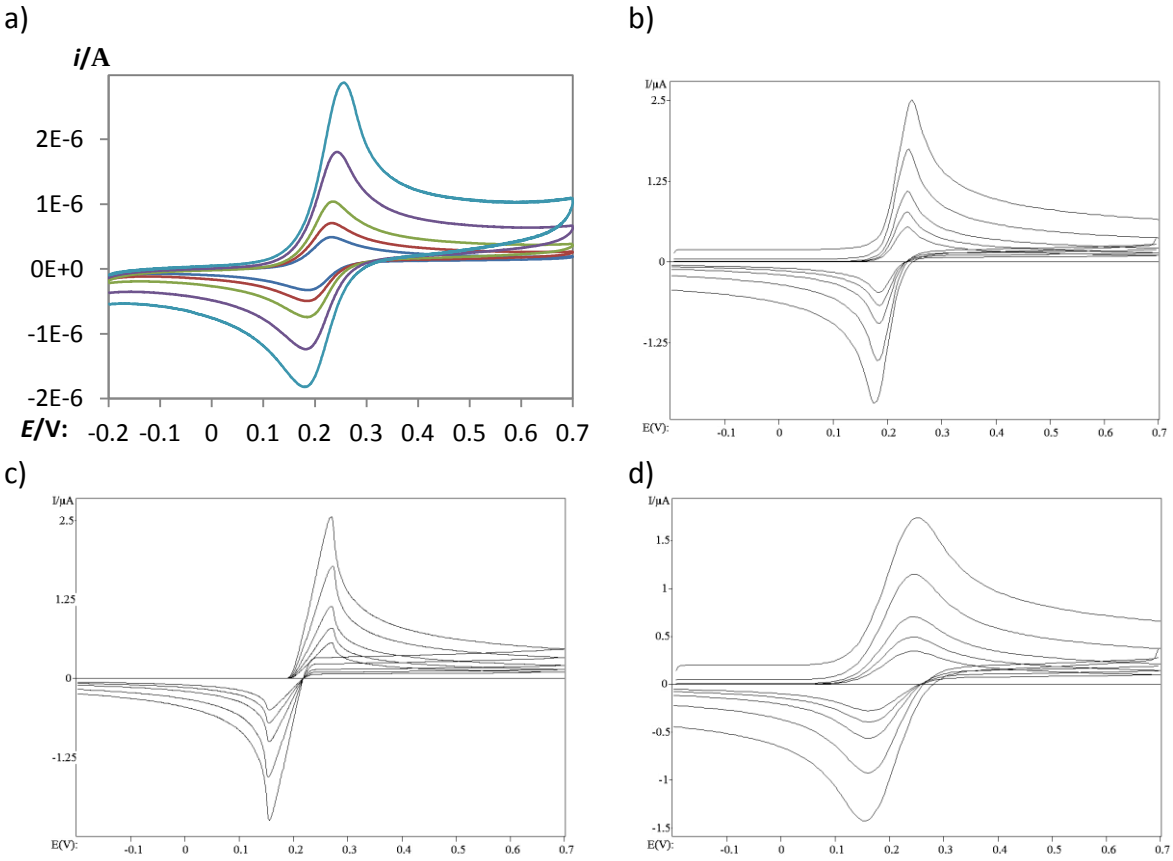

Figure 5.8: *Cyclic voltammograms of $(FcTT)_8$: a) experimental data; b) simulation assuming 8 steps of 1 e^- (peak separation 65 mV); c) simulation assuming 1 step of 8 e^- (peak separation 112 mV); d) simulation assuming 1 step of 1 e^- (peak separation 105 mV). (100 µM, 10 mM sodium phosphate buffer, 100 mM NaCl at rt, between 5 mV s^{-1} and 100 mV s^{-1}).*

From observation of the shapes of the simulated cyclic voltammograms, the best fitting is the situation in which the 8 electrons are not exchanged in one single step, but in separate steps. The simulation in which only one electron is exchanged displays broader oxidation waves than what is observed experimentally and the current intensity for the oxidation and reduction peaks is smaller. Therefore, it is more likely that all the 8 electrons are exchanged, as the intensity of current of the simulation fits better the experimental observation.

However, there is no evidence to support the hypothesis of the 8 electrons being transferred all at the same potential, or at different potential depending on their position on the FcNA strand. In the second case, two options are possible: in the first the electrons are exchanged all at different potentials because the oxidation of each of them affects the oxidation potential of the others; in the second, the FcNA strand being rather symmetrical, two equivalent ferrocene centres could be oxidised at the same potential and then affect the oxidation potential of the ferrocene centres next to them in the strand. Another useful piece of information that could help to further understand the dynamics of the electron transfer processes occurring is the difference between the redox potentials in the above mentioned steps. The influence of each redox centre on the others could be small, reflected in potential differences of only a few mV, or large, with potential difference of several mV. Further simulations were then performed to understand if the electrons are transferred all at exactly the same redox potential (0.210 V), or at different potentials (Figure 5.9). The different potentials assumed are reported in Table 5.2 and Table 5.3 and they were chosen with small differences of 2 or 4 mV, or large differences of 10 mV or 20 mV, in order to have extreme cases which would make the comparison easier.

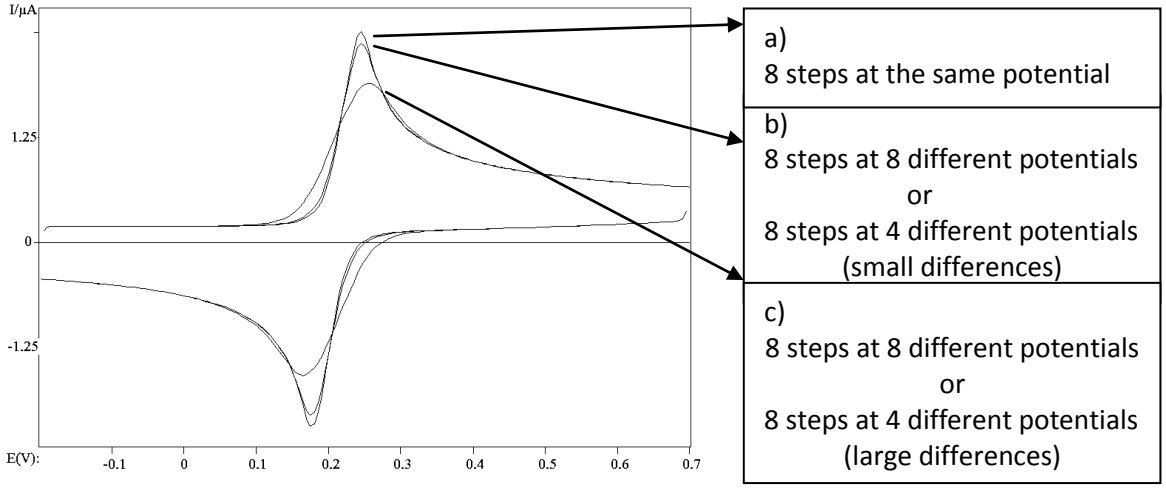

Figure 5.9: *Digital simulations of the cyclic voltammograms of $(FcTT)_8$ assuming 8 step of 1 e^- (a) at the same potential or (b and c) at different potentials (100 μM, 10 mM sodium phosphate buffer, 100 mM NaCl, at rt, scan rate 100 mV s^{-1}.)*

Table 5.2: *Potential values used for the simulations where the potential is assumed to be the same for equivalent redox centres, with differences of 4 mV and 20 mV.*

Electron Transfer Steps	Potential (small difference)	Potential (large difference)
First two steps	0.204 V	0.180 V
3rd and 4th step	0.208 V	0.200 V
5th and 6th step	0.212 V	0.220 V
Last two steps	0.216 V	0.240 V

Table 5.3: *Potential values used for the simulations where the potential is assumed to change in each electron transfer step, with differences of 2 mV and 10 mV.*

Electron Transfer Steps	Potential (small difference)	Potential (large difference)
First step	0.203 V	0.175 V
2nd step	0.205 V	0.185 V
3rd step	0.207 V	0.195 V
4th step	0.209 V	0.205 V
5th step	0.211 V	0.215 V
6th step	0.213 V	0.225 V
7th step	0.215 V	0.235 V
Last step	0.217 V	0.245 V

From the observation of the simulated voltammograms it is evident that the differences in the potentials are not large, otherwise the oxidation and reduction waves become broad and the intensity of current is smaller than that observed experimentally. However, it is difficult to assess whether the potential is different for each ferrocene centre or only for non-equivalent ones, because the simulated voltammograms display the same features (Figure 5.9b). It is perhaps more likely that the potential is slightly different for each electron transfer step, with those ferrocene units still in their reduced forms becoming slightly thermodynamically harder to oxidise when influenced by the decreased electron density in their surroundings.

5.3 Addition of DNA-A_{16}

An experiment in which a complementary strand of DNA-A_{16} was added to $(FcTT)_8$ was performed and the response was followed by cyclic voltammetry (Figure 5.10).

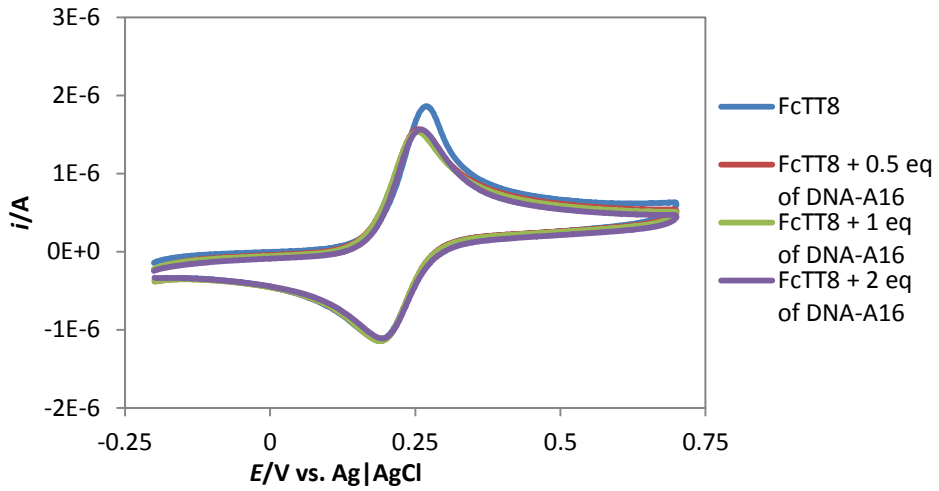

Figure 5.10: *Cyclic voltammograms of $(FcTT)_8$ in the free form and upon addition of the complementary strand of DNA-A_{16}. (100 µM, 10 mM sodium phosphate buffer, 100 mM NaCl at 18 ^{o}C, scan rate 50 mV s^{-1}.)*

The conditions were the same used for the electrochemical characterisation of $(FcTT)_8$ in aqueous buffer (100 µM solution in 10 mM sodium phosphate and 100 mM NaCl at pH 7.0). The additions of DNA-A_{16} were performed with up to 4 µL of concentrated solution in water, in order not to affect significantly the concentration of $(FcTT)_8$ in solution. Addition of 0.5 equivalents, 1 equivalent and 2 equivalents were performed in order to follow the binding of the complementary strands. A small shift of 7 mV was observed but only for the oxidation peak, towards less positive potential. A separate UV/Vis study performed within the group has revealed that any interaction with DNA-A_{16} is minimal, even after allowing 2 hours in solution for the formation of the duplex. This is most likely due to the conformation of the strand of $(FcTT)_8$ not exactly fitting the strand of complementary DNA, which is not flexible enough to adapt its conformation to form a stable duplex. However, the small changes observed in the CVs are possibly due to weak Coulombic association of negatively charged DNA with the oxidised ferrocene; the increased electron density in proximity of the ferrocene units, caused by the negative charges born by the phosphate groups in the backbone of the DNA strands added, would explain the small shift.

5.4 Addition of PNA-A_{16}

After the experiments with addition of DNA-A_{16} it was then decided to switch to PNA-A_{16}, which is a DNA analogue with 16 adenine nucleobases, as a complementary strand to be added to our $(FcTT)_8$ probe. PNA is more flexible than DNA, due to the replacement of the entire backbone with a peptide chain (Figure 5.11).[15-16] The flexibility might make it easier to adapt to the conformation of $(FcTT)_8$ to form a duplex, thus binding more strongly than DNA.

Moreover, PNA differs from DNA by the absence of phosphate groups in the backbone, therefore no negative charge is present and the complementary strand of $(FcTT)_8$ would not experience repulsive interactions.

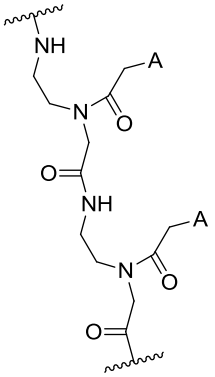

Figure 5.11: *Chemical structure of a generic strand of PNA, where A designates the nucelobase adenine.*

The duplex formation experiment was performed according to the same procedure used for the addition of DNA-A_{16} described in Section 5.3, and under the same conditions (100 µM solution in 10 mM sodium phosphate and 100 mM NaCl at pH 7.0), with the response followed by cyclic voltammetry. The addition of 0.5, 1 and 2 equivalents of PNA-A_{16} was undertaken in order to follow the binding of the complementary strand (Figure 5.12).

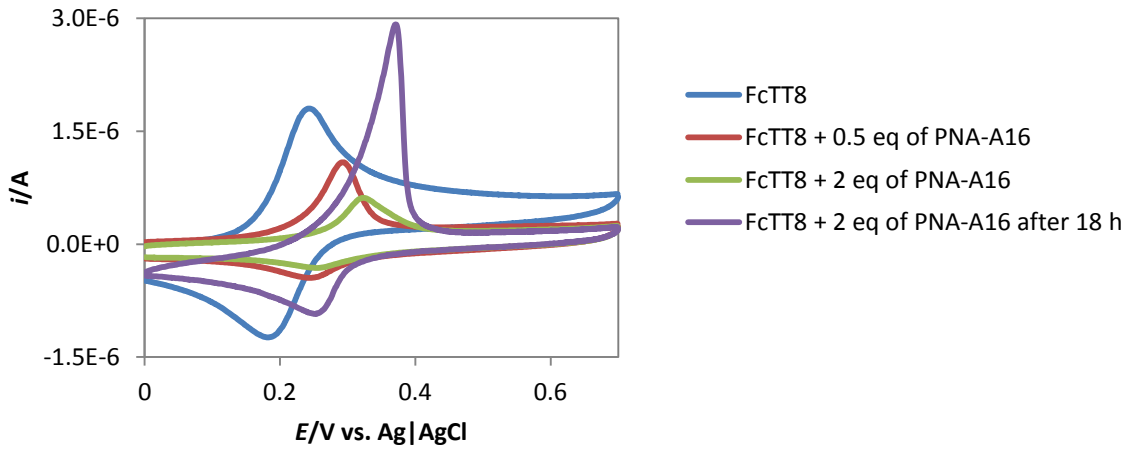

Figure 5.12: *Cyclic voltammograms of $(FcTT)_8$ in the free form and upon addition of the complementary strand of PNA-A_{16}. (100 µM, 10 mM sodium phosphate buffer, 100 mM NaCl at 18 ^{o}C, scan rate 50 mV s^{-1}.)*

A significant shift towards more positive potentials was observed upon addition of 0.5 equivalents of PNA-A_{16} (38 mV); the shift increased following addition of 1 and 2 equivalents (up to 75 mV). However, a precipitate formed and the solution turned cloudy. It was observed that, after leaving the solution to equilibrate, the precipitate redissolved, possibly because of slow kinetics in the interaction between the two complementary strands that delayed complete formation of the duplex and its solubilisation. The solution was therefore allowed to rest overnight and a cyclic voltammogram was then re-recorded. A wave with a slightly larger potential shift (81 mV) was observed with higher peak intensity (Figure 5.12). This wave displayed a very small return peak, indicating the occurrence of an electrochemical reaction, or a large difference in the diffusion coefficients for the oxidised and reduced forms.

After addition of 2 equivalents of PNA-A_{16} the scan rate dependence of the species formed was probed by cyclic voltammetry, varying the sweep rate between 10 mV s^{-1} and 100 mV s^{-1} (Figure 5.13) with the data obtained reported in Table 5.4.

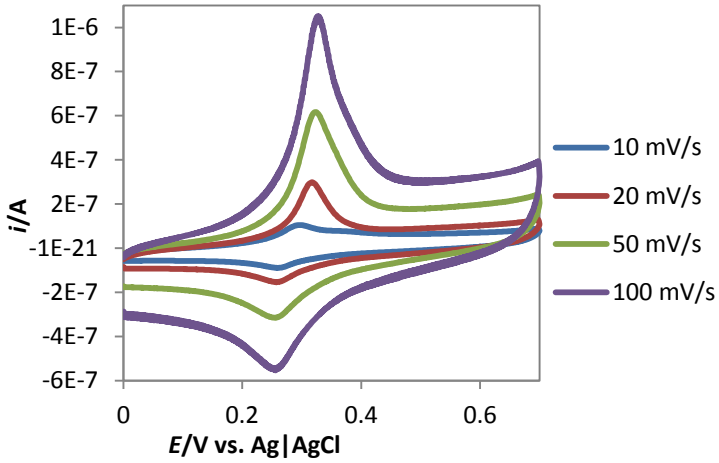

Figure 5.13: *Cyclic voltammograms of $(FcTT)_8$ with 2 equivalents of PNA-A_{16} at various scan rates. (100 µM, 10 mM sodium phosphate buffer, 100 mM NaCl at 18 ^{o}C.)*

Table 5.4: *Data obtained from the cyclic voltammograms in Figure 5.12 and Figure 5.13.*

Scan Rate/mV s^{-1}	i_p^a/A	i_p^c/A	i_p^a/i_p^c	E_p^a/mV	E_p^c/mV	E_p^a-E_p^c/mV	$E^{0'}$/mV
10	7.17×10^{-8}	-5.26×10^{-8}	1.36	297	257	40	277
20	2.44×10^{-7}	-9.48×10^{-8}	2.57	317	257	60	287
50	5.03×10^{-7}	-2.02×10^{-7}	2.49	323	256	67	289
100	8.63×10^{-7}	-3.56×10^{-7}	2.42	327	256	71	291
50 after 18h	2.39×10^{-6}	-8.90×10^{-7}	2.68	341	249	92	295

The electrochemical reversibility is lower in comparison with the free form of the probe $(FcTT)_8$. The kinetics are slower, and the different size of the peaks is possibly related to easier hybridisation when the oligomer is in its oxidised rather than reduced form. For the sample after the formation of the duplex overnight, the reversibility is again poorer, and the peak separation between E_p^a and E_p^c is increased (from 67 mV to 92 mV), which is possibly caused by formation of the duplex, hence leading to a slower mass transport in solution. This is supported by the calculations of the diffusion coefficients from the Randles-Sevcik equation (as in paragraph 5.2), using 8 as number of electron transferred. The peak currents, i_p, for the oxidised form and the reduced form were plotted against the sweep rate (Figure 5.14).

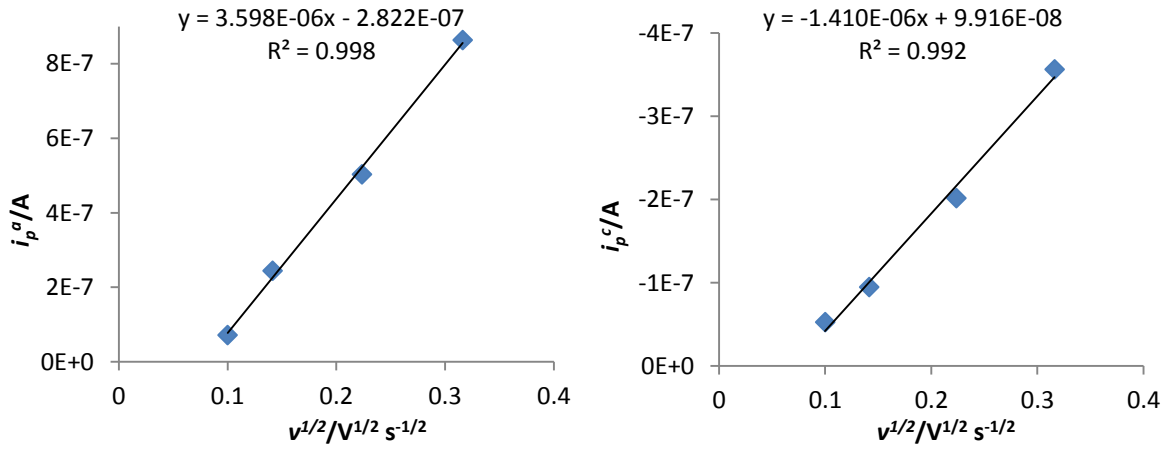

Figure 5.14: *Dependence of anodic (left) and cathodic (right) peak height (i_p) on scan rate (v).*

The values of D obtained for the oxidised form and the reduced form are reported in Table 5.5, together with the values obtained for $(FcTT)_8$ in the free form, for an immediate comparison.

Table 5.5: *Diffusion coefficients calculated for $(FcTT)_8$ as a single strand and as a duplex with PNA-A_{16} in 10 mM sodium phosphate buffer and 100 mM NaCl at 100 µM conc. at 18 ^{o}C.*

	Reduced Form	**Oxidised Form**
$(FcTT)_8$	2.35216 x 10^{-6} cm^2 s^{-1}	1.266 x 10^{-6} cm^2 s^{-1}
$(FcTT)_8$ + PNA-A_{16}	6.10394x 10^{-7} cm^2 s^{-1}	9.374 x 10^{-8} cm^2 s^{-1}

Preliminary UV-Vis measurements performed in the group have indicated that there is an interaction between $(FcTT)_8$ and PNA-A_{16} under the same conditions, and this dissociated by heating to *ca.* 31 ^{o}C. Therefore, to provide further evidence for the potential shift being caused by the formation of a duplex, the solution obtained after allowing the two strands to react overnight was heated slowly and the cyclic voltammograms at 50 mV s^{-1} were monitored every 3 °C of increased temperature, between 21 °C and 66 °C (Selected CVs are provided in Figure 5.15).

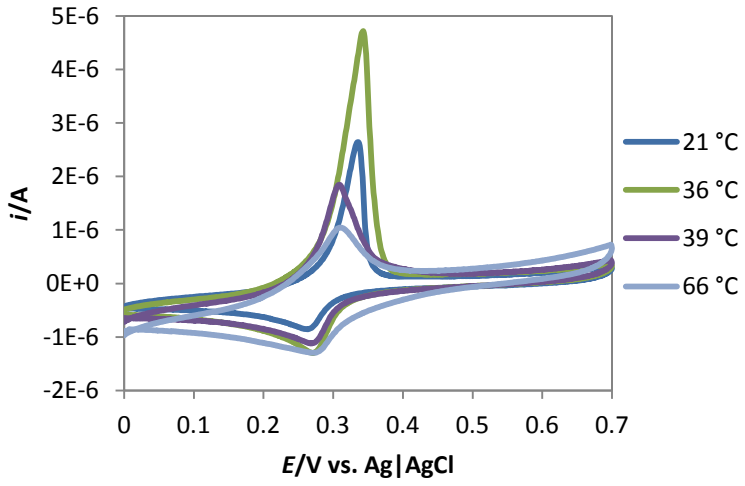

Figure 5.15: *Cyclic voltammograms of $(FcTT)_8$ with 2 equivalents of PNA-A_{16} at different temperatures. (100 µM, 10 mM sodium phosphate buffer, 100 mM NaCl, 50 mV s^{-1}.)*

Initially increasing the temperature from 21 °C to 36 °C caused an increase in peak intensity, as could be predicted assuming a higher mobility of the species in solution and a smaller resistance of the solution.[25] Between 36 °C and 39 °C an abrupt change in the voltammogram was observed, with decreased peak intensity and a shift towards less positive potential: this phenomenon could indicate that the duplex is no longer formed. The temperature recorded was higher than that observed in the UV-Vis experiments. A higher temperature might be needed if thermal equilibrium is difficult to reach in the presence of the glass bridge tube, which separates the analyte solution from the heated buffer solution. However, the duplex did not disappear completely: the potential did not reach the value observed for the $(FcTT)_8$ in its free form (from 307 mV to 288 mV instead of 214 mV). Increasing the temperature up to 66 °C did not affect the potential (290 mV) although it affected the peak height ratio (i_p^a/i_p^c = 1.27) and the peak separation (E_p^a-E_p^c = 39 mV). After the experiment, the solution was cooled down to room temperature and left to rest overnight (Figure 5.16).

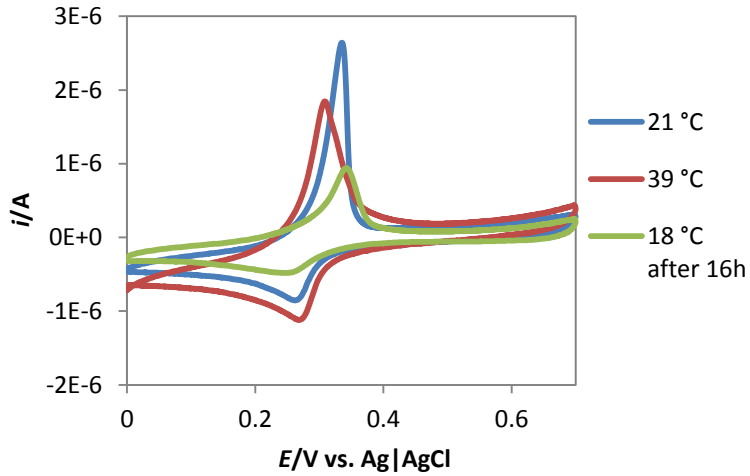

Figure 5.16: *Cyclic voltammograms of $(FcTT)_8$ with 2 equivalents of PNA-A_{16} at different temperatures: after formation of the duplex (21 °C), after disruption of the duplex (39 °C), and after allowing the duplex to reform (18 °C after 16 h). (100 µM, 10 mM sodium phosphate buffer, 100 mM NaCl, 50 mV s^{-1}.)*

The potential went back to the original shift of ca. 300 mV, but with a reduced peak height, which is perhaps a result of some precipitation.

5.5 Conclusions and Future Work

The bioorganometallic DNA analogue $(FcTT)_8$ was successfully synthesised and characterised. Its novelty exists through the replacement of the backbone of DNA with repeating ferrocene based units functionalised with nucleobases. Its electrochemical behaviour was investigated in its free form, and upon formation of duplexes with complementary strands of DNA and PNA. The latter indicated that there was an interaction which could be followed by cyclic voltammetry.

Future work will initially focus on gaining more information on the electrochemical properties of $(FcTT)_8$, specifically the electron transfer process and the absolute number of electrons exchanged *n*. A method to determine *n* has been developed by Amatore and coworkers,[26] based on the comparison of currents measured using two different electrochemical techniques on the same system. It was evaluated that the uncertainty is lower when comparing chronoamperometry and steady state voltammetry at a microelectrode. The mathematical expression that describes the current differs depending on the form of diffusion characteristic of the technique. In chronoamperometry, for an electrode that is planar, the change in current with respect to time is directly proportional to the square root of the diffusion coefficient, according to the Cottrell equation (Equation 5.1).

$$i = nFACD^{1/2}(\pi\theta)^{-1/2} \qquad \textbf{\textit{Equation 5.1}}$$

where:

i = peak current (A)

n = number of electrons transferred per molecule

F = Faraday constant

A = electrode surface area (cm^2)

C = bulk concentration (mol/cm^3)

D = diffusion coefficient of solution species (cm^2/s)

θ = step (s)

In steady state cyclic voltammetry at a microelectrode with spherical diffusion, the current is directly proportional to the diffusion coefficient (Equation 5.2).

$$i^{lim} = 4nFrCD \qquad \textbf{\textit{Equation 5.2}}$$

where:

i^{lim} = limiting current (A)

n = number of electrons transferred per molecule

F = Faraday constant

r = radius of the electrode (cm)

C = bulk concentration (mol/cm^3)

D = diffusion coefficient of solution species (cm^2/s)

The value of *n* can be obtained after mathematical treatment of Equation 5.1 and 5.2 for the system under investigation and for an internal reference (e.g. ferrocenemethanamine, for which *n* is known to be 1). The mathematical treatment is given below:

(FcTT)$_8$ $i_{FcNA} = nFACD_a{}^{1/2}(\pi\theta)^{-1/2}$

$$\frac{i_{FcNA}}{i_{FcCH_2NH_2}} = \frac{nD_a{}^{1/2}}{D_b{}^{1/2}} = A$$

Ferrocenemethanamine $i_{FcCH_2NH_2} = FACD_b{}^{1/2}(\pi\theta)^{-1/2}$

(FcTT)$_8$ $i_{FcNA}{}^{lim} = 4nFrCD_a$

$$\frac{i_{FcNA}{}^{lim}}{i_{FcCH_2NH_2}{}^{lim}} = \frac{nD_a}{D_b} = B$$

Ferrocenemethanamine $i_{FcCH_2NH_2}{}^{lim} = 4FrCD_b$

$$n = \frac{A^2}{B}$$

Further work could consist of the synthesis and characterisation of alternative artificial nucleic acids with different nucleobases. Adenine functionalised FcNA (FcAA)$_8$ could be synthesised and its interaction with complementary (FcTT)$_8$ probed. Further control experiments could be carried out, for example adding non-complementary strands of PNA and checking that no potential shift is observed. This would allow distinction between specific and non-specific binding. Probes of opposite chirality (Figure 5.17) could also be investigated, to study the effect of the chirality on the binding to DNA, PNA and complementary FcNA.

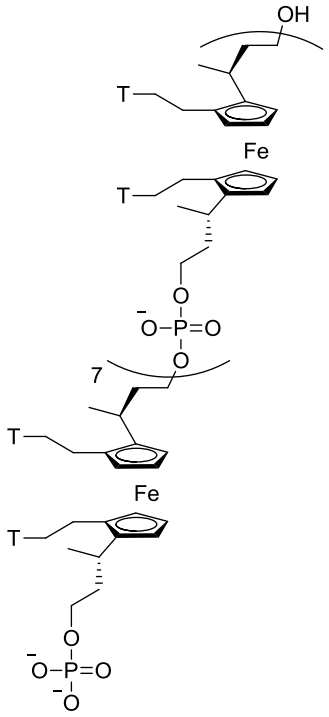

Figure 5.17: *Structure of the oligomer (FcTT)$_8$ with (*R,R,R$_p$,R$_p$*) chirality.*

Finally, experiments to detect mercury could be performed using (FcTT)$_8$, as mercury is well known to bridge thymine units.[27-29] For the (FcTT)$_8$ system, there is the possibility to bind up to 16 mercury ions, therefore improving on the sensitivity of other DNA-based mercury sensors that have been reported.[27-29]

5.6 References

1. Khakshoor, O.; Kool, E. T., *Chem. Commun.* **2011,** *47*, 7018-7024.
2. Bell, N. M.; Micklefield, J., *Chembiochem* **2009,** *10*, 2691-2703.
3. Pinheiro, V. B.; Holliger, P., *Curr. Opin. Chem. Biol.* **2012,** *16*, 245-252.
4. Whittell, G. R.; Manners, I., *Adv. Mater.* **2007,** *19*, 3439-3468.
5. Clever, G. H.; Shionoya, M., *Coord. Chem. Rev.* **2010,** *254*, 2391-2402.

6. Johannsen, S.; Megger, N.; Bohme, D.; Sigel, R. K. O.; Muller, J., *Nat. Chem.* **2010,** *2*, 229-234.
7. Seiler, P.; Dunitz, J. D., *Acta Crystallogr. B* **1979,** *35*, 1068-1074.
8. Watson, J. D.; Crick, F. H. C., *Nature* **1953,** *171*, 737-738.
9. Ihara, T.; Sasahara, D.; Shimizu, M.; Jyo, A., *Supramol. Chem.* **2009,** *21*, 207-217.
10. Li, D.; Song, S. P.; Fan, C. H., *Acc. Chem. Res.* **2010,** *43*, 631-641.
11. Song, H. F.; Li, X. H.; Long, Y. T.; Schatte, G.; Kraatz, H. B., *Dalton Trans.* **2006**, 4696-4701.
12. Chatelain, G.; Brisset, H.; Chaix, C., *New J. Chem.* **2009,** *33*, 1139-1147.
13. Nguyen, H. V.; Zhao, Z.-y.; Sallustrau, A.; Horswell, S. L.; Male, L.; Mulas, A.; Tucker, J. H. R., *Chem. Commun.* **2012,** *48*, 12165-12167.
14. Nguyen, H. V.; Sallustrau, A.; Male, L.; Thornton, P. J.; Tucker, J. H. R., *Organometallics* **2011,** *30*, 5284-5290.
15. Nielsen, P. E.; Haaima, G., *Chem. Soc. Rev.* **1997,** *26*, 73-78.
16. Corradini, R.; Sforza, S.; Tedeschi, T.; Totsingan, F.; Manicardi, A.; Marchelli, R., *Curr. Top. Med. Chem.* **2011,** *11*, 1535-1554.
17. Kang, D.; Zuo, X.; Yang, R.; Xia, F.; Plaxco, K. W.; White, R. J., *Anal. Chem.* **2009,** *81*, 9109-9113.
18. Valincius, G.; Niaura, G.; Kazakeviciene, B.; Talaikyte, Z.; Kazemekaite, M.; Butkus, E.; Razumas, V., *Langmuir* **2004,** *20*, 6631-6638.
19. Han, S. W.; Seo, H.; Chung, Y. K.; Kim, K., *Langmuir* **2000,** *16*, 9493-9500.
20. Silva, M.; Pombeiro, A. J. L.; Dasilva, J.; Herrmann, R.; Deus, N.; Castilho, T. J.; Silva, M., *J. Organomet. Chem.* **1991,** *421*, 75-90.
21. Emilia, M.; Silva, N.; Pombeiro, A. J. L.; Dasilva, J.; Herrmann, R.; Deus, N.; Bozak, R. E., *J. Organomet. Chem.* **1994,** *480*, 81-90.
22. Brett, C. M. A.; Oliveira, A. M., *Voltammetric Sensors in Electroanalysis*. Oxford University Press: 1998.
23. Randles, J. E. B., *Trans. Faraday Soc.* **1948,** *44*, 327-338.
24. Sevcik, A., *Collect. Czech. Chem.Commun.* **1948,** *13*, 349-377.
25. Bard, A. J.; Faulkner, L. R., *Electrochemical Methods, Fundamentals and Applications*. Wiley, New York, 2001.
26. Amatore, C.; Azzabi, M.; Calas, P.; Jutand, A.; Lefrou, C.; Rollin, Y., *J. Electroanal. Chem.* **1990,** *288*, 45-63.
27. Miyake, Y.; Togashi, H.; Tashiro, M.; Yamaguchi, H.; Oda, S.; Kudo, M.; Tanaka, Y.; Kondo, Y.; Sawa, R.; Fujimoto, T.; Machinami, T.; Ono, A., *J. Am. Chem. Soc.* **2006,** *128*, 2172-2173.
28. Liu, S. J.; Nie, H. G.; Jiang, J. H.; Shen, G. L.; Yu, R. Q., *Anal. Chem.* **2009,** *81*, 5724-5730.
29. Tanaka, Y.; Oda, S.; Yamaguchi, H.; Kondo, Y.; Kojima, C.; Ono, A., *J. Am. Chem. Soc.* **2007,** *129*, 244-245.

CHAPTER 6: EXPERIMENTAL

6.1 Synthesis

6.1.1 General

Commercially available solvents and reagents were used without further purification, except Et_2O, MeOH, THF, MeCN and CH_2Cl_2, which were dried in Pure Solv™ Solvent Purification Systems, and DMSO, which was distilled from CaH_2 and kept under argon and in presence of activated molecular sieves.[1] All reactions were carried out under an argon atmosphere with the exclusion of moisture. Thin layer chromatography plates were visualized under UV light or by potassium permanganate stain. Flash chromatography was carried out using silica 60, with the eluent specified. Elemental analysis was determined on a CE Instruments EA1110 elemental analyser. ^{1}H NMR spectra were recorded at 300 MHz on a Bruker AVIII300 NMR spectrometer, ^{13}C NMR spectra at 100 MHz on a Bruker AVIII400 NMR spectrometer, at room temperature. Chemical shifts (δ) are in ppm and coupling constants (J) are in Hz. MS were recorded with a Waters/Micromass spectrometer using the ES+ method. Optical rotations were measured on a digital polarimeter. Analytical HPLC was performed using a reversed phase C18 column with a water/MeCN method (0-40 mins 0% MeCN – 100% MeCN; 40-50 mins, 100% MeCN; 50-60 mins, 0% MeCN) with Flow Rate 1.0 mL/min and monitoring at 210 nm. Semi-prep HPLC was performed using a reversed phase C18 column with a water/MeCN method (0-10 mins 90% MeCN – 95% MeCN; 10-20 mins, 100% MeCN; 20-25 mins, 90% MeCN) with flow rate 1.0 mL/min and monitoring at 220 nm. The enantiomeric excess of the receptors was calculated from the area of the peaks obtained in the chiral HPLC performed used an AD column and a 10% (planar chiral ureas) or 20% (central chiral ureas) IPA in hexane mixture of eluents with a flow rate of 1 mL/min, and a

20% IPA in hexane mixture of eluents with a flow rate of 5 mL/s (binol based receptors) and monitoring at 210 nm.

6.1.2 General procedure for the synthesis of ferrocenylmethanamines A[2-3]

To a solution of ferrocenecarboxaldehyde (2.19 mmol) in EtOH (5 mL) a solution of hydroxylamine hydrochloride (4.39 mmol) in water (1.5 mL) was added under argon, followed by sodium acetate (6.57 mmol). The mixture was heated under reflux for 3 hours, cooled and concentrated under reduced pressure. $CHCl_3$ (6 mL) was added dropwise and the mixture was stirred for an additional 30 minutes. The precipitated solid was filtered off and the filtrate was concentrated under vacuum to give the oxime as brown-red oil. The crude ferrocenecarboxaldehyde oxime (2.05 mmol) was dissolved in dry THF (18 mL) and an excess of lithium aluminum hydride (10 mmol) was added portionwise with care. The mixture was stirred under argon for 6 hours. Toluene (18 mL) was added to the solution followed by ethyl acetate (3.5 mL) with caution. A few drops of 5M NaOH were then added until precipitation of inorganics was complete. The mixture was filtered yielding a yellow filtrate and a gummy solid residue. The residue was washed with copious amounts of toluene/MeOH (80:20). The filtrate was then evaporated to dryness and inorganic impurities removed by dissolution in dichloromethane followed by filtration and evaporation of the organic filtrate. The product was further purified by flash column chromatography on silica using as eluent CH_2Cl_2, to a mixture 9:1 CH_2Cl_2/MeOH and addition of triethylamine (1 mL), to yield the desired product.

6.1.3 Synthesis of 1-ferrocenylmethanamine 2.12

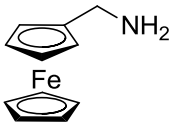

Obtained from ferrocenecarboxaldehyde (0.466 g, 2.19 mmol), the oxime was obtained as a brown-red oil (0.437 g, yield 94%). ^{1}H NMR (300 MHz, $CDCl_3$) δ = 8.00 (1 H, s, C*H*=N), 4.85-4.81 (1 H, m, *ortho* H of Cp), 4.54 (1 H, m, *ortho* H of Cp), 4.38 (2 H, m, *meta* H of Cp), 4.23 (5 H, m, unsubstituted Cp ring). Ferrocenecarboxaldehyde oxime (0.437 g, 2.05 mmol) was then reduced with an excess of lithium aluminum hydride (0.38 g, 10 mmol) to yield the desired product as an orange-yellow solid (0.366 g, yield 83%). Mp 98–100 °C; ^{1}H NMR (300 MHz, $CDCl_3$) δ = 4.33 (2 H, s, *ortho* H of Cp), 4.23 (2 H, s, *meta* H of Cp), 4.16 (5 H, s, unsubstituted Cp ring), 3.77 (2 H, s, CpCH_2N), 2.13 (2 H, br s, –NH_2). ^{13}C NMR (101 MHz, $CDCl_3$) δ = 86.5 (C, unsubstituted Cp ring), 68.4 (CH, Cp ring), 67.8 (CH, Cp ring), 48.2 (CH_2, CpCH_2N); Electrospray MS analysis: Calc. for $C_{11}H_{11}Fe$: 199.0. Found: 199.3. Characterisation data is in agreement with the literature data.[4]

6.1.4 Synthesis of (2*S*,4*S*)-4-(Hydroxymethyl)-2-ferrocenyl-1,3-dioxane 2.14[5]

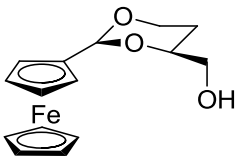

To a solution of ferrocenecarboxaldehyde (2.0 g, 9.3 mmol) in trimethylorthoformate (12 mL) was added a catalytic amount of *para*-toluensulfonic acid monohydrate (5% mol equiv) and the dark solution was stirred at 80°C overnight. Anhydrous sodium carbonate was then added while the stirring solution was allowed to cool at room temperature. The suspension was dissolved in Et_2O (50 mL) and filtered on Celite, and the filter cake was washed with ether until the filtrate was colourless. After concentration under reduced pressure and drying under

vacuum, the crude acetal was quantitatively isolated and directly used in the next step. A solution of (-)-1,2,4-butanetriol (1.2 g, 11.2 mmol) in CH_3Cl (12 mL) was mixed with 6 g of activated molecular sieves, and a catalytic amount of *para*-toluensulfonic acid. The crude acetal was diluted with CH_3Cl (6 mL) and added to the previous solution. The reaction mixture was stirred overnight at room temperature and treated as before with anhydrous sodium carbonate, before filtration on Celite, washing with CH_2Cl_2 and concentration under reduce pressure. The crude acetal was purified by flash column chromatography on silica gel (1:1 hexane/EtOAc, Rf = 0.4) yielding the desired product as orange crystals (1.922 g, yield 75%). Mp 98–100 °C; $[\alpha]_D^{21}$ = -18.3 (*c* 0.95, chloroform); ^{1}H NMR (300 MHz, $CDCl_3$) δ = 4.36 (2 H, m, CH_2), 4.21 (2 H, d, *ortho* H of Cp), 4.19 (5 H, s, unsubstituted Cp ring), 4.16 (2 H, t, *meta* H of Cp), 3.99-3.85 (2 H, m, CH_2), 3.78-3.57 (2 H, m, CH_2), 2.06 (1 H, dd, *J* = 7.7, 5.3 Hz, OH), 1.95-1.76 (1 H, m, CH), 1.47-1.35 (1 H, m, CH). ^{13}C NMR (101 MHz, $CDCl_3$) δ = 100.2 (CH, Cp*C*H), 85.8 (C, Cp ring), 77.2 (CH, *C*HCH_2OH), 68.9 (CH, unsubstituted Cp ring), 68.0 (CH, Cp ring), 66.6 (CH, Cp ring), 66.5 (CH, Cp ring), 66.5 (CH_2, CH_2CH_2O), 65.8 (CH_2, CH_2OH), 26.9 (CH_2, $CHCH_2CH_2$); Electrospray MS analysis: Calc. for $C_{15}H_{18}O_3NaFe$: 325.1. Found: 325.0. Characterisation data is in agreement with the literature data.[5]

6.1.5 Synthesis of (2*R*,4*R*)-4-(Hydroxymethyl)-2-ferrocenyl-1,3-dioxane 2.14[5]

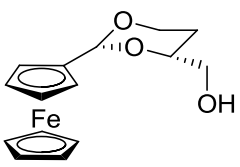

Obtained from ferrocenecarboxaldehyde (1.67 g, 7.80 mmol), the crude acetal was purified by flash chromatography on silica gel (1:1 hexane/EtOAc, Rf = 0.4) yielding the desired product as orange crystals

(1.4573 g, yield 62%). $[\alpha]_D^{21}$ = +16.4 (*c* 0.96, chloroform). Characterisation data is in agreement with the literature data,[5] and with data for the other enantiomer.

6.1.6 Synthesis of (2*S*,4*S*)-4-(Methoxymethyl)-2-ferrocenyl-1,3-dioxane 2.15[5]

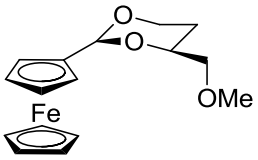

A dry shlenk tube was loaded with a solution of **(*2S,4S*)-2.14** (1.92 g, 6.36 mmol) in dry THF (24 mL) and cooled to 0°C. To the stirred solution was added slowly NaH, 60% in mineral oil (510 mg, 12.7 mmol) because of hydrogen evolution. The reaction mixture was stirred at room temperature for 30 minutes and methyl iodide (1.20 mL, 19.1 mmol) was added. After stirring the solution at room temperature for 1 hour the reaction was quenched with a slow addiction of MeOH (8 mL) and diluted with water. After standard workup the crude was purified by flash column chromatography on silica gel (1:4 Et_2O/hexane, Rf = 0.6) and an orange oil that partially solidified after standing was obtained (1.893 g, yield 94%). $[\alpha]_D^{21}$ = -16.0 (*c* 0.60, chloroform); ^{1}H NMR (300 MHz, $CDCl_3$) δ = 4.36 (2 H, CH_2), 4.22 (2 H, d, *ortho* H of Cp), 4.19 (5 H, s, unsubstituted Cp ring), 4.13 (2 H, t, *meta* H of Cp), 4.02-3.84 (2 H, m, CH_2), 3.56 (2 H, dd, *J* = 10.3, 6.1, CH_2), 3.45 (3 H, s, -OC*H*$_3$), 1.80 (1 H, m, CH), 1.50-1.52 (1 H, m, CH). ^{13}C NMR (101 MHz, $CDCl_3$) δ = 100.1 (CH, Cp*C*H), 86.1 (C, Cp ring), 76.1 (CH, *C*HCH$_2$OMe), 75.7 (CH_2, CH_2*C*H$_2$O), 68.9 (CH, unsubstituted Cp ring), 67.9 (CH, Cp ring), 66.7 (CH_2, *C*H$_2$OMe), 66.7 (CH, Cp ring), 59.5 (CH_3, O*C*H$_3$), 28.1 (CH_2, CH*C*H$_2$CH$_2$); Electrospray MS analysis: Calc. for $C_{16}H_{20}O_3NaFe$: 339.2. Found: 339.0. Characterisation data is in agreement with the literature data.[5]

6.1.7 Synthesis of (2*R*,4*R*)-4-(Methoxymethyl)-2-ferrocenyl-1,3-dioxane 2.15[5]

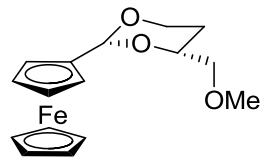

Obtained from **(2*R*,4*R*)-2.14** (1.40 g, 4.65 mmol), the crude was purified by flash column chromatography on silica gel (1:4 Et_2O/hexane, Rf = 0.6) and an orange oil was obtained. (1.257 g, yield 86%). $[\alpha]_D^{21}$ = +14.0 (*c* 0.40, chloroform). Characterisation data is in agreement with the literature data,[5] and with data for the other enantiomer.

6.1.8 Synthesis of (*R*)-2-methyl-ferrocenecarboxaldehyde 2.16[5-6]

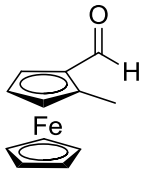

A dry shlenk tube was loaded with a solution of **(2*S*,4*S*)-2.15** (1.88 g, 5.96 mmol) in dry Et_2O (25 mL), cooled to -78°C in an acetone/dry ice bath, and *t*-Buli (4 mL of 1.7M solution in pentane) was added dropwise (a bright yellow precipitate was observed after the addition of *t*-BuLi). The cooling bath was removed after 15 minutes and the solution was stirred at room temperature for 1 hour. Methyl iodide (0.56 mL, 8.96 mmol) was added neat (disappearing of precipitate was observed after addition of the electrophile) to the solution cooled to -78°C and stirred at room temperature overnight. The mixture was then quenched with saturated solution of sodium carbonate and the organic phase was separated and dried under reduced pressure. The crude was treated with HCl 1M (8 mL) and MeOH (25 mL) and the solution was stirred at room temperature for 2 hours. The reaction mixture was diluted with water and extracted with ethyl acetate. After standard work-up the crude aldehyde was purified by flash column chromatography on silica gel (9:1 hexane/Et_2O, Rf = 0.3) and the pure aldehyde was obtained, after further purification by dissolution in methanol and filtration gave the product as a brown solid

(0.831 g, yield 61%). $[\alpha]_D^{21}$ = +31.7 (*c* 0.23, chloroform); ^{1}H NMR (300 MHz, MeOD) δ = 10.06 (1 H, s, -C*H*O), 4.73 (1 H, s, *meta* H of Cp), 4.62 (1 H, s, *ortho* H of Cp), 4.57 (1 H, s, *ortho* H of Cp), 4.25 (5 H, s, unsubstituted Cp ring), 2.26 (3 H, s, CpCH_3). ^{13}C NMR (101 MHz, $CDCl_3$) δ = 193.8 (CH, *C*HO), 87.1 (C, Cp ring), 87.1 (C, Cp ring), 75.0 (CH, Cp ring), 71.0 (CH, Cp ring), 70.2 (CH, unsubstituted Cp ring), 69.5 (CH, Cp ring), 13.5 (CH_3, Cp*C*H_3); Electrospray MS analysis: Calc. for $C_{12}H_{12}ONaFe$: 251.0. Found: 251.0. Characterisation data is in agreement with the literature data.[5]

6.1.9 Synthesis of (*S*)-2-methyl-ferrocenecarboxaldehyde 2.16[5-6]

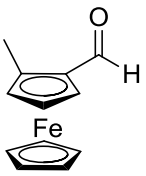

Obtained from **(2*R*,4*R*)-2.15** (1.23 g, 3.89 mmol), the crude aldehyde was purified by flash chromatography on silica gel (9:1 hexane/Et_2O, Rf = 0.3) and the pure aldehyde was obtained as a brown solid (0.667 g, yield 75%). $[\alpha]_D^{21}$ = -27.8 (*c* 0.63, chloroform). Characterisation data is in agreement with the literature data,[5] and with data for the other enantiomer.

6.1.10 Synthesis of (*R*)-1-(2-methylferrocenyl)methanamine 2.17

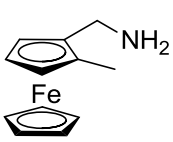

Using the general procedure **A**, **(*R*)-2.16** (0.815 g, 3.60 mmol) was reacted to give the oxime as a brown-red oil (0.685 g, yield 78%). ^{1}H NMR (300 MHz, $CDCl_3$) δ = 8.12 (1 H, s, C*H*=N), 4.56-4.45 (1 H, m, *meta* H of Cp), 4.34-4.23 (2 H, m, *ortho* H of Cp), 4.14 (5 H, m, unsubstituted Cp ring), 2.12(3 H, s, CH_3). The oxime (0.685 g, 2.80 mmol) was then reduced with an excess of lithium aluminum hydride (0.49 g, 13 mmol) to yield the

desired product as brown yellow oil (0.272 g, yield 42%). $[\alpha]_D^{21}$ = +34.8 (*c* 1.55, chloroform); ^{1}H NMR (300 MHz, $CDCl_3$) δ = 4.21 (1 H, s, *ortho* H of Cp), 4.09 (2 H, s, *meta* H of Cp), 4.02 (5 H, s, unsubstituted Cp ring), 3.67 (2 H, s, CpCH_2N), 1.97 (3 H, s, CpCH_3). ^{13}C NMR (101 MHz, $CDCl_3$) δ = 88.7 (C, Cp ring), 82.4 (C, Cp ring), 69.7 (CH, Cp ring), 68.9 (CH, unsubstituted Cp ring), 66.8 (CH, Cp ring), 65.3 (CH, Cp ring), 40.0 (CH_2, CpCH_2NH_2), 13.0 (CH_3, CpCH_3); Electrospray MS analysis: Calc. for $C_{12}H_{13}Fe^+$: 213.0. Found: 213.1; HRMS analysis: Calc. for $C_{12}H_{15}NNaFe$: 252.0452. Found: 252.0450.

6.1.11 Synthesis of (*S*)-1-(2-methylferrocenyl)methanamine 2.18

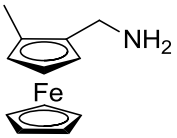

Using the general procedure **A**, **(*S*)-2.16**(0.658 g, 2.89 mmol) was reacted to give the oxime as a brown-red oil (0.664 g, yield 95%). The oxime (0.664 g, 2.73 mmol) was then reduced with an excess of lithium aluminum hydride (0.45 g, 12 mmol) to yield the desired product as brown yellow oil (0.406 g, yield 65%). $[\alpha]_D^{21}$ = -29.3 (*c* 0.60, chloroform); HRMS analysis: Calc. for $C_{12}H_{15}NFe$: 229.0554. Found: 229.0545. Characterisation data is in agreement with data for the other enantiomer.

6.1.12 Synthesis of (*S*)-*N*-(1-Phenylbutoxy)-phthalimide 3.10[7]

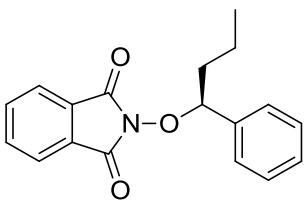

N-hydroxyphthalimide (2.18 g, 13.4 mmol), (*R*)-1-Phenylbutanol (1.0 g, 6.7 mmol) and PhP_3 (3.57g, 1.3 mmol) were placed in a 250 mL shlenk tube with dry THF (60 mL). The mixture was cooled to 0°C and DIAD (3.0 mL, 6.7 mmol) was added dropwise over 10 minutes at the same

temperature. The mixture was stirred at 0°C for 30 minutes and then allowed to warm to room temperature. Then it was stirred at 50°C for 4 days (the mixture became pale yellow and clear). The solvent was evaporated and the solid was then dissolved in CH_2Cl_2 (30 mL) and washed with a saturated solution of $NaHCO_3$ (4x25 mL). The aqueous layers were combined and extracted with CH_2Cl_2 (30 mL). The organic phases were combined, dried over $MgSO_4$ and then evaporated to obtain a yellow oil. The mixture was purified by flash column chromatography on silica (4:1 hexane/Et_2O, Rf = 0.38) and a white solid was obtained (1.32 g, yield 67%). ^{1}H NMR (300 MHz, $CDCl_3$) δ = 7.83-7.59 (4 H, m, phthalimide Ar*H*), 7.51-7.38 (2 H, m, *ortho H* of Ph), 7.37-7.21 (3 H, m, *meta* and *para H* of Ph), 5.35 (1 H, t, *J* = 7.1 Hz, PhC*H*), 2.28-2.11 (1 H, m, PhCHC*H*H), 1.99-1.80 (1 H, m, PhCHCH*H*), 1.58-1.30 (2 H, m, CH_3CH_2), 0.99 (3 H, t, *J* = 7.4 Hz, CH_3). ^{13}C NMR (101 MHz, $CDCl_3$) δ = 163.7 (C, *C*O), 138.3 (C, CH_2CCO), 134.2 (CH, Ar), 128.9 (CH, Ar), 128.8 (C, NOCH*C*), 128.3 (CH, Ar), 128.1 (CH, Ar), 123.3 (CH, Ar), 89.1 (CH, NO*C*H), 36.9 (CH_2, NOCH*C*H_2), 19.0 (CH_2, NOCHCH_2*C*H_2), 13.9 (CH_3); Electrospray MS analysis: Calc. for $C_{18}H_{17}NO_3Na$: 318.1. Found: 318.1; HRMS analysis: Calc. for $C_{18}H_{17}NO_3Na$: 318.1106. Found: 318.1111. Characterisation data is in agreement with the literature data.[7]

6.1.13 Synthesis of (*E*)-(*S*)-(-)-*O*-(1-Phenylbutyl)ferrocene-1-carboxaldoxime 3.11[8]

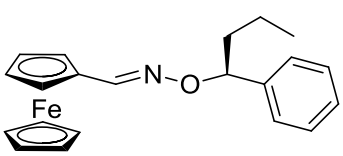

(*S*)-3.10 (1.32 g, 4.47 mmol) was dissolved in EtOH (50 mL) at 40°C. Hydrazine monohydrate (0.3 mL, 6 mmol) was added dropwise under Ar. The solution turned orange and then yellow. The mixture was refluxed for 1 hour and a white precipitate formed.

Ferrocenecarboxaldehyde (1.92 g, 9 mmol) was added at room temperature and the mixture was stirred overnight at room temperature. The crude was purified by flash column chromatography on silica gel (9:1 hexane/Et_2O, Rf = 0.5) to give a red solid (0.75 g, 46%). $[\alpha]_D^{21}$ = +245 (*c* 0.0373, chloroform); ^{1}H NMR (300 MHz, $CDCl_3$) δ = 7.98 (1 H, s, CpC*H*), 7.42-7.30 (4 H, m, *ortho* and *meta H* of Ph), 7.29-7.19 (1 H, m, *para H* of Ph), 5.13 (1 H, t, *J* = 6.9 Hz, PhC*H*), 4.54-4.48 (1 H, m, *ortho H* on substituted Cp ring), 4.48-4.43 (1 H, m, *ortho H* on substituted Cp ring), 4.34-4.27 (2 H, m, *meta H* on substituted Cp ring), 4.09 (5 H, s, unsubstituted Cp ring), 2.07-1.92 (1 H, m, PhCHC*H*H), 1.85-1.71 (1 H, m, PhCHCH*H*), 1.53-1.30 (2 H, m, CH_3CH_2), 0.98 (3 H, t, *J* = 7.4 Hz, CH_3). ^{13}C NMR (101 MHz, $CDCl_3$) δ = 148.8 (C, Cp ring), 142.9 (C, NOCH*C*), 128.1 (CH, Ar), 127.2 (CH, Ar), 126.8 (CH, Ar), 84.7 (CH, NO*C*HC), 69.8 (CH, Cp ring), 69.6 (CH, Cp ring), 69.1 (CH, unsubstituted Cp ring), 68.0 (CH, Cp ring), 67.2 (CH, Cp*C*HNO), 38.2 (CH_2, NOCH*C*H_2), 18.9 (CH_2, NOCHCH_2*C*H_2), 14.0 (CH_3); Electrospray MS analysis: Calc. for $C_{21}H_{23}NONa$: 384.1. Found: 384.0; HRMS analysis: Calc. for $C_{21}H_{23}NONa$: 384.1027. Found: 384.1025. Characterisation data is in agreement with the literature data.[8]

6.1.14 Synthesis of (*E*)-(*R*)-(-)-*O*-(1-Phenylbutyl)ferrocene-1-carboxaldoxime 3.11[8]

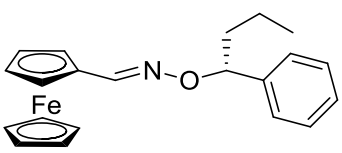

Obtained from **(*R*)-*3.10*** (1.5 g, 5.08 mmol) and ferrocenecarboxaldehyde (2.14 g, 10 mmol) as a red solid (1.56 g, 85%). $[\alpha]_D^{21}$ =-213 (*c* 0.324, chloroform). Characterisation data is in agreement with the literature data,[8] and with data for the other enantiomer.

6.1.15 Synthesis of *N*(1*S*,1'*S*)-1-ferrocenyl-2-phenyl-*N*(1-phenylbutoxy)-1-ethylamine 3.12[8]

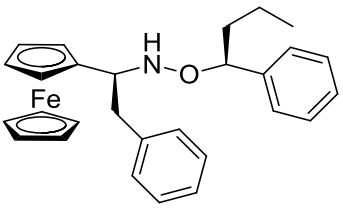

(*S*)-3.11 (0.74 g, 2.05 mmol) was dissolved in dry toluene (50 mL) in dry glassware and $BF_3{\cdot}Et_2O$ (0.8 mL, 6.37 mmol) was added at -78°C and stirred for 30 minutes. Benzylmagnesium Chloride (7 mL 1.0 M in Et_2O, 7 mmol) was added at -78 °C over 40 minutes. The reaction mixture was stirred for 1 hour and 30 minutes at -78 °C, and then quenched with saturated aqueous solution of ammonium chloride (10 mL). The mixture was warmed to room temperature and washed with water (10 mL) and Et_2O (10 mL), extracted from the aqueous layer and washed with saturated sodium bicarbonate, dried over anhydrous magnesium sulphate and evaporated. This was then purified by flash column chromatography on silica gel (95:5 hexane/Et_2O with 0.5% of triethylamine, Rf = 0.6) to give the desired product (0.788 g, yield 85%). ^{1}H NMR (300 MHz, $CDCl_3$) δ = 7.53 – 7.00 (10 H, m, ArH), 5.76 (1 H, s, NH), 4.58 (1 H, dd, *J* = 7.7, 5.9 Hz, CH), 4.15-3.76 (10H, m, Cp rings, CpC*H*), 3.29 (1 H, dd, *J* = 13.1, 6.0 Hz, CpCHC*H*H), 2.86 (1 H, dd, *J* = 13.1, 7.3 Hz, CpCHCH*H*), 1.94-1.71 (1 H, m, PhCHC*H*H), 1.69-1.44 (1 H, m, PhCHCH*H*), 1.43–1.17 (2 H, m, $CH_3C\mathit{H_2}$), 0.95 (3 H, t, *J* = 7.2 Hz, $C\mathit{H_3}$). ^{13}C NMR (101 MHz, $CDCl_3$) δ = 143.3 (C, Ar), 139.3 (C, Ar), 129.7 (CH, Ar), 128.37 (CH, Ar), 128.0 (CH, Ar), 127.4 (CH, Ar), 126.6 (CH, Ar), 125.9 (CH, Ar), 88.7 (C, Cp ring), 85.1 (CH, O*C*H), 68.2 (CH, unsubstituted Cp ring), 67.5 (CH, Cp ring), 66.8 (CH, Cp ring), 66.3 (CH, Cp ring), 61.5 (CH, Cp*C*H), 40.8 (CH_2, CpCH*C*H_2), 38.6 (CH_2, OCH*C*H_2), 19.2 (CH_2, OCHCH_2*C*H_2), 14.1 (CH_3); Electrospray MS analysis: Calc. for $C_{28}H_{31}NONaFe$: 476.2. Found: 476.1; HRMS analysis: Calc. for $C_{28}H_{31}NONaFe$: 476.1653. Found: 476.1640. Characterisation data is in agreement with the literature data.[8]

6.1.16 Synthesis of *N*(1*R,1'R*)-1-Ferrocenyl-2-phenyl-*N*(1-phenylbutoxy)-1-ethylamine 3.12

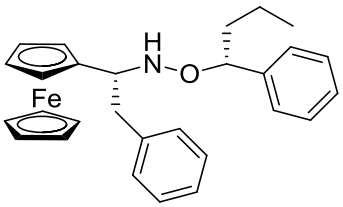

Obtained from **(*R*)-3.11** (1.55 g, 4.29 mmol) and benzylmagnesium chloride (13 mL 1.0 M in Et_2O, 13 mmol) as a brown solid (0.58 g, yield 30%). Electrospray MS analysis: Calc. for $C_{28}H_{31}NONaFe$: 476.2. Found: 476.1. Characterisation data is in agreement with the literature data,[8] and with data for the other enantiomer.

6.1.17 Synthesis of (*S*)-1-ferrocenyl-2-phenyl-ethylamine 3.13[8]

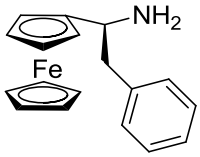

Zinc dust (4 g, 60 mmol) was added to **(*SS*)-3.12** (0.78 g, 1.72 mmol) dissolved in THF (0.5 mL) and a mixture of acetic acid and water (40 mL, 1:1) to obtain a milky solution. The mixture was placed in an unltrasound bath at 40 °C for 6 hours, after which the solution became transparent and yellow coloured. The zinc was filtered on celite and rigorously washed with water and Et_2O. The filtrate was extracted with Et_2O (2x20 mL), the aqueous layer basified to pH 12 with 4 M NaOH and then saturated ammonium chloride was added to disperse the emulsion. The solution was then further extracted with ethyl acetate (3x20 mL); the organic phase was washed with brine, dried over anhydrous magnesium sulphate, filtered and evaporated to yield the crude amine. This was then purified with flash column chromatography through silica gel using CH_2Cl_2 to remove the impurities and then 9:1 CH_2Cl_2/MeOH to collect the desired product (0.15 g, yield 29%). $[\alpha]_D^{21}$ = +9.6 (*c* 1.00, chloroform); ^{1}H NMR (300 MHz, $CDCl_3$) δ = 7.48-7.03 (5 H, m, Ar*H*), 4.33 – 4.06 (9 H, stack, H of Cp rings), 4.05-3.90 (1 H, m, CpC*H*N), 3.12 (2 H, s, NH_2), 3.04 (1 H, dd, *J* = 13.3, 4.2 Hz, CpCHC*H*H), 2.79 (1 H, dd, *J* = 13.2, 8.6 Hz, CpCHCH*H*). ^{13}C

NMR (101 MHz, $CDCl_3$) δ = 138.7 (C, Ar), 129.4 (CH, Ar), 128.4 (CH, Ar), 126.4 (CH, Ar), 68.4 (CH, unsubstituted Cp ring), 67.6 (CH, Cp ring), 67.5 (CH, Cp ring), 67.0 (CH, Cp ring), 65.4 (C, Cp ring), 52.2 (CH, Cp*C*H), 45.5 (CH_2, CpCH*C*H_2); Electrospray MS analysis: Calc. for $C_{18}H_{17}Fe$: 289.1. Found: 289.1. Characterisation data is in agreement with the literature data.[8]

6.1.18 Synthesis of (*R*)-1-ferrocenyl-2-phenyl-ethylamine 2.19[8]

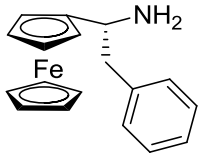

Obtained from **(*RR*)-3.12** (0.4 g, 0.75 mmol) as a yellow solid (0.18 g, yield 79%). $[\alpha]_D^{21}$ = -9.6 (*c* 1.00, chloroform); ^{1}H NMR (300 MHz, $CDCl_3$) δ = 7.36 – 7.11 (5 H, m, Ar*H*), 4.29 – 4.03 (9 H, m, stack, H of Cp rings), 3.92 (1 H, s, CpC*H*N), 3.00 (1 H, dd, *J* = 13.2, 4.2 Hz, CpCHC*H*H), 2.70 (1 H, dd, *J* = 13.2, 8.9 Hz, CpCHCH*H*), 1.75 (2 H, broad s, N*H*$_2$); ^{13}C NMR (101 MHz, $CDCl_3$) δ = 139.2 (C, Ar), 129.4 (CH, Ar), 128.4 (CH, Ar), 126.3 (CH, Ar), 68.3 (CH, unsubstituted Cp ring), 67.5 (CH, Cp ring), 67.4 (CH, Cp ring), 66.9 (CH, Cp ring), 65.4 (C, Cp ring), 52.3 (CH, Cp*C*H), 46.1 (CH_2, CpCH*C*H_2); Electrospray MS analysis: Calc. for $C_{18}H_{17}Fe^+$: 289.1. Found: 289.2; HRMS analysis: Calc. for $C_{18}H_{17}Fe$: 289.0680. Found: 289.0678. Characterisation data is in agreement with the literature data,[8] and with data for the other enantiomer.

6.1.19 General procedure for the synthesis of urea receptors B[9]

To a solution of ferrocenylmethanamine (0.78 mmol) dissolved in dry CH_2Cl_2 (10 mL), cooled at 0°C, was added dropwise a solution of 4-nitrophenylisocyanate (1.13 mmol) in dry CH_2Cl_2 (4 mL). The cold bath was removed and the solution was stirred at room temperature for 6.5

hours. After concentration under reduced pressure the crude urea derivative was recovered as a light brown powder, redissolved in dichloromethane and filtered under vacuum to separate a yellow insoluble compound and obtain a dark orange coloured solution. The filtrate was concentrated under reduced pressure, dissolved in CH_2Cl_2 and purified by flash column chromatography on silica gel (95:5 CH_2Cl_2/EtOAc) to give the urea.

6.1.20 Synthesis of *N*-(4-nitrophenyl)-*N'*-ferrocenemethyl-urea 2.10[10]

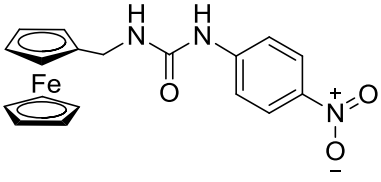

Using the general procedure **B**, **2.12** (0.18 g, 0.78 mmol) was reacted with 4-nitrophenylisocyanate (0.185 g, 1.13 mmol) and purified by flash column chromatography on silica gel (95:5 CH_2Cl_2/EtOAc, Rf = 0.2) to give the urea as a brown powder (144 mg, yield 48%). Crystallographic quality crystals were obtained by slow evaporation of CH_2Cl_2 and Et_2O from a saturated solution at room temperature. Mp 120–122 °C; IR (neat)/ cm^{-1} 3376, 3240, 1641, 1612, 1598, 1546, 1506, 1462, 1408, 1327, 1298, 1251, 1040, 853, 829, 746; ^{1}H NMR (300 MHz, CD_2Cl_2) δ = 8.18 (2 H, d, *J* = 9.2 Hz, Ar*H*), 7.58 (2 H, d, *J* = 9.3 Hz, Ar*H*), 6.75 (1 H, s, ArN*H*C), 4.99 (1 H, t, *J* = 4.7 Hz, CH_2N*H*C), 4.27-4.24 (2 H, m, *ortho* H of Cp), 4.22 (2 H, s, *meta* H of Cp), 4.21 (5 H, s, unsubstituted Cp ring), 4.20-4.17 (2 H, m, Cp*C*H_2N). ^{13}C NMR (101 MHz, CD_2Cl_2) δ = 146.0 (C, CO), 125.5 (CH, Ar), 118.1 (CH, Ar), 86.5 (C, Ar), 85.4 (C, Ar), 69.0 (CH, unsubstituted Cp ring), 68.7 (CH, Cp ring), 68.6 (CH, Cp ring), 66.1 (C, Cp ring), 40.1 (CH_2, Cp CH_2); Electrospray MS analysis: Calc. for $C_{18}H_{17}N_3O_3NaFe$: 402.1. Found: 402.1; HRMS analysis: Calc. for $C_{18}H_{17}N_3O_3NaFe$: 402.0517. Found: 402.0522. Anal. Calc. for $C_{18}H_{17}N_3O_3Fe$:

C, 57.01; H, 4.52; N, 11.08. Found: C, 57.01; H, 4.87; N, 10.98. Characterisation data is in agreement with the literature data.[10]

6.1.21 Synthesis of (*R*)-*N*-(4-nitrophenyl)-*N'*-[2-methyl-ferrocenemethyl]-urea 2.8

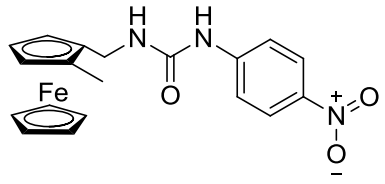

Using the general procedure **B**, **2.17** (183 mg, 0.80 mmol) was reacted with 4-nitrophenylisocyanate (164 mg, 1.00 mmol) and purified by flash column chromatography on silica gel (95:5 CH_2Cl_2/EtOAc, Rf = 0.7) to give the urea as a yellow powder (221 mg, yield 70%). Crystallographic quality crystals were obtained by slow evaporation of CH_2Cl_2 and Et_2O from a saturated solution at room temperature. Mp 82–84°C; $[\alpha]_D^{21}$ = +75.3 (*c* 0.74, chloroform); IR (neat)/cm^{-1} 3339, 3094, 2922, 1672, 1614, 1548, 1492, 1412, 1324, 1301, 1220, 1175, 1104, 1034, 998, 849, 747, 691; ^{1}H NMR (400 MHz, CD_2Cl_2) δ = 8.04 (2 H, d*, J* = 9.2 Hz, Ar*H*), 7.45 (2 H, d*, J* = 9.2 Hz, Ar*H*), 6.89 (1 H, s, ArN*H*C), 4.95 (1 H, t, *J* = 4.5 Hz, CH_2N*H*C), 4.22 (1 H, dd, *J* = 14.2 Hz, 5.7 Hz, CpC*H*HN), 4.11 – 4.01 (3 H, m, H of Cp), 3.99 (5 H, s, unsubstituted Cp ring), 3.92 (1 H, t, *meta* H of Cp), 1.91 (2 H, s, CpCH_3). ^{13}C NMR (101 MHz, CD_2Cl_2) δ = 154.0 (C, CO), 146.0 (C, Ar), 142.6 (C, Ar), 125.5 (CH, Ar), 118.1 (CH, Ar), 83.7 (C, Cp ring), 83.5 (C, Cp ring), 70.5 (CH, Cp ring), 69.6 (CH, unsubstituted Cp ring), 68.3 (CH, Cp ring), 66.4 (CH, Cp ring), 38.8 (CH_2), 13.1c (CH_3); Electrospray MS analysis: Calc. for $C_{19}H_{19}N_3O_3NaFe$: 416.1. Found: 416.0; HRMS analysis: Calc. for $C_{19}H_{19}N_3O_3NaFe$: 416.0674. Found: 416.0679. Anal. Calc. for $C_{19}H_{19}N_3O_3Fe{\cdot}H_2O$: C, 57.51; H, 4.93; N, 10.59. Found: C, 57.51; H, 4.86; N, 10.57; %ee = 97%.

6.1.22 Synthesis of (*S*)-*N*-(4-Nitrophenyl)-*N*'-[2-methyl-ferrocenemethyl]-urea 2.9

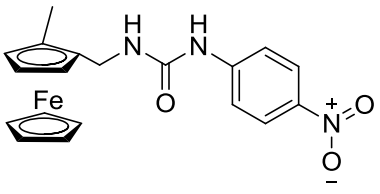

Using the general procedure **B**, **2.18** (160 mg, 0.70 mmol) was reacted with 4-nitrophenylisocyanate (164 mg, 1.00 mmol) and purified by flash column chromatography on silica gel (95:5 CH_2Cl_2/EtOAc, Rf = 0.7) to give the urea as brown yellow flakes (206 mg, yield 75%). Crystallographic quality crystals were obtained by slow evaporation of CH_2Cl_2 and Et_2O from a saturated solution at room temperature. Mp 78–80°C; $[\alpha]_D^{21}$ = -70.8 (*c* 1.03, chloroform); HRMS analysis: Calc. for $C_{19}H_{19}N_3O_3NaFe$: 416.0674. Found: 416.0677. Anal. Calc. for $C_{19}H_{19}N_3O_3Fe$: C, 58.03; H, 4.87; N, 10.69. Found: C, 58.10; H, 4.89; N, 10.80; %ee = 91%. Characterisation data is in agreement with data for the other enantiomer.

6.1.23 Synthesis of *N*,*N*'-bis[1-ferrocenylmethyl]-urea 2.7[11]

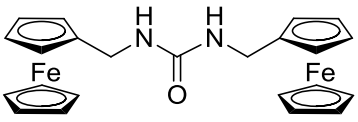

2.12 (64 mg, 0.30 mmol) was dissolved in toluene (1 mL) and added dropwise to a stirred mixture of 1,1'-carbonyl diimidazole (24 mg, 0.15 mmol) and toluene (3 mL). The mixture was stirred at room temperature overnight, then the crystallized solid imidazole was removed by filtration and the filtrate was concentrated in vacuo, dissolved in CH_2Cl_2, washed with water (3x10 mL), dried over anhydrous sodium sulphate, filtered and concentrated in vacuo. The crude was purified by flash column chromatography (1:1 light petroleum/EtOAc) to yield the desired product as yellow crystalline needles (34 mg, 51%). Mp 232–236°C; ^{1}H NMR (300 MHz, CD_2Cl_2) δ = 4.45 (2 H, s, N*H*), 4.11 (4 H, s, H of substituted Cp ring), 4.08 (8 H, s, H of unsubstituted Cp ring), 4.04 (4 H, s, H of substituted Cp ring), 3.97 (4 H, d, J = 5.4, CpC*H*$_2$); ^{13}C

NMR (101 MHz, CD_2Cl_2) δ = 157.5 (C, CO), 86.6 (C, Cp ring), 68.9 (CH, unsubstituted Cp ring), 68.5 (CH, Cp ring), 68.4 (CH, Cp ring), 40.1 (CH_2); Electrospray MS analysis: Calc. for $C_{23}H_{24}Fe_2N_2ONa$: 479.1; HRMS analysis: Calc. for $C_{23}H_{24}Fe_2N_2ONa$: 479.0485. Found: 479.0486. Anal. Calc. for $C_{23}H_{24}Fe_2N_2O$: C, 60.56; H, 5.30; N, 6.14. Found: C, 60.67; H, 5.36; N, 6.03. Characterisation data is in agreement with the literature data.[11]

6.1.24 Synthesis of Isolipoic Acid 3.2[12]

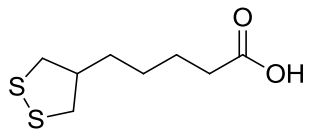

Sulfur (42 mg, 1.30 mmol) and sodium sulphide hydrate (315 mg, 1.30 mmol) were added to a stirred solution of **3.14** (435 mg, 1.30 mmol) in DMF (15 mL) and the resulting reaction mixture was heated at 85 °C for 4.5 h. The mixture was then cooled to room temperature, water (30 mL) and Et_2O (30 mL) were added, and the layers were separated. The aqueous layer was extracted with Et_2O (5x30 mL). The combined organic extracts were washed with brine (45 mL) and dried with anhydrous magnesium sulphate, and solvents were removed under reduced pressure. The crude was purified by flash column chromatography on silica gel (1:1 Hexane/EtOAc, Rf = 0.5) to give the acid as a yellow solid (174 mg, yield 64%). Mp 70-72°C; IR (neat)/cm^{-1} 2929, 2855, 1695, 1461, 1411, 1302, 1260, 1210, 943, 746, 712; ^{1}H NMR (300 MHz, CD_2Cl_2) δ = 3.25 (2 H, dd, J = 11.0, 6.6Hz, SCH*H*), 2.80 (2 H, dd, J = 11.0, 6.6 Hz, SCH*H*), 2.54 (1 H, sept, J = 6.6Hz, CH_2CH-$(CH_2S)_2$), 2.36-2.40 (2 H, m, COCH_2), 1.63-1.71 (2 H, m, CH_2), 1.50-1.56 (2 H, m, CH_2), 1.41-1.47 (2 H, m, CH_2); Electrospray MS analysis: Calc. for $C_8H_{14}O_2S_2$: 205. Found: 205.

6.1.25 General procedure for the synthesis of disulfides C

An ice cold solution of **3.2** (0.29 mmol) and triethylamine (0.29 mmol) in dry toluene (2 mL) was stirred for 10 minutes, after which a solution of diphenylphosphoryl azide (0.29 mmol) in dry toluene (1 mL) was added dropwise over a period of 2 h. After removal of the ice bath it was allowed to cool to room temperature and heated under reflux for 4 h. Ferrocenylamine (0.29 mmol) in dry toluene (1 mL) was pipetted into the stirring solution. The mixture was stirred at room temperature overnight. The solvent was then removed under reduced pressure. The crude product was purified by flash column chromatography (98:2 CH_2Cl_2/MeOH) and solvent evaporated to give a dark orange oily product.

6.1.26 Synthesis of Ferrocenyl Isolipoic Achiral Urea 3.3

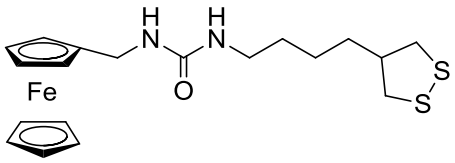

Using the general procedure **C**, **2.12** (21 mg, 0.097 mmol) was reacted with **3.2** (20 mg, 0.097 mmol), triethylamine (10 mg, 0.097 mmol) and diphenylphosphorylazide (27 mg, 0.097 mmol) and purified by flash column chromatography on silica gel (98:2 CH_2Cl_2/MeOH Rf = 0.7) to give the urea as a dark orange oil (34 mg, yield 84%). IR (neat)/cm^{-1} 3356, 2923, 2852, 1634, 1568, 1467, 1260, 1105, 842, 750; ^{1}H NMR (300 MHz, CD_2Cl_2) δ = 4.62 (1 H, s, $FcCH_2NH$), 4.52 (1 H, s, CH_2CH_2NH), 4.17-4.18 (2 H, m, *ortho* H of Cp), 4.16 (5 H, s, unsubstituted Cp ring), 4.12-4.13 (2 H, m, *meta* H of Cp), 4.07 (2 H, d, *J* = 6.0 Hz, $CpCH_2N$), 3.24 (2H, dd, J = 9.0, 6.6Hz, SCH*H*), 3.17 (2H, q, J = 6.6 Hz, $CONHCH_2$), 2.78 (2H, dd, J = 9.0, 6.6 Hz, SCH*H*), 2.52 (1H, sept, J = 6.6Hz, CH_2CH-$(CH_2S)_2$), 1.46-1.58 (4H, m, CH_2), 1.35-1.45 (2H, m, CH_2).^{13}C NMR (101 MHz, CD_2Cl_2) δ = 157.9 (C, CO), 85.8 (C, Cp ring),

68.6 (CH, Cp ring), 68.1 (CH, Cp ring), 47.7 (CH, $SCH_2\mathit{C}H$), 43.9 (CH_2, $S\mathit{C}H_2$), 40.4 (CH_2, $NH\mathit{C}H_2CH_2$), 39.9 (CH_2, $CpCH_2$), 33.5 (CH_2, $NHCH_2\mathit{C}H_2/SCH_2CH\mathit{C}H_2$), 30.4 ($CH_2$, $NHCH_2\mathit{C}H_2/SCH_2CH\mathit{C}H_2$), 25.8 ($CH_2$, $NHCH_2CH_2\mathit{C}H_2$); Electrospray MS analysis: Calc. for $C_{19}H_{26}FeN_2OS_2Na$: 441.1. Found: 441.2; HRMS analysis: Calc. for $C_{19}H_{26}FeN_2OS_2Na$: 441.0734. Found: 441.0751.

6.1.27 Synthesis of (*R*)-Ferrocenyl Isolipoic Planar Chiral Urea 3.4

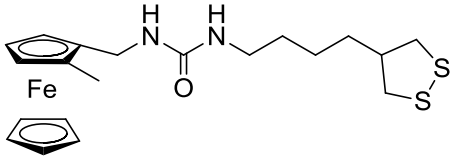

Using the general procedure **C**, **2.17** (66.7 mg, 0.291 mmol) was reacted with **3.2** (60 mg, 0.291 mmol), triethylamine (30 mg, 0.291 mmol) and diphenylphosphorylazide (91 mg, 0.291 mmol) and purified by flash column chromatography on silica gel (98:2 CH_2Cl_2/MeOH Rf = 0.7) to give the urea as a dark orange oil (105 mg, yield 83%). IR (neat)/cm^{-1} 3308, 2921, 2858, 1617, 1570, 1245, 1104, 1031, 999, 807; ^{1}H NMR (300 MHz, CD_2Cl_2) δ = 4.26-4.34 (2 H, m, N*H*), 4.18-4.25 (2 H, m, Fc$C\mathit{H}_2$), 4.03-4.13 (7 H, m, *ortho* H of Cp and unsubstituted Cp ring), 3.98-4.02 (1 H, m, *meta* H of Cp), 3.26 (2 H, dd, J = 9.0, 6.6Hz, $SC\mathit{H}_2$), 3.19 (2 H, q, J = 6.6 Hz, $CONHC\mathit{H}_2$), 2.81 (2 H, dd, J = 9.0, 6.6Hz, SCH*H*), 2.54 (1 H, sept, J = 6.6Hz, $CH_2C\mathit{H}$-$(CH_2S)_2$), 2.01 (3 H, s, $C\mathit{H}_3$), 1.47-1.59 (4 H, m, $C\mathit{H}_2$), 1.35-1.46 (2 H, m, $C\mathit{H}_2$).^{13}C NMR (101 MHz, CD_2Cl_2) δ = 157.6 (C, CO), 84.3 (C, Cp ring), 83.7 (C, Cp ring), 70.1 (CH, Cp ring), 69.6 (CH, Cp ring), 68.1 (CH, Cp ring), 66.1 (CH, Cp ring), 47.7 (CH, $SCH_2\mathit{C}H$), 43.9 (CH_2, $S\mathit{C}H_2$), 40.4 (CH_2, $NH\mathit{C}H_2CH_2$), 38.6 (CH_2, $CpCH_2$), 33.5 (CH_2, $NHCH_2\mathit{C}H_2/SCH_2CH\mathit{C}H_2$), 30.4 ($CH_2$, $NHCH_2\mathit{C}H_2/SCH_2CH\mathit{C}H_2$), 25.8 ($CH_2$, $NHCH_2CH_2\mathit{C}H_2$), 13.0

(CH_3); Electrospray MS analysis: Calc. for $C_{20}H_{29}FeN_2OS_2Na$: 455.1. Found: 455.2; HRMS analysis: Calc. for $C_{20}H_{29}FeN_2OS_2Na$: 455.0890. Found: 455.0892; %ee = 95%.

6.1.28 Synthesis of (*S*)-Ferrocenyl Isolipoic Planar Chiral Urea 3.5

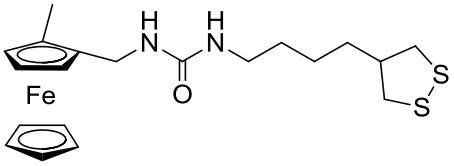

Using the general procedure **C**, **2.18** (66.7 mg, 0.291 mmol) was reacted with **3.2** (60 mg, 0.291 mmol), triethylamine (30 mg, 0.291 mmol) and diphenylphosphorylazide (91 mg, 0.291 mmol) and purified by flash column chromatography on silica gel (98:2 CH_2Cl_2/MeOH Rf = 0.7) to give the urea as a dark orange oil (66 mg, yield 52%). IR (neat)/cm^{-1} 3314, 2920, 2854, 1618, 1578, 1246, 1104, 1031, 998, 808; ^{1}H NMR (300 MHz, CD_2Cl_2) δ = 4.18-4.38 (4 H, m, N*H* and FcC*H*$_2$), 4.06-4.13 (7 H, m, *ortho* H of Cp and unsubstituted Cp ring), 3.99-4.02 (1 H, m, *meta* H of Cp), 3.14-3.31 (4 H, m, SC*H*$_2$ and CONHC*H*$_2$), 2.81 (2 H, dd, J = 9.0, 6.6Hz, SCH*H*), 2.54 (1 H, sept, J = 6.6Hz, CH_2CH-$(CH_2S)_2$), 2.00 (3 H, s, C*H*$_3$), 1.47-1.59 (4 H, m, C*H*$_2$), 1.36-1.46 (2 H, m, C*H*$_2$).^{13}C NMR (101 MHz, CD_2Cl_2) δ = 157.6 (C, CO), 83.9 (C, Cp ring), 83.3 (C, Cp ring), 69.9 (CH, Cp ring), 69.2 (CH, Cp ring), 67.8 (CH, Cp ring), 65.8 (CH, Cp ring), 47.7 (CH, SCH_2CH), 43.9 (CH_2, SCH_2), 40.4 (CH_2, $NHCH_2CH_2$), 38.6 (CH_2, $CpCH_2$), 33.5 (CH_2, $NHCH_2CH_2$/SCH_2CHCH_2), 30.4 (CH_2, $NHCH_2CH_2$/SCH_2CHCH_2), 25.8 (CH_2, $NHCH_2CH_2CH_2$), 13.0 (CH_3); Electrospray MS analysis: Calc. for $C_{20}H_{29}FeN_2OS_2Na$: 455.1. Found: 455.2; HRMS analysis: Calc. for $C_{20}H_{29}FeN_2OS_2Na$: 455.0890. Found: 455.0899; %ee = 94%.

6.1.29 Synthesis of (*S*)-Ferrocenyl Isolipoic Central Chiral Urea 3.6

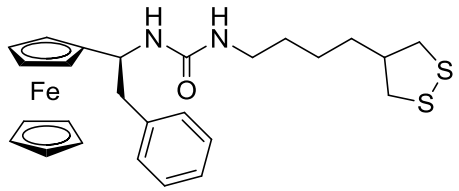

Using the general procedure **C**, **3.13** (88.8 mg, 0.291 mmol) was reacted with isolipoic acid (60 mg, 0.291 mmol), triethylamine (30 mg, 0.291 mmol) and diphenylphosphorylazide (91 mg, 0.291 mmol) and purified by flash column chromatography on silica gel (98:2 CH_2Cl_2/MeOH Rf = 0.7) to give the urea as a dark orange oil (73 mg, yield 49%). IR (neat)/cm^{-1} 3311, 2924, 2855, 1626, 1558, 1250, 1105, 1027, 1000, 812, 698; ^{1}H NMR (300 MHz, CD_2Cl_2) δ = 7.13-7.34 (5 H, stack, Ar*H*), 4.89 (1 H, q, *J* = 4.7 Hz, CH_2CH_2NH), 4.52 (1 H, d, *J* = 9.1 Hz, $FcCH_2NH$), 4.17 (5 H, s, unsubstituted Cp ring), 4.12-4.15 (2 H, m, Cp*H*), 4.08-4.11 (1 H, m, Cp*H*), 4.04-4-07 (1 H, m, Cp*H*), 3.24 (2 H, dd, J = 9.0, 6.6Hz, SCH*H*), 3.08-3.18 (4 H, m, PhCH_2 and $COCH_2$), 2.92-2.99 (1 H, m, CpC*H*), 2.79 (2 H, dd, J = 9.0, 6.6Hz, SCH*H*), 2.53 (1 H, sept, J = 6.6Hz, CH_2CH-$(CH_2S)_2$), 1.41-1.53 (4 H, m, CH_2), 1.35-1.41 (2 H, m, CH_2).^{13}C NMR (101 MHz, CD_2Cl_2) δ = 157.4 (C, CO), 138.2 (C, Ar), 129.6 (CH, Ar), 128.2 (CH, Ar), 126.4 (CH, Ar), 91.2 (C, Cp ring), 68.6 (CH, unsubstituted Cp ring), 67.7 (CH, Cp ring), 67.5 (CH, Cp ring), 67.0 (CH, Cp ring), 66.2 (CH, Cp ring), 50.6 (CH, CpCH), 47.7 (CH, SCH_2CH), 43.9 (CH_2, $NHCH_2CH_2$), 43.2 (CH_2, SCH_2), 40.3 (CH_2, $CpCHCH_2$), 33.5 (CH_2, $NHCH_2CH_2$/SCH_2CHCH_2), 30.4 (CH_2, $NHCH_2CH_2$/SCH_2CHCH_2), 25.8 (CH_2, $NHCH_2CH_2CH_2$); Electrospray MS analysis: Calc. for $C_{26}H_{32}FeN_2OS_2Na$: 531.1. Found: 531.2; HRMS analysis: Calc. for $C_{26}H_{32}FeN_2OS_2Na$: 531.1203. Found: 531.1203; %ee = 82%. Characterisation data is in agreement with the data for the other enantiomer, synthesised in the Moody group in Nottingham by Kevin Joly.

6.1.30 Synthesis of 2,2'-Bis-(methoxymethoxy)-(*R*)-binaphthyl 4.19[13]

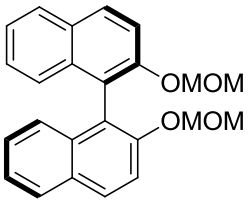

To a 250 mL round bottomed flask, (*R*)-Binol (4.0 g, 14 mmol), $CH_3OCH_2OCH_3$ (14.0 g, 184 mmol) and CH_2Cl_2 (100 mL) were added. P_2O_5 (16.6 g, 117 mmol) was then added to the reaction mixture in 5 portions. The mixture was then stirred for 1 hour, and the reaction was quenched with saturated aqueous Na_2CO_3 (100 mL). The organic layer was separated and the aqueous layer was extracted with CH_2Cl_2 (2x10 mL). The resulting organic fractions were combined, dried with anhydrous magnesium sulphate and concentrated under vacuum. The yellow oil obtained was purified by flash column chromatography on silica gel (9:1 EtOAc/hexane) to yield the product as a white solid (3.45 g, yield 66%). ^{1}H NMR (300 MHz, $CDCl_3$) δ = 7.95 (2 H, d, *J* = 8.9 Hz, Ar*H*), 7.87 (2 H, d, *J* = 8.2 Hz, Ar*H*), 7.58 (2 H, d, *J* = 9.0 Hz, Ar*H*), 7.34 (2 H, ddd, *J* = 8.2, 6.6, 1.4 Hz, Ar*H*), 7.25 – 7.19 (2 H, m, Ar*H*), 7.18 – 7.12 (2H, m, Ar*H*), 5.09 (2H, d, *J* = 6.8 Hz, OC*H*HO), 4.98 (2H, d, *J* = 6.8 Hz, OCH*HO*), 3.14 (6H, s, C*H*$_3$); ^{13}C NMR (101 MHz, $CDCl_3$) δ = 152.7 (C, Ar), 134.0 (C, Ar), 129.9 (C, Ar), 129.4 (CH, Ar), 127.9 (CH, Ar), 126.3 (CH, Ar), 125.6 (CH, Ar), 124.1 (CH, Ar), 121.3 (C, Ar), 117.3 (CH, Ar), 95.3 (CH_2), 55.8 (CH_3); Electrospray MS analysis: Calc. for $C_{24}H_{22}O_4Na$: 397.1. Found: 397.2. HRMS analysis: Calc. for $C_{24}H_{22}O_4Na$: 397.1416. Found: 397.1419. Characterisation data is in agreement with the literature data.[13]

6.1.31 Synthesis of 2,2'-Bis-(methoxymethoxy)-(*S*)-binaphthyl 4.19[13]

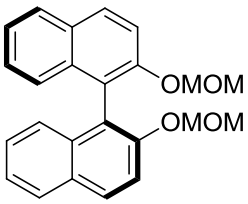

Obtained from (*S*)-Binol (4.0 g, 14 mmol), the crude was purified by flash column chromatography and a white solid was obtained (3.79 g, yield 73%). Characterisation data is in agreement with the literature

data,[13] and with data for the other enantiomer.

6.1.32 Synthesis of (*R*)-3,3'-Diformyl-2,2'-bis(methoxymethoxy)-1,1'-binaphthyl 4.20[13]

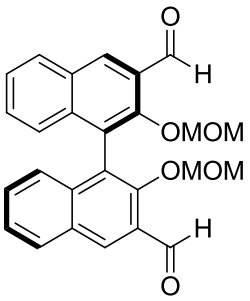

Under Argon, *n*-BuLi (2.5 M in hexanes, 12.0 mL, 30 mmol) was added to a solution of **(*R*)-4.19** (3.79 g, 10 mmol) in dry Et_2O (150 mL) at room temperature. The resulting mixture was stirred for 2 hours. While the reaction proceeded, a change in colour was observed, going from colourless to orange and then milky brown. The mixture was then cooled to 0 °C and DMF (3.1 mL, 40 mmol) was added. The solution turned almost immediately into a milky green colour, and was allowed to warm to room temperature, and then stirred for 4 hours, with obtainment of a white solution. Saturated NH_4Cl (70 mL) was then added to quench the reaction. The organic layer was separated, and the aqueous phase was extracted with EtOAc (3x20 mL). The organic phase was washed with H_2O and brine, and dried over anhydrous magnesium sulphate. The solution was concentrated with a rotary evaporator and purified by flash column chromatography on silica gel (4:1 hexane/EtOAc, Rf = 0.17) to yield the desired product (1.94 g, yield 45%). ^{1}H NMR (300 MHz, $CDCl_3$) δ = 10.55 (2 H, s, ArC*H*O), 8.62 (2 H, s, Ar*H*), 8.08 (2 H, dd, *J* = 8.2, 1.3 Hz, Ar*H*), 7.53 (2 H, ddd, *J* = 8.2, 6.8, 1.3 Hz, Ar*H*), 7.43 (2 H, ddd, *J* = 8.3, 6.8, 1.4 Hz, Ar*H*), 7.22 (2 H, d, *J* = 8.5 Hz, Ar*H*), 4.84 – 4.57 (4 H, m, OCH_2O), 2.87 (6 H, s, CH_3); ^{13}C NMR (101 MHz, $CDCl_3$) δ = 190.6 (CH, CHO), 154.1 (C, Ar), 136.7 (C, Ar), 132.3 (CH, Ar), 130.3 (CH, Ar), 130.1 (CH, Ar), 129.6 (CH, Ar), 128.9 (C, Ar), 126.3 (C, Ar), 126.1 (C, Ar), 125.9 (CH, Ar), 100.6 (CH_2), 57.0 (CH_3); Electrospray MS analysis: Calc. for $C_{26}H_{22}O_6Na$: 453. Found: 453. Characterisation data in agreement with the literature data.[13]

6.1.33 Synthesis of (*S*)-3,3'-Diformyl-2,2'-bis(methoxymethoxy)-1,1'-binaphthyl 4.20[13]

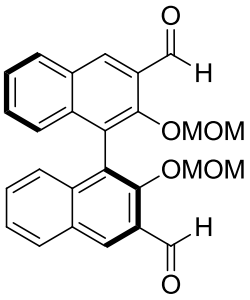

Obtained from **(*S*)-4.19** (3.45 g, 9.22 mmol), the crude was purified by flash column chromatography and a white solid was obtained (3.69 g, yield 93%). Characterisation data is in agreement with the literature data,[13] and with data for the other enantiomer.

6.1.34 Synthesis of (*R*)-3,3'-Diformyl-2,2'-dihydroxy-1,1'-binaphthyl 4.1[13]

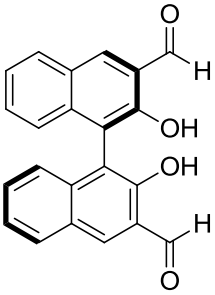

(*R*)-4.20 was dissolved in a minimum amount of CH_2Cl_2, EtOH (50 mL) and HCl (6 M, 50 mL) were added successively, and the mixture was heated under reflux for about 10 hours. The resulting yellow solution was concentrated using a rotary evaporator. Water (100 mL) was then added, and the solution was extracted with CH_2Cl_2 (3x100 mL). The combined organic fractions were dried over anhydrous sodium sulphate. After removal of the solvent, the residue was purified by flash column chromatography on silica gel (CH_2Cl_2) to yield the product as a bright yellow powder (1.30 g, yield 93%). $[\alpha]_D^{21}$ = -197.2 (*c* 1.00, chloroform); ^{1}H NMR (300 MHz, $CDCl_3$) δ = 10.59 (2 H, s, ArC*H*O), 10.19 (2 H, s, ArO*H*), 8.35 (2 H, s, Ar*H*), 8.01 – 7.98 (2 H, m, Ar*H*), 7.49 – 7.34 (4 H, m, Ar*H*), 7.24 – 7.15 (2 H, m, Ar*H*); ^{13}C NMR (101 MHz, $CDCl_3$) δ = 196.8 (CH, CHO), 153.7 (C, Ar), 138.5 (CH, Ar), 137.4 (C, Ar), 130.7 (CH, Ar), 130.0 (CH, Ar), 127.7 (C, Ar), 124.9 (CH, Ar), 124.5 (CH, Ar), 122.1 (C, Ar), 116.5 (C, Ar); Electrospray MS analysis: Calc. for $C_{22}H_{14}O_4Na$: 365.1. Found: 365.0. Characterisation data is in agreement with the literature data.[13]

6.1.35 Synthesis of (*S*)-3,3'-Diformyl-2,2'-dihydroxy-1,1'-binaphthyl 4.1[13]

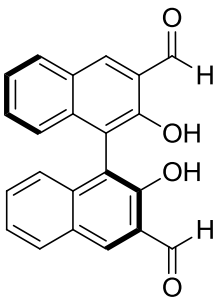

Obtained from **(*S*)-4.20** (3.69 mg, 8.57 mmol), the crude was purified by flash column chromatography and a bright yellow solid was obtained (1.04 g, yield 39%). $[\alpha]_D^{21}$ =197.6 (*c* 1.00, chloroform); Electrospray MS analysis: Calc. for $C_{22}H_{14}O_4Na$: 365.1. Found: 365.0. Characterisation data is in agreement with the literature data,[13] and with data for the other enantiomer.

6.1.36 General procedure for the synthesis of binol receptors D[14-15]

4.1 (0.22 mmol) was dissolved in dry CH_2Cl_2 (20 mL) in the presence of 4 Å molecular sieves, and combined with ferrocenylamine (0.66 mmol). The reaction mixture was heated at reflux overnight. The solution was cooled to room temperature and filtered. The filtrate was concentrated under vacuum to give the corresponding crude Schiff base. This was then dissolved in a mixture of dry CH_2Cl_2 (5 mL) and MeOH (anhydrous, 10 mL) and cooled to 0 °C. $NaBH_4$ (0.66 mmol) was added in small portions. The reaction mixture was allowed to proceed at room temperature for 2 hours and 30 minutes. The solvent was removed, and the residue was dissolved in CH_2Cl_2 (30 mL) and HCl (0.2 M, 30 mL). After stirring for 1 hour, the organic layer was separated and washed with 0.5 M NaOH aqueous solution (15 mL), water (15 mL) and brine (15 mL) and dried over anhydrous magnesium sulphate. After evaporation of the solvent the desired product was obtained as a light brown solid.

6.1.37 Synthesis of achiral (*R*)-binol receptor 4.8

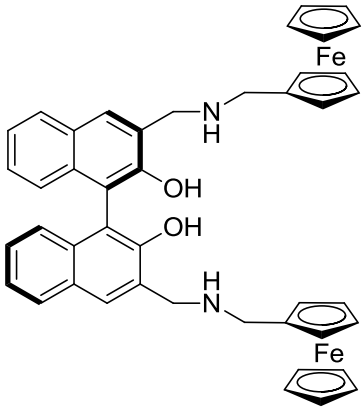

Obtained using general procedure **D** from **(*R*)-4.1** (69 mg, 0.22 mmol) and **2.12** (142 mg, 0.66 mmmol), the desired product was obtained as a light brown solid (147 mg, yield 90%). Mp 126–128 °C; IR (neat)/cm^{-1} 3316, 3080, 2920, 2850, 1626, 1505, 1424, 1375, 1353, 1314, 1251, 1148, 1105, 1022, 931, 905, 885, 814, 777, 747, 693; ^{1}H NMR (300 MHz, $CDCl_3$) δ = 7.79 (2 H, d, *J* = 7.7 Hz, Ar*H*), 7.66 (2 H, s, Ar*H*), 7.30 – 7.26 (2 H, m, Ar*H*), 7.22 – 7.19 (4 H, m, Ar*H*), 5.30 (2 H, s, ArO*H*) 4.24 (4 H, d, *J* = 6.8 Hz, -CH_2), 4.14 (4 H, d, *J* = 1.8 Hz, *H* of substituted Cp ring), 4.10 (4 H, t, *J* = 1.9 Hz, *H* of substituted Cp ring), 4.09 (10 H, s, *H* of unsubstituted Cp ring), 3.58 (4 H, s, -CH_2); ^{13}C NMR (101 MHz, $CDCl_3$) δ = 154.0 (C, Ar), 133.9 (C, Ar), 128.2 (C, Ar), 127.7 (CH, Ar, HO-CCCCH*C*H), 126.0 (CH, Ar), 125.0 (C, Ar), 124.9 (CH, Ar), 122.9 (CH, Ar), 116.7 (C, Ar), 84.9 (C, Cp ring), 68.6 (CH, Cp ring), 68.5 (CH, unsubstituted Cp ring), 68.1 (CH, Cp ring), 52.4 (CH_2, Cp*C*H_2), 47.5 (CH_2, Ar*C*H_2); Electrospray MS analysis: Calc. for $C_{44}H_{40}Fe_2N_2O_2K$: 779.1. Found: 779.3; $C_{44}H_{40}Fe_2N_2O_2Na$: 763.2. Found: 763.2; $C_{44}H_{41}Fe_2N_2O_2$: 741.2. Found: 741.2. HRMS analysis: Calc. for $C_{44}H_{40}Fe_2N_2O_2Na$: 763.1702. Found: 763.1686. Analytical reversed phase C18-HPLC (water/MeCN method, flow Rate 1.0 mL/min, monitoring at 210 nm): ret. time 25.4 mins; %ee = 83%.

6.1.38 Synthesis of achiral-(*S*)-binol receptor 4.9

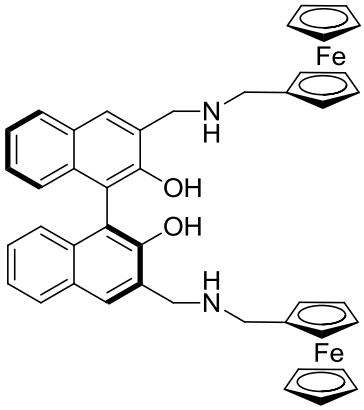

Obtained using general procedure **D** from **(*S*)-4.1** (69 mg, 0.22 mmol) and **2.12** (142 mg, 0.66 mmmol), the desired product was obtained as a light brown solid (140 mg, yield 86%). Mp 124–126 °C; Electrospray MS analysis: Calc. for $C_{44}H_{41}Fe_2N_2O_2$: 741.2. Found: 741.2. HRMS analysis: Calc. for $C_{44}H_{41}Fe_2N_2O_2$: 741.1867. Found: 741.1869. Characterisation data is in agreement with data for the other enantiomer. Analytical reversed phase C18-HPLC (water/MeCN method, flow Rate 1.0 mL/min, monitoring at 210 nm): ret. time 25.4 mins; %ee = 99%.

6.1.39 Synthesis of planar chiral (*RR*)-methyl-(*R*)-binol receptor 4.10

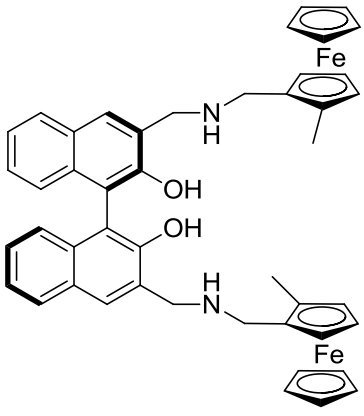

Obtained using general procedure **D** from **(*R*)-4.1** (64 mg, 0.2 mmol) and **2.17** (142 mg, 0.62 mmmol), the desired product was obtained as a light brown solid (147 mg, yield 96%). Mp 138–140 °C with decomposition; IR (neat)/cm^{-1} 3312, 3076, 2911, 2844, 1626, 1505, 1425, 1376, 1353, 1313, 1251, 1149, 1105, 1077, 1031, 999, 947, 933, 883, 805, 778, 747, 694; ^{1}H NMR (300 MHz, $CDCl_3$) δ = 7.77 (2 H, d, *J* = 7.7 Hz, Ar*H*), 7.65 (2 H, s, Ar*H*), 7.29 – 7.24 (2 H, m, Ar*H*), 7.21 – 7.18 (4 H, m, Ar*H*), 5.30 (2 H, s, ArO*H*), 4.30 – 4.21 (4 H, m, -C*H*$_2$), 4.06 (4 H, t, *J* = 2.6 Hz, *H* of substituted Cp ring), 4.00 (10 H, s, *H* of unsubstituted Cp ring), 3.97 (2 H, t, *J* = 2.4 Hz, *H* of substituted Cp ring), 3.73 (2 H, d, *J* = 13.2 Hz, -C*H*H), 3.58 (2 H, d, *J* = 13.2 Hz, -

CH*H*), 1.95 (6 H, s, FcC*H*$_3$); ^{13}C NMR (101 MHz, $CDCl_3$) δ = 154.0 (C, Ar), 134.0 (C, Ar), 128.2 (C, Ar), 127.7 (CH, Ar, HO-CCCCH*C*H), 126.0 (CH, Ar), 125.1 (C, Ar), 124.9 (CH, Ar), 122.9 (CH, Ar), 116.8 (C, Ar), 83.4 (C, Cp ring), 69.8 (CH, Cp ring), 69.1 (CH, unsubstituted Cp ring), 68.4 (CH, Cp ring), 65.9 (CH, Cp ring), 52.7(CH_2, Cp*C*H_2), 46.3 (CH_2, Ar*C*H_2), 13.2 (CH_3); Electrospray MS analysis: Calc. for $C_{46}H_{45}Fe_2N_2O_2$: 769.2. Found: 769.3. HRMS analysis: Calc. for $C_{46}H_{45}Fe_2N_2O_2$: 769.2180. Found: 763.2184. Analytical reversed phase C18-HPLC (water/MeCN method, flow Rate 1.0 mL/min, monitoring at 210 nm): ret. time 26.5 mins; %de = 89%.

6.1.40 Synthesis of planar chiral (*RR*)-methyl-(*S*)-binol receptor 4.11

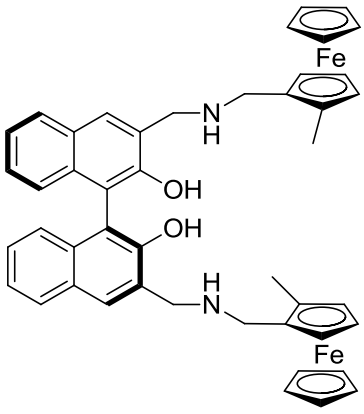

Obtained using general procedure **D** from **(*S*)-4.1** (121 mg, 0.39 mmol) and **2.17** (262 mg, 0.96 mmmol), the desired product was obtained as a light brown solid (255 mg, yield 85%). Mp 136–138 °C with decomposition; Electrospray MS analysis: Calc. for $C_{46}H_{45}Fe_2N_2O_2$: 769.2. Found: 769.4. HRMS analysis: Calc. for $C_{46}H_{45}Fe_2N_2O_2$: 769.2180. Found: 763.2182. Characterisation data is in agreement with data for the other diastereoisomer. Analytical reversed phase C18-HPLC (water/MeCN method, flow Rate 1.0 mL/min, monitoring at 210 nm): ret. time 26.6 mins; %de = 99%.

6.1.41 Synthesis of central chiral (*RR*)-benzyl-(*R*)-binol receptor 4.12

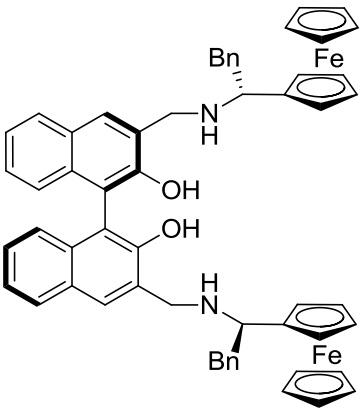

Obtained using general procedure **D** from **(*R*)-4.1** (23 mg, 0.075 mmol) and **2.19** (69 mg, 0.226 mmmol), the desired product was obtained as a light brown solid after purification through semi-prep reversed phase C18-HPLC with water/MeCN method (0-10 mins 90% MeCN – 95% MeCN; 10-20 mins, 100% MeCN; 20-25 mins, 90% MeCN) with flow rate 1.0 mL/min and monitoring at 220 nm (ret. time 15 mins) (60 mg, yield 87%). Mp 112–114 °C; IR (neat)/cm^{-1} 3026, 2922, 2850, 1627, 1602, 1496, 1428, 1375, 1354, 1311, 1251, 1149, 1106, 1028, 999, 933, 885, 818, 778, 746, 698; ^{1}H NMR (300 MHz, $CDCl_3$) δ = 7.75 (2 H, d, *J* = 7.8 Hz, Ar*H*), 7.59 (2 H, s, Ar*H*), 7.23 – 7.03 (16 H, m, Ar*H*), 4.26 (2 H, d, *J* = 13.6 Hz, $ArCH_2NH$), 4.21 – 4.04 (18 H, m, Fc*H*), 3.98 (2 H, s, ArO*H*), 3.78 (2 H, dd, *J* = 7.8, 5.5 Hz, $FcCHCH_2$), 3.29 – 2.89 (4 H, m, -CH_2), 1.99 (4 H, s, -CH_2); ^{13}C NMR (101 MHz, $CDCl_3$) δ = 153.6 (C, Ar), 138.5 (C, Ar), 133.8 (C, Ar), 129.3 (CH, Ar), 128.5 (CH, Ar), 128.2 (C, Ar), 127.6 (CH, Ar), 127.5 (CH, Ar), 126.4 (CH, Ar), 125.9 (CH, Ar), 125.8 (C, Ar), 124.9 (CH, Ar), 122.9 (CH, Ar), 116.5 (C, Ar), 90.4 (C, Cp ring), 68.6 (CH, unsubstituted Cp ring), 67.5 (CH, Cp ring), 67.1 (CH, Cp ring), 67.0 (CH, Cp ring), 58.1 (CH, Cp*C*H), 50.6 (CH_2, Ar*C*H_2), 42.1 (CH_2, CpCH*C*H_2); Electrospray MS analysis: Calc. for $C_{58}H_{53}Fe_2N_2O_2$: 921.3. Found: 921.4. HRMS analysis: Calc. for $C_{58}H_{53}Fe_2N_2O_2$: 921.2806. Found: 921.2776. Analytical reversed phase C18-HPLC (water/MeCN method, flow Rate 1.0 mL/min, monitoring at 210 nm): ret. time 47.7 mins; %de = 68%.

6.1.42 Synthesis of central chiral (*SS*)-benzyl-(*S*)-binol receptor 4.13

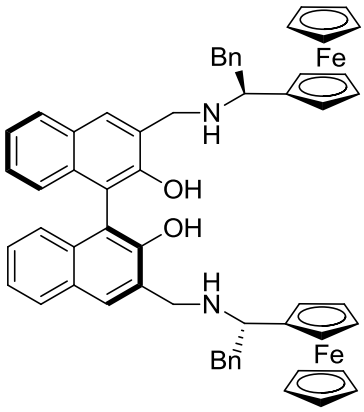

Obtained using general procedure **D** from **(*S*)-4.1** (16 mg, 0.052 mmol) and **3.13** (48 mg, 0.157 mmmol), the desired product was obtained as a light brown solid after purification through semi-prep reversed phase C18-HPLC with water/MeCN method (0-10 mins 90% MeCN – 95% MeCN; 10-20 mins, 100% MeCN; 20-25 mins, 90% MeCN) with flow rate 1.0 mL/min and monitoring at 220 nm (ret. time 15 mins) (42 mg, yield 87%). Mp 112–116 °C; Electrospray MS analysis: Calc. for $C_{58}H_{53}Fe_2N_2O_2$: 921.3. Found: 921.2. HRMS analysis: Calc. for $C_{58}H_{53}Fe_2N_2O_2$: 921.2806. Found: 921.2804. Characterisation data is in agreement with data for the other enantiomer. Analytical reversed phase C18-HPLC (water/MeCN method, flow Rate 1.0 mL/min, monitoring at 210 nm): ret. time 47.8 mins; %de = 64%.

6.1.43 Synthesis of central chiral (*SS*)-benzyl-(*R*)-binol receptor 4.15

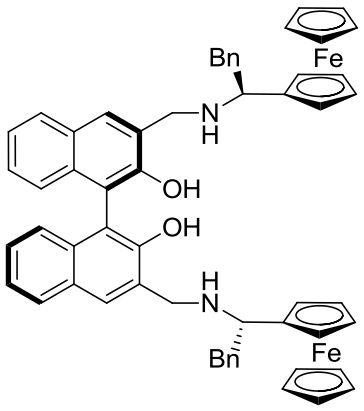

Obtained using general procedure **D** from **(*R*)-4.1** (15 mg, 0.047 mmol) and **3.13** (43 mg, 0.141 mmmol), the desired product was obtained as a light brown solid after purification through semi-prep reversed phase C18-HPLC with water/MeCN method (0-10 mins 90% MeCN – 95% MeCN; 10-20 mins, 100% MeCN; 20-25 mins, 90% MeCN) with flow rate 1.0 mL/min and monitoring at 220 nm (ret. time 15 mins) (35 mg, yield 82%). Mp 114–116 °C; ^{1}H NMR (300 MHz, $CDCl_3$) δ = 7.74 (2 H, d, *J* = 7.7 Hz, Ar*H*), 7.56 (2 H, s, Ar*H*), 7.26 – 7.05

(16 H, m, Ar*H*), 4.18 (6 H, m, $ArCH_2N$*H,* Fc*H*), 4.13 – 4.04 (14 H, m, Fc*H*), 4.04 – 3.92 (2 H, m, ArO*H*), 3.79 (2 H, dd, *J* = 7.9, 5.5 Hz, FcC*H*CH_2), 3.27 – 2.96 (4 H, m, -C*H*$_2$), 1.99 (4 H, s, -C*H*$_2$); ^{13}C NMR (75 MHz, $CDCl_3$) δ = 151.6 (C, Ar), 136.7 (C, Ar), 131.8 (C, Ar), 127.4 (CH, Ar), 126.6 (CH, Ar), 126.3 (C, Ar), 125.7 (CH, Ar), 125.6 (CH, Ar), 124.5 (CH, Ar), 123.9 (CH, Ar), 123.1 (C, Ar), 122.3 (CH, Ar), 120.9 (CH, Ar), 114.6 (C, Ar), 88.7 (C, Cp ring), 66.6 (CH, unsubstituted Cp ring), 65.7 (CH, Cp ring), 65.7 (CH, Cp ring), 65.2 (CH, Cp ring), 56.5 (CH, Cp*C*H), 48.9 (CH_2, Ar*C*H_2), 40.1 (CH_2, CpCH*C*H_2); Electrospray MS analysis: Calc. for $C_{58}H_{52}Fe_2N_2O_2Na$: 943.3. Found: 943.3; Calc. for $C_{58}H_{53}Fe_2N_2O_2$: 921.3. Found: 921.3. HRMS analysis: Calc. for $C_{58}H_{53}Fe_2N_2O_2$: 921.2806. Found: 921.2803. Characterisation data is in agreement with data for the other diastereoisomers. Analytical reversed phase C18-HPLC (water/MeCN method, flow Rate 1.0 mL/min, monitoring at 210 nm): ret. time 47.8 mins; %de = 64%.

6.1.44 Synthesis of central chiral (*RR*)-benzyl-(*S*)-binol receptor 4.14

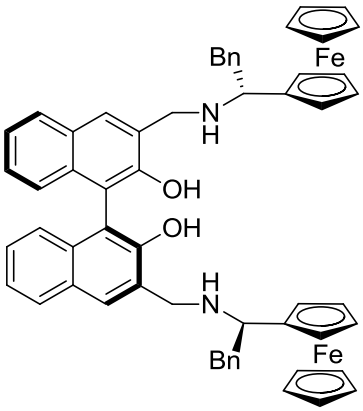

Obtained using general procedure **D** from **(*S*)-4.1** (23 mg, 0.075 mmol) and **2.19** (69 mg, 0.226 mmmol), the desired product was obtained as a light brown solid after purification through semi-prep reversed phase C18-HPLC with water/MeCN method (0-10 mins 90% MeCN – 95% MeCN; 10-20 mins, 100% MeCN; 20-25 mins, 90% MeCN) with flow rate 1.0 mL/min and monitoring at 220 nm (ret. time 15 mins) (59 mg, yield 85%). Mp 110–114 °C; Electrospray MS analysis: Calc. for $C_{58}H_{53}Fe_2N_2O_2$: 921.3. Found: 921.4. HRMS analysis: Calc. for $C_{58}H_{53}Fe_2N_2O_2$: 921.2806. Found: 921.2790. Characterisation data is in agreement with data

for the other enantiomer. Analytical reversed phase C18-HPLC (water/MeCN method, flow Rate 1.0 mL/min, monitoring at 210 nm): ret. time 47.8 mins; %de = 69%.

6.1.45 Synthesis of the TBA carboxylate salts of 2.3-2.5[9]

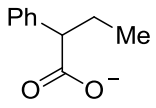

2.3

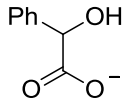

2.4

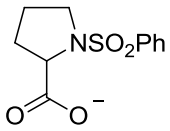

2.5

The carboxylic acid (6 mmol) was dissolved in methanol (6 mL) and tetrabutylammonium hydroxide (1M in MeOH, 6mmol) was added. The solution was stirred overnight at room temperature. The solvent was removed and the residue dried under high vacuum. The salt was crystallized after washing with Et_2O, leaving in the fridge overnight and then under high vacuum the whole day. ^{1}H NMR of **2.3** (300 MHz, $CDCl_3$) δ = 7.49 (2 H, d, *J* = 7.0 Hz, Ar*H*), 7.20 (2 H, t, *J* = 7.4 Hz, Ar*H*), 7.09 (1 H, t, *J* = 7.3 Hz, Ar*H*), 3.38 – 3.27 (1 H, m, C*H*COO$^-$), 3.23 – 3.04 (8 H, m, TBA CH_2), 2.21 – 2.06 (1H, m, CH_3C*H*H), 1.80 – 1.62 (1 H, m, CH_3C*H*H), 1.59 – 1.43 (8 H, m, TBA CH_2), 1.41 – 1.27 (8 H, m, TBA CH_2), 1.05 – 0.86 (15 H, m, CH_3, TBA CH_3). ^{1}H NMR of **2.4** (300 MHz, $CDCl_3$) δ = 7.54 (2 H, d, *J* = 7.2 Hz, Ar*H*), 7.22 (2 H, t, *J* = 7.3 Hz, Ar*H*), 7.13 (1 H, t, *J* = 7.2 Hz, Ar*H*), 4.80 (1 H, s, O*H*), 3.38 (1 H, s, C*H*COO$^-$), 3.20 – 3.04 (8 H, m, TBA CH_2), 1.59 – 1.41 (8 H, m, TBA CH_2), 1.44 – 1.26 (8 H, m, TBA CH_2), 0.95 (12 H, t, *J* = 7.2 Hz, TBA CH_3). ^{1}H NMR of **2.5** (300 MHz, $CDCl_3$) δ = 7.92 (2 H, d, *J* = 6.7 Hz, Ar*H*), 7.64 – 7.44 (3 H, m, Ar*H*), 4.19 (1 H, dd, *J* = 8.6, 3.6 Hz, C*H*COO$^-$), 3.61 – 3.50 (2 H, m, CH_2CHCOO$^-$), 3.41 – 3.30 (8 H, m, TBA CH_2), 3.24 – 3.14 (2 H, m, NCH$_2$CH_2), 2.22 – 1.89 (2 H, m, NCH_2), 1.79 – 1.62 (8 H, m, TBA CH_2), 1.59 – 1.37 (8 H, m, TBA CH_2), 1.02 (12 H, t, *J* = 7.3 Hz, TBA CH_3).

6.2 UV-Vis Studies

UV-Vis measurements were performed using a Cary 5000 spectrophotometer or a Shimadzu UV-1800 spectrophotometer. The receptor (0.025 mM) was titrated with a solution of the guest (6.25 mM) dissolved in the stock solution of the host, to avoid dilution effects. In each titration, the change in absorption intensity was monitored at different wavelengths (between 350 and 410 nm). Binding constants are determined using the Benesi-Hildebrand method.[16] In each titration in DMSO the absorption change is monitored between 365 and 410 nm, and the value of 1/(ΔA) is plotted against the value of 1/[guest], giving a value of the binding constant (presented as log*K*) obtained from the division of the intercept by the gradient, at a specific wavelength. The binding constant was calculated as the average of the ten values obtained from the plots in the wavelengths range, a plot every 5 nm. Each titration was repeated at least once and the experimental error was estimated on the range of log*K* values obtained from the different titrations.

6.3 NMR Studies

6.3.1 ^{1}H NMR Titrations

NMR measurements were performed at 300 MHz on a Bruker AVIII300 NMR spectrometer and at 400 MHz on a Bruker AV400 NMR spectrometer. The receptor (5 mM) was titrated with a solution of the guest (50 mM) dissolved in the stock solution of the host, to avoid dilution effects. After each addition of guest solution, a ^{1}H NMR spectrum was recorded and signals corresponding to the urea protons were noted. The binding constant values, *K*, were determined from the titrations data, using the WinEqNMR software.[17-18]

6.3.2 ^{1}H NMR Job plots[19-20]

Solutions of the host and the guest were prepared (5 mM) in CD_2Cl_2. These solutions were then combined with the following host:guest ratio (in µl): 500:0, 450:50, 400:100, 350:150, 300:200, 250:250, 200:300, 150:350, 100:400 and 50:450. A ^{1}H NMR experiment was recorded of each resulting solution, and shift of significant peaks upon complexation was observed. The concentration of the complex formed was calculated using the data obtained through Equation 6.1 and then plotted against the mole fraction of host.

$$[complex]_{n:500-n} = [H]_{n:500-n}\left(\frac{\delta_{obs}-\delta_0}{\delta_{comp}-\delta_0}\right) \qquad \textbf{Equation 6.1}$$

where:

n = volume of host (µl)

[*H*] = concentration of host in solution (mM)

δ_{obs} = observed shift of the proton resonance monitored

δ_0 = shift of the proton resonance observed for the host in absence of substrate

δ_{comp} = shift of the proton resonance observed for the host upon full complexation

6.4 Electrochemical Studies

6.4.1 Studies on receptors in solution

Electrochemical studies were performed on a BAS 100W electrochemical analyser, with BAS 100W software. All measurements were carried out at 298 K in dry CH_3CN or dry CH_2Cl_2, in which was dissolved tetrabutylammomiun hexafluorophosphate as supporting electrolyte (0.1 M). A conventional 3-electrode system was employed. The working electrode (WE) was

a platinum disc electrode (diameter: 1.6 mm). Silver/silver chloride (Ag|AgCl) was used as an external reference electrode and a platinum wire was used as auxiliary electrode. Decamethylferrocene, dmfc (0.2-0.8 mM) was used as an internal reference and its redox couple was unaffected by the addition of guests. All cyclic voltammograms were carried out at a scan rate of 100 mV s^{-1} unless otherwise stated. All square wave voltammograms were carried out using a step of 1 mV, with a pulse amplitude of 25 mV and a frequency of 15 Hz. The cells and the volumetric flasks used were cleaned using a 1:1 solution of ammonia and hydrogen peroxide, rinsed 10 times using MilliQ® water, purified with a Millipore Elix-Gradient A10 system (18 MΩ cm, toc ≤ 5 ppb, Millipore, France), and dried in the oven overnight. Prior to use, the platinum electrode was polished by hand using an eight pattern on aqueous slurries of 0.05 µm alumina powder pads and then thoroughly rinsed in deionised water followed by MeOH and drying in a directed stream of nitrogen. To check the electrochemical reversibility of the host, voltammetric cycles were performed at different scan rates (100, 300, 500, 700 and 1000 mV^{-1}) between -250 and 700 mV (vs. Ag/AgCl) with plots of anodic peak current versus the square root of the scan rate, giving a straight line. Formal potentials of each receptor, $E^{o\prime}$, where $E^{o\prime} = (E_p^a + E_p^c)/2$, were independent of scan rate. The receptor (0.5 mM) was titrated with aliquots from a solution of guest (0.05 M) and the shift in the ferrocene-centred redox wave of the receptor monitored. Additions were continued until no further shifts were observed to indicate that the receptor was fully complexed. Control studies in the absence of the receptors revealed that the guests showed no redox activity in regions where complexation-induced shifts in potential were observed. Titrations were also used to determine any chiral sensing effects. The observed shift in

electrode potential was evaluated for the addition of each aliquot of enantiomers and plotted against molar equivalents of guest.

6.4.2 Studies on receptors on SAMs

Electrochemical studies were performed on a BAS 100W electrochemical analyser, with BAS 100W software. All measurements were carried out at 298 K in dry CH_2Cl_2, in which tetrabutylammomiun hexafluorophosphate ($TBAPF_6$) was dissolved as a supporting electrolyte (0.1 M). A conventional 3-electrode system was employed. The working electrode (WE) was a gold disc electrode from Bioanalitical Systems. Inc. (diameter: 1.6 mm). Silver/silver chloride (Ag/AgCl) was used as an external reference electrode and a platinum wire was used as auxiliary electrode. Decamethylferrocene, dmfc (in a concentration comparable to the concentration of the analyte) was used as an internal reference and its redox couple was unaffected by the addition of carboxylate salts. All cyclic voltammograms were carried out at a scan rate of 500 mV s^{-1} unless otherwise stated. All square wave voltammograms were measured using a step of 1 mV, with a pulse amplitude of 25 mV and a frequency of 15 Hz. The cells and the volumetric flasks used were cleaned using a 1:1 solution of ammonia and hydrogen peroxide, rinsed 10 times using MilliQ® water, purified with a Millipore Elix-Gradient A10 system (18 MΩ cm, toc ≤ 5 ppb, Millipore, France), and dried in the oven overnight. Prior to use, the gold electrode was polished by hand using an eight pattern on an abrasive microcloth pad, then a 3 μm diamond solution on a nylon pad, then aqueous slurries of 0.05 μm alumina powder pads and then thoroughly rinsed in MilliQ® water followed by an electrochemically polishing, running different scans (*ca.* 20) in

a 0.1 M sulfuric acid solution. To check the electrochemical reversibility of the host, voltammetric cycles were performed at different scan rates (100, 300, 500, 700 and 1000 mV^{-1}) between -250 and 700 mV (vs. Ag|AgCl) with plots of anodic peak current versus the scan rate, giving a straight line. Formal potentials of each receptor, $E^{o\prime}$, where $E^{o\prime} = (E_p^a + E_p^c)/2$, were independent of scan rate. The SAMs were obtained soaking the electrode in a 1.5 mM solution of the receptor, for a variable time of 5 minutes for the achiral receptor, 30 minutes for the planar chiral receptors and 2 hours for the central chiral receptors. Mixed monolayers were prepared by soaking the electrode in a 1.5 mM solution of hexanethiol overnight, washing the electrode with dry CH_2Cl_2 and then soaking it for a variable time of 5 minutes for the achiral receptor, 20 minutes for the planar chiral receptor and 30 minutes for the central chiral receptors.

6.4.3 Studies on DNA analogues

The cyclic voltammograms were recorded using a 3-electrode cell consisting of a gold working electrode of 1.6 mm diameter, a platinum wire as auxiliary electrode and an Ag|AgCl reference electrode. All potentials were quoted versus Ag|AgCl. The working electrode was immersed in 100 μL of a 0.1 mM solution of $FcTT_8$ in buffer (10 mM phosphate, 100 mM NaCl, pH 7.0), which was separated from the electrolyte solution of the same buffer with a glass holder terminating in a glass frit. Solutions were saturated with argon before measurements. Glassware and cells were cleaned prior to use with a 1:1 mixture of ammonia and hydrogen peroxide solution, followed by rinsing with copious quantities of ultrapure water and dried in the oven overnight. Ultrapure water, purified with

a Millipore Elix-Gradient A10 system (18 MΩ cm, toc ≤ 5 ppb, Millipore, France) was used throughout. The working electrode was cleaned by mechanical polishing with aqueous slurries of successively finer grades of alumina, followed by potential cycling running different scans (*ca.* 20) in a 0.1 M sulfuric acid solution. Measurements were carried out with a BioAnalytical Systems Inc. (BASi) EC epsilon potentiostat. The voltammograms were recorded at different scan rates, varying from 10 mV s^{-1} to 200 mV s^{-1}.

6.5 AFM Studies

AFM studies were performed using an Agilent Technologies scanning probe microscope with video access for Picoplus PicoSPM II. The same plates of approximately 1 cm^2 area of 100 nm thick gold on a silicon wafer used for the ellipsometry experiments were immersed in the same way in a 1.5 mM solution of each of the receptors for the same time as in the previous studies. The cantilevers were cleaned by thorough washing with EtOH and by treatment with UV/ozone. AFM images were then recorded using contact AFM. The set-point was chosen at 0.8 V. 10 µm x 10 µm images were recorded.

6.6 Ellipsometry

Ellipsometry studies were performed on a Jobin Yvon Horiba UVISEL FUV200 ellipsometer and data was treated using DeltaPsi 2 software. A plate of approximately 1 cm^2 area of 100 nm thick gold on silicon wafer was washed with EtOH, dried with a stream of nitrogen and cleaned by treatment with UV/ozone, and then immersed in a 1.5 mM solution of each of the receptors for the same time as for the functionalisation of the gold electrode used in the

electrochemical studies. A model included in the software was used, to take into account the nature of the substrate used, the tethering group and the presence of functional groups such as ferrocene. Before the experiments, measurement of the thickness of the blank gold plates was carried out. The values were then subtracted from the observed thickness by the software, to obtain the thickness of the monolayer

6.7 Fluorescence Studies

Fluorescence studies were performed using a Horiba Fluorolog-3 Model FL3-22 spectrofluorometer (double-grating excitation and double-grating emission monochromators). The wavelength of excitation was 340 nm. The excitation slit was set at 4.0 nm and the emission slit at 4.0 nm, unless otherwise stated. The scan speed was set at 1.0 nm s^{-1}. Spectra were recorded between 360 nm to 550 nm, after subtracting the solvent background signal and noise signals. The stock solutions of the sensors were freshly prepared for each measurement. Host solutions were prepared in 1.0 x 10^{-5} M concentration in toluene with 0.03% or 1% of DME (dimethoxyethane), toluene/THF 2% or in CH_2Cl_2. For the fluorescence enhancement studies, a receptor solution was mixed with the guest solution at room temperature in a 5 mL volumetric flask and diluted to the desired concentration.

6.8 References

1. Perin, D. D.; Armarego, W. L. F., *Purification of Laboratory Chemicals*. Oxford: **1989**.
2. Huikai, S.; Qingmin, W.; Runqiu, H.; Heng, L.; Yonghong, L., *J. Organomet. Chem.* **2002,** *655*, 182-185.
3. Beer, P. D.; Smith, D. K., *J. Chem. Soc. Dalton Trans.* **1998**, 417-423.
4. Kraatz, H. B., *J. Organomet. Chem.* **1999,** *579*, 222-226.
5. Riant, O.; Samuel, O.; Flessner, T.; Taudien, S.; Kagan, H. B., *J. Org. Chem.* **1997,** *62*, 6733-6745.
6. Sokolov, V. I.; Troitskaya, L. L.; Reutov, O. A., *J. Organomet. Chem.* **1979,** *182*, 537-546.
7. Moody, C. J.; Lightfoot, A. P.; Gallagher, P. T., *J. Org. Chem.* **1997,** *62*, 746-748.
8. Laurent, P.; Miyaji, H.; Collinson, S. R.; Prokes, I.; Moody, C. J.; Tucker, J. H. R.; Slawin, A. M. Z., *Org. Lett.* **2002,** *4*, 4037-4040.
9. Willener, Y.; Joly, K. M.; Moody, C. J.; Tucker, J. H. R., *J. Org. Chem.* **2008,** *73*, 1225-1233.
10. Miyaji, H.; Collinson, S. R.; Prokes, I.; Tucker, J. H. R., *Chem. Commun* **2003**, 64-65.
11. Lorenzo, A.; Aller, E.; Molina, P., *Tetrahedron* **2009,** *65*, 1397-1401.
12. Joly, K. M.; Mirri, G.; Willener, Y.; Horswell, S. L.; Moody, C. J.; Tucker, J. H. R., *J. Org. Chem.* **2010,** *75*, 2395-2398.
13. Zhang, H. C.; Huang, W. S.; Pu, L., *J. Org. Chem.* **2001,** *66*, 481-487.
14. Lin, J.; Rajararn, A. R.; Pu, L., *Tetrahedron* **2004,** *60*, 11277-11281.
15. Yu, S. S.; DeBerardinis, A. M.; Turlington, M.; Pu, L., *J. Org. Chem.* **2011,** *76*, 2814-2819.
16. Benesi, H. A.; Hildebrand, J. H., *J. Am. Chem. Soc.* **1949,** *71*, 2703-2707.
17. Hynes, M. J., *J. Chem. Soc. Dalton Trans.* **1993**, 311-312.
18. Molard, Y.; Bassani, D. M.; Desvergne, J. P.; Moran, N.; Tucker, J. H. R., *J. Org. Chem.* **2006,** *71*, 8523-8531.
19. Huang, C. Y., *Methods Enzymol.* **1982,** *87*, 509-525.
20. Job, P., *Ann Chim.* **1928,** *9*, 113-203.

APPENDIX

Table 1: Crystal data and structure refinement for receptor **2.6.**

Empirical formula	$C_{37}\ H_{36}\ Fe_2\ N_2\ O,\ H_2O$
Formula weight	654.39
Temperature	120 K
Wavelength	0.71073 Å
Crystal system	Orthorhombic
Space group	P 2(1) 2(1) 2(1)
Unit cell dimensions	a = 6.2750 Å α= 90°
	b = 19.7316 Å β= 90°
	c = 24.4396 Å γ = 90°
Volume	3026.01 $Å^3$
Z	4
Density (calculated)	1.436 mg/m^3
Absorption coefficient	0.996 mm^{-1}
F(000)	1368
Crystal size	0.24 x 0.04 x 0.02 mm^3
Theta range for data collection	3.21 to 25.02°
Index ranges	-7<=h<=7, -19<=k<=23, -29<=l<=29
Reflections collected	26247
Independent reflections	5342 [R(int) = 0.0912]
Completeness to theta = 25.02°	99.8%
Absorption correction	Semi-empirical from equivalents
Max. and min. transmission	0.9804 and 0.7960
Refinement method	Full-matrix least-squares on F2
Data / restraints / parameters	5342 / 83 / 394
Goodness-of-fit on F2	1.043
Final R indices [I>2sigma(I)]	R1 = 0.0499, wR2 = 0.0736
R indices (all data)	R1 = 0.0752, wR2 = 0.0792
Absolute structure parameter	0.050
Largest diff. peak and hole	0.372 and -0.305 Å

Table 2: Crystal data and structure refinement for receptor **2.7.**

Empirical formula	C_{23} H_{24} Fe_2 N_2 O
Formula weight	456.14
Temperature	120 K
Wavelength	0.71073 Å
Crystal system	Orthorhombic
Space group	P 2_1 2_1 2_1
Unit cell dimensions	a = 8.5102 Å α = 90°
	b = 8.7702 Å β= 90°
	c = 26.0912 Å γ = 90°
Volume	1947.35 $Å^3$
Z	4
Density (calculated)	1.556 mg/m^3
Absorption coefficient	1.506 mm^{-1}
F(000)	944
Crystal size	0.23 x 0.02 x 0.02 mm^3
Theta range for data collection	3.12 to 27.48°
Index ranges	-10<=h<=10, -11<=k<=11, -33<=l<=33
Reflections collected	13280
Independent reflections	4389 [R(int) = 0.0656]
Completeness to theta = 27.48°	99.4%
Absorption correction	Semi-empirical from equivalents
Max. and min. transmission	0.9705 and 0.7233
Refinement method	Full-matrix least-squares on F2
Data / restraints / parameters	4389 / 40 / 254
Goodness-of-fit on F2	1.169
Final R indices [I>2sigma(I)]	R1 = 0.0671, wR2 = 0.1164
R indices (all data)	R1 = 0.0932, wR2 = 0.1287
Absolute structure parameter	0.16
Largest diff. peak and hole	0.521 and -0.521 Å

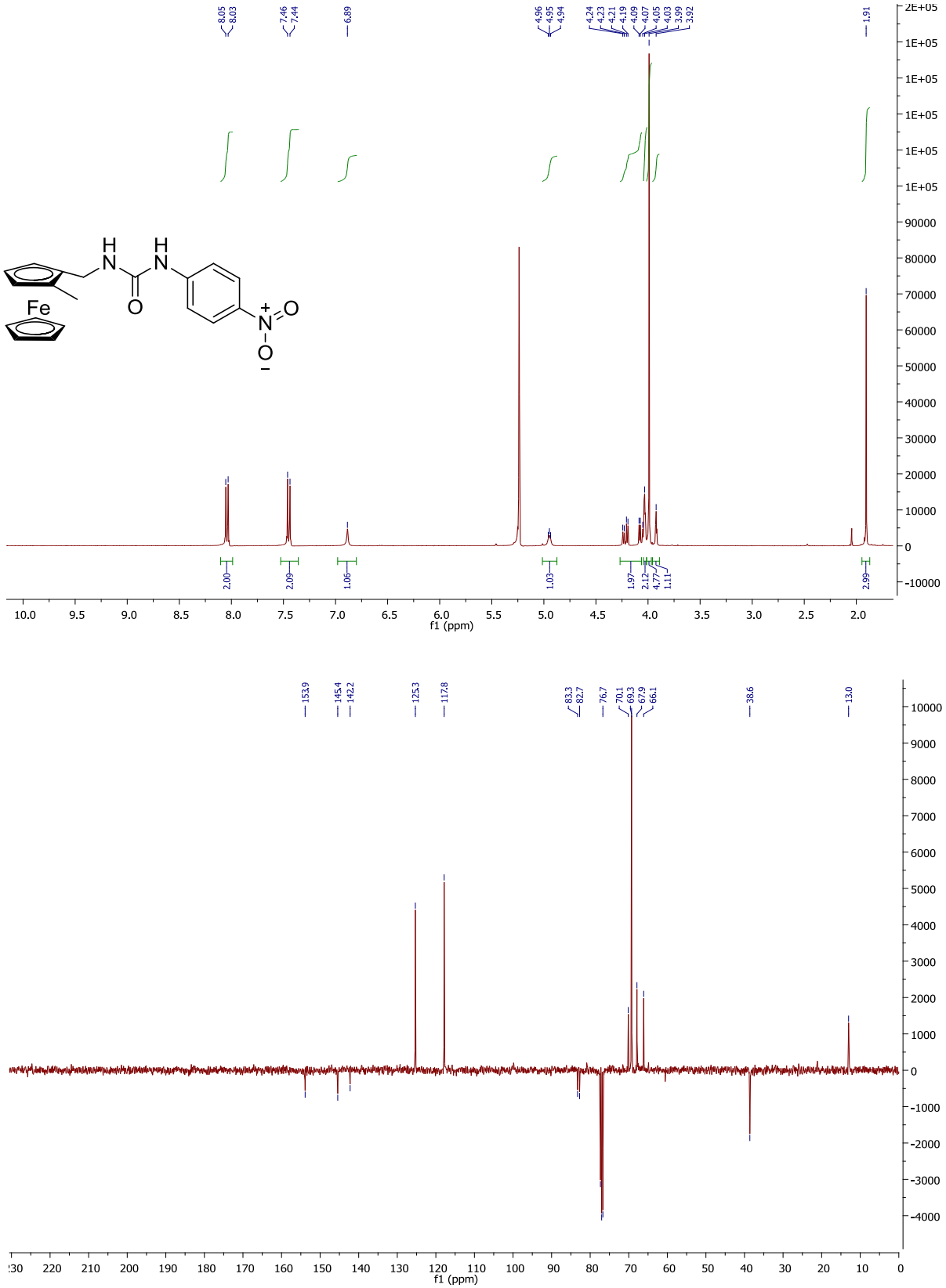

Figure 1: ^{1}H NMR and ^{13}C (DEPT-135) NMR spectra of receptor **2.8** in CD_2Cl_2.

Table 3: Crystal data and structure refinement for receptor **2.8.**

Empirical formula	$C_{19}H_{19}FeN_3O_3$, 0.5(H_2O)
Formula weight	402.23
Temperature	120 K
Wavelength	0.71073 Å
Crystal system	Monoclinic
Space group	P 2_1
Unit cell dimensions	a = 11.1740 Å α = 90°
	b = 7.2448 Å β = 92.1200°
	c = 22.0107 Å γ = 90°
Volume	1780.62 $Å^3$
Z	4
Density (calculated)	1.500 mg/m^3
Absorption coefficient	0.875 mm^{-1}
F(000)	836
Crystal size	0.62 x 0.14 x 0.10 mm^3
Theta range for data collection	2.96 to 27.48°
Index ranges	-14<=h<=14, -9<=k<=9, -27<=l<=28
Reflections collected	19184
Independent reflections	7983 [R(int) = 0.0464]
Completeness to theta = 27.48°	99.6%
Absorption correction	Semi-empirical from equivalents
Max. and min. transmission	0.9176 and 0.6131
Refinement method	Full-matrix least-squares on F2
Data / restraints / parameters	7983 / 4 / 488
Goodness-of-fit on F2	1.040
Final R indices [I>2sigma(I)]	R1 = 0.0434, wR2 = 0.0880
R indices (all data)	R1 = 0.0555, wR2 = 0.0933
Absolute structure parameter	0.036
Largest diff. peak and hole	0.383 and -0.559 Å

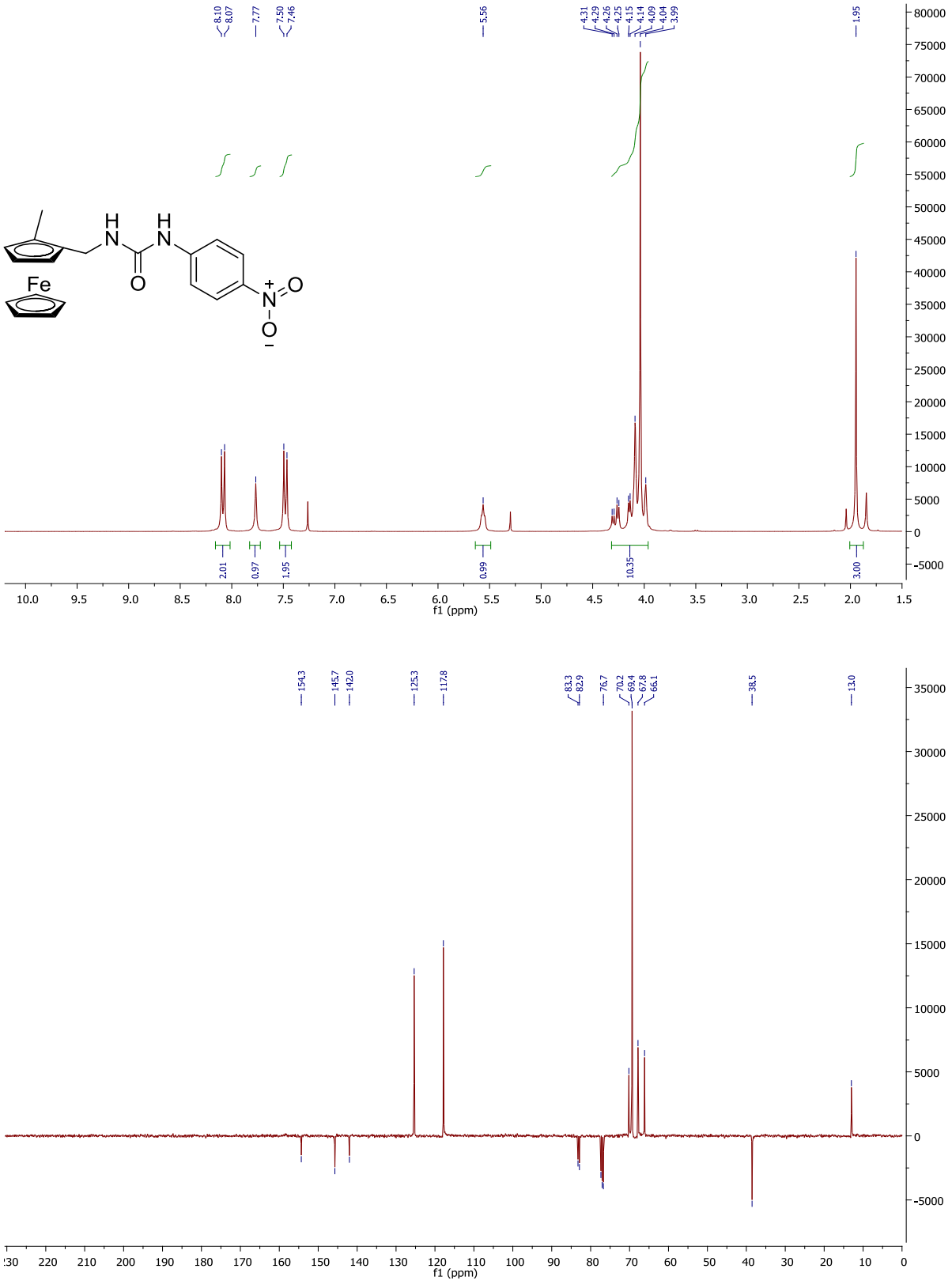

Figure 2: ^{1}H NMR and ^{13}C (DEPT-135) NMR spectra of receptor **2.9** in $CDCl_3$.

Table 4: Crystal data and structure refinement for receptor **2.9.**

Empirical formula	$C_{19}H_{19}FeN_3O_3$, 0.5(H_2O)
Formula weight	402.23
Temperature	120 K
Wavelength	0.71073 Å
Crystal system	Monoclinic
Space group	P 2_1
Unit cell dimensions	a = 11.1747 Å α = 90°
	b = 7.2439 Å β = 92.116°
	c = 22.0137 Å γ = 90°
Volume	1780.76 $Å^3$
Z	4
Density (calculated)	1.500 mg/m^3
Absorption coefficient	0.875 mm^{-1}
F(000)	836
Crystal size	0.32 x 0.09 x 0.03 mm^3
Theta range for data collection	2.96 to 27.48°
Index ranges	-14<=h<=14, -8<=k<=9, -28<=l<=28
Reflections collected	22029
Independent reflections	7713 [R(int) = 0.0752]
Completeness to theta = 27.48°	99.4%
Absorption correction	Semi-empirical from equivalents
Max. and min. transmission	0.9742 and 0.7672
Refinement method	Full-matrix least-squares on F2
Data / restraints / parameters	7713 / 4 / 486
Goodness-of-fit on F2	1.014
Final R indices [I>2sigma(I)]	R1 = 0.0542, wR2 = 0.0998
R indices (all data)	R1 = 0.0863, wR2 = 0.1118
Absolute structure parameter	0.056
Largest diff. peak and hole	0.410 and -0.485 Å

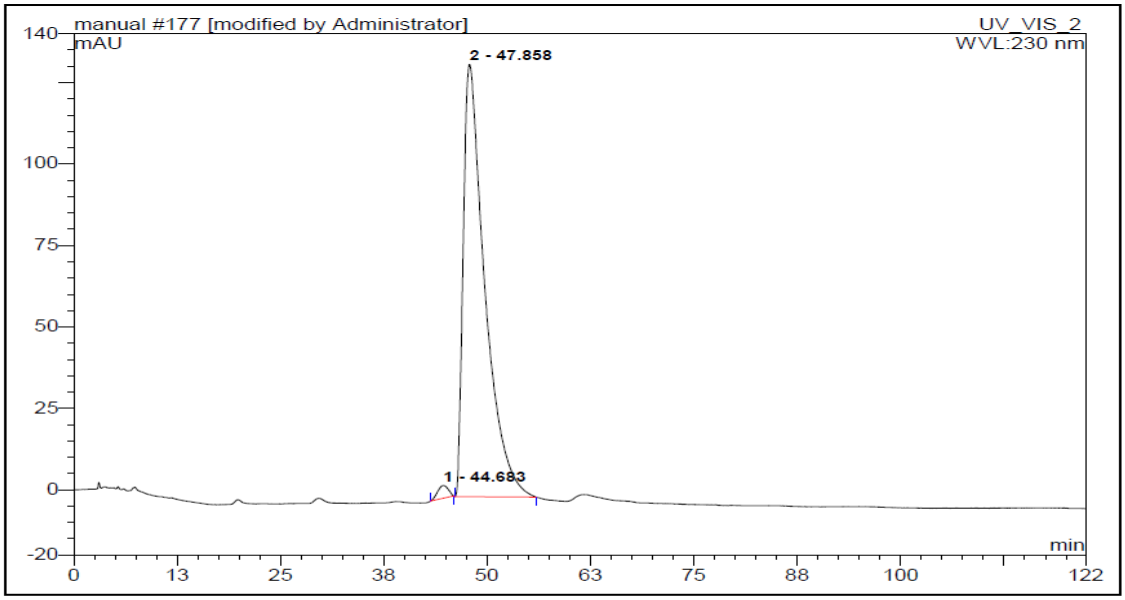

No.	Ret.Time min	Peak Name	Height mAU	Area mAU*min	Rel.Area %	Amount	Type
1	44.68	n.a.	3.927	5.867	1.45	n.a.	BMB*
2	47.86	n.a.	132.790	399.995	98.55	n.a.	BMB
Total:			136.717	405.862	100.00	0.000	

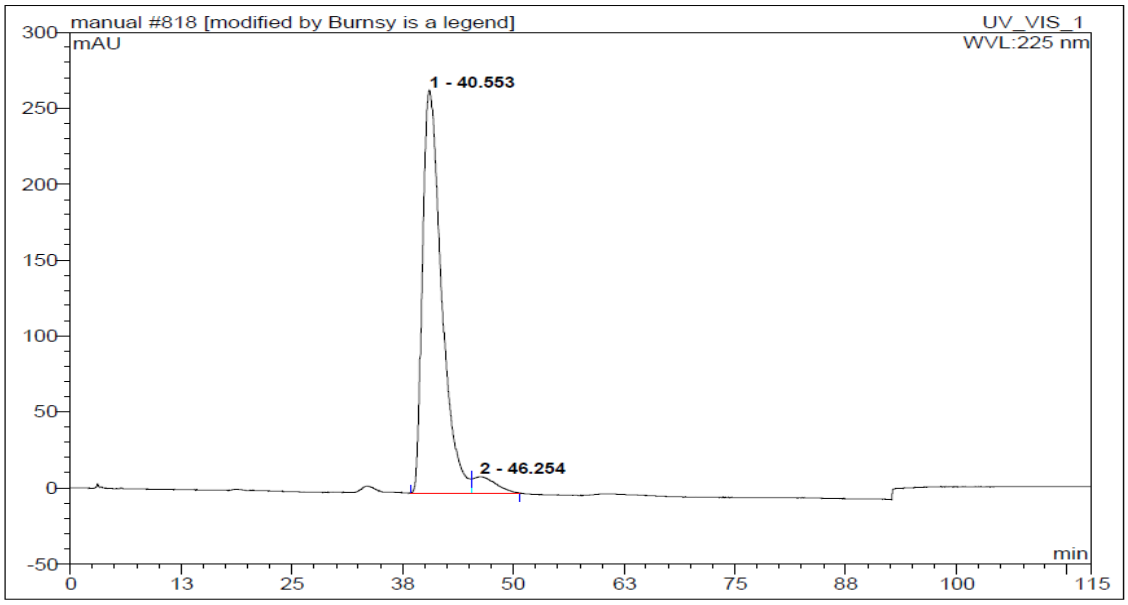

No.	Ret.Time min	Peak Name	Height mAU	Area mAU*min	Rel.Area %	Amount	Type
1	40.55	n.a.	265.312	661.326	95.37	n.a.	BM
2	46.25	n.a.	10.706	32.105	4.63	n.a.	MB
Total:			276.018	693.431	100.00	0.000	

Figure 3: Chiral HPLC of receptors **2.8** (top) and **2.9** (bottom) (10% IPA in hexane, AD column, 1 mL/min).

Table 5: Crystal data and structure refinement for receptor **2.10.**

Empirical formula	$C_{18} H_{17} Fe N_3 O_3$
Formula weight	379.20
Temperature	120 K
Wavelength	0.71073 Å
Crystal system	Monoclinic
Space group	Cc
Unit cell dimensions	a = 5.7835 Å α= 90°
	b = 30.636 Å β= 96.405°
	c = 9.2241 Å γ = 90°
Volume	1624.2 $Å^3$
Z	4
Density (calculated)	1.551 mg/m^3
Absorption coefficient	0.952 mm^{-1}
F(000)	784
Crystal size	0.20 x 0.09 x 0.01 mm^3
Theta range for data collection	3.47 to 25.03°
Index ranges	-6<=h<=6, -36<=k<=36, -10<=l<=10
Reflections collected	8429
Independent reflections	2707 [R(int) = 0.0445]
Completeness to theta = 25.03°	99.6%
Absorption correction	Semi-empirical from equivalents
Max. and min. transmission	0.9905 and 0.8325
Refinement method	Full-matrix least-squares on F2
Data / restraints / parameters	2707 / 2 / 227
Goodness-of-fit on F2	1.067
Final R indices [I>2sigma(I)]	R1 = 0.0374, wR2 = 0.0783
R indices (all data)	R1 = 0.0419, wR2 = 0.0811
Absolute structure parameter	0.13
Largest diff. peak and hole	0.265 and -0.345 Å

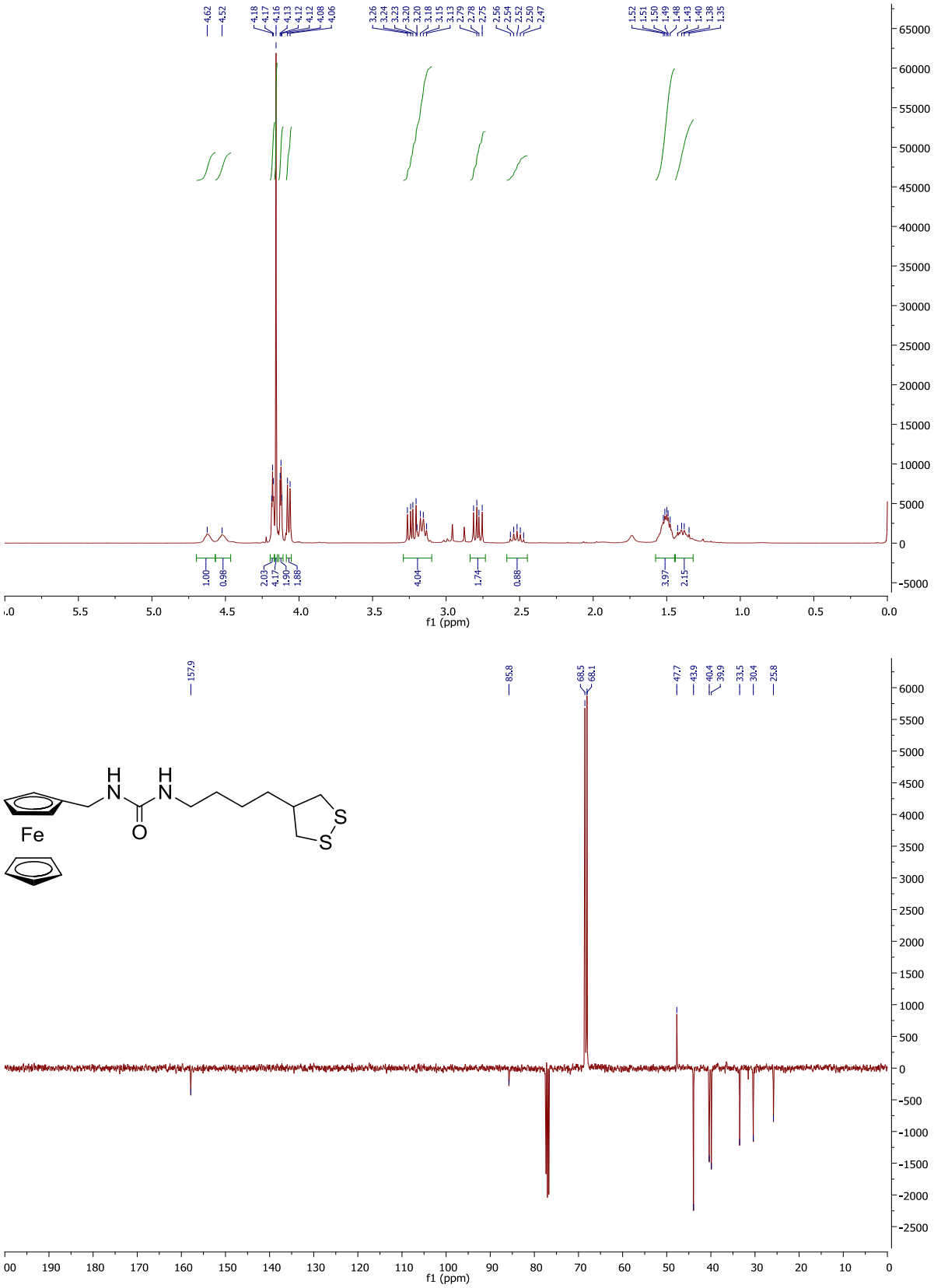

Figure 4: ^{1}H NMR and ^{13}C (DEPT-135) NMR spectra of receptor **3.3** in $CDCl_3$.

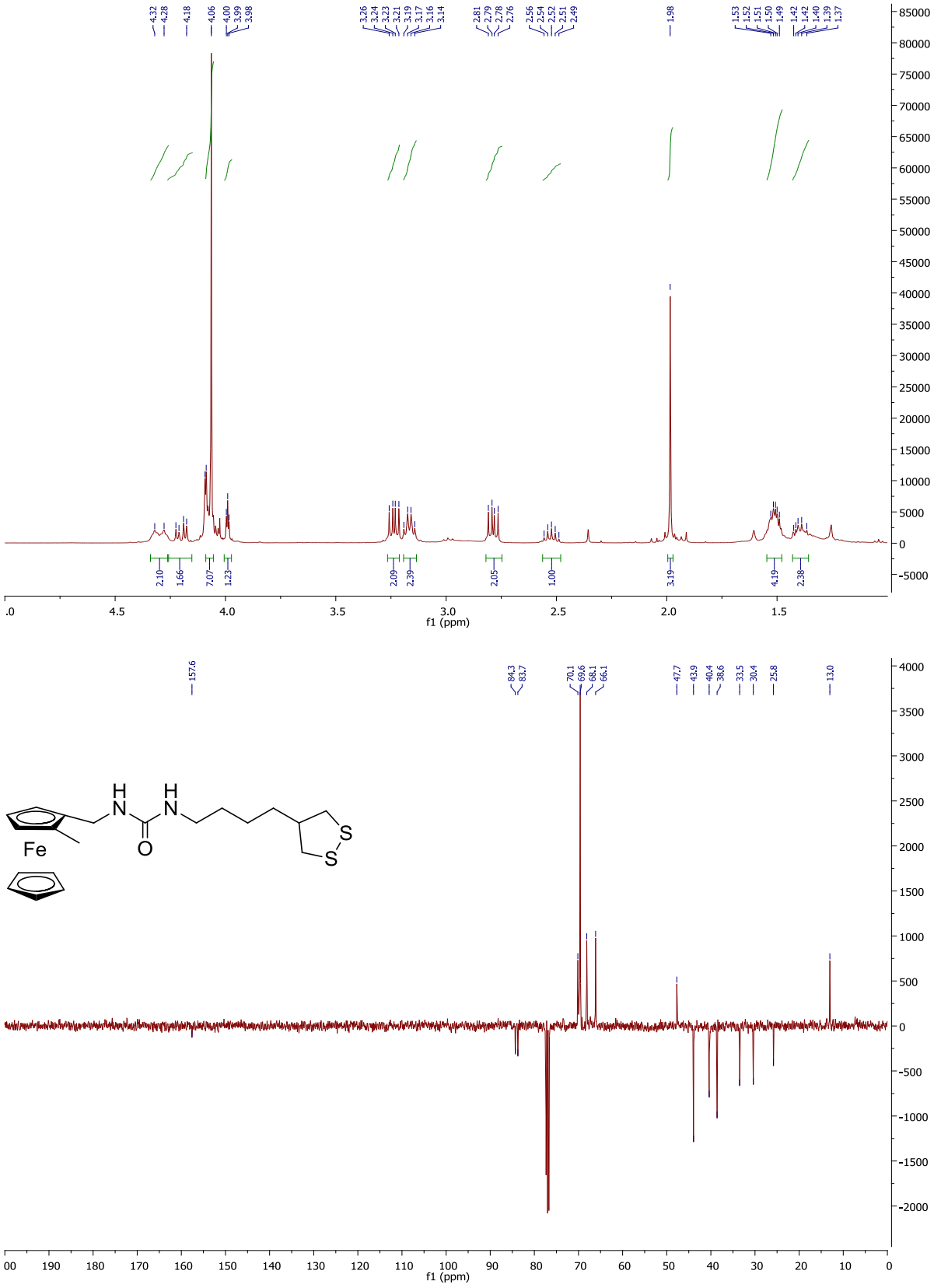

Figure 5: ^{1}H NMR and ^{13}C (DEPT-135) NMR spectra of receptor **3.4** in $CDCl_3$.

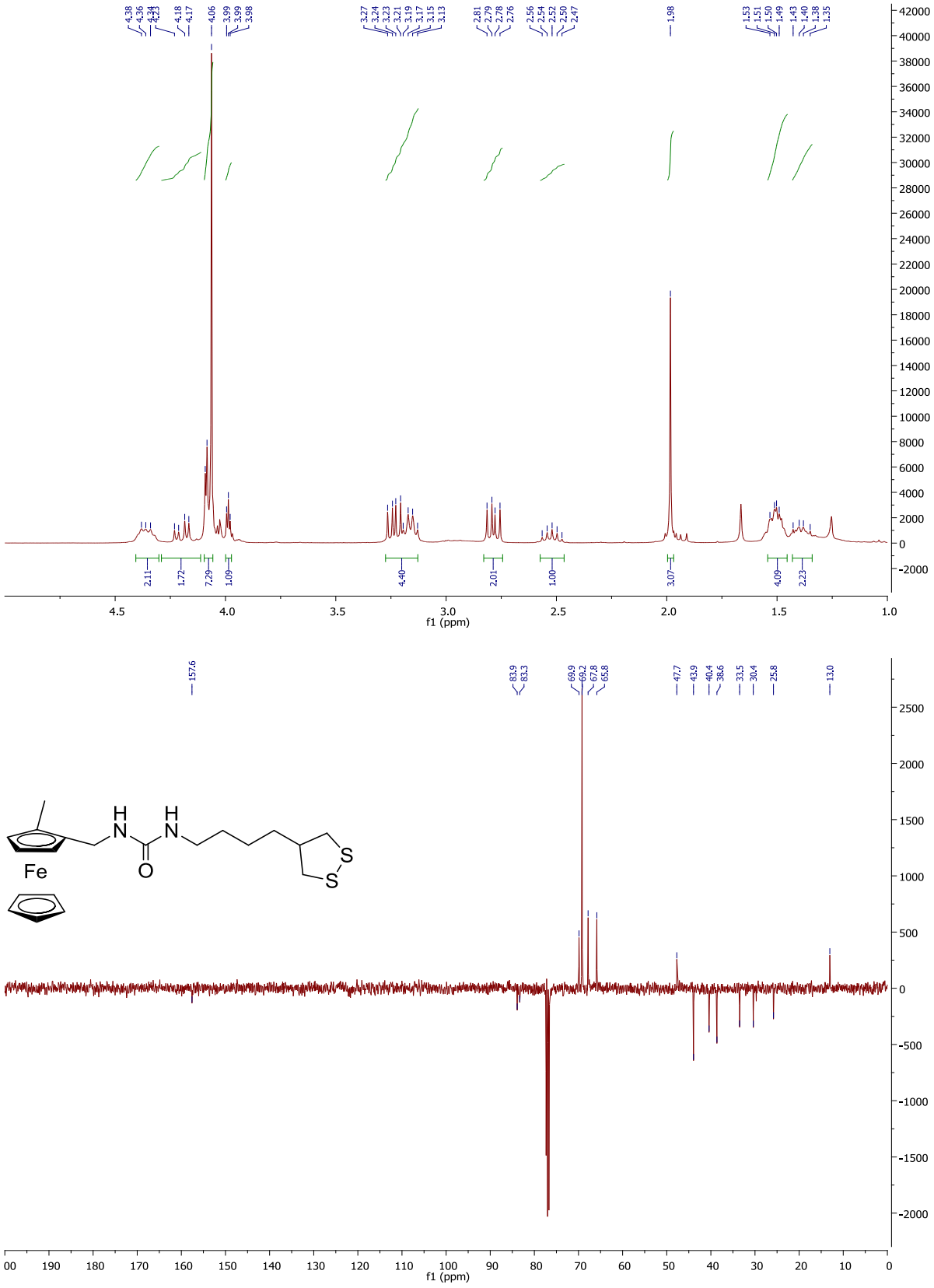

Figure 6: ^{1}H NMR and ^{13}C (DEPT-135) NMR spectra of receptor **3.5** in $CDCl_3$.

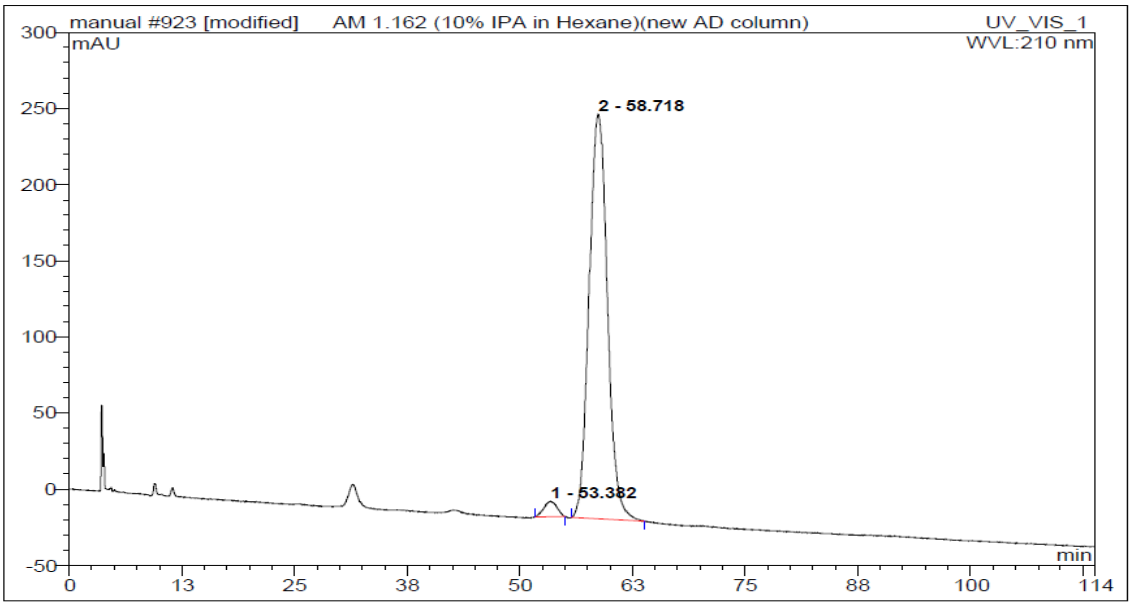

No.	Ret.Time min	Peak Name	Height mAU	Area mAU*min	Rel.Area %	Amount	Type
1	53.38	n.a.	10.117	16.919	2.64	n.a.	BMB*
2	58.72	n.a.	265.810	624.652	97.36	n.a.	BMB*
Total:			275.927	641.570	100.00	0.000	

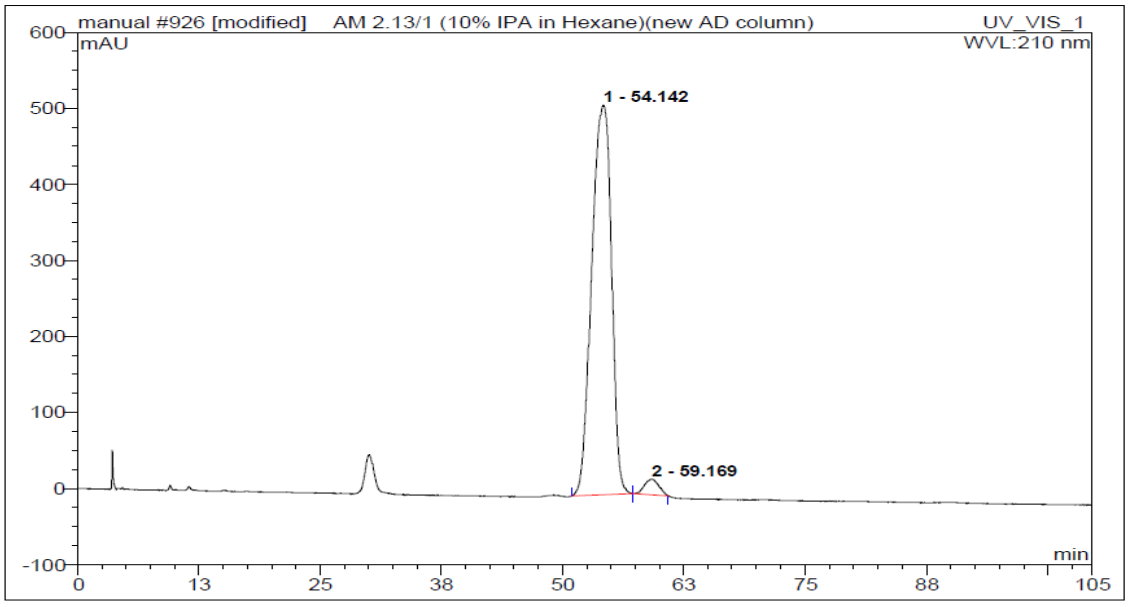

No.	Ret.Time min	Peak Name	Height mAU	Area mAU*min	Rel.Area %	Amount	Type
1	54.14	n.a.	512.748	1208.487	97.15	n.a.	BMB*
2	59.17	n.a.	20.567	35.462	2.85	n.a.	BMB*
Total:			533.315	1243.948	100.00	0.000	

Figure 7: Chiral HPLC traces of receptors **3.4** (top) and **3.5** (bottom) (10% IPA in hexane, AD column, 1 mL/min).

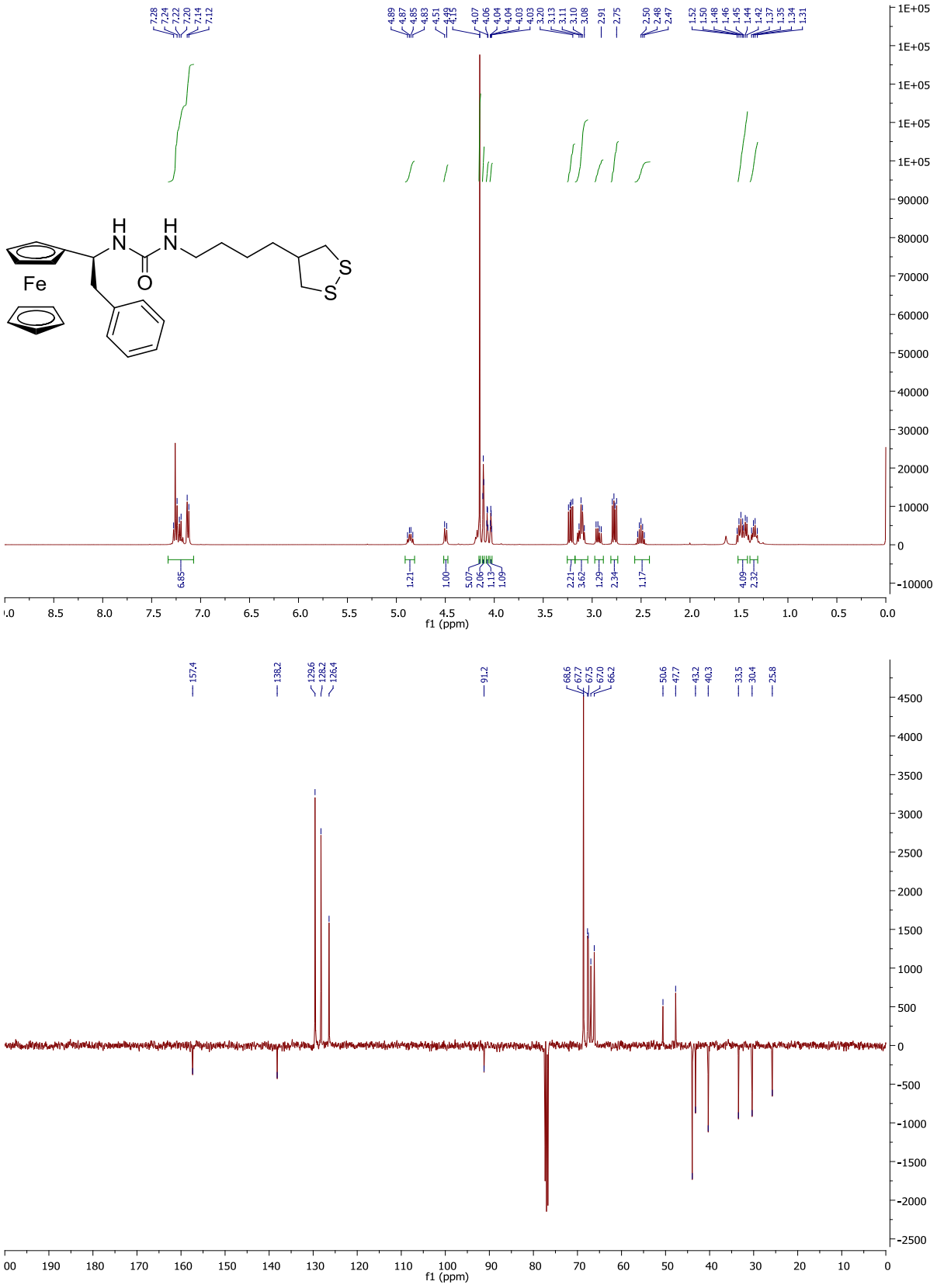

Figure 8: ^{1}H NMR and ^{13}C (DEPT-135) NMR spectra of receptor **3.6** in $CDCl_3$.

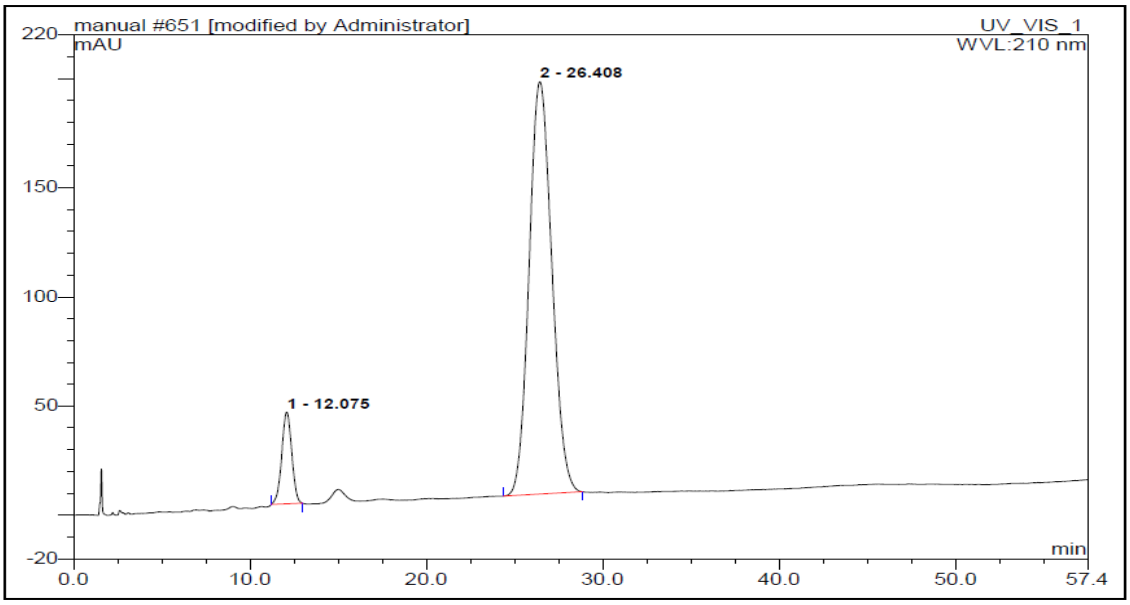

No.	Ret.Time min	Peak Name	Height mAU	Area mAU*min	Rel.Area %	Amount	Type
1	12.08	n.a.	42.038	27.580	8.90	n.a.	BMB*
2	26.41	n.a.	188.892	282.358	91.10	n.a.	BMB
Total:			230.930	309.937	100.00	0.000	

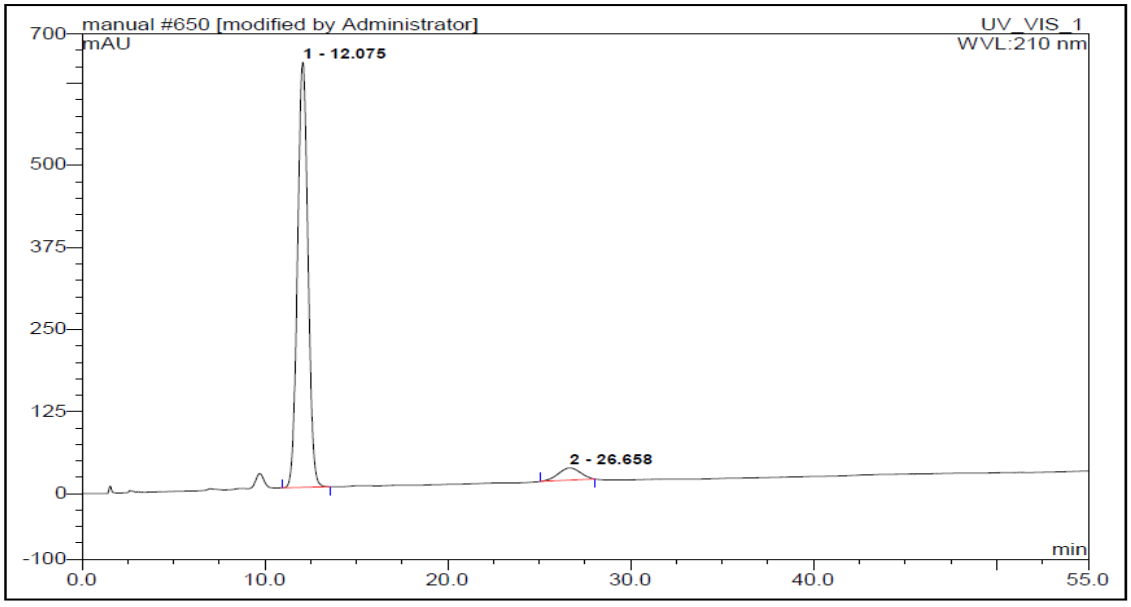

No.	Ret.Time min	Peak Name	Height mAU	Area mAU*min	Rel.Area %	Amount	Type
1	12.08	n.a.	647.710	428.891	94.35	n.a.	BMB
2	26.66	n.a.	18.458	25.689	5.65	n.a.	BMB*
Total:			666.168	454.580	100.00	0.000	

Figure 9: Chiral HPLC of receptors **3.6** (top) and **3.7** (bottom) (20% IPA in hexane, AD column, 2 mL/min).

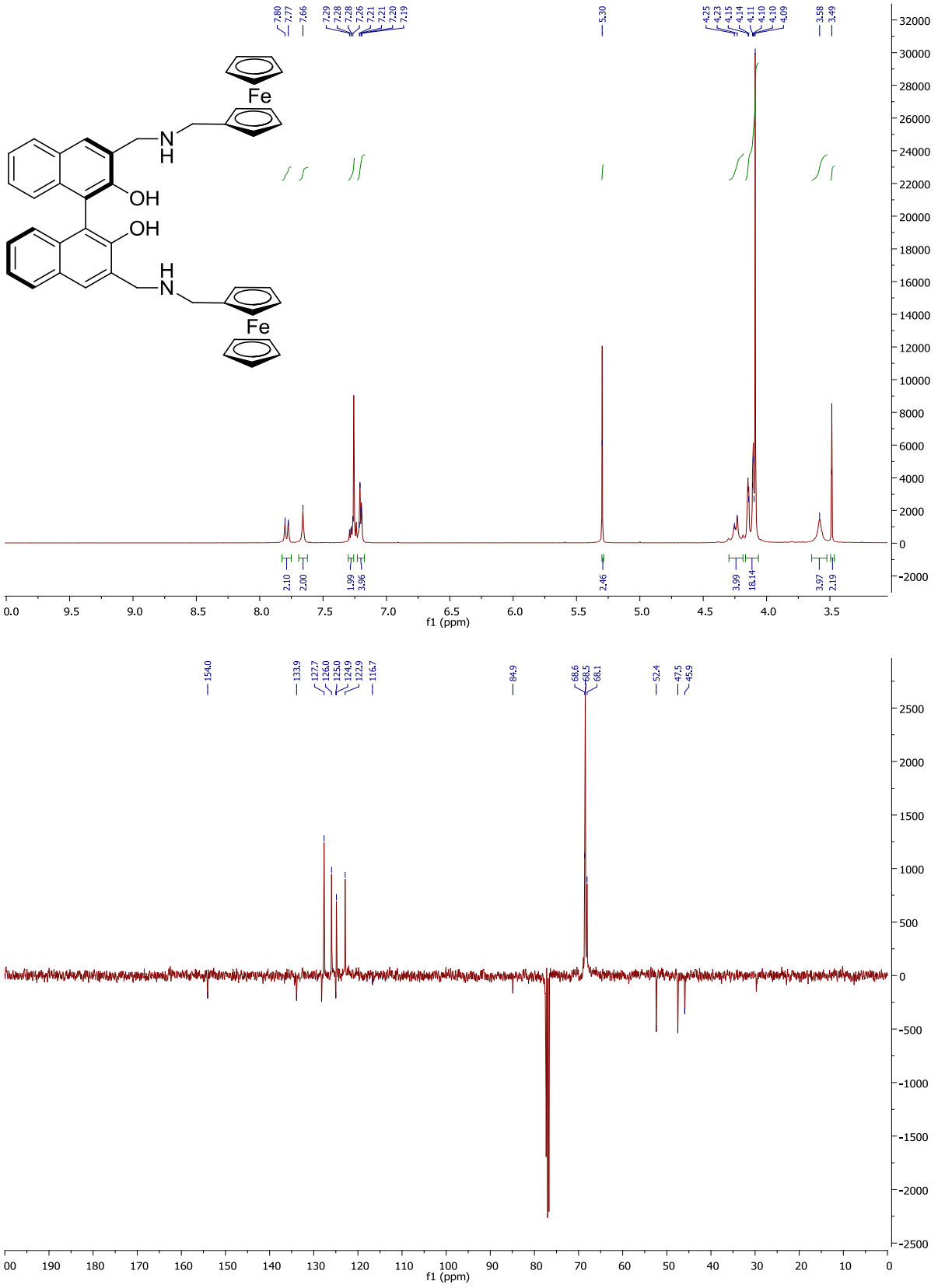

Figure 10: ^{1}H NMR and ^{13}C (DEPT-135) NMR spectra of receptor **4.8** in $CDCl_3$.

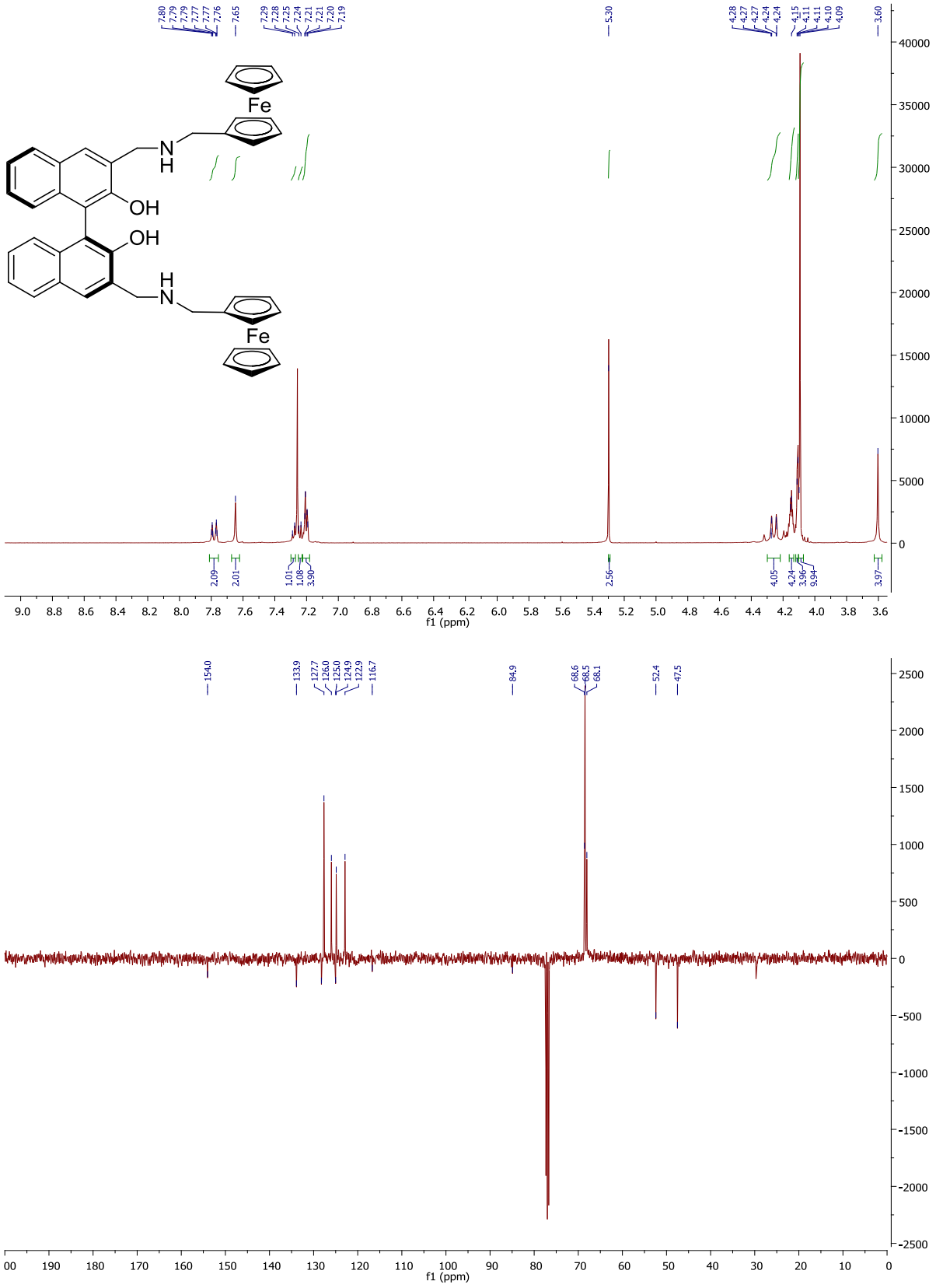

Figure 11: ^{1}H NMR and ^{13}C (DEPT-135) NMR spectra of receptor **4.9** in $CDCl_3$.

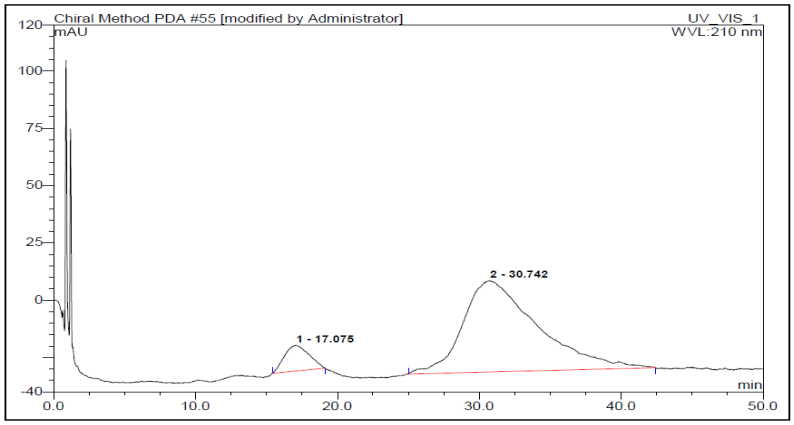

No.	Ret.Time min	Peak Name	Height mAU	Area mAU*min	Rel.Area %	Amount	Type
1	17.08	n.a.	11.295	22.591	8.50	n.a.	BMB*
2	30.74	n.a.	39.893	243.089	91.50	n.a.	BMB*
Total:			51.188	265.679	100.00	0.000	

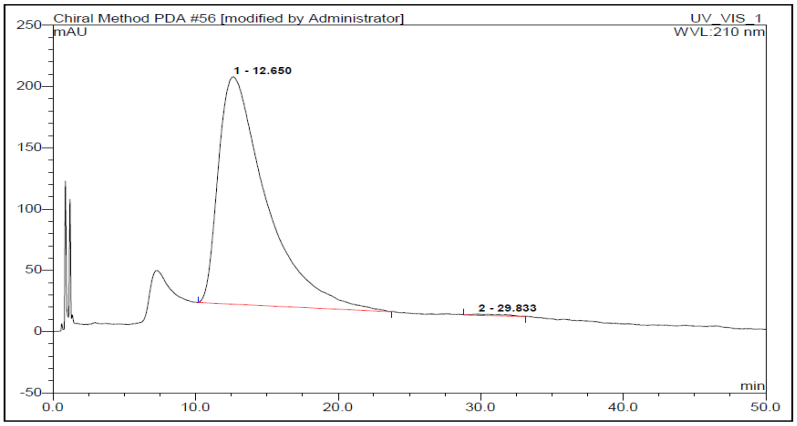

No.	Ret.Time min	Peak Name	Height mAU	Area mAU*min	Rel.Area %	Amount	Type
1	12.65	n.a.	185.545	722.594	99.62	n.a.	BMB*
2	29.83	n.a.	1.063	2.727	0.38	n.a.	BMB*
Total:			186.608	725.320	100.00	0.000	

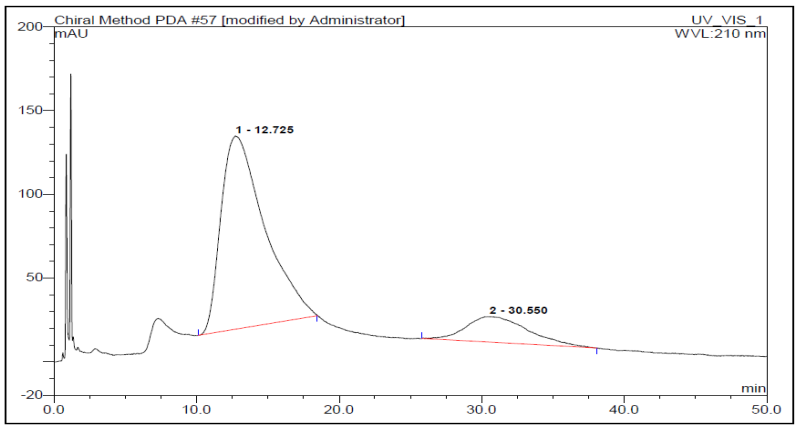

No.	Ret.Time min	Peak Name	Height mAU	Area mAU*min	Rel.Area %	Amount	Type
1	12.73	n.a.	115.419	408.726	84.12	n.a.	BMB*
2	30.55	n.a.	15.222	77.147	15.88	n.a.	BMB*
Total:			130.641	485.873	100.00	0.000	

Figure 12: Chiral HPLC of **4.8**, **4.9** and a mixture of both (top to bottom) (20% IPA in hexane, AD column, 5 mL/min).

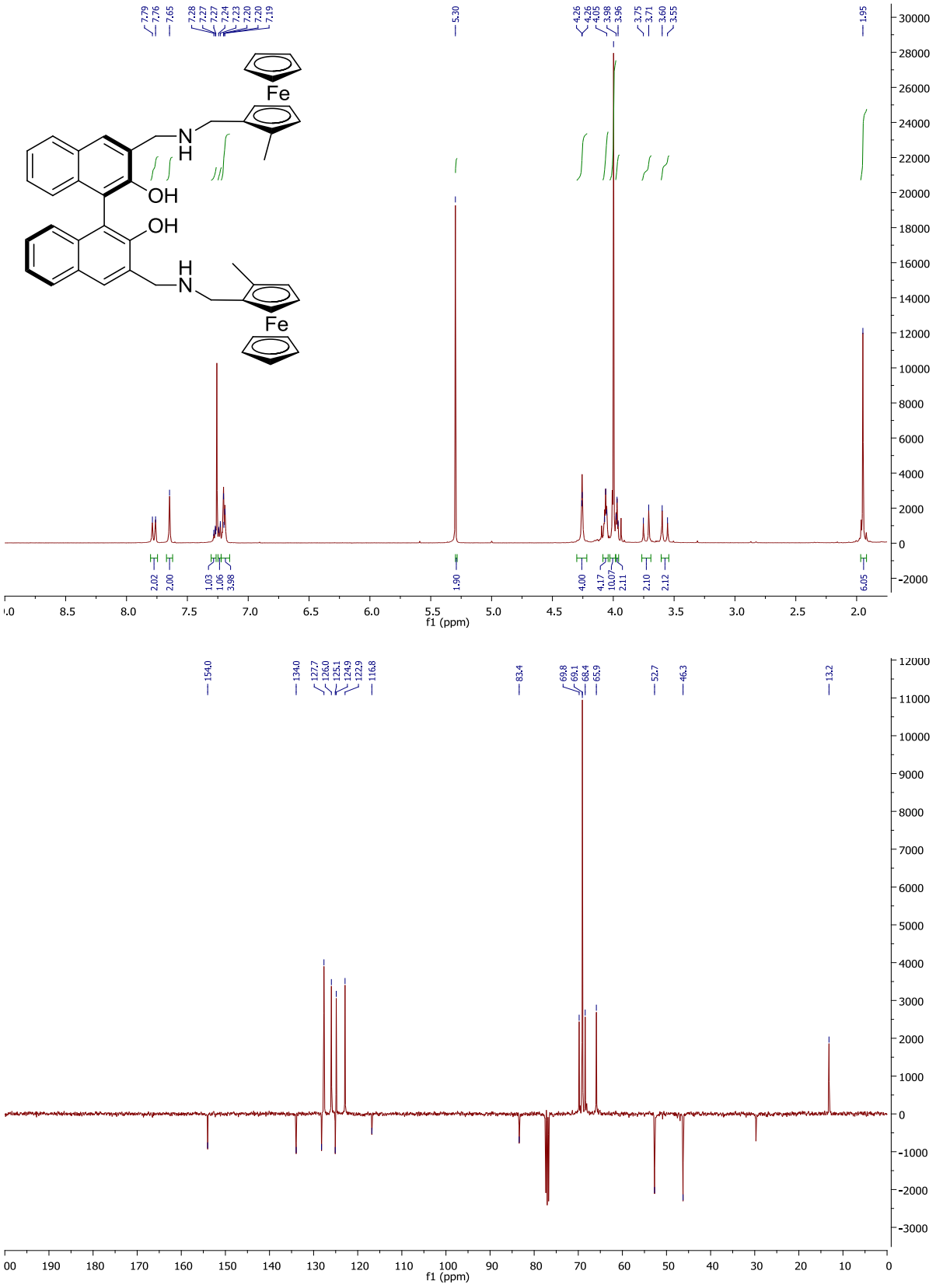

Figure 13: ^{1}H NMR and ^{13}C (DEPT-135) NMR spectra of receptor **4.10** in $CDCl_3$.

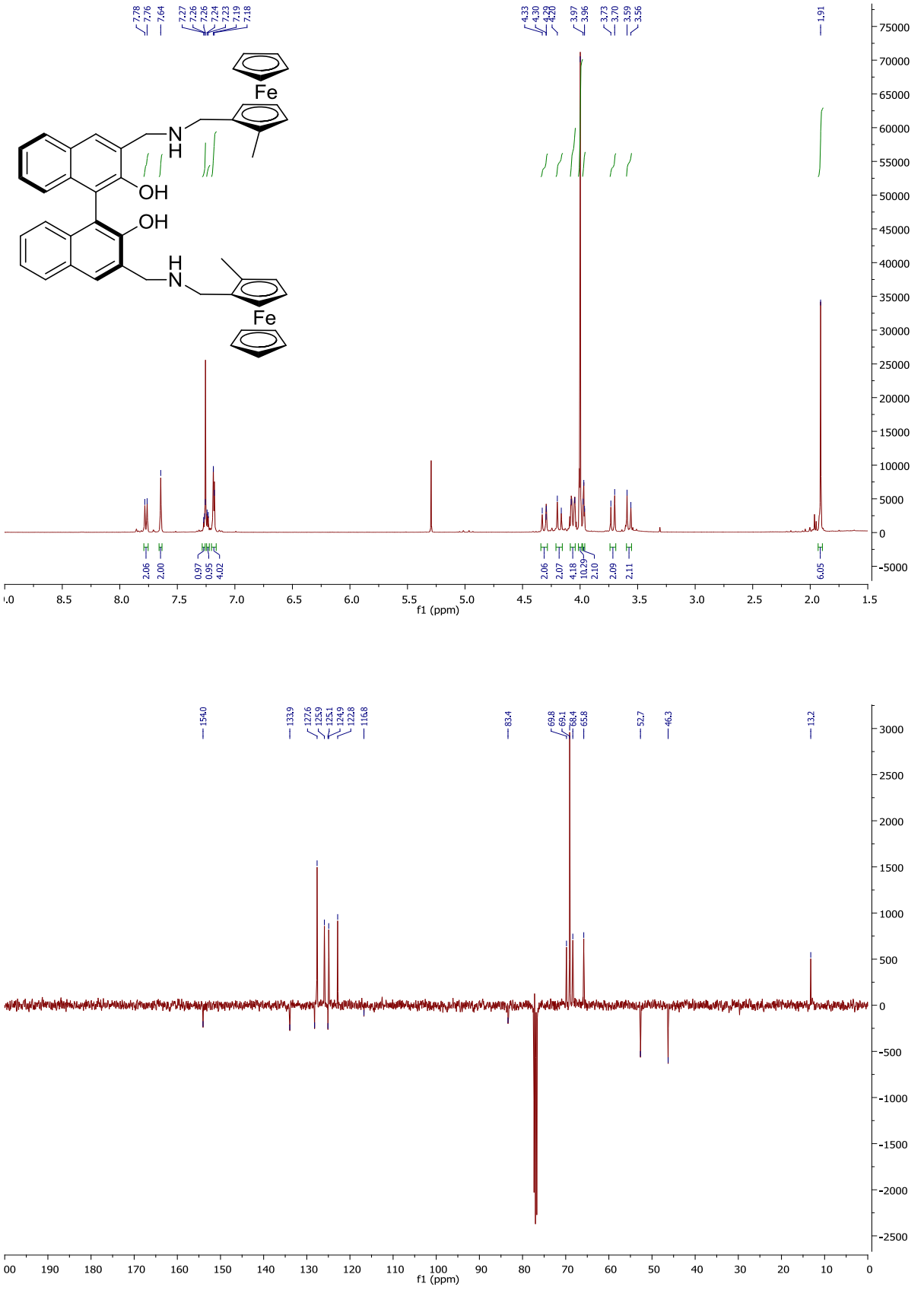

Figure 14: ^{1}H NMR and ^{13}C (DEPT-135) NMR spectra of receptor **4.11** in $CDCl_3$.

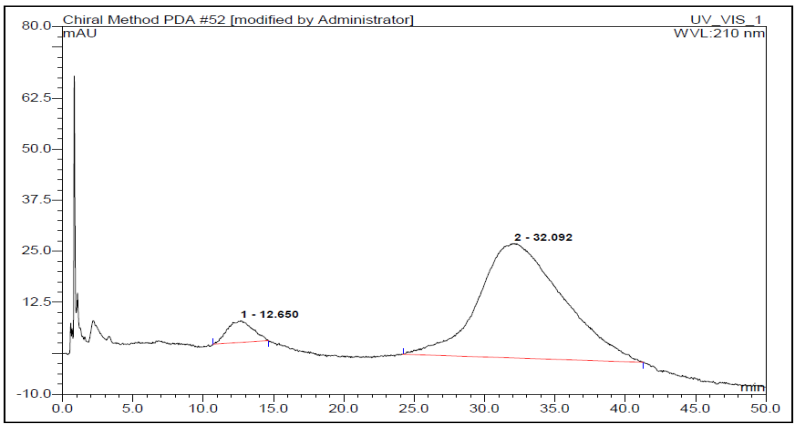

No.	Ret.Time min	Peak Name	Height mAU	Area mAU*min	Rel.Area %	Amount	Type
1	12.65	n.a.	5.326	11.215	5.46	n.a.	BMB*
2	32.09	n.a.	28.043	194.206	94.54	n.a.	BMB*
Total:			33.369	205.422	100.00	0.000	

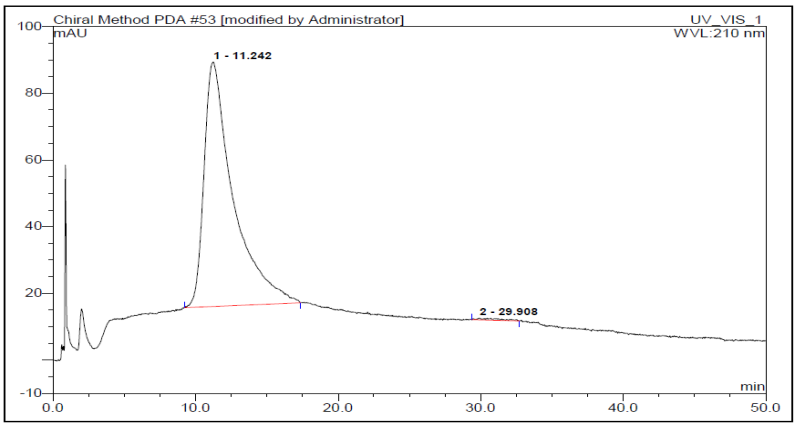

No.	Ret.Time min	Peak Name	Height mAU	Area mAU*min	Rel.Area %	Amount	Type
1	11.24	n.a.	73.318	173.887	99.44	n.a.	BMB*
2	29.91	n.a.	0.614	0.980	0.56	n.a.	BMB*
Total:			73.932	174.867	100.00	0.000	

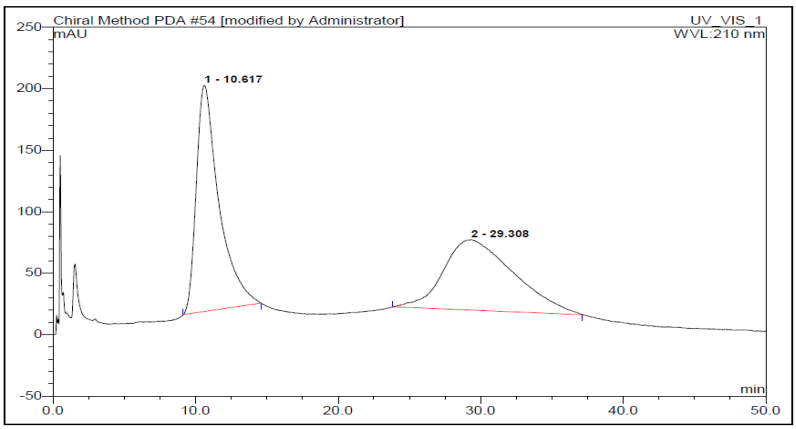

No.	Ret.Time min	Peak Name	Height mAU	Area mAU*min	Rel.Area %	Amount	Type
1	10.62	n.a.	183.950	339.266	50.96	n.a.	BMB*
2	29.31	n.a.	57.211	326.432	49.04	n.a.	BMB*
Total:			241.161	665.697	100.00	0.000	

Figure 15: Chiral HPLC of **4.10**, **4.11** and a mixture of both (top to bottom) (20% IPA in hexane, AD column, 5 mL/min).

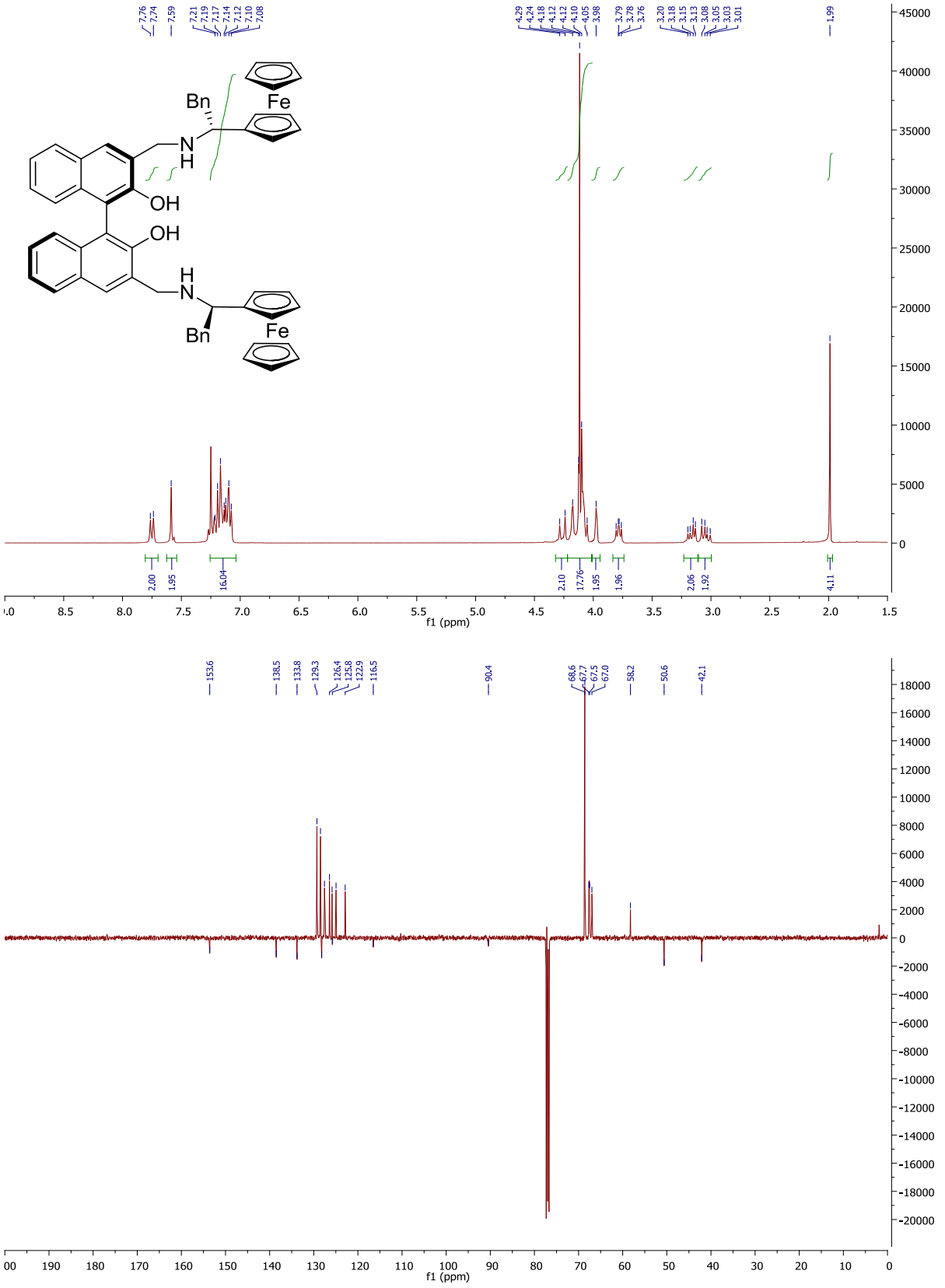

Figure 16: ^{1}H NMR and ^{13}C (DEPT-135) NMR spectra of receptor **4.12** in $CDCl_3$.

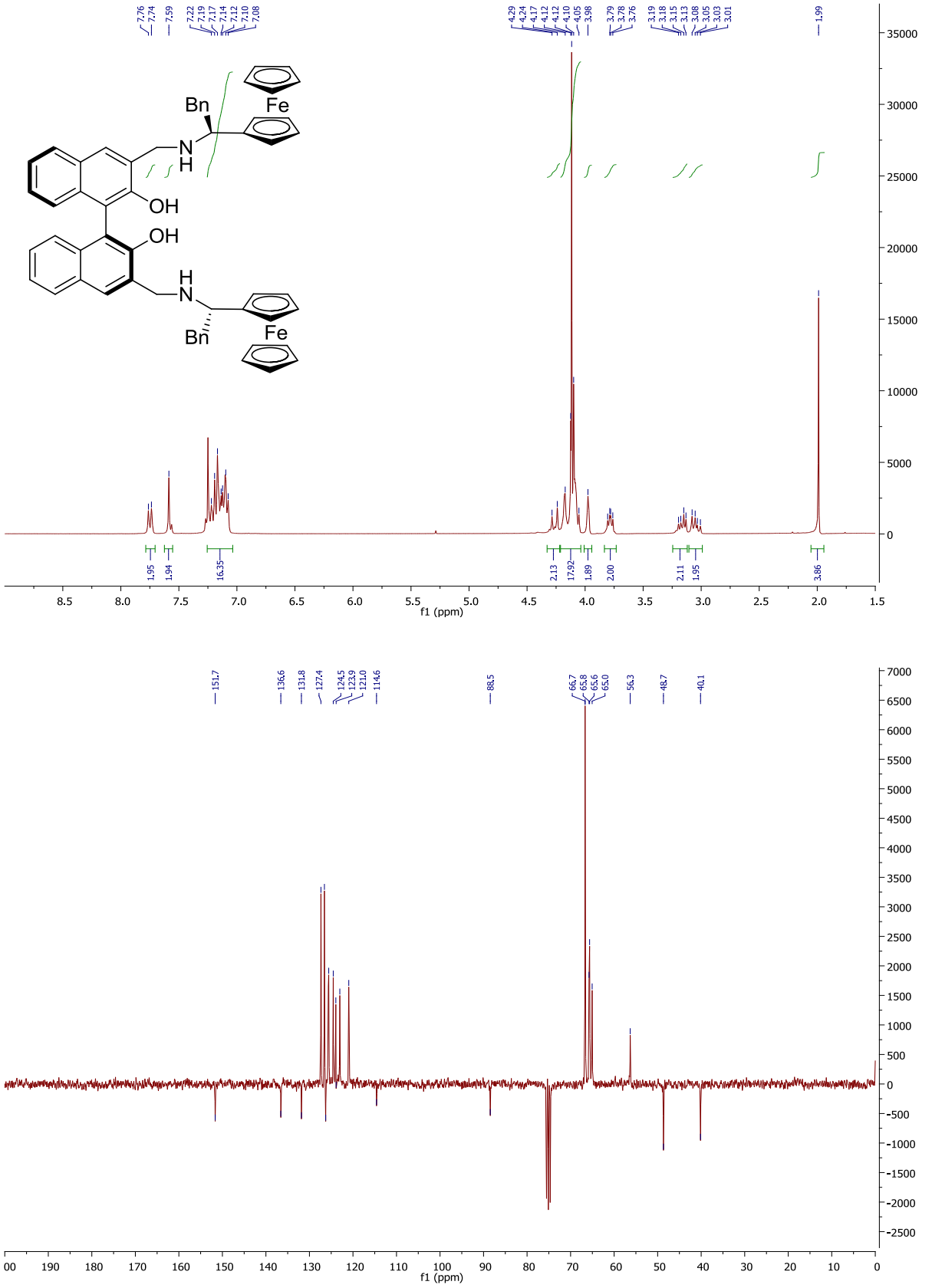

Figure 17: ^{1}H NMR and ^{13}C (DEPT-135) NMR spectra of receptor **4.13** in $CDCl_3$.

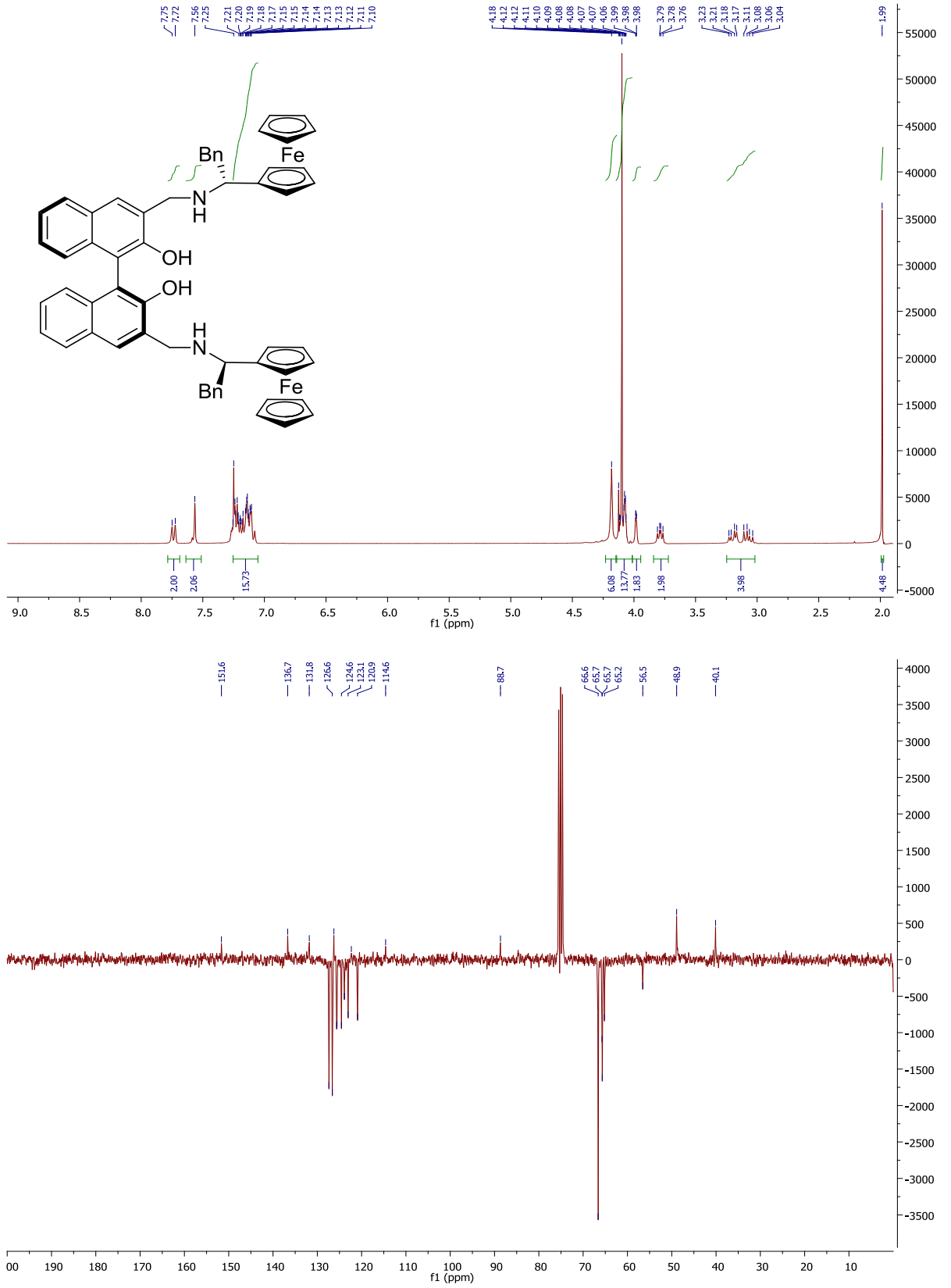

Figure 18: ^{1}H NMR and ^{13}C (DEPT-135) NMR spectra of receptor **4.14** in $CDCl_3$.

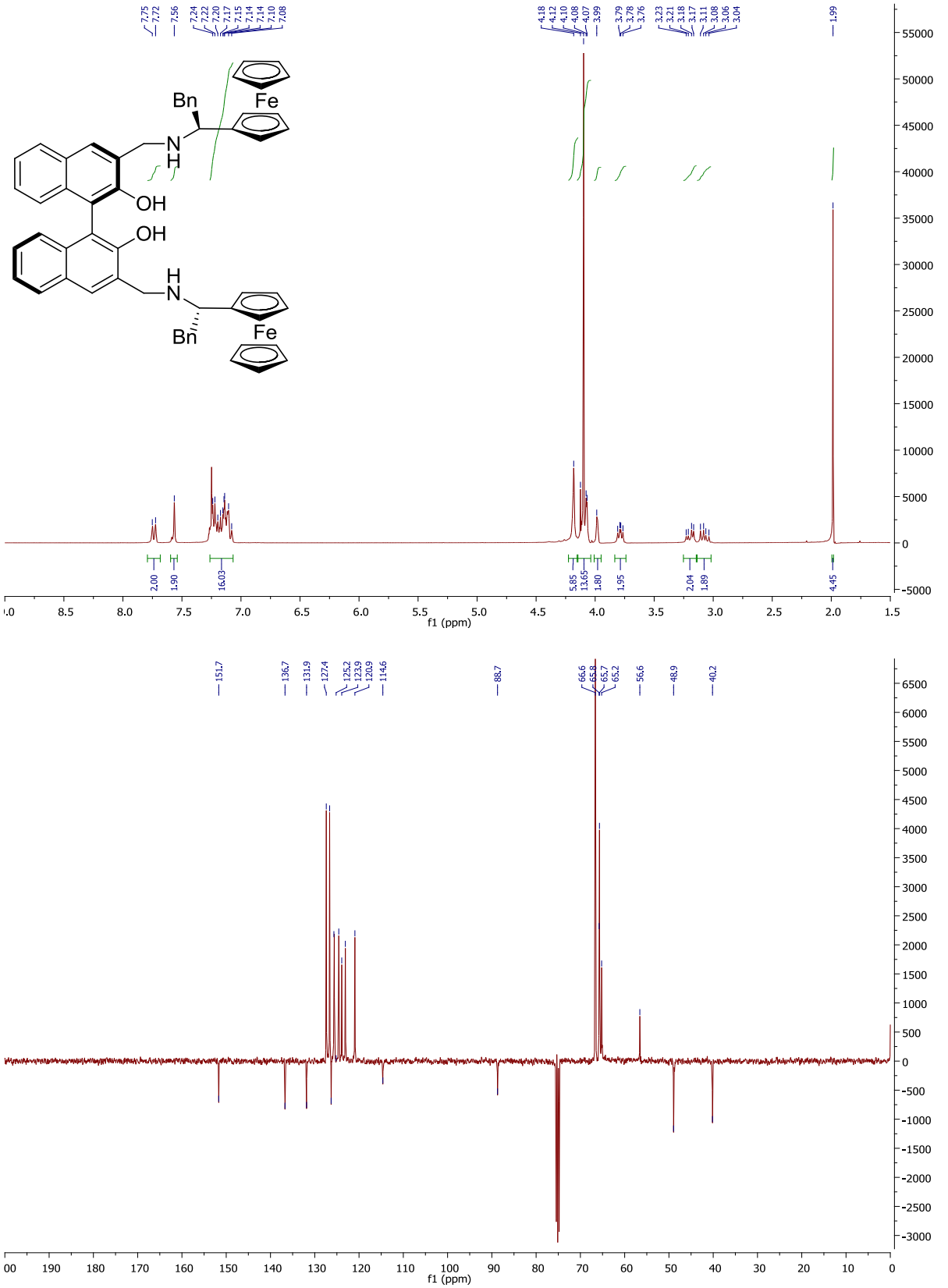

Figure 19: ^{1}H NMR and ^{13}C (DEPT-135) NMR spectra of receptor **4.15** in $CDCl_3$.

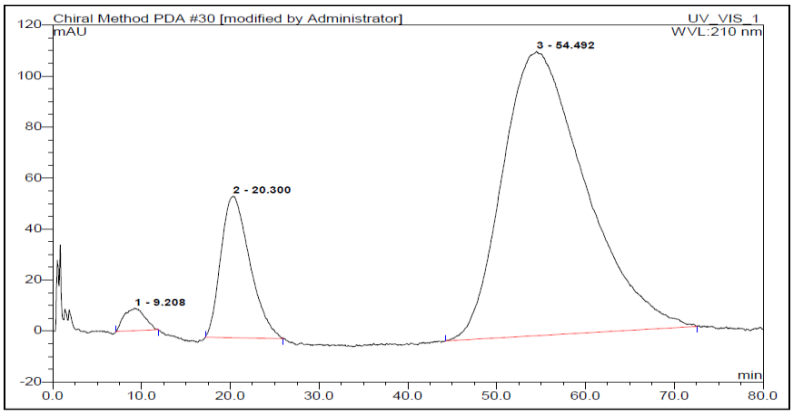

No.	Ret.Time min	Peak Name	Height mAU	Area mAU*min	Rel.Area %	Amount	Type
1	9.21	n.a.	8.869	23.725	1.65	n.a.	BMB*
2	20.30	n.a.	55.509	209.531	14.55	n.a.	BMB*
3	54.49	n.a.	111.571	1206.538	83.80	n.a.	BMB*
Total:			175.949	1439.794	100.00	0.000	

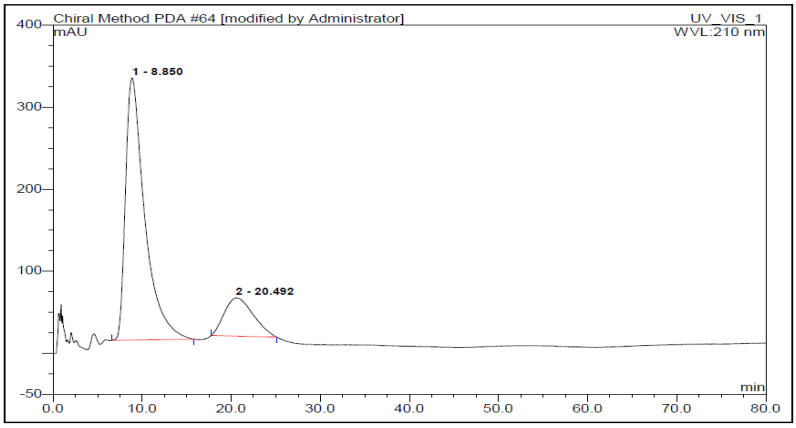

No.	Ret.Time min	Peak Name	Height mAU	Area mAU*min	Rel.Area %	Amount	Type
1	8.85	n.a.	319.821	798.562	82.04	n.a.	BMB*
2	20.49	n.a.	46.620	174.778	17.96	n.a.	BMB*
Total:			366.441	973.341	100.00	0.000	

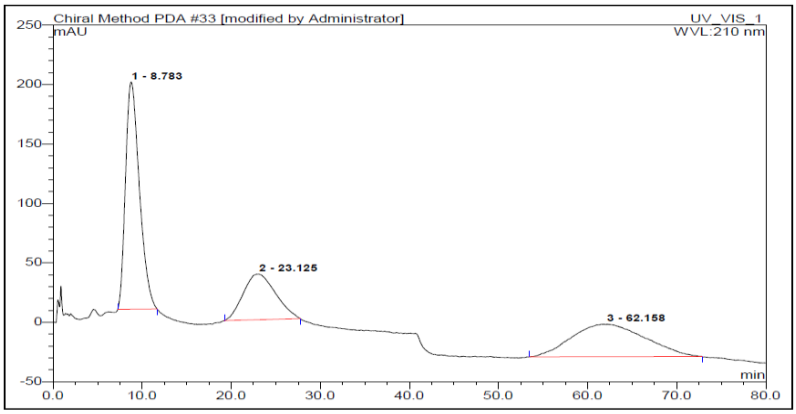

No.	Ret.Time min	Peak Name	Height mAU	Area mAU*min	Rel.Area %	Amount	Type
1	8.78	n.a.	191.173	345.326	44.90	n.a.	BMB*
2	23.13	n.a.	38.428	161.439	20.99	n.a.	BMB*
3	62.16	n.a.	27.499	262.388	34.11	n.a.	BMB*
Total:			257.100	769.154	100.00	0.000	

Figure 20: Chiral HPLC of **4.12**, **4.15** and a mixture of both (top to bottom) (20% IPA in hexane, AD column, 5 mL/min).

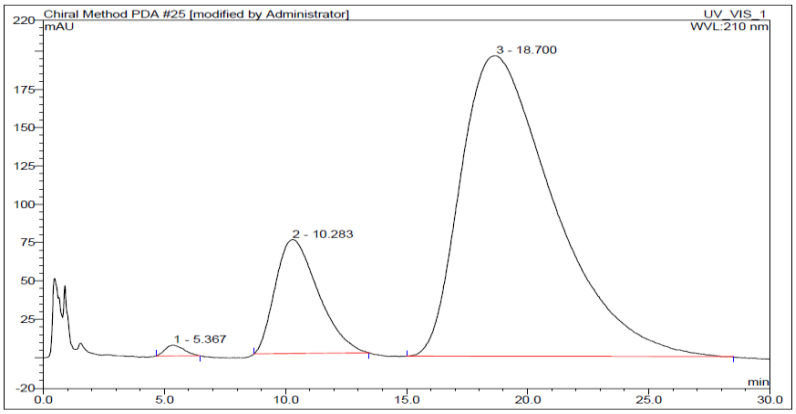

No.	Ret.Time min	Peak Name	Height mAU	Area mAU*min	Rel.Area %	Amount	Type
1	5.37	n.a.	7.084	6.394	0.62	n.a.	BMB*
2	10.28	n.a.	74.395	152.681	14.77	n.a.	BMB*
3	18.70	n.a.	196.028	874.786	84.61	n.a.	BMB*
Total:			277.507	1033.860	100.00	0.000	

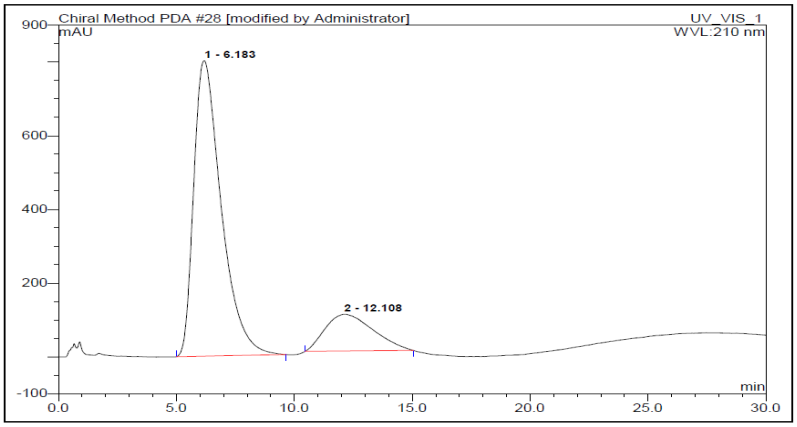

No.	Ret.Time min	Peak Name	Height mAU	Area mAU*min	Rel.Area %	Amount	Type
1	6.18	n.a.	802.068	1083.659	82.20	n.a.	BMB*
2	12.11	n.a.	99.324	234.739	17.80	n.a.	BMB*
Total:			901.392	1318.399	100.00	0.000	

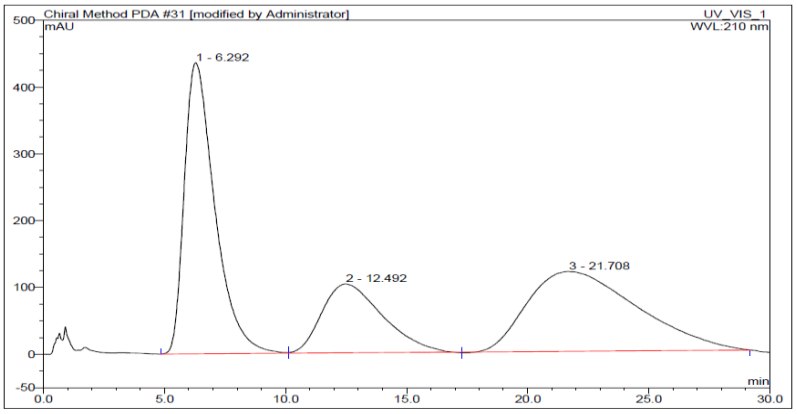

No.	Ret.Time min	Peak Name	Height mAU	Area mAU*min	Rel.Area %	Amount	Type
1	6.29	n.a.	435.712	637.730	40.76	n.a.	BM
2	12.49	n.a.	103.007	298.068	19.05	n.a.	M
3	21.71	n.a.	119.398	628.685	40.18	n.a.	MB*
Total:			658.117	1564.482	100.00	0.000	

Figure 21: Chiral HPLC of **4.13**, **4.14** and a mixture of both (top to bottom) (20% IPA in hexane, AD column, 5 mL/min).